IMPACT OF STOCHASTIC RENEWABLE DISTRIBUTED GENERATION ON URBAN DISTRIBUTION NETWORKS

A Dissertation
Presented to
The Academic Faculty

by

Insu Kim

In Partial Fulfillment
of the Requirements for the Degree
Doctor of Philosophy in the
School of Electrical and Computer Engineering

Georgia Institute of Technology
December 2014

IMPACT OF STOCHASTIC RENEWABLE DISTRIBUTED GENERATION ON URBAN DISTRIBUTION NETWORKS

Approved by:

Dr. Miroslav M. Begovic, Advisor
School of Electrical and Computer Engineering
Georgia Institute of Technology

Dr. Maryam Saeedifard
School of Electrical and Computer Engineering
Georgia Institute of Technology

Dr. Thomas G. Habetler
School of Electrical and Computer Engineering
Georgia Institute of Technology

Dr. John Crittenden
School of Civil and Environmental Engineering
Georgia Institute of Technology

Dr. Ajeet Rohatgi
School of Electrical and Computer Engineering
Georgia Institute of Technology

Date Approved: June 24, 2014

Dedicated to my loving and missing parents for their endless love and devotion.

I would like to express my deepest love and thanks to my parents and wife.

ACKNOWLEDGEMENTS

There were ups, downs, good, and bad times during my doctoral study. Without the helps from many people, I could not finish this long journey successfully.

I would never have been able to finish my dissertation without the guidance of my advisor and my committee members, collaboration with my colleagues, help from my friends, and support from my family. I would like to express my deepest appreciation to my advisor, Dr. Miroslav Begovic, for motivating me, providing excellent guidance on this research, caring about my progress, showing patience, promoting independence, and providing an interactive atmosphere for doing research. He was not only my role model for walking the academic journey but also my strongest advocate, encouraging me to explore many aspects of the field so that I could contribute to the field and even tackle practical issues beyond the textbooks. I would also like to extend my sincere thanks to Dr. Thomas Habetler, Dr. Ajeet Rohatgi, Dr. Maryam Saeedifard, and Dr. John Crittenden for serving as committee members and providing their ideas and criticisms that helped shape this dissertation.

I would like to express my deepest gratitude to Dr. Miroslav Begovic and Dr. John Crittenden for providing me with the infrastructure, the guidance, the patience, and the financial support for this research. I would also like to express my gratitude to Dr. Hyunju Jeong, Jean Ann James, Rajatha Bhat, the colleagues, the students, and the staff at the Brook Byers Institute for Sustainable Systems for providing their help, support, and critiques throughout the process of writing my dissertation.

I had a wonderful chance to work with Dr. Ronald Harley at Georgia Tech, Frank Lambert, and Dr. Yamille del Valle at NEETRAC. In addition, I am thankful for my colleagues who worked with me, Raeey Regassa, Yi Deng, and Yi Du, for insightful discussions and valuable comments.

I must also thank to my master's degree advisor, Dr. Chulhwan Kim, and professors at Sungkyunkwan University in South Korea, Dr. Junho Lee, Dr. Dongryeol Shin, Dr. Chungyuen Won, and Dr. Hyoungkee Choi. Especially, my graduate studies at Georgia Tech would not have begun at all without their supportive recommendation and encouragement.

I would like to thank Professor William H. Kersting and Roger Dugan for our discussions pertaining to three-phase power-flow algorithms. Specially, I would like to thank Jane Chisholm who has helped me to practice and improve my written English.

I would like to thank Dr. Yeonho Jung, Dr. Jinwoo Park, Dr. Ockoo Lee, Kwangil Kim, and Dr. Jongseok Moon for their help and encouragement. I really spent joyful times with them during my doctoral study. Moreover, I would like to express my appreciation for the support from my Korean friends. Dr. Namhun Cho, Dr. Sangtaek Han, Dr. Yongnam Cho, Dr. Sungyun Choi, Yonghee Lee, and Jongkook Park were supportive during my difficulties. I would also like to thank visiting scholars, Dr. Beung-Jin Kim and Dr. Sungsam Kim.

Finally, I am deeply indebted to my parents, even though are not with us, Jongsoon Kim and Namsoon Kook, and parents-in-law, Kyoungil Kim and Sungja Kim, for their unconditional love and dedication. I sincerely appreciate to my brother, Namwoo Kim, who prays for me and my sister, Aeshim Kim, for her support and patience. In addition, I would like to express my appreciation to all the relatives for supporting my family throughout this doctoral study. I also want to thank to my wife, Jeongha Kim. She has provided endless support, cheering me up during times of frustration. She has stood beside me through good times and bad. For all these and much more, I would like to dedicate my dissertation to them.

TABLE OF CONTENTS

LIST OF TABLES

LIST OF FIGURES

NOMENCLATURE

CHAPTER 2

A_F = constant matrix of the equation for voltage

B_F = constant matrix of the equation for impedance

C_B = constant matrix of the equation for current

$\delta_{V_{a,j}}^{(k)}$ = angle of the voltage of phase *a* at the j^{th} bus at the k^{th} iteration

$\tilde{I}_A$ = current of phase *A* of the primary side

$\tilde{I}_{AB}$ = current between phases *A* and *B* of the primary side

$\tilde{I}_a$ = current of phase *a* of the secondary side

$\tilde{I}_{ab}$ = current between phases *a* and *b* of the secondary side

$\tilde{I}_{bk,i}$ = current flowing at breakpoint *i*

$\tilde{I}_{constant\ I,j}$ = current of the constant current load at the j^{th} bus

$\tilde{I}_{constant\ PQ,j}$ = current of the constant power load at the j^{th} bus

$\tilde{I}_{constant\ Z,j}$ = current of the constant impedance load at the j^{th} bus

$\tilde{I}_j^{(k)}$ = current flowing at the j^{th} bus at the k^{th} iteration

$\tilde{I}_H$ and $\tilde{I}_L$ = current of the high- and low-voltage sides

$\Delta\tilde{I}_{bk,i}^{(k)}$ = incremental change in the current of breakpoint *i* at the k^{th} iteration

$\Delta I_{pos,q,j}^{(k)}$ = incremental reactive current change in the positive sequence of the j^{th} P-V bus at the k^{th} iteration

$\Delta\tilde{I}_{qa,j}^{(k)}$ = incremental reactive current change in phase *a* of the j^{th} P-V bus at the k^{th} iteration

$N_1 / N_2 = E_1 / E_2 = I_2 / I_1 = n_t$ = the turns ratio

$S_{scheduled,j} = P_j + jQ_j = |S| \angle \delta_{s_j}$ = scheduled power at the j^{th} bus

Tap = position of the tap, typically $-16 \leq Tap \leq 16$

$\tilde{V}_{AN}$, $\tilde{V}_{AG}$, and $\tilde{V}_{AB}$ = line-to-neutral voltage of phase *A*, line-to-ground voltage of phase *A*, and line-to-line voltage of phases *A* and *B* of the primary side

$\tilde{V}_{an}$, $\tilde{V}_{a'g}$, and $\tilde{V}_{a'b'}$ = line-to-neutral voltage of phase *a*, line-to-ground voltage of phase a', and line-to-line voltage phases a' and b' of the secondary side

$\tilde{V}_{bk,i}$ = voltage of breakpoint *i*

$\tilde{V}_j^{(k)} = \left|\tilde{V}_j^{(k)}\right| \angle \delta_{V_j^{(k)}} = V_j^{(k)} \angle \delta_{V_j^{(k)}}$ = voltage at the j^{th} bus at the k^{th} iteration

$\tilde{V}_H$ and $\tilde{V}_L$ = voltage of the high- and low-voltage sides

$V_{nominal,j}$ = magnitude of the nominal voltage at the j^{th} bus

$V_{pos,j}^{(k)}$ = positive-sequence voltage of the j^{th} bus at the k^{th} iteration

$V_{pos,j,target}$ = target voltage of the positive sequence at bus *j*

$\Delta V_{pos,j}^{(k)}$ = incremental voltage change in the positive sequence of the j^{th} P-V bus at the k^{th} iteration

Y_j = all shunt admittances connected to the j^{th} bus

Z_{ij} = line impedance between the i^{th} and j^{th} buses

Z_T = Thevenin -equivalent impedance matrix of the breakpoints

$Z_{pos,j}$ = positive-sequence impedance of the j^{th} P-V bus

$Z_{Sensitivity}$ = P-V sensitivity impedance

$\left|Z_{pos,ij+jk}\right|$ = magnitude of the positive-sequence impedance of the sum of lines *ij* and *jk*

CHAPTER 5

C = {c|c is the customer type such as residential, commercial, and industrial customers}

$C_i(P_{Gi})$ = the total operating costs of generating unit *i* in *$/hour*

ef = the emission factor in *kg/MBtu* or *gallons/MBtu*

$EO_i(P_{Gi})$ = the emission output of generating unit *i* in *kg/hour*

E_{TB} = the total actual generation of the test bed in *GWh*

$\tilde{E}_{TB}$ = the total generation of the composite load profile of the test bed in *GWh*

fp_i = the equivalent fuel price of generating unit *i* in *$/MBtu*

F_i = the fuel input of generating unit *i* in *MBtu/hour*

$F\left(P_{S_{j,i}}\right)$ = the fuel input of thermal generating unit *j* during interval *i* in *MBtu/hour*

$i_{\max}$ = the maximum interval in hydrothermal coordination

n = the number of loads

n_i = the number of hours during interval *i*

N = the number of generating units

N_H = the number of hydroelectric units

N_S = the number of steam turbines

m = the number of buses

P_c = { $P_c \mid P_c$ is the active power profile of customer type *c* in hourly intervals in *kW*}

P_{Gi} = the net power output of generating unit *i* in *MW*

$P_{Gi}(t)$ and $P_{Gi}(t-1)$ = power outputs of generating unit *i* at times *t* and (*t*-1) in *MW*, respectively

$\tilde{P}_{TB}$ = the composite load profile of the test bed in hourly intervals in *GW*

$\hat{P}_{TB}$ = the unknown load profile of the test bed in hourly intervals in *GW*

P_{Hi} = hydroelectricity generation during interval *i* or of unit *i* in *MW*

$P_{Hk,i}$ = the generation of hydroelectric unit *k* during interval *i* in *MW*

$P_{Sj,i}$ = the generation of thermal unit *j* during interval *i* in *MW*

q_i = water discharge during interval *i* or of unit *i* in *acre-ft/hour*

$q_i\left(P_{Hi}\right)$ = water discharge of hydroelectric unit *i* in *acre-ft/hour*

$q_i(P_{H_{k,i}})$ = water discharge of hydroelectric unit *k* during interval *i* in *acre-ft/hour*

q_{Tot} = total water discharge in daily intervals in *acre-ft*

$r_{i,Min}$ and $r_{i,Max}$ = min and max ramp ratios of generation unit *i*, respectively

T = the total time interval

W_c = the population percentage of customer type *c* in *%*

W_i = the weight of objective function *i* from 0 to 1

$WO_i(P_{Gi})$ = the water output of generating unit *i* in *gallons/hour*

λ = the Lagrangian multiplier for load balancing

γ = the Lagrangian multiplier for water balancing

SUMMARY

The main objective of this study is to analyze the impact of the stochastic renewable distributed generation (DG) system on the urban distribution network. Renewable DG systems, particularly photovoltaic (PV) systems, dispersed on the distribution network may, in spite of their relatively small individual capacities, change the behavior of such a network. Therefore, this study (1) develops tools and algorithms useful for planning, designing, and operating such a network, (2) addresses some of the issues in the analysis of the impact of renewable DG systems on such a network, and (3) designs a framework for streamlining the future development and the smooth integration of renewable DG systems into the urban distribution network.

The objective of Task 1 of this research was to propose a useful method of analyzing the impact of stochastic renewable DG systems, particularly PV systems, on urban distribution networks. Using the backward and forward sweep method implemented in MATLAB, this study developed an algorithm for three-phase power flow that models power system components, including distribution systems, transformers, and PV systems. To model the influence of the inherent uncertainty of the input, the location, and the capacity of the PV system, this study implemented a stochastic simulation algorithm combined with the power-flow algorithm. It also accelerated the stochastic algorithm using a method of variance reduction, including importance sampling, and the sampling of representative clusters and extreme points, which reduced the extremely heavy computational burden that the stochastic simulation inevitably imposed. Then this study analyzed inherent uncertainties such as the inputs, the locations, and the capacities of residential PV systems stochastically installed on urban distribution networks by performing several stochastic simulations. While doing this research, this study found that if PV systems, the power output of which is estimated by solar radiation and

meteorological data of the Atlanta area in typical meteorological year (TMY) data sets in hourly intervals, are dispersed randomly throughout the IEEE 123-bus test feeder as an example of the urban distribution network, with a capacity equal to ten percent of total peak demand, they can decrease the amount of energy produced by non-PV solar plants, particularly by about 3.8-6.7 percent in the case study. That is, stochastically dispersed PV systems could not only save energy generated from other generation resources, which typically burn more polluting fuel, but also handle peaks in consumption. Lastly, this study investigated methods of acceleration of stochastic simulations by the near-normal distribution for the system capacity and azimuth angle random variables of the PV system and reduced a stochastic simulation time by sampling representative clusters and extreme points.

In Task 2, this study developed a genetic algorithm in MATLAB that solves an optimization problem that maximizes the reliability (or minimizes the frequency and the duration of failure) of urban distribution networks enhanced by protection devices (i.e., the recloser, the fuse, and the switch) and renewable DG. Using the backward and forward method, this study implemented an analytical method that simulates all possible permanent and transient faults and evaluated the reliability of an urban distribution network housing a combination of fuses, switches, reclosers, and DG systems. Then it analyzed the impact of both the DG system, including the effect of the islanded operation of the DG system, and the protection device, on the reliability of the urban distribution network. The results from the reliability analysis of urban distribution networks such as IEEE 34- and 123-bus feeders showed that although the recloser installed on such test feeders increases the frequency of a failure because of its multiple reclosing characteristics and lock-out state, it could reduce the duration of a failure, or the SAIDI. In the case of a transient fault, the recloser can prevent a downstream fuse from burning, so fewer customers will experience outages. In addition, as a result of its islanded operation, the DG system can reduce the duration of a failure. However, since renewable

DG systems, particularly PV systems, produce power only during the daytime, they do not significantly reduce the annual failure duration, even with a 100 percent capacity of peak demand. Therefore, to maximize the reliability of urban distribution networks, which would be enhanced by PV systems, the PV systems would have to be enhanced by various storage systems or methods of optimizing their locations, capacities, and islanded zones.

The objective of Task 3 of this study was to present a useful method for analyzing the impact of geographically dispersed DG systems, particularly PV systems, on statewide and nationwide power grids. Using the methods of Lagrangian optimization and hydrothermal coordination, this study developed an algorithm for environmentally constrained generation resource allocation that minimizes both fuel costs and ecological impact, including the impact of water consumption. Then, this study (1) analyzed, as an example of the statewide power grid of the future, the power system of the state of Georgia in 2010, (2) modeled the load consumption and the water inflow of the power system, (3) synthesized third-order power output functions for costs, emissions, and water consumption from actual heat-rate data, and (4) estimated the power output of PV systems geographically dispersed throughout the state and hydroelectric resources of the state in hourly intervals. Lastly, it performed simulations for the generation resource allocation of the power system in hourly intervals. As a result of this research, this study concluded that the statewide power grid enhanced by geographically dispersed PV systems can cope with peaks and reduce the amount of energy generated from fast dispatchable gas-fired plants, which typically burn expensive fuel, particularly by about 3.1 percent in the case study assuming that PV systems, the power output of which is estimated by solar radiation and meteorological data of 19 locations of the state in TMY data sets, with a capacity of ten percent of the peak of the state are geographically dispersed throughout the state.

Viewed in hourly intervals, the PV system appears to have a more stable output than usual. Rapid variations in short-term PV generation, typically in minute intervals, result from transient cloudiness and weather disturbances in the atmosphere. Therefore, this study modeled the short-term intermittency of transient cloudiness using the Markov chain Monte Carlo method and estimated the generation of geographically dispersed PV systems with a capacity of ten percent of the peak of the state in one-minute intervals. This study found that the statewide power grid enhanced by geographically distributed PV systems operating in one-minute intervals could still cope with peaks. However, since PV systems operating in these intervals can suddenly decrease their output, they create an additional need for a spinning reserve that copes with uncertainty involved in their output. In fact, because of their intermittency, or sudden energy shortages and overages, PV systems can increase fossil fuel consumption of faster dispatchable spinning reserves, which typically burn the most expensive fuel. Thus, the smooth integration of renewables into statewide or nationwide power grids necessitates the further investigation of a source of supplementary energy, especially for peak power and spinning reserves, and changes in the costs of generation resulting from their intermittency.

CHAPTER 1

INTRODUCTION

1.1 Motivation and Background

To maximize reliability and to minimize costs, utilities generate, transmit, and distribute electricity in centralized power systems. However, they may soon be able to abandon centralization for two reasons. For one, small power generation has advanced to the point of viable application in micro-turbine, cogeneration, and small power photovoltaic (PV) systems and other generation technologies. When electricity from a power plant is not available, small distributed power generation can provide reliable power by operating in the "islanding" mode. Furthermore, because of "green" electricity initiatives, the installation of cleaner and smaller power generation systems has become less costly and more efficient.

The 1970's witnessed the advent of the commercial PV power industry. During that time, PV modules were prohibitively expensive, but since then, their real prices have decreased 70 percent. In the early 1980s, the political climate in the United States ended substantial funding for solar energy research. Since the nation represented nearly 80 percent of the global market of solar energy at that time, this substantial reduction in funding in the United States virtually halted the development of solar energy around the world [1, 2]. In 2004, renewable energy sources (74.5 percent of which are produced from hydroelectric plants and 0.001 percent from solar PV generators in the United States) produced only 9.6 percent of the electricity generation in the United States and 18.6 percent globally [3-5]. In 2009, all the nations of the world produced 3,900 TWh of renewable energy, only 20 TWh of which (0.1 percent of 20,043 TWh of world electric energy) was produced by solar PV generators and 3,252 TWh (16.2 percent of world

electric energy) of which was generated by hydroelectric plants. However, the world net generation of solar PV is projected to increase from 20 TWh in 2009 to 740 TWh (2.0 percent of 36,250 TWh of projected global electric energy) in 2035, growing at an average annual rate of 15 percent [6], even rising to 11 percent of projected global electric energy in 2050 [7].

1.1.1 Cost Evolution of PV

Figure 1 illustrates a roadmap for the levelized cost of electricity (LCOE) of PV that quantifies the need for technology development to attain grid parity. In Figure 1, LCOE contours are plotted as a function of module cost in $/Wp (Wp means the maximum power output of a solar panel area of 1 m^2 at 25 °C on an ideal sunny day) and module efficiency (in percent) for a location in Phoenix, Arizona. This assumes a balance of system (BOS) cost of $2/W for 20 percent efficient modules. For example, 18 percent to 20 percent efficient modules at prices of $1.2/Wp to $1.4/Wp can produce electricity at 10 ¢/kWh (which can be often defined as grid parity for residential applications defined in sunny areas of the United States). Figure 1 indicates that the cost effectiveness of PV can be a function of module technology such as efficiency, which has been steadily improving (as presented in Figure 3), and module prices, which have been continuously decreasing (as presented in Figure 4).

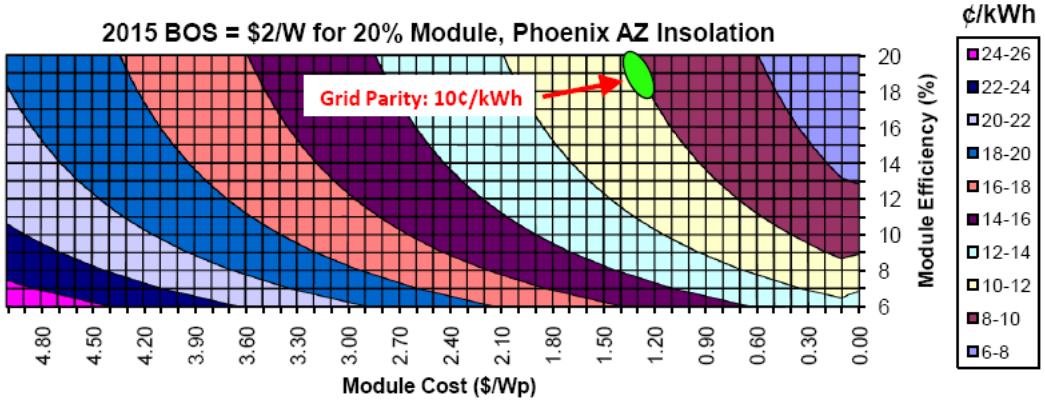

Figure 1. Relationship between module cost, efficiency, and the cost of electricity [8]

1.1.2 PV Module Technologies

PV systems consist of PV modules (interconnected by PV cells with a p-n junction diode structure), inverters, batteries, electrical components, and mounting systems. The fundamental building block of a PV system is the PV module, which can be classified by wafer-based crystalline silicon (c-Si) and thin films. In Figure 2, c-Si (such as single crystalline [sc-Si] with an efficiency of 14-20 percent and multi-crystalline [mc-Si] with an efficiency of 13-15 percent) accounts for 85-90 percent of the global market share in 2008, thin films (such as cadmium telluride [CdTe] with an efficiency of 9-11 percent, amorphous silicon [a-Si] with an efficiency of 6-9 percent, and copper indium gallium selenide [CIS] with an efficiency of 10-12 percent) represent 10-15 percent of the global market share, concentrating PV under 1 percent, and organic solar cells under 1 percent [7]. Figure 3 shows PV module efficiencies, which have been steadily improving during the last three decades.

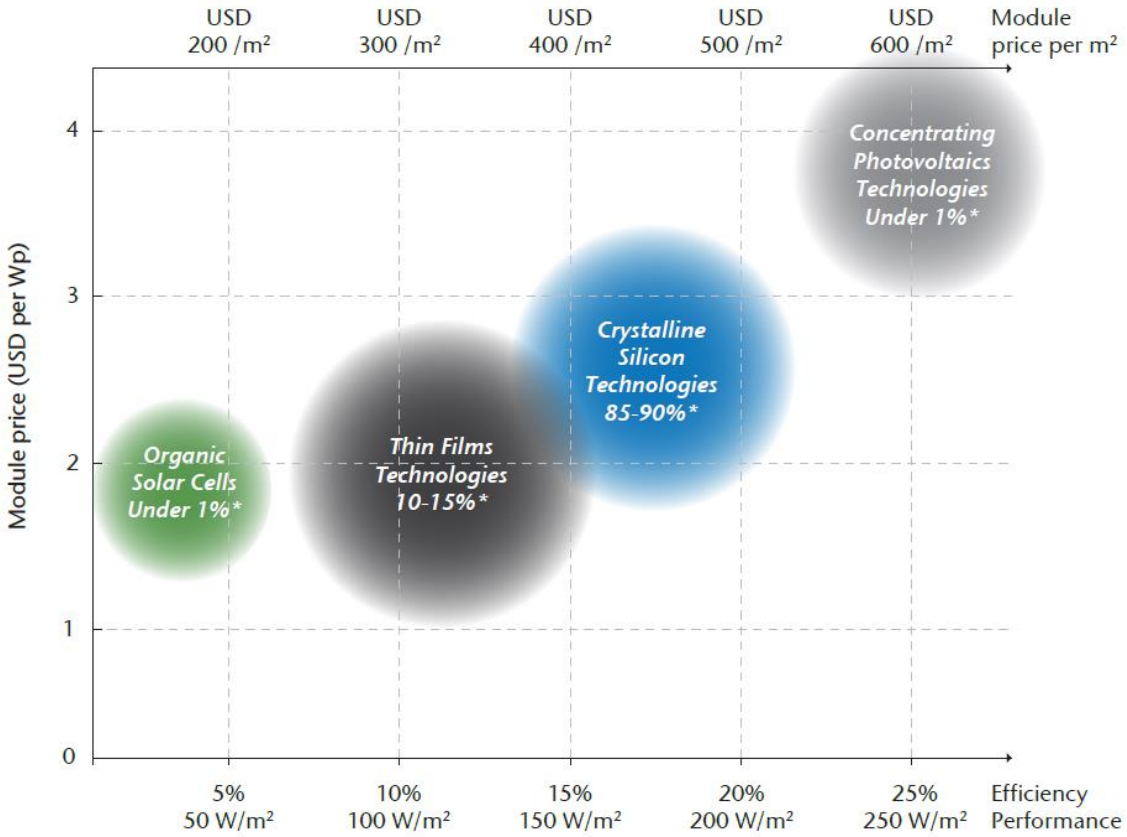

Figure 2. Market shares and prices of PV module technologies [7].

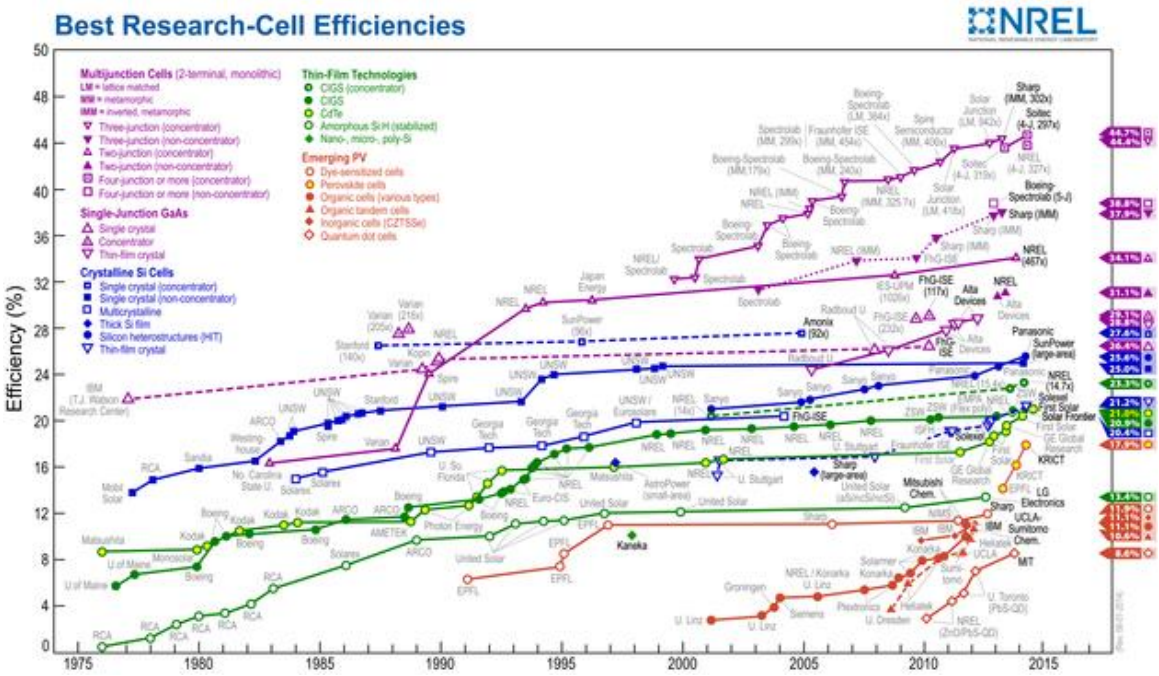

Figure 3. PV module efficiencies [9]

1.1.3 PV for Grid Parity

For more than 50 years, c-Si (crystalline silicon), the dominant market share of which increased from 68 percent to 90 percent between 1990 and 2007, has been a mainstream material for manufacturing PV cells, modules, and panels [8]. Figure 4 shows the learning curve, referred to as the "experience curve," for c-Si PV module prices, defined as the function of the cumulative production of PV modules in the world from 1976 to 2012. It indicates that in the past three decades, the prices of c-Si modules have decreased by approximately 20 percent whenever the cumulative production of PV modules has doubled. At the end of 2011, the prices of PV modules declined to \$0.95/Wp from \$1/Wp, which corresponds to a cost of generating electricity of 10 ¢/kWh, or 100 \$/MWh, and which is defined as grid parity for residential applications in sunnier areas of the United States, with a cumulative installed capacity of 77 GW [10]. In fact, in sunnier areas such as the southern United States, PV may be able to compete with conventional sources of energy.

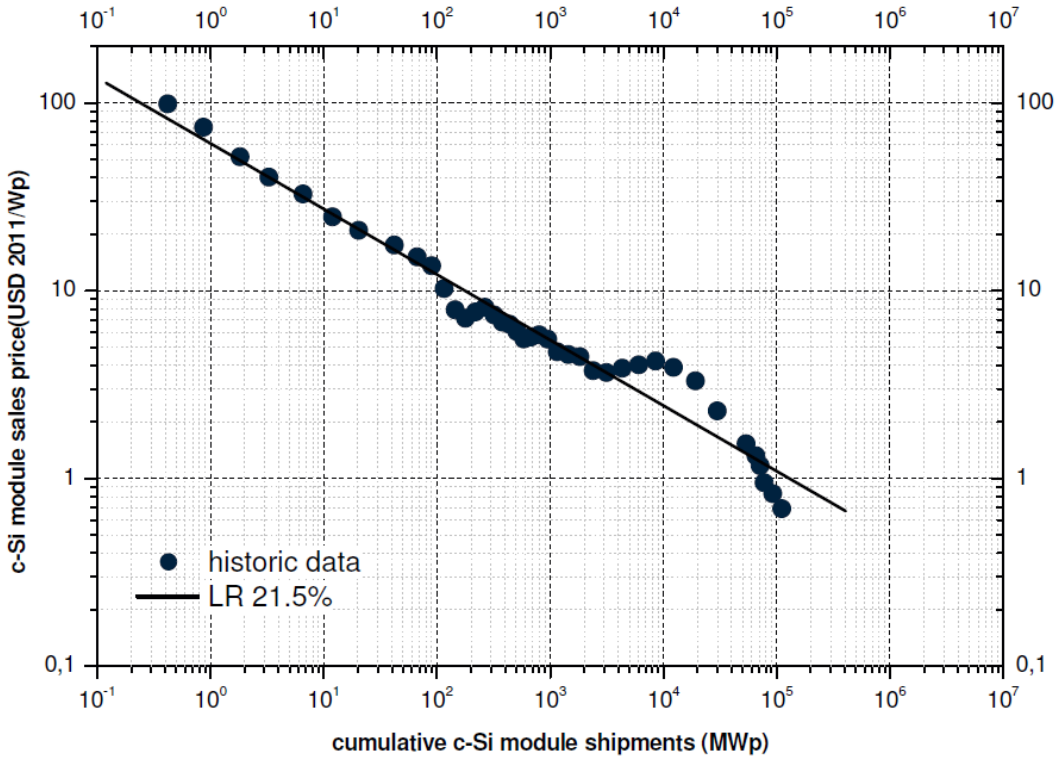

Figure 4. Learning curve for the c-Si PV industry from 1976 to 2012 [10].

1.1.4 Global Trend of Cumulative Installed PV Capacity

At the end of 2012, the global cumulative installed capacity of PV reached the mark of 100 GW, almost 138.9 GW of PV in 2013, as shown in Figure 5. In 2013, China accounted for 18.6 GW of cumulative installed capacity of PV, so the nation was the leading nation while the Americas represented 13.7 GW. Europe remains the leading region with a cumulative installed capacity of 81.5 GW. Figure 5 shows that the PV market has continuously grown over the past decade, even during economic hard times [11].

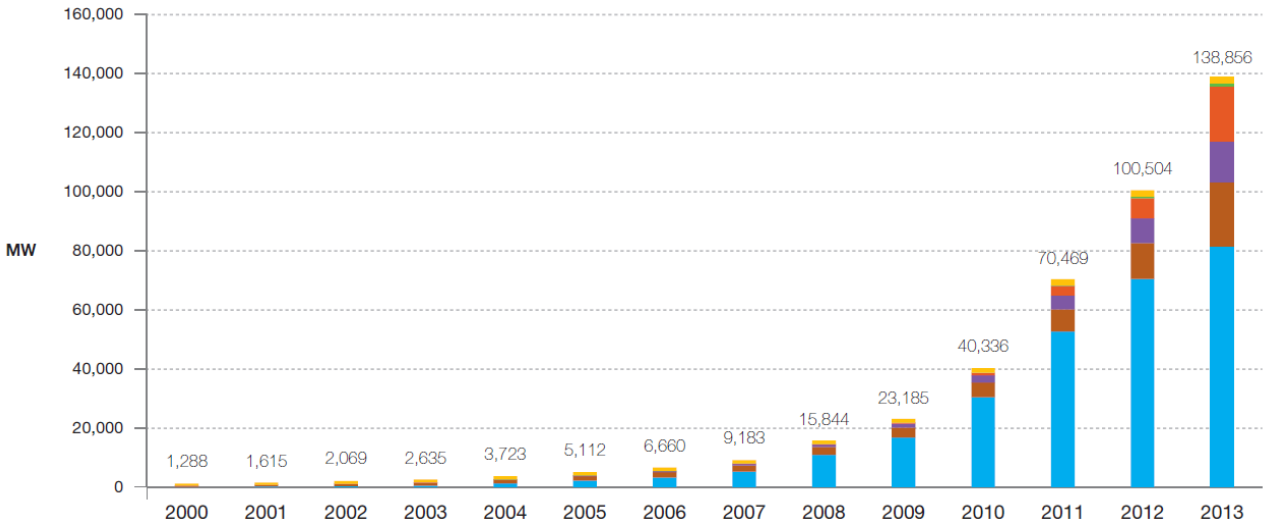

	2000	2001	2002	2003	2004	2005	2006	2007	2008	2009	2010	2011	2012	2013
RoW	751	807	887	964	993	1,003	1,108	1,150	1,226	1,306	1,590	2,098	2,098	2,098
MEA	n/a	n/a	n/a	n/a	1	1	1	2	3	25	80	205	570	953
China	19	24	42	52	62	70	80	100	140	300	800	3,300	6,800	18,600
Americas	21	24	54	102	163	246	355	522	828	1,328	2,410	4,590	8,365	13,727
APAC	368	496	686	916	1,198	1,502	1,827	2,098	2,628	3,373	4,951	7,513	12,159	21,992
Europe	129	265	399	601	1,306	2,291	3,289	5,312	11,020	16,854	30,505	52,764	70,513	81,488
Total	**1,288**	**1,615**	**2,069**	**2,635**	**3,723**	**5,112**	**6,660**	**9,183**	**15,844**	**23,185**	**40,336**	**70,469**	**100,504**	**138,856**

Figure 5. Global cumulative installed PV capacity [11].

1.1.5 Global Interest in Renewable Energy

Interest in renewable energy, including PV, the market of which has experienced continuous growth, has been growing since the recent catastrophic events in Japan such as the meltdowns of triple nuclear reactors at the Fukushima Daiichi Power Plant (which were seriously damaged by an earthquake and the following tsunami, in March 2011). In addition, in June 2011, the German government announced a plan to shut down all nuclear reactors, which currently provide 27 percent of the electricity generation of the country, by 2022 and increase renewable energy generation to partially offset the resulting loss of generation [12]. The French government, which derives over 75 percent of the country's electricity generation from nuclear energy, plans to reduce nuclear generation by five percent, and the Italian government announced a halt in new nuclear initiatives. While these plans are not directly related to the rapid growth of PV, they will

result in energy shortages that the proliferation of all renewable energy, including PV, can make up for [8].

1.2 Grid-Connected PV

Electric power utilities in the United States are focusing on boosting renewable energy, including PV, in their distribution networks because of (1) a significant reduction in the costs of PV systems (which is caused from the rapid growth of PV module installations), (2) present regulations that require the increased production of renewables such as renewable portfolio standards (RPS) or renewable electricity standards (RES), and (3) financial incentives for PV systems such as rebates, grants, and government subsidies. These grid-connected PV systems are classified by the following scales [8, 13]:

- Small-scale PV systems with a capacity under 20 kW, which are usually installed on the roof of residential houses.
- Medium-scale PV systems with a capacity of between 100 and 500 kW, which are usually installed on rooftops of small commercial buildings or integrated within a building itself.
- Utility-scale PV systems with a capacity of between 500 kW and 10 MW, or above 10 MW, which are installed in solar power stations.

These grid-connected PV systems will have the following most common impacts on distribution networks:

(1) *Energy savings caused from reverse power flow.* The most obvious effect of PV systems installed on distribution networks is reductions in energy consumption because of the reverse power flow of PV systems into the distribution network. They can also reduce the emissions and the costs of energy production by using less fuel from fossil-fuel plants, particularly the avoided costs caused by reducing gas turbines for peak power generation that burns the most expensive fuel.

(2) *Reliability.* In case of an outage, PV systems with relatively high capacity may be able to provide a distribution network with some power, especially when equipped with storage systems, so the network supplied by the PV systems will become an island and not experience an outage. In fact, the islanded operation of PV systems can reduce the duration of a failure. In other words, it can improve reliability. Therefore, PV systems may have an impact on the reliability of the urban distribution network.

(3) *Short-term intermittency of PV generation.* Because PV systems may suddenly and unpredictably decrease or increase their output, utilities may have to prepare for sudden energy shortages or overages (e.g., the voltage deviation, or a maximum difference between voltage without PV systems and that with full-capacity PV systems, can be defined as a ramping capability criterion of the PV system). These rapid variations in their output caused by transient cloudiness and weather disturbances in the atmosphere lead to fluctuations in feeder voltages, increase the fossil fuel consumption of conventional power plants in order to make up for sudden and severe energy shortages, and create a need for an additional spinning reserve to cover uncertainty involved in their output. In fact, to complement sudden and severe energy shortages caused from their intermittency, many electric utilities may burn expensive fossil fuel, or keeping a sufficient spinning reserve.

(4) *Voltage rise.* One of the main concerns of electric power utilities is overvoltage along their feeders when their networks are enhanced by various distributed generation (DG) systems, particularly PV systems in this study. The voltage rise can be significant when high-capacity PV systems are installed on lightly loaded feeders, which are common in rural areas. This condition also may cause voltage exceeding utility planning limits and affect overvoltage protection and coordination.

(5) *Voltage and current imbalance.* A single-phase PV system can offset local feeder loads by injecting active power into a single phase of the distribution network but cause imbalance in phase voltages and currents. For example, phase *a* connected to a single-phase PV system experiences reverse power flow but other phases *b* and *c* do not.

(6) *Interaction with voltage-controlled capacitor banks, load tap change transformers, and voltage regulators.* Voltage rise and fluctuations may increase the operation of voltage-controlled capacitor banks, load tap changer transformers, and voltage regulators, particularly those set to a forward operation mode, a line drop compensation mode, or their loading limits. In fact, their frequent operations can worsen life cycles and increase maintenance cycles. Furthermore, they in turn may cause additional reactive power fluctuations and affect Volt/VAr control (or Volt/VAr optimization), Volt/Watt control, dynamic VAr control, and conservation voltage reduction [8, 13].

(7) *Power losses.* PV systems with low or moderate capacity generally reduce local feeder loading, particularly during the daytime, and distribution line losses (proportional to the square of line currents). However, PV systems with high capacity may increase the magnitude of currents because of reverse power flow, thereby increasing distribution line losses. In fact, the more power high-capacity PV systems inject into the distribution network, the more loss the distribution network may experience because of reverse power flow.

(8) *Total harmonic distortion (THD) increase.* Power electronics equipment for plug-in electric vehicles, distribution energy storages, inverter-based devices, and PV systems connected to distribution networks may deteriorate power quality such as THD. Their interconnection to the grid in the presence of capacitor banks also addresses other harmonic issues such as resonance [8].

(9) *Overcurrent and overvoltage protection.* The interconnection of PV systems to the grid may affect the operation of overcurrent and overvoltage protection devices (e.g., fuses, reclosers, and relays) because of the increased magnitude of line currents caused from the reverse power flow of PV systems. In addition, the islanded operation of PV systems can convert a radial network into a meshed network, cause temporary overvoltage, and disrupt the overall coordination of overcurrent and overvoltage devices.

(10) *Reactive power support.* Present regulations require that DG systems maintain terminal voltage within a specified range, typically within 0.95 to 1.05 PU of the rated voltage level, and operate at or near unity power factor [14]. To maintain voltage within this range, present DG systems can produce active and reactive power, but mostly producing active power at unity power factor, based on present standards. In addition, since various DG systems such as PV systems, wind farms, and microturbines enhanced by inverters with the capability of Volt/VAr control are being deployed in distribution networks, they may provide additional reactive power within their capacity limits to maintain voltage within 0.95 to 1.05 PU of the rated voltage level.

1.3 Three Main Impacts of PV Systems

Despite the various advantages of PV systems, electric power utilities are not sufficiently motivated to allow interconnections of customer-owned generators (which would consist of a number of PV installations) to their distribution networks, the main reasons being more operational than economic. The potential impact of DG on the deterioration of reliability and the power quality of systems sometimes outweighs the anticipated benefits. Therefore, utilities tend to subject non-utility generation to extensive technical analysis. Conversely, regulating authorities such as the federal energy regulatory commission act in favor of DG owners and tend to request that

interconnections be as easy and transparent as possible [15]. Thus, some of the issues in the analysis of such interactions should be addressed on the impact of the DG system on (1) the urban distribution network, (2) reliability (from the perspective of small- or distribution-scale impacts caused from the DG system), and (3) statewide or nationwide power grids (from the perspective of large- or utility-scale impacts). In other words, the severity of steady-state and transient issues resulting from the integration of the DG system in general and the PV system in particular into urban distribution, statewide, or nationwide power grids can be examined by analyzing the various impacts of DG systems on such grids. Therefore, the main objectives of this study are to examine (1) the impact of DG systems stochastically dispersed throughout urban distribution networks, (2) the impact of DG systems on the reliability of urban distribution networks, and (3) the impact of DG systems geographically distributed on statewide or nationwide power grids.

1.4 Impact of Stochastic Renewable DG on Urban Distribution Networks

To analyze the impact of DG systems on urban distribution networks at small- or distribution-scales, this study initially models uncertainty of the DG systems. The inherent uncertainty of the input, the location, and the capacity of DG systems can be modeled by optimized stochastic methods that require tens of thousands of the sub-hourly power-flow calculations. Therefore, it firstly discusses the related prior work and the problem statement on an algorithm for three-phase power flow.

1.4.1 Related Prior Work of the Three-Phase Power-Flow Algorithm for the Analysis of the Impact of the DG System

The related prior work on an algorithm for three-phase power flow for the analysis of the impact of the DG system has not analyzed the impact of the uncertainties of the DG system. For example, neither the conventional Newton-Raphson and fast decoupled power-flow techniques nor the modified Newton-Raphson and fast decoupled

power-flow techniques were suitable for the analysis of radial distribution power systems [16]. However, several faster and more efficient algorithms for the radial distribution system have been developed [17]. These algorithms directly solve the power-flow problem of a radial network by applying Kirchhoff's voltage law (KVL) and Kirchhoff's current law (KCL), both of which are referred to as the "backward and forward sweep method." However, these algorithms are not capable of solving the power flow of the meshed power system network. To solve the problem, [18] proposed a modified power-flow algorithm for the meshed network. This algorithm bi-directionally accumulates current flow at breakpoints after injecting current and calculates the breakpoint current using the method of iterative multi-port compensation, based on the fixed tangent method [16, 17, 19, 20]. However, these algorithms cannot directly analyze the impact of DG systems on radial or meshed urban distribution networks enhanced by various DG systems with the inherent uncertainty of their inputs, locations, and capacities. In addition, since various DG systems such as PV, wind farms, and microturbines enhanced by inverters with the capability of Volt/VAr control are being deployed in urban distribution networks, present regulations require that the DG system maintain its terminal voltage within a specified range, typically 0.95 to 1.05 PU of the rated voltage level [14]. To stay within this range, the DG bus that produces active and reactive power for its terminal voltage (which means the Volt/VAr control) was modeled as a P-V bus [17, 18, 21]. On the other hand, the DG bus that reduces only active power as a negative constant power source was modeled as a P-Q bus [17]. Therefore, this study will implements an algorithm that will be able to model the DG bus of the high-penetration capacity as either a P-Q or P-V bus and combines the algorithm with a stochastic algorithm (which will be discussed in the next section).

1.4.2 Problem Statement of the Three-Phase Power-Flow Algorithm for the Analysis of the Impact of the DG System

The related prior work for power-flow analysis is not appropriate for analyzing the impact of the uncertainties of the DG system because they cannot directly analyze the impact of DG systems on radial or meshed urban distribution networks enhanced by various DG systems with the inherent uncertainty of their inputs, locations, and capacities [16-20]. Thus, the objective of this study is to develop a three-phase power-flow algorithm capable of analyzing the impact of DG systems stochastically dispersed on urban distribution networks. For this purpose, the algorithm implements the backward sweep that sums current flows at each bus in the backward direction and the forward sweep that calculates voltage drops in the forward direction, codes of which are presented in Appendix B [16-20]. Since DG connected to the radial network may convert a radial network into a meshed network, the algorithm analyzes the meshed network by the method of iterative breakpoint compensation, which injects nodal currents and expresses as a Thevenin-equivalent circuit by viewing such a network from the breakpoint [16-20]. In addition, it models power system components, including distribution systems, voltage regulators, and transformers, and integrates the simulation program for the PV system into the power-flow algorithm because various DG systems such as PV, wind farms, and microturbines are being deployed in urban distribution networks [22-25]. Furthermore, present regulations require that the DG system maintain its terminal voltage within a specified range, typically 0.95 to 1.05 PU of the rated voltage level [14]. To stay within this range, the DG bus should be modeled as either a P-V bus if the DG system is able to produce active and reactive power for its terminal voltage or a P-Q bus if the DG system is not able to control its terminal voltage [17, 18, 21]. Therefore, this study implements an algorithm that will be able to model the DG bus of the high-penetration capacity as

either a P-Q or P-V bus and combines the algorithm with a stochastic algorithm that will be discussed in the next section.

1.4.3 Related Prior Work of the Analysis of the Impact of Stochastic Renewable DG on Urban Distribution Networks

Algorithms for analyzing the effect of the DG system can be classified as both non-stochastic (which typically uses the deterministic method such as power-flow algorithms) and stochastic methods. One study using the former method quantified the benefits of PV systems by examining the relationship between the generation of a PV system and peak loads from the standpoint of energy savings, loss, and emissions as well as a reliability and economic analysis [26]. Another study presented a method of calculating distribution line losses reduced by the PV system and optimizing the plant size and the feeder configuration [27]. In addition, many studies modified the algorithm for power-flow analysis to determine the effects of the DG system. One study investigated the effect of a PV system installed on radial and looped feeders from the perspective of power quality such as the voltage, active power, and loss using MATPOWER in MATLAB [28]. Another study developed a three-phase power-flow algorithm for shipboard power systems that analyzes the effect of the DG system with various capacities in twelve cases with varying loads [21].

Stochastic methods model the influence of the many uncertainties of stochastically dispersed DG systems by repeatedly conducting random sampling. One study removed the uncertainty of loads and the input of DG, or the wind speed, in the distribution system [29, 30]. Other research analyzed the performance of DG systems dispersed across a 69-bus test feeder using the stochastic Monte Carlo method enhanced by the method of sampling representative clusters and boundary points [31, 32]. Using the stochastic Monte Carlo method, a recent study developed a power-flow algorithm that models the load and the PV system as random variables, so it removed the uncertainty of

solar energy and load variations [33]. Another recent study showed that the capacity of the PV system is affected by policy incentives, personal characteristics, income level, age, race, and education [34]. However, neither of these non-stochastic and stochastic studies examined the inherent high-dimensional uncertainty of the input, the location, and the capacity of the DG system, variables that are not known in the planning stage of the power system. In addition, these studies did not examine the effect of the DG system from the standpoint of long-term, typically annual, operation. The high-dimensionality of uncertainty requires a very large number of simulations, possible only with a fast-performing optimization algorithm. Therefore, this study develops a stochastic simulation algorithm combined with the fine-tuned three-phase power-flow algorithm (which is discussed in the previous section). Then, to reduce the number of computational steps that the stochastic simulation inevitably imposes, this study accelerates this combined algorithm with methods of variance reduction (including importance sampling, stratification sampling presented in [35, 36]) and the sampling of representative clusters and extreme points proposed in [31, 32].

1.4.4 Problem Statement of the Analysis of the Impact of Stochastic Renewable DG on Urban Distribution Networks

(1) Challenge in the Analysis of the Impact of Stochastic Renewable DG on Urban Distribution Networks

In anticipation of the increased penetration of DG systems in general and PV systems in particular, their cumulative effect on the distribution network may, in spite of their relatively small individual capacities, change the behavior of the distribution network in which they are installed. The accurate modeling of such a distribution network enhanced by PV systems is challenging for the following reasons: Renewable PV systems are normally neither owned nor operated by a utility, their outputs are a stochastic quantity-dependent on meteorological and other input conditions, and the

locations, the capacities, and the operational statuses of individual systems are not known in the planning stage [24]. In other words, one challenge in analyzing the impact of the DG system is the inherent uncertainties of its inputs, locations, and capacities.

(2) Uncertainty of DG Systems

Algorithms for analyzing the effect of the DG system can be classified as both non-stochastic and stochastic methods [21, 26-33]. However, these both non-stochastic and stochastic studies did not examine the inherent high-dimensional uncertainty of the input, the location, and the capacity of the DG system, not known in the planning stage of the power system. To analyze the effects of a DG system, particularly the PV system, on urban distribution networks, this study proposes a stochastic simulation algorithm that models the following uncertainties:

1) *Location*. Residential small-capacity PV systems can be dispersed anywhere across the distribution network.
2) *Generation*. Since the generation of the PV system depends on a probabilistic quantity, its generation is not known in the planning stage.
3) *Capacity and field orientation*. The capacity and the field orientation of individual PV systems may differ.

To model the inherent uncertainties of the location, the capacity, and the field orientation of the PV system, this study proposes a scenario of residential PV systems with a capacity of ten percent of total peak demand stochastically dispersed throughout the urban distribution network. In the scenario, this study determines the annual effect of not only savings in energy and emissions but also changes in generation costs resulting from residential PV systems. In fact, it determines the annual power production (in kWh/year/household), the annual energy savings (in kWh/year/ household), the emissions savings (in kg/year/household or gallons/year/household), and the generation cost changes (in $/year/household) of residential PV systems stochastically dispersed throughout the urban distribution network.

(3) Stochastic Simulation

In the scenario of stochastically dispersed residential PV systems, to remove their uncertainties and to determine the annual energy production and savings of residential PV systems, this study proposes a stochastic (Monte Carlo) simulation (which is usually used to estimate expectation values) combined with the power-flow algorithm (presented in the previous two sections). Then this study defines uncertainty in the input and the power output of PV systems such as the capacity, the azimuth angle, the tilt angle, and the module material of the PV system [37-39] and surveys the actual distribution of the capacity of residential PV systems in California in 2014 (because of the unknown distribution of residential PV systems in Georgia) [40]. This study also uses the IEEE 123-bus test feeder as the urban distribution network [41] and load profiles for residential, commercial, industrial, agricultural and pumping, and large industrial customers, obtained from an actual utility in kW in hourly intervals in 2007 [42]. In addition, it uses an energy mix of the state of Georgia [43] and residential PV systems as an example of a DG system dispersed throughout an urban distribution network. Lastly, it performs annual stochastic simulations during sufficiently long periods in hourly intervals and analyzes the impact of residential PV systems stochastically dispersed in the Atlanta area from the perspective of energy, particularly regarding peak power, electricity generation costs, and emissions.

(4) Variance Reduction

A (naive) Monte Carlo simulation as stochastic simulation methods of accounting for uncertainty is based on repeated random sampling, which creates a serious computation burden on rare events that can be reduced by the method of importance sampling and stratification sampling [35, 36]. This study applies importance sampling to random sampling for the system capacity and azimuth angle random variables in the proposed stochastic simulation. In other words, it reduces variance by sampling more extensively near the important area (which is defined by optimal importance sampling)

when finding the expectation value of annual PV power production, which is a function of the capacities, the azimuth and tilt angles, and the modules of PV systems. In fact, to reduce variance in the expected value, that is, to obtain the more accurate expected value, this study accelerates the stochastic simulation with the methods of variance reduction, including importance sampling for the system capacity and azimuth angle random variables and stratification sampling for the tilt angle random variable. Lastly, it quantifies the effects of the methods of variance reduction, including importance sampling and stratification sampling.

1.5 Reliability Enhancement Through a Reconfiguration of Urban Distribution Networks Enhanced by DG

To analyze the impact of DG systems on the reliability of urban distribution networks at small- or distribution-scales, this study discusses the related prior work and the problem statement on reliability enhancement through a reconfiguration of urban distribution networks enhanced by DG.

1.5.1 Related Prior Work of Reliability Enhancement Through a Reconfiguration of Urban Distribution Networks Enhanced by DG

The method of evaluating the reliability of a distribution network can be classified into two methods: the analytical method and the stochastic method. One study presented an analytical method that provided a mathematical model of the reliability configuration and the mean value of the reliability index [44-46]. However, since the mean value does not contain the probability distribution and the dispersion of the relevant reliability index, a stochastic process simulation such as the Monte Carlo technique, which evaluates the variability of the reliability index, has been proposed [47, 48]. Residential, commercial, and industrial customers can use the results of the stochastic method for cost analysis [47]. Recently, another study provided a method for evaluating reliability using the duration

curve of a load, which is divided into two regions, not supplied and supplied loads, a connection matrix that expresses the system configuration, and an impact factor that examines the effect of sustained and momentary interruptions of a system failure [49]. In addition, a recent study provided a method of representing the logical relationship between nodes and branches in the distribution network in a matrix form [50].

Recently, to enhance the reliability of distribution networks, many studies have proposed near-optimal solutions that maximize the reliability of conventional feeders protected by reclosers and investigated the effects of protection devices, particularly the recloser. One study presented a genetic algorithm that determines an optimal recloser position and improves reliability [51, 52]. Another study presented selection models for genetic evolution such as the fitness-based roulette model, the scaled roulette model, the tournament model, and the elitist model [53-55]. Since the superiority of the genetic algorithm arises from its crossover operation (which generates a better solution by exchanging genetic information) and mutation operation (in which better populations of experiencing changes approach the best population while avoiding convergence to the local minimum), many studies presented the crossover probability in the range of 0.5-1.0 [53, 56] and the mutation probability in the range of 0.005-0.1 [53, 56]. Another study provided a method of simulating social behavior in systems such as an ant colony. The algorithm found a near-optimum solution for switch relocation [57]. One study suggested that a recloser placed in the middle of a distribution line might improve feeder-wide reliability by about 25 percent [51]. Another study showed that the three reclosing operations of the recloser could prevent nearly 93 percent of faults [58]. In addition, a recent study showed that downstream transient faults prevented by the recloser could improve the system average interruption duration index (SAIDI), but not the system average interruption frequency index (SAIFI) [59].

These analytical, stochastic methods, and evolutionary algorithms, however, are not capable of analyzing the urban distribution network housing a combination of fuses,

switches, reclosers, and high-capacity DG systems. Therefore, to determine the reliability index of a more practical distribution network housing a combination of fuses, switches, and reclosers, this study (1) proposes an analytical method of implementing the backward and forward sweep method by KCL and KVL, (2) implements various protection schemes presented in [46] and the fuse-saving strategy typically used in urban distribution networks, and (3) examines the effect of protection devices on the reliability of the urban distribution network.

1.5.2 Problem Statement

A commonly used method of improving reliability is to strategically place protection devices such as breakers, switches, fuses, and reclosers within the distribution network. Since small-scale and decentralized DG systems, particularly the PV system in this study, have been incorporated into power systems, an optimization problem for the strategic placement of protection devices has to be solved for urban distribution networks enhanced by DG systems. However, because of the large size of the search space of the optimization problem and the inherent complexity of the power system, solving the optimization problem for the strategic placement of protection devices requires a fast and efficient algorithm for system analysis.

The method of evaluating the reliability of a distribution network can be classified into three methods: (1) the analytical method that provides a mathematical model of the reliability configuration and the mean value of the reliability index [44-46], (2) the stochastic method that evaluates the variability of the reliability index [47, 48], and (3) many heuristic search algorithms that propose near-optimal solutions that maximize the reliability of conventional feeders protected by reclosers and switches [51, 52, 57]. These analytical, stochastic methods, and evolutionary algorithms, however, are not capable of analyzing the urban distribution network housing a combination of fuses, switches, reclosers, and high-capacity DG systems. To determine the reliability index of more

practical distribution networks housing a combination of fuses, switches, and reclosers, this study proposes an analytical method of implementing the backward and forward sweep method by KCL and KVL (which evaluates reliability indices such as the SAIFI and the SAIDI of urban distribution networks housing a combination of fuses, switches, and reclosers).

As mentioned before, nowadays, since small-scale, local, and decentralized DG systems have been incorporated into power systems, this study proposes a genetic algorithm that determines the optimal allocation of protection devices (i.e., the recloser, the fuse, and the switch) on urban distribution networks enhanced by the DG system. In addition, it verifies both the proposed optimization algorithm and the analytical method using (1) bus 4 of the Roy Billinton Test System (RBTS) (which consists of five load busbars from buses 2 to 6 and practical elements such as transformers, switches, busbars, lines, and cables [45]), (2) the IEEE 34-bus test feeder without the DG system [23, 41], and (3) the IEEE 123-bus test feeder enhanced by twenty DG systems [23, 41]. Finally, it analyzes the impact of both the DG system, including the effect of the islanded operation of the DG system [14], and the protection device on the reliability of the urban distribution network. As a result, this study will propose tools and algorithms useful for planning, designing, and operating urban distribution networks enhanced by DG systems and protection devices from the standpoint of reliability.

1.6 Impact of Geographically Distributed Renewable DG Systems on Environmentally Constrained Generation Resource Allocation

To analyze the impact of geographically distributed renewable DG systems on environmentally constrained generation resource allocation at large- or utility-scales, this study discusses the related prior work and the problem statement of environmentally constrained generation resource allocation.

1.6.1 Related Prior Work of the Analysis of the Impact of Geographically Distributed Renewable DG Systems on Environmentally Constrained Generation Resource Allocation

In the late 1960's, several states in the United States began to impose constraints on emissions such as sulfur dioxide (SO_2), nitrogen oxides (NO_X), and carbon dioxide (CO_2). During that time, utilities added the constraints to an objective function to minimize emissions and the costs of generating electricity. In 1990, Clean Air Act amendments emphasized the environmental problems of the release of pollutants and greenhouse gases into the atmosphere. For the past several decades, since various DG systems, particularly the PV system in this study, have been incorporated into power systems, the utilities may have to modify the objective of their resource allocation problems that optimize power generation in order to minimize fuel costs.

Fuel costs and emissions have been deemed constraints in many techniques. One of the techniques minimized a cubic-order objective function with the constraints of fuel costs and emissions such as SO_2 and NO_X by Lagrange optimization [60]. Another technique used a stochastic formulation method to examine uncertainty in the costs of system production and load demand via multiple runs and simulated a trade-off relationship of objective functions by the weighted sum method [61]. In addition, many studies introduced a genetic algorithm [62, 63] and evolutionary programming [64] that solved the problem of the non-commensurable objective function. Another more recent study presented an optimization method of simulating social behavior such as particle swarm optimization [65] and bacterial foraging optimization [66]. However, these studies do not address the ecological impact of water. Energy and water infrastructures are closely linked to production and consumption. With increasing awareness of the sustainability of energy and water infrastructures, this link may require the addition of the water consumption constraints to the objective function.

When viewed in hourly intervals, PV systems seem to have a more stable output than usual. Therefore, one study claimed that rapid variations in short-term PV generation result from transient cloudiness and weather disturbances in the atmosphere [67, 68]. Since current PV generation affected by transient cloudiness depends only on previous generation, rapid variations in PV generation can be modeled by optimized Markov chain methods [69-71]. Thus, to model the short-term intermittency of the transient cloudiness of a test bed, this study will use Markov chain Monte Carlo (MCMC) simulation.

1.6.2 Problem Statement

(1) Challenge in the Analysis of the Short-term Intermittency of Geographically Distributed Renewable DG Generation

The proliferation of PV systems can offer various benefits such as peak load and electrical loss reductions, reactive and voltage support, and reliability improvement [51]. On the other hand, viewed in hourly intervals, PV systems seem to have a more stable output than usual. Rapid variations in short-term PV generation, typically in one-minute intervals, result from transient cloudiness and weather disturbances in the atmosphere [67, 68]. In addition, PV systems can create an additional need for spinning reserves that cope with uncertainty involved in their output. In fact, because of their intermittency, or sudden energy shortages and overages, they may increase the fossil fuel consumption of faster dispatchable spinning reserves, which typically burn the most expensive fuel. Therefore, this study will model the short-term intermittency of transient cloudiness [67-71] and estimate the generation of PV systems geographically dispersed throughout a test bed in hourly and minute intervals [72].

(2) Modeling of the Short-term Intermittency of Geographically Distributed Renewable DG Generation

As mentioned before, the increased number of DG systems, particularly PV systems in this study, offers not only opportunities such as a reduction in peak load and

loss but also potential for use in Volt/VAr management and control [51]. However, it also creates a need for additional spinning reserve that covers uncertainty involved in their output. In fact, the deployment of PV systems may increase the consumption of fossil fuels because of their intermittency. In addition, viewed in hourly resolution (averaged every hour), the PV system seems to have a more stable output than usual. Rapid variations in short-term PV generation, typically in minute-averaging resolution, result from transient cloudiness in the atmosphere [67, 68]. Unfortunately, solar radiation data in minute intervals for the power system model of the state of Georgia in 2010 as a test bed are not available from the current national solar radiation database [73]. Therefore, this study synthesizes the short-term intermittency, typically one-minute intervals, of PV systems geographically dispersed on a statewide or nationwide power grid in hourly and minute intervals using the MCMC (Markov chain Monte Carlo) method [69-72]. To calculate the transition probability matrix required as input data for the MCMC method, this study obtains actual solar data in minute-by-minute resolution from nine test sites located in Colorado, Arizona, New Mexico, and Utah from 2008 to 2012 [74] and selects a transition probability matrix calculated from one of the areas that shows an annual output that most closely resembles that of the test bed. This study assumes that all PV systems oriented at an azimuth of 180° (facing south) and a tilt angle of 30° are geographically dispersed across the representative 19 locations of the test bed [73]. Then, as input data to the MCMC simulation, this study uses hourly solar data obtained from the 19 locations of the test bed in the TMY3 format [69-73]. Lastly, it analyzes the impact of their intermittency on energy, especially for peak power and spinning reserve, electricity generation costs, and emissions.

(3) Algorithm for Generating Resource Allocation of Merging Fuel Costs, Emissions, and Water Consumption

Fuel costs and emissions in resource allocation problems have been considered constraints in many techniques [60, 61, 75]. In addition, many studies introduced

evolutionary algorithms that solved the optimization problem of the non-commensurable objective function [62-66]. However, these studies do not address the ecological impact of water. Energy and water infrastructures are closely or directly linked to production and consumption. With increasing awareness of the sustainability of energy and water infrastructures, this link requires the addition of the water consumption constraints to the objective function. Therefore, this study presents an algorithm for generating resource allocation with a scalar objective function that merges fuel costs and emissions with a water consumption constraint.

The objective of this study is (1) to present tools and algorithms useful for analyzing the impact of geographically dispersed DG systems, particularly PV systems in this study, on local, statewide, or nationwide generation resource allocation in hourly and minute intervals and (2) to address some of the issues in the analysis of the impact of DG systems on such resource allocation. For this purpose, this study first develops an algorithm for generation resource allocation that minimizes ecological impact, including water consumption, and fuel costs, and synthesizes cubic-order output functions for costs, emissions, and water consumption from heat rate data [60, 75-78]. Second, it proposes, as a test bed, the power system model of the state of Georgia in 2010 [43], approximates the load consumption [79] and the water inflow of the test bed [80], and estimates the power output of geographically dispersed PV systems in hourly and minute-by-minute resolutions [72] and the hydroelectric resources of the test bed [80]. Next, the study performs simulations for generation resource allocation in hourly and minute-by-minute resolutions. Finally, it analyzes the impact of dispersed PV systems from a long-term, typically annual, perspective of energy, specifically for peak power, electricity generation costs, and emissions.

1.7 Summary of Problem Statement

The main objectives of this study are to examine (1) the impact of DG systems stochastically dispersed throughout urban distribution networks, (2) the impact of DG systems on the reliability of urban distribution networks, and (3) the impact of DG systems geographically distributed on statewide or nationwide power grids.

The objective of the analysis of the impact of stochastic renewable DG on urban distribution networks from the perspective of small- or distribution-scale impacts is to propose a useful method of analyzing their impacts on urban distribution networks. Using the backward and forward sweep method implemented in MATLAB, this study develops an algorithm for three-phase power flow that models power system components, including distribution systems, transformers, and the PV system. To model the influence of the inherent uncertainty of the input, the location, and the capacity of the PV system, this study implements a stochastic simulation algorithm combined with the power-flow algorithm. It also accelerates the stochastic simulation algorithm using the methods of variance reduction, including importance sampling and stratification sampling, and the sampling of representative clusters and extreme points, which reduces the extremely heavy computational burden that the stochastic simulation inevitably imposes. Then it analyzes inherent uncertainties such as the inputs, the locations, and the capacities of residential PV systems installed on urban distribution networks by performing several stochastic simulations. It also quantifies the effects of the method of variance reduction, including importance sampling, and analyzes the impact of stochastically dispersed residential PV systems on the urban distribution network from the perspective of reductions in energy consumption, particularly regarding peak power, the changes in electricity generation costs, and emissions savings.

The objective of the analysis of reliability enhancement through a reconfiguration of urban distribution networks enhanced by DG is to propose tools and algorithms useful for planning, designing, and operating such distribution networks from the standpoint of

reliability. For this purpose, this study develops a genetic algorithm in MATLAB that solves an optimization problem that maximizes the reliability (or minimizes the frequency and the duration of failure) of urban distribution networks enhanced by protection devices (i.e., the recloser, the fuse, and the switch) and renewable DG. Using the backward and forward sweep method, this study implements an analytical method that simulates all possible permanent and transient faults and evaluates the reliability of the urban distribution network housing a combination of fuses, switches, reclosers, and DG systems. Then it analyzes the impact of both the DG system, including the effect of the islanded operation of the DG system, and the protection device, on the reliability of the urban distribution network

The objective of the analysis of the impact of geographically distributed renewable DG systems on environmentally constrained generation resource allocation from the perspective of large- or utility-scale impacts is to present a useful method for analyzing their impacts on statewide or nationwide power grids. Using the methods of the Lagrangian optimization and hydrothermal coordination, this study develops an algorithm for environmentally constrained generation resource allocation that minimizes both fuel costs and ecological impact, including the impact of water consumption. Then, this study (1) analyzes, as an example of the statewide power grid, the power system of the state of Georgia in 2010, (2) models the load consumption and the water inflow of the power system, (3) synthesizes third-order power output functions for costs, emissions, and water consumption from actual heat-rate data, and (4) estimates the power output of geographically dispersed PV systems and hydroelectric resources of the power system in hourly and minute intervals. Next, it performs simulations for the generation resource allocation of the power system in hourly and minute-by-minute resolutions. Lastly, it analyzes the impact of geographically dispersed PV systems from a long-term, typically annual, perspective of energy, specifically for peak power and spinning reserve, electricity generation costs, and emissions.

1.8 Dissertation Overview

The remainder of this dissertation, which analyzes (1) the impact of the stochastic renewable DG system, particularly the PV system in this study, on urban distribution networks, (2) the impact of DG systems on the reliability of urban distribution networks, and (3) the impact of DG systems geographically distributed on statewide or nationwide power grids, is organized as follows:

Chapter 2 proposes an algorithm for three-phase power flow that models power system components, including distribution systems, transformers, and PV systems with multiple sub-arrays as a generator. Using the backward and forward sweep method implemented in MATLAB, the algorithm calculates the three-phase power flow of urban radial and meshed distribution networks enhanced by various DG systems and represents the DG bus as a P-Q or P-V bus.

Chapter 3 presents a useful method for analyzing the impact of stochastic renewable DG systems, particularly PV systems, on urban distribution networks. To model the influence of the inherent uncertainty of the input, the location, and the capacity of the PV system, this study implements a stochastic simulation algorithm combined with the power-flow algorithm (presented in the previous section). This study also accelerates the stochastic simulation algorithm using methods of variance reduction, including importance sampling and stratification sampling, and the sampling of representative clusters and extreme points, all of which reduce the extremely heavy computational burden caused from the stochastic simulation. Finally, it analyzes inherent uncertainties such as the inputs, the locations, and the capacities of residential PV systems stochastically dispersed on urban distribution networks by performing several stochastic simulations in sufficiently long intervals.

Chapter 4 suggests a genetic algorithm that solves an optimization problem that maximizes the reliability (or minimizes the frequency and the duration of failure) of urban distribution networks enhanced by protection devices (i.e., the recloser, the fuse,

and the switch) and renewable DG systems. Using the backward and forward sweep method in MATLAB, this study implements an analytical method that simulates all possible permanent and transient faults and evaluates the reliability of the urban distribution network housing a combination of fuses, switches, reclosers, and DG systems. Then it analyzes the impact of both the DG system, including the effect of the islanded operation of the DG system, and the protection device on the reliability of the urban distribution network.

Chapter 5 introduces a useful method for analyzing the impact of geographically dispersed DG systems, particularly PV systems, on local, statewide, or nationwide power grids. Using methods of the Lagrangian optimization and hydrothermal coordination, this study develops an algorithm for environmentally constrained generation resource allocation that minimizes both fuel costs and ecological impact, including water consumption. Then this study (1) proposes, as a test bed, a power system model of the state of Georgia in 2010, (2) models the load consumption and the water inflow of the test bed, (3) synthesizes third-order power output functions for costs, emissions, and water consumption from actual heat-rate data, and (4) estimates the power output of geographically dispersed PV systems and hydroelectric resources of the test bed in hourly and minute intervals. Finally, it performs simulations for the generation resource allocation of the test bed in minute and hourly intervals.

Chapter 6 summarizes the main conclusions, the accomplishments, the contributions, and the future work of this dissertation.

CHAPTER 2

ALGORITHM FOR THE THREE-PHASE POWER-FLOW ANALYSIS OF DISTRIBUTION NETWORKS

2.1 Overview

An excellent example of a DG (distributed generation) system may be PV (photovoltaic) systems, which are most effectively dispersed as a large number of relatively small systems. For example, they may be installed on the roof of individual houses, integrated within a building itself, or installed in any location in which electricity is required. As DG systems with various capacities, specifically PV systems in this study, have been deployed in the urban distribution network, they may change the behavior of the distribution network. Therefore, accurate and efficient system analysis algorithms capable of analyzing the impact of various DG systems on various types of microgrids and distribution networks are required. However, formulating such algorithms may be difficult because of the inherent uncertainty of the input, the location, and the capacity of the DG system, not known in the planning stage of the power system. Many uncertainties can be modeled by optimized stochastic methods, very computer-intensive processes that require tens of thousands of sub-hourly power-flow calculations for each annual stochastic simulation. Thus, this study initially introduces an algorithm that can analyze the three-phase power flow of urban radial and meshed networks enhanced by DG systems. The next chapter of this study will discuss how this algorithm analyzes the impact of DG systems stochastically dispersed on urban distribution networks.

2.2 Introduction

The related prior work for power-flow analysis is not appropriate for analyzing

the impact of the uncertainties of the DG system because they cannot directly analyze the impact of DG systems on radial or meshed urban distribution networks enhanced by various DG systems with the inherent uncertainty of their inputs, locations, and capacities [16-20]. Thus, the objective of this study is to develop an algorithm that can calculate the three-phase power flow of urban radial and meshed networks enhanced by various DG systems. It implements the backward and forward sweep method and iterative compensation methods for meshed networks in MATLAB, models power system components, including distribution systems, transformers, and PV systems, and calculates the three-phase power flow of urban radial and meshed networks enhanced by DG systems, particularly the PV system in this study. In addition, since various DG systems, including PV, are being deployed in urban distribution networks, this study integrates the simulation program for the PV system into the power-flow algorithm. Furthermore, present regulations require that the DG system maintain its terminal voltage within a specified range, typically 0.95 to 1.05 PU of the rated voltage level [14]. Therefore, to stay within this range, the DG bus should be modeled as a P-V bus if the DG system produces active and reactive power for its terminal voltage (which means the Volt/VAr control) [17, 18, 21]. Therefore, the proposed algorithm will be able to model the DG bus of the high-penetration capacity as either a P-Q or P-V bus.

2.3 Algorithm for Solving Three-Phase Power Flow

2.3.1 Backward and Forward Sweep Method

The backward and forward sweep method, which solves the three-phase power flow of a radial distribution network, implements KCL, KVL, and the iterative method [17, 22]. In the backward sweep, current flow at the j^{th} bus in Figure 6 is

$$\tilde{I}_j^{(k)} = \left(\frac{S_j}{\tilde{V}_j^{(k-1)}} \right)^* + Y_j \tilde{V}_j^{(k-1)} . \qquad (1)$$

Then, the backward sweep sums the current flow at each bus in the backward direction as

follows:

$$\tilde{I}_i^{(k)} = \tilde{I}_j^{(k)} + \sum_{m \in M} \tilde{I}_m^{(k)}, \qquad (2)$$

where M = all other buses connected to the i^{th} bus, excluding the j^{th} bus.

The forward sweep calculates voltage drops. The source voltage is the nominal voltage, and all bus voltages are calculated from the source bus using current obtained in the previous backward sweep routine:

$$\tilde{V}_j^{(k)} = \tilde{V}_i^{(k)} - Z_{ij}\,\tilde{I}_j^{(k)}. \qquad (3)$$

The calculation of mismatched power examines convergence. These three steps iterate until they achieve convergence, as follows:

$$\Delta S_j^{(k)} = \tilde{V}_j^{(k)} (\tilde{I}_j^{(k)})^* - Y_j^* \,|\tilde{V}_j^{(k)}|^2 - S_{j,scheduled}. \qquad (4)$$

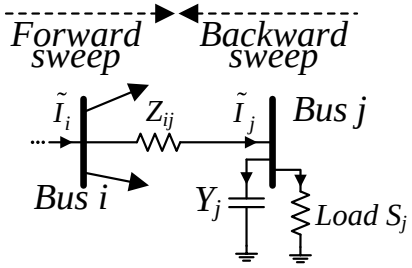

Figure 6. Current flowing at the j^{th} bus.

2.3.2 Analysis of the Meshed Network

DG connected to the radial network may convert a radial network into a meshed network. The power flow of the meshed network can be solved by the method of iterative breakpoint compensation, which injects nodal currents [17-20]. The meshed network in Figure 7 is expressed as a Thevenin-equivalent circuit by viewing such a network from the breakpoint.

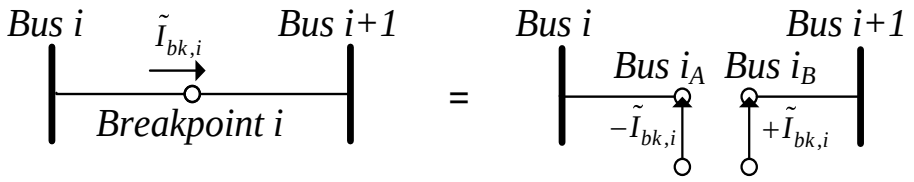

Figure 7. Breakpoint that injects nodal currents.

Thus, the voltage of the breakpoint is the Thevenin-equivalent impedance multiplied by

the current of the breakpoint, as follows:

$$\begin{bmatrix} \tilde{V}_{bk,1} \\ \vdots \\ \tilde{V}_{bk,i} \\ \vdots \\ \tilde{V}_{bk,n} \end{bmatrix} = Z_T \begin{bmatrix} \tilde{I}_{bk,1} \\ \vdots \\ \tilde{I}_{bk,i} \\ \vdots \\ \tilde{I}_{bk,n} \end{bmatrix} = \begin{bmatrix} Z_{11} & \cdots & Z_{1j} & \cdots & Z_{1n} \\ & & \vdots & & \\ Z_{i1} & & Z_{ij} & & Z_{in} \\ & & \vdots & & \\ Z_{n1} & \cdots & Z_{nj} & \cdots & Z_{nn} \end{bmatrix} \begin{bmatrix} \tilde{I}_{bk,1} \\ \vdots \\ \tilde{I}_{bk,i} \\ \vdots \\ \tilde{I}_{bk,n} \end{bmatrix}, \quad (5)$$

where n = the number of breakpoints.

To determine the breakpoint impedance, this study removes all load and sources from the network and injects nodal currents in two directions as shown in Figure 7. For example, to determine the j^{th} column of the breakpoint impedance matrix, this study injects the breakpoint current in the backward direction of the following:

$$\tilde{I}_{bk,i} = \begin{cases} -1.0\angle 0^{\circ}\ PU & \text{where } i = j \\ 0 & \text{where } i \neq j \end{cases}, \quad (6)$$

in the forward direction of the following:

$$\tilde{I}_{bk,i} = \begin{cases} +1.0\angle 0^{\circ}\ PU & \text{where } i = j \\ 0 & \text{where } i \neq j \end{cases}, \quad (7)$$

where $i=1,...,n$.

After the forward sweep calculating voltage drops, this study calculates the j^{th} column of the Thevenin-equivalent breakpoint impedance by

$$Z_{T,ij} = \frac{\tilde{V}_{bk,i}}{\tilde{I}_{bk,i}}, \quad (8)$$

where $i=1,...,n$.

After determining all the breakpoint impedance, the backward sweep calculates an incremental change in the current flowing at the breakpoint by

$$\Delta\tilde{I}_{bk,i}^{(k)} = Z_T^{-1}\tilde{V}_{bk,i}^{(k-1)}. \quad (9)$$

Then, the backward sweep bi-directionally updates the current of each meshed bus by the incremental change in the current flowing at the breakpoint.

$$\tilde{I}_i^{(k)} = \tilde{I}_i^{(k-1)} - \Delta\tilde{I}_{bk,i}^{(k)}, \quad (10)$$

$$\tilde{I}_{i+1}^{(k)} = \tilde{I}_{i+1}^{(k-1)} + \Delta\tilde{I}_{bk,i}^{(k)} . \quad (11)$$

The forward sweep calculates voltage drops. All of the above algorithms iterate these steps until they achieve convergence.

2.3.3 Modeling of P-Q and P-V Buses of the DG System

Since current regulations of DG require that the terminal voltage of the DG system be maintained within a specified range, typically 0.95 to 1.05 PU of the rated voltage level [14], this study develops a power-flow algorithm that represents a DG bus of high-penetration capacity as a P-Q or P-V bus from [17, 18, 21]. Methods of modeling a DG bus are as follows:

(1) A DG system on a P-Q bus reduces only active power as a negative constant power source.

(2) A DG system on a P-V bus provides active and reactive power so that it can maintain terminal voltage within a specified range.

A DG bus was modeled in [17, 18, 21] as a P-V bus that provided reactive power or reactive current that maintained the terminal voltage of the DG system. The incremental terminal voltage of the positive sequence was incremental reactive current multiplied by the impedance of the positive sequence:

$$\Delta V_{pos,j}^{(k)} = \Delta I_{pos,q,j}^{(k)} Z_{pos,j} , \quad (12)$$

where $j = 1,2,3,\ldots,N$ and N = the number of DG buses.

Equation (12) suggests that the terminal voltage of the DG system can be maintained within a specified value by an incremental change in the reactive current if the impedance of the positive sequence, referred to as the P-V bus sensitivity impedance, is known.

To describe how to determine the sensitivity impedance, this study evaluates the simple radial network with three buses and two DG systems in Figure 8. The diagonal entry of the positive-sequence sensitivity impedance of the P-V bus is the sum of the positive-sequence impedance from the P-V bus to the root bus (bus *i*) after the removal of

all loads and sources from the network. The off-diagonal entry is the sum of the positive-sequence impedance from a bus that two P-V buses share to the root bus (bus *i*) after the removal of all loads and sources from the network. The sensitivity impedance matrix for Figure 8 can be expressed as:

$$Z_{Sensitive} = \begin{matrix} \\ P_{DG,j} \\ P_{DG,k} \end{matrix} \begin{matrix} \begin{matrix} P_{DG,j} & P_{DG,k} \end{matrix} \\ \begin{bmatrix} |Z_{pos,ij}| & |Z_{pos,ij}| \\ |Z_{pos,ij}| & |Z_{pos,ij+jk}| \end{bmatrix} \end{matrix}. \quad (13)$$

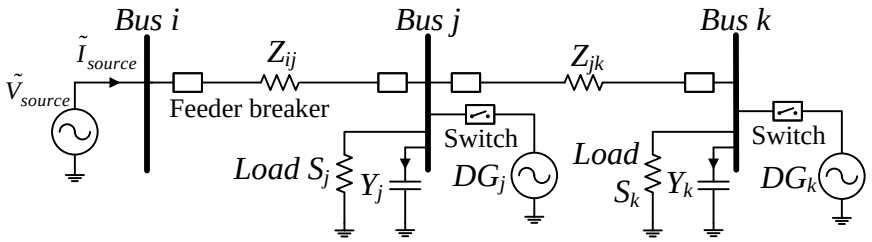

Figure 8. A simple radial network with three buses and two distributed generators.

After determining the sensitivity impedance, to maintain the terminal voltage within a specified range, this study iterates in the following steps:

Step 1. Calculate the positive-sequence voltage of the DG bus. That is, difference between the target and positive-sequence voltage of the DG bus is calculated by

$$\Delta V_{pos,j}^{(k)} = V_{pos,j,target} - V_{pos,j}^{(k)}. \quad (14)$$

Step 2. Calculate the reactive current to be injected. If the positive-sequence voltage of the DG system is not equal to the target voltage, then reactive power is injected, determined by

$$\Delta\tilde{I}_{qa,j}^{(k)} = \Delta I_{pos,q,j}^{(k)} \angle\left(sign\left(\Delta V_{pos,j}^{(k)}\right) \times 90° + \delta_{V_{a,j}}^{(k)} \right), \quad (15)$$

$$\Delta\tilde{I}_{qb,j}^{(k)} = \Delta I_{pos,q,j}^{(k)} \angle\left(sign\left(\Delta V_{pos,j}^{(k)}\right) \times 90° + \delta_{V_{b,j}}^{(k)} \right), \quad (16)$$

$$\Delta\tilde{I}_{qc,j}^{(k)} = \Delta I_{pos,q,j}^{(k)} \angle\left(sign\left(\Delta V_{pos,j}^{(k)}\right) \times 90° + \delta_{V_{c,j}}^{(k)} \right). \quad (17)$$

The positive mismatch from (14) indicates the leading phase angle of the incremental reactive current of the positive sequence, $\Delta I_{pos,q,j}^{(k)}$, in (12), which

suggests that the DG system provides reactive power as a capacitive load. The negative mismatch from (14) indicates the lagging phase angle of the incremental reactive current of the positive sequence in (12), which suggests that the DG system consumes reactive power as an inductive load.

Step 3. Check the voltage mismatch. The reactive power that can be injected depends on the rating of the inverter used in the DG system. If the reactive power to be injected is greater than the feasible operating range of the reactive power of the inverter, the reactive power is set to the maximum limit, or reactive and active power is fixed at a predefined power factor that indicates that the DG bus is treated as a P-Q bus. These three steps iterate until they achieve convergence.

2.4 Modeling of Power System Components

2.4.1 Modeling of the Load

The load of the power system can be classified into three types: constant power load, referred to as "constant PQ"; constant impedance load, referred to as "constant Z"; and constant current load, referred to as "constant I." The backward sweep of the proposed algorithm for three-phase power-flow analysis calculates the current flowing through a load as follows:

$$\tilde{I}_{constant\ PQ,j} = \left(\frac{S_{scheduled,j}}{\tilde{V}_j^{(k)}} \right)^*, \tag{18}$$

$$\tilde{I}_{constant\ Z,j} = \frac{\tilde{V}_j^{(k)}}{\frac{|V_{nominal,j}|^2}{S_{scheduled,j}^*}}, \tag{19}$$

$$\tilde{I}_{constant\ I,j} = \left| \left(\frac{S_{scheduled,j}}{V_{nominal,j}} \right)^* \right| \angle \left(\delta_{V_j^{(k)}} - \delta_{s_j} \right). \tag{20}$$

For example, the capacitor banks are modeled as a constant impedance load [22].

2.4.2 Modeling of the Transformer

Figure 9 shows the transformer connected by the grounded wye-grounded wye configuration. The backward sweep sums up the current in each bus and the forward sweep calculates voltage drops in the general matrix form by

$$\begin{bmatrix} \tilde{I}_A \\ \tilde{I}_B \\ \tilde{I}_C \end{bmatrix} = C_B \begin{bmatrix} \tilde{I}_a \\ \tilde{I}_b \\ \tilde{I}_c \end{bmatrix}, \tag{21}$$

$$\begin{bmatrix} \tilde{V}_{ag} \\ \tilde{V}_{bg} \\ \tilde{V}_{cg} \end{bmatrix} = A_F \begin{bmatrix} \tilde{V}_{AG} \\ \tilde{V}_{BG} \\ \tilde{V}_{CG} \end{bmatrix} - B_F \begin{bmatrix} \tilde{I}_a \\ \tilde{I}_b \\ \tilde{I}_c \end{bmatrix}. \tag{22}$$

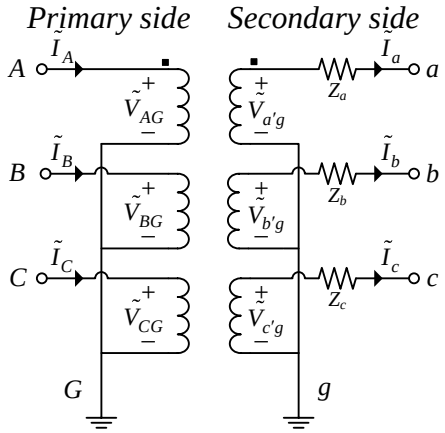

Figure 9. Transformer connected by the grounded wye-grounded wye configuration.

In the case of the ungrounded wye connection, line-to-ground voltage such as $\tilde{V}_{ag}$ and $\tilde{V}_{AG}$ in (22) indicates line-to-neutral voltage such as $\tilde{V}_{an}$ and $\tilde{V}_{AN}$. Table 1 summarizes the turns ratio, A_F and B_F, used in the forward sweep, and C_B, used in the backward sweep for all the connections of the three-phase transformer. The other detailed connections of the other transformers are presented in Appendix A.

2.4.3 Modeling of the Voltage Regulator

In Figure 10, this study models the voltage regulator, which automatically maintains a constant voltage level, by the autotransformer with multiple taps, typically 32 taps. The current standard classifies the voltage regulator into types A and B [22, 25], in

which one tap indicates an increase or a decrease in the voltage by 0.00625 per unit (PU). Thus, the forward sweep of the algorithm for power-flow analysis calculates a voltage decrease or increase by

$$\tilde{V}_H = \left(1+\frac{N_2}{N_1}\right)\tilde{V}_L = \left(1+0.00625Tap\right)\tilde{V}_L . \qquad (23)$$

The backward sweep of the algorithm calculates the current by

$$\tilde{I}_L = \left(1+\frac{N_2}{N_1}\right)\tilde{I}_H = \left(1+0.00625Tap\right)\tilde{I}_H . \qquad (24)$$

Table 1. The connection of the three-phase transformer [22]

Connection	Turns Ratio n_t	Forward Sweep		Backward Sweep
		A_F	B_F	C_B
Grounded Wye-Grounded Wye	$\frac{\tilde{V}_{AG}}{\tilde{V}_{a'g}}=\frac{\tilde{V}_{BG}}{\tilde{V}_{b'g}}=\frac{\tilde{V}_{CG}}{\tilde{V}_{c'g}}=n_t \quad \frac{\tilde{I}_A}{\tilde{I}_a}=\frac{\tilde{I}_B}{\tilde{I}_b}=\frac{\tilde{I}_C}{\tilde{I}_c}=\frac{1}{n_t}$	$\frac{1}{n_t}I$	$Z_{abc}I$	$\frac{1}{n_t}I$
Delta-Grounded Wye	$\frac{\tilde{V}_{AB}}{\tilde{V}_{b'g}}=\frac{\tilde{V}_{BC}}{\tilde{V}_{c'g}}=\frac{\tilde{V}_{CA}}{\tilde{V}_{a'g}}=-n_t \quad \frac{\tilde{I}_{BA}}{\tilde{I}_b}=\frac{\tilde{I}_{CB}}{\tilde{I}_c}=\frac{\tilde{I}_{AC}}{\tilde{I}_a}=\frac{1}{n_t}$	$\frac{1}{n_t}D_1$	$Z_{abc}I$	$\frac{1}{n_t}D_2$
Delta-Delta	$\frac{\tilde{V}_{AB}}{\tilde{V}_{a'b'}}=\frac{\tilde{V}_{BC}}{\tilde{V}_{b'c'}}=\frac{\tilde{V}_{CA}}{\tilde{V}_{c'a'}}=n_t \quad \frac{\tilde{I}_{AB}}{\tilde{I}_{ba}}=\frac{\tilde{I}_{BC}}{\tilde{I}_{cb}}=\frac{\tilde{I}_{CA}}{\tilde{I}_{ac}}=\frac{1}{n_t}$	$\frac{1}{3n_t}D_3$	$\frac{Z}{3}D_4\ (Z_{ab}=Z_{bc}=Z_{ca}=Z)$	$\frac{1}{n_t}I$
Ungrounded Wye-Delta	$\frac{\tilde{V}_{AN}}{\tilde{V}_{a'b'}}=\frac{\tilde{V}_{BN}}{\tilde{V}_{b'c'}}=\frac{\tilde{V}_{CN}}{\tilde{V}_{c'a'}}=n_t \quad \frac{\tilde{I}_A}{\tilde{I}_{ba}}=\frac{\tilde{I}_B}{\tilde{I}_{cb}}=\frac{\tilde{I}_C}{\tilde{I}_{ac}}=\frac{1}{n_t}$	$\frac{1}{3n_t}D_5$	$\frac{Z}{3}D_4\ (Z_{ab}=Z_{bc}=Z_{ca}=Z)$	$\frac{1}{3n_t}D_2$
Open Grounded Wye-Open Delta	$\frac{\tilde{V}_{AG}}{\tilde{V}_{a'b'}}=\frac{\tilde{V}_{BG}}{\tilde{V}_{b'c'}}=n_t \quad \frac{\tilde{I}_A}{\tilde{I}_{ba}}=\frac{\tilde{I}_B}{\tilde{I}_{cb}}=\frac{1}{n_t}$	$\frac{1}{3n_t}D_6$	$\frac{Z}{3}D_7\ (Z_{ab}=Z_{bc}=Z)$	$\frac{1}{n_t}D_8$

where

$$I=\begin{bmatrix}1&0&0\\0&1&0\\0&0&1\end{bmatrix}, Z_{abc}=\begin{bmatrix}Za&0&0\\0&Zb&0\\0&0&Zc\end{bmatrix}, D_1=\begin{bmatrix}1&0&-1\\-1&1&0\\0&-1&1\end{bmatrix}, D_2=\begin{bmatrix}1&-1&0\\0&1&-1\\-1&0&1\end{bmatrix}, D_3=\begin{bmatrix}2&-1&-1\\-1&2&-1\\-1&-1&2\end{bmatrix}, D_4=\begin{bmatrix}1&0&0\\0&1&0\\-1&-1&0\end{bmatrix},$$

$$D_5=\begin{bmatrix}2&1&0\\0&2&1\\1&0&2\end{bmatrix}, D_6=\begin{bmatrix}2&1&0\\-1&1&0\\-1&-2&0\end{bmatrix}, D_7=\begin{bmatrix}2&0&-1\\-1&0&-1\\-1&0&2\end{bmatrix}, D_8=\begin{bmatrix}1&0&0\\0&0&-1\\0&0&0\end{bmatrix}.$$

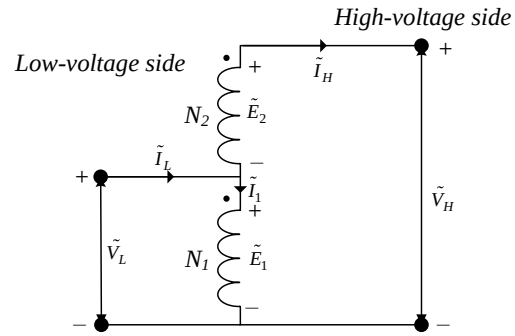

Figure 10. Type A step-voltage regulator.

2.4.4 Modeling of the Renewable PV System

The University Center of Excellence for Photovoltaics at the Georgia Institute of Technology developed a complete simulator for the PV system utilizing the most rigorous models available today and provided a more accurate way of modeling PV systems with multiple sub-arrays that can be oriented and tilted differently or located in different planes [24]. In a simplified PV system, Figure 11 shows a PV array, which receives insolation from the sun and transforms it into DC power fed through an inverter that converts DC power into AC power and provides to the local load and the grid. To determine the impact of PV systems dispersed throughout the urban distribution network in the next chapter, this study models the PV system as a generator and integrates the simulation program for the PV system into the algorithm for three-phase power-flow analysis.

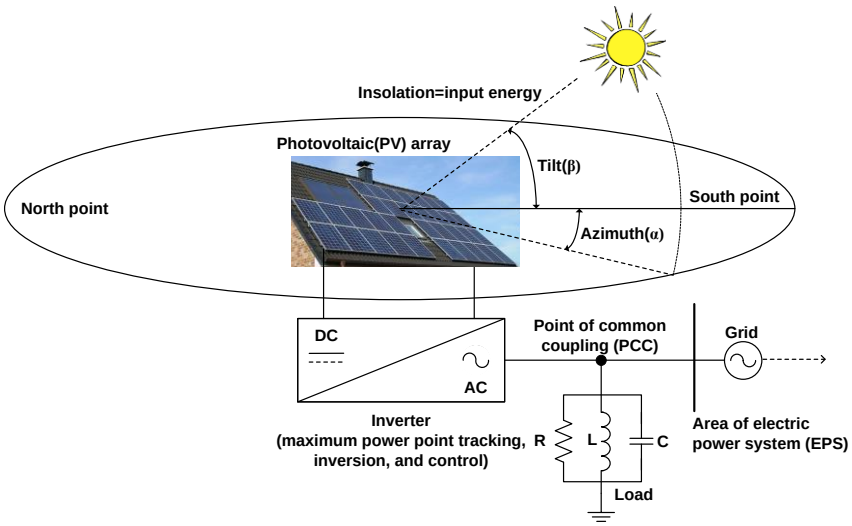

Figure 11. A simplified PV system.

2.5 Implementation of the Power-Flow Algorithm

This study implements the algorithm for solving three-phase power flow, which is based on the backward and forward sweep method, the iterative compensation method for the meshed network, and the representation method of the DG bus as a P-Q or P-V bus. The algorithm uses MATLAB to model common power system components such as the

load (i.e., the constant power, constant current, and constant impedance loads), the transformer, the voltage regulator, and the shunt capacitor bank. Figure 12 shows the procedure of the proposed algorithm, which implements the backward and forward sweep method, analyzes the meshed network, and represents the DG bus as either a P-Q or P-V bus. For example, when DG systems are present on the distribution network, the proposed algorithm treats the DG system as either a P-Q bus if the DG system is not able to control its terminal voltage or a P-V bus if the DG system is able to control its terminal voltage.

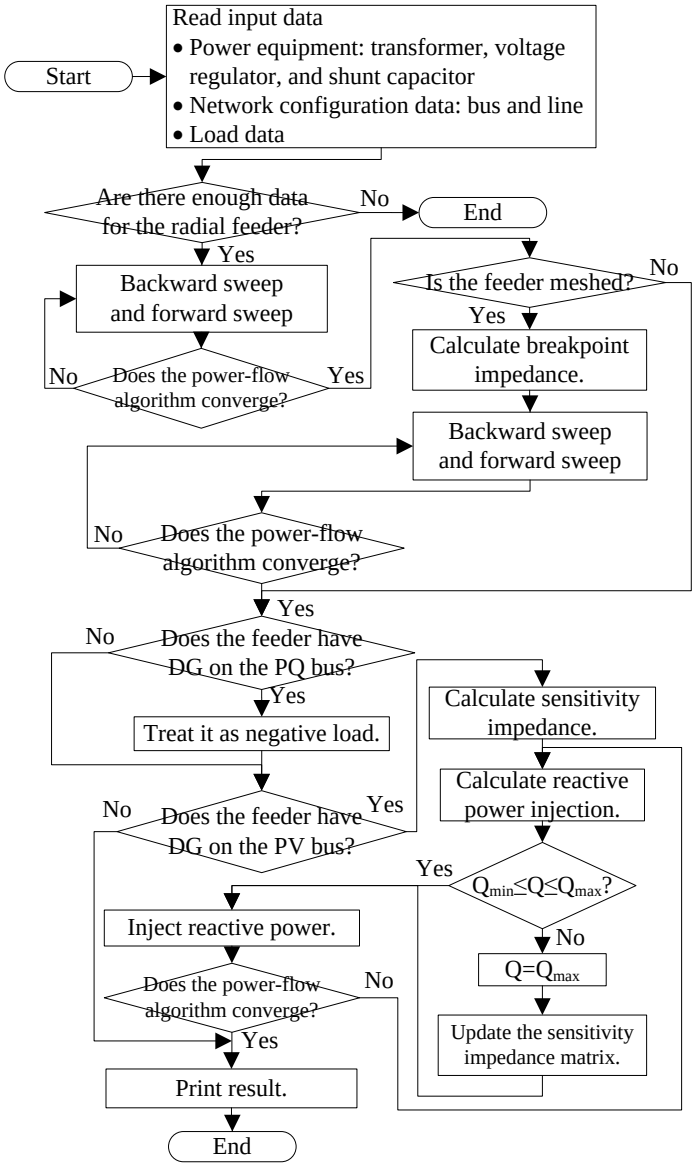

Figure 12. Flowchart of the proposed algorithm for three-phase power-flow analysis.

2.6 Verification of the Power-Flow Algorithm

2.6.1 Urban Distribution Networks

The IEEE PES Distribution System Analysis Subcommittee developed test feeders for the distribution system that consists of well-defined and extremely complex networks such as 4-, 13-, 34-, 37-, 123-, and 8,500-bus test feeders for research study purposes [23, 41]. For example, the feeder in Figure 13, characterized by a very complex configuration and several switches for alternative paths, is appropriate for testing the problem of a voltage drop through very long lines, voltage regulators, and shunt capacitor banks. This study verifies the proposed power-flow algorithm using 4-, 13-, 34-, 37-, and 123-bus test feeders. Three-phase total active power (P) in kW, reactive power (Q) in kVar, current (I), loss, and voltage (V) from the proposed power-flow algorithm in Table 2 are the same as those in [41]. The detailed comparisons of solutions presented from [41] and those from the proposed algorithm for each test feeder are presented in Appendices C and D.

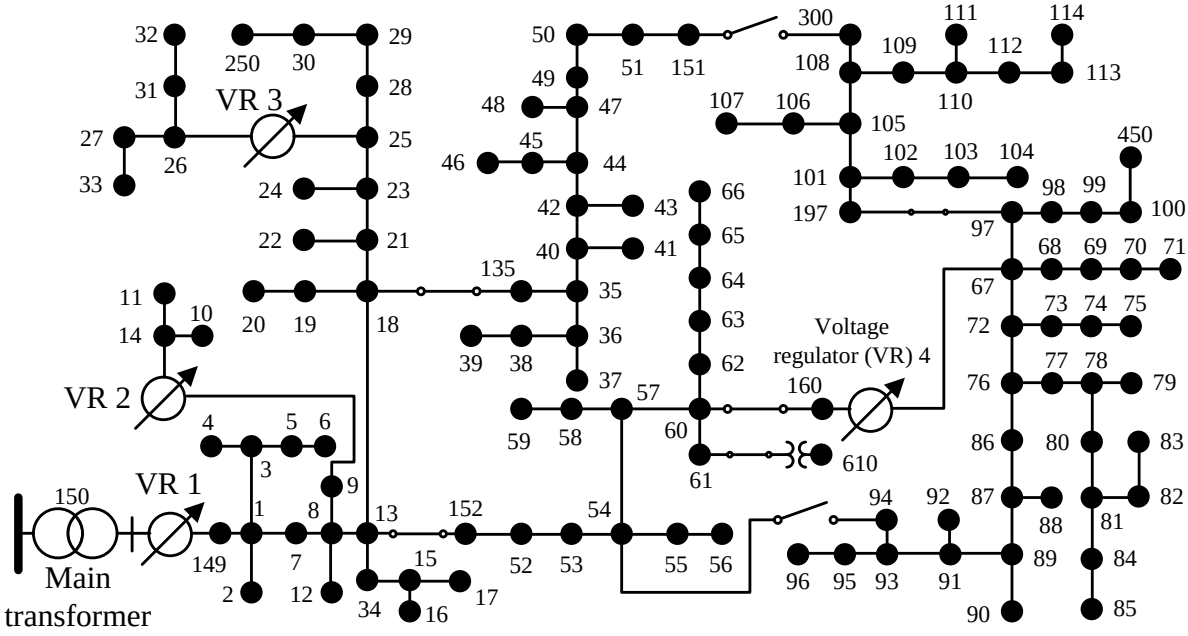

Figure 13. The IEEE 123-bus test feeder.

Table 2. Power-flow analysis of IEEE 4-, 13-, 34-, 37-, and 123-bus test feeders

Test Feeder Name	Phase	Total Active (P) and Reactive Power (Q)	Total Current (I) at Slack Bus	Total Active Power Loss	Voltages (V) of All Buses
		% Error of P and Q to IEEE Solution	% Error of Magnitude and Angle to IEEE Solution	% Error of Loss to IEEE Solution	Average of % Error of Magnitude of V to IEEE Solution
4	A	-	-0.01%, -0.05%	-	0.0108%
	B		0.01%, 0.03%		0.0134%
	C		-0.02%, -0.02%		0.0085%
13	A	0.00%, 0.03%	0.01%, 0.04%	-0.08%	0.003%
	B	-0.00%, 0.01%	0.00%, 0.00%	0.19%	0.002%
	C	0.00%, 0.03%	0.01%, -0.00%	0.09%	0.003%
34	A	-0.02%, 0.55%	0.01%, 0.50%	-0.16%	0.003%
	B	-0.00%, 0.90%	0.02%, 0.05%	-0.04%	0.003%
	C	-0.02%, 2.03%	-0.02%, -0.04%	-0.11%	0.003%
37	A	0.01%, 0.00%	0.00%, -0.02%	-0.01%	0.004%
	B	-0.00%, 0.01%	0.00%, -0.00%	-0.02%	0.002%
	C	-0.00%, -0.01%	-0.00%, 0.00%	-0.01%	0.003%
123	A	0.00%, 0.14%	0.02%, 0.15%	0.22%	0.009%
	B	-0.01%, 0.09%	0.00%, 0.01%	-0.69%	0.006%
	C	-0.00%, 0.13%	0.01%, -0.02%	-0.11%	0.003%

2.6.2 Power-Flow Analysis of a Meshed Network

This study modifies the IEEE 123-bus test feeder in Figure 13 by adding five breakpoints that convert the feeder into the meshed network. To validate the proposed algorithm, this study examined the voltage and the current between the breakpoint while decreasing the line impedance between the i^{th} and j^{th} buses, shown in Table 3. For example, when the line impedance of phase *A* between buses 300 and 151 is infinite, which can be viewed as an open circuit, the voltage and the current between the two buses are $114.389 \angle 145.0044°$ V and 0 A, respectively. If the line impedance between the two buses decreases to zero, which corresponds to a short circuit or a meshed network, the voltage and the current of phase *A* between the two buses are 0 V and $137.86 \angle -93.93°$ A, respectively. In fact, to calculate the power flow at breakpoints, the proposed algorithm changes the open-circuit breakpoints to a short circuit by the iterative compensation method. Table 4 shows the current, the voltage, and the Thevenin-equivalent impedance of the breakpoint. After sixteen iterations, the power-flow algorithm converged. The voltage and the current of all meshed phases are zero and non-

zero, which indicates successful results. To examine how the iterative compensation method for the meshed network determines the voltage and the current of the breakpoint, this study plots their values during iterative compensation. Figure 14 and Figure 15 show that the initial zero current and the initial non-zero voltage of the breakpoint, respectively, reach the final solution during iterative compensation.

Table 3. Line impedances decreasing from infinite to zero

Bus	Line Impedance	Voltage between Buses in V			Current Flowing between Buses in A		
	Ω	Phase *A*	Phase *B*	Phase *C*	Phase *A*	Phase *B*	Phase *C*
300-151	∞ (Open Circuit)	114.389 ∠ 145.0044°	37.292 ∠ -9.5132°	74.780 ∠ -92.9939°	0	0	0
	$10^7 Z_{bk}$	114.388 ∠ 145.0043°	37.292 ∠ -9.5132°	74.779 ∠ -92.9936°	0.0017 ∠ -86.77°	0.0006 ∠ 113.45°	0.0008 ∠ 37.97°
	$10^5 Z_{bk}$	114.26 ∠ 144.99°	37.28 ∠ -9.50°	74.70 ∠ -92.97°	0.17 ∠ -86.78°	0.06 ∠ 113.45°	0.08 ∠ 37.97°
	$10^3 Z_{bk}$	101.90 ∠ 143.45°	35.82 ∠ -8.01°	66.83 ∠ -90.52°	16.24 ∠ -87.14°	5.82 ∠ 113.37°	7.98 ∠ 38.42°
	$10 Z_{bk}$	0.23 ∠ 71.69°	0.54 ∠ 76.93°	1.09 ∠ 82.53°	138.07 ∠ -94.08°	67.21 ∠ 116.66°	86.36 ∠ 46.58°
	0 (Short Circuit)	0	0	0	137.86 ∠ -93.93°	67.42 ∠ 116.83°	85.50 ∠ 46.71°

Table 4. Results of five breakpoints inserted into the IEEE 123-bus test feeder

Bus	Breakpoint Phase	Phase	Breakpoint Voltage (V_{bk})	Breakpoint Current (I_{bk})	Thevenin-equivalent Breakpoint Impedance (Z_{bk})
		-	|V|(°)	|A|(°)	Ω
300-151	*ABC*	*A*	0	137.86(-93.93°)	0.6352+1.4698i
		B	0	67.42(116.83°)	0.6293+1.4504i
		C	0	85.50(46.71°)	0.6349+1.4536i
085-075	*C*	*A*	13.99(00.29°)	0	0
		B	19.89(00.32°)	0	0
		C	0	15.89(22.12°)	0.6934+0.8827i
011-020	*A*	*A*	0	57.61(12.60°)	0.4701+0.6022i
		B	81.07(-00.66°)	0	0
		C	49.45(-00.53°)	0	0
071-114	*A*	*A*	0	33.70(-46.12°)	0.8010+0.9365i
		B	10.12(00.17°)	0	0
		C	15.52(00.03°)	0	0
094-054	*A*	*A*	0	159.00(-87.85°)	0.3768+0.7847i
		B	92.48(02.13°)	0	0
		C	87.36(-00.03°)	0	0

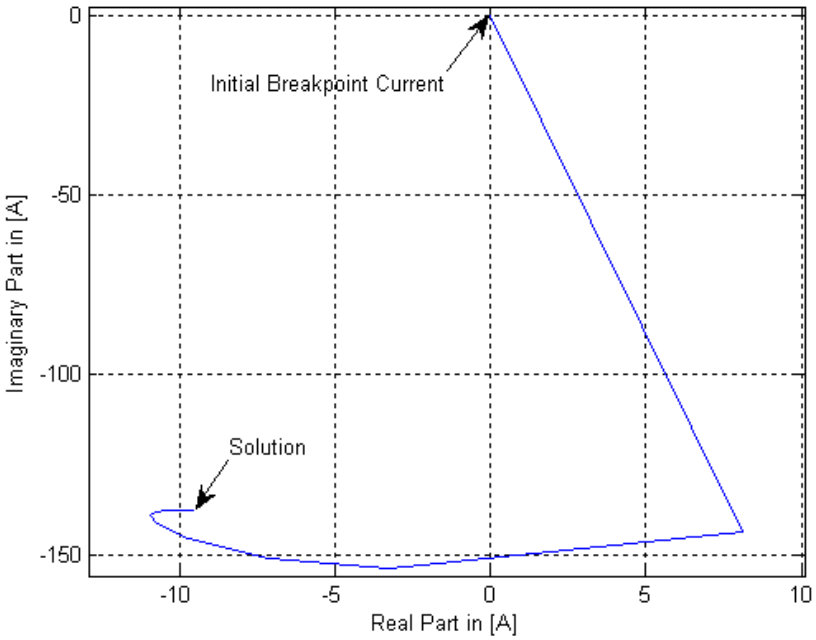

Figure 14. Convergence of the breakpoint current of phase *A* at 300-151 buses during iterative compensation.

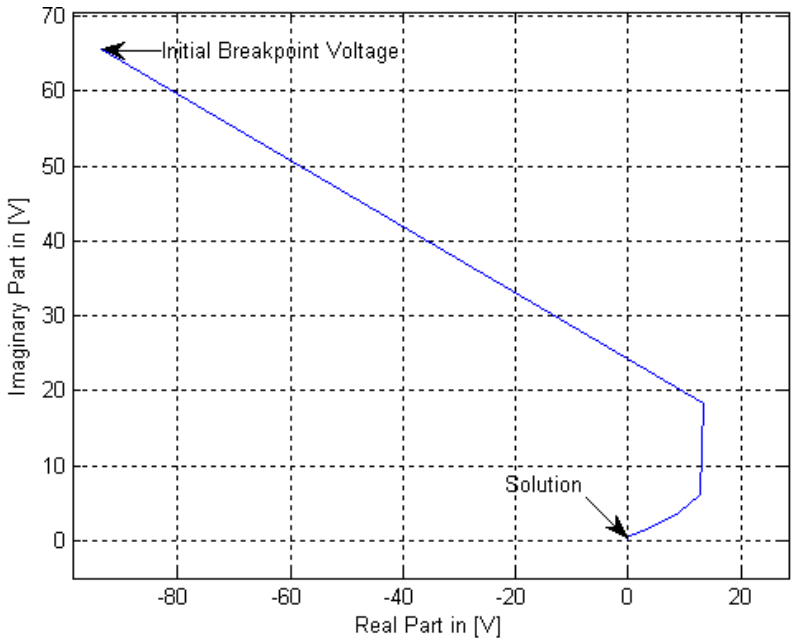

Figure 15. Convergence of the breakpoint voltage of phase *A* at 300-151 buses during iterative compensation.

2.6.3 Integration of the Simulation Program for the PV System into the Three-Phase Power-Flow Algorithm

For three-phase power-flow analysis, this study models the PV system as a generator and integrates a simulation program developed by the University Center of Excellence for Photovoltaics at the Georgia Institute of Technology. This study compares the generation of the PV system integrated into the proposed power-flow algorithm to that of the system advisor model (SAM) developed by the National Renewable Energy Laboratory [81]. Figure 16 shows the generation of the 315 kW PV system, installed in the Atlanta area, oriented at a 90° azimuth angle, which indicates that the PV system faces east, and a 15° tilt angle. Both the proposed algorithm and the SAM are based on version 2 of typical meteorological year (TMY) weather data, a national weather database collected from 229 locations in the United States between 1961 and 1990.

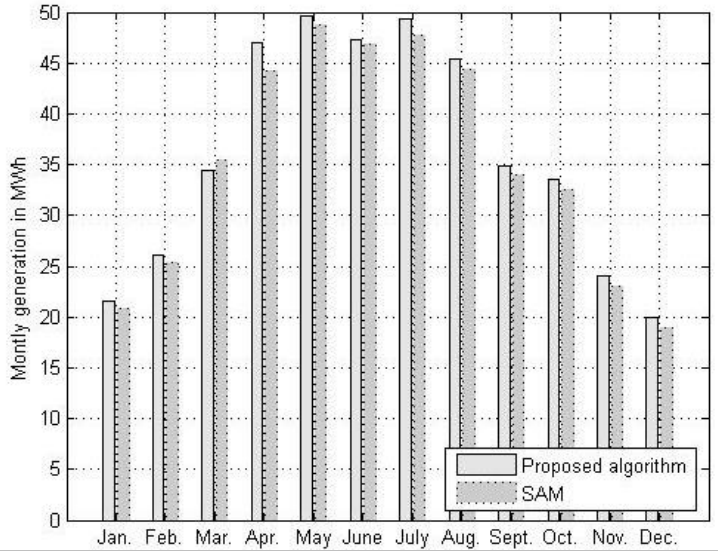

Figure 16. Comparison of the proposed power-flow algorithm and the system advisor model.

Illustrating the proposed power-flow algorithm that models the PV system as a generator, Figure 17 shows the impact of PV on feeder load demand, or how the load decreases as a result of PV generation. This study treated the 362 kW PV system (which corresponds to the 10 % PV system in Figure 17) installed in the Atlanta area and oriented at a 180° azimuth angle (facing south) and a 30° tilt angle as a negative load. In

other words, this study modeled a PV bus as a P-Q bus, presented in Section 2.3.3.

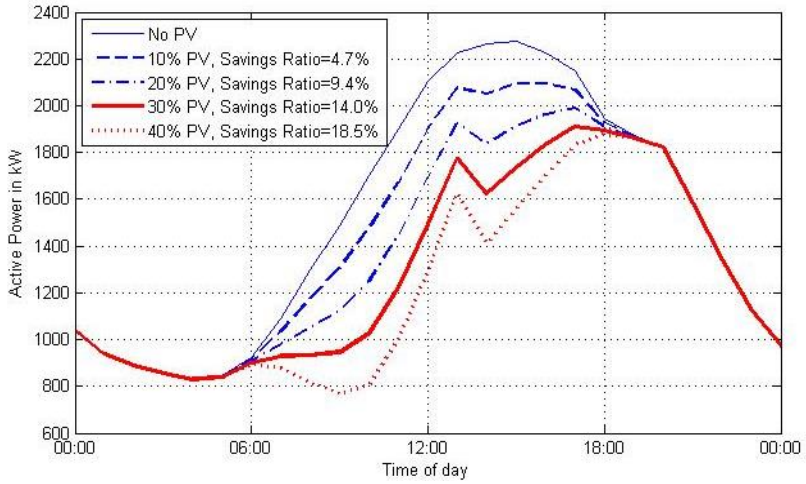

Figure 17. The effect of PV generation on peak demand on a typical day

2.6.4 Representation of the DG Bus as a P-Q or P-V Bus

This study adds three distributed generators to the IEEE 37-bus test feeder, supplied by the three-phase transformer of 2,500 kVA, shown in Figure 18, and proposes three scenarios with distributed generators with small, medium, and high capacities.

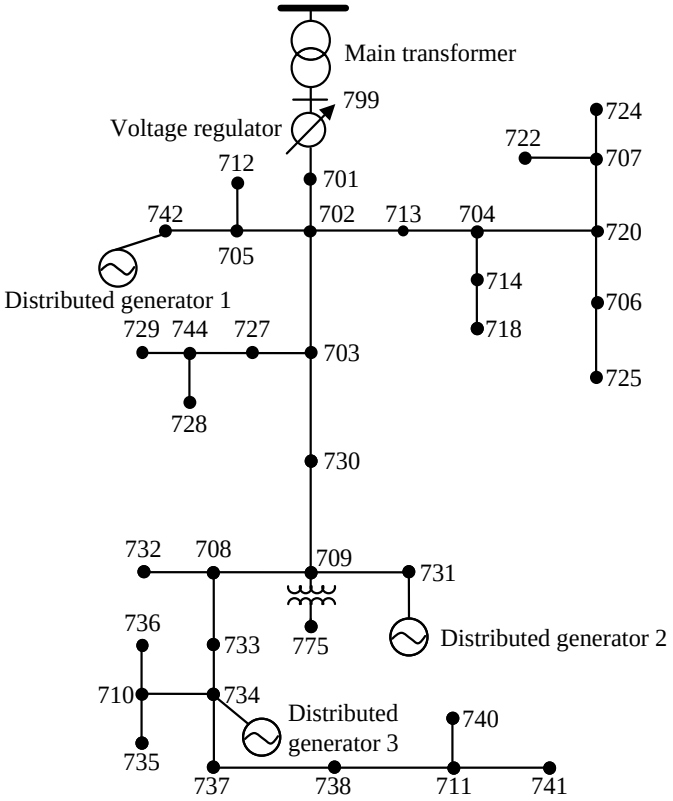

Figure 18. The IEEE 37-bus test feeder enhanced by three distributed generators.

Table 5 represents three small-capacity generators of 50, 100, and 100 kVA added to the feeder and a DG bus operating as a P-V bus. Since the reactive power of the three generators required for target voltage violates their capacity limits, the proposed algorithm changes the DG bus into a P-Q bus after setting its reactive power to its limit. Then the capacity of distributed generator 1 on bus 742 increases from 50 to 500 kVA. As a result of the increased capacity, distributed generator 1 maintains its terminal voltage within the target voltage, but the others fail. Finally, the three high-capacity generators, which increase to 500, 900, and 900 kVA, inject sufficient reactive power, so they maintain their target voltages. The convergence criterion does not exceed 0.00001.

Table 5. Representation of the DG bus as a P-Q or P-V bus

Scenario Number	Bus	DG Capacity	Mode	Positive-Sequence Voltage (Line-to-Neutral)	
				Target	Regulated
		kVA	P-V, P-Q	PU	PU
Reference	742	0	-	1.01298	
	731	0	-	1.00253	
	734	0	-	0.99663	
1	742	50	P-V→P-Q	1.01000	1.01466
	731	100	P-V→P-Q	1.00000	1.00567
	734	100	P-V→P-Q	1.00000	1.00002
2	742	500	P-V	1.01000	1.01001
	731	100	P-V→P-Q	1.00000	1.00252
	734	100	P-V→P-Q	1.00000	0.99687
3	742	500	P-V	1.01000	1.01001
	731	900	P-V	1.00000	1.00001
	734	900	P-V	1.00000	1.00000

2.7 Conclusion

The main objective of this study has been to develop an algorithm that analyzes the three-phase power flow of urban radial and meshed networks enhanced by DG (distribution generation) systems, particularly the PV system examined in this study. This study (1) has developed an accurate and fast algorithm for three-phase power-flow analysis based on the backward and forward sweep method in MATLAB, a method of iterative compensation for the meshed network, and a method of representing the DG bus as a P-Q or P-V bus; (2) has modeled common power system components such as the load (constant power, constant current, and constant impedance loads), the transformer, the voltage regulator, and the shunt capacitor bank; and (3) has verified the algorithm using IEEE 4-, 13-, 34-, 37-, and 123-bus test feeders, which are well-defined and extremely complex distribution networks. The proposed algorithm for three-phase power-flow analysis has exhibited the following three characteristics:

(1) Accurate power-flow analysis of urban radial and meshed distribution networks

(2) Successful representation of the DG bus as either a P-Q or P-V bus

(3) Successful integration of the PV simulation program into the power-flow algorithm

The results of the power-flow analysis of radial and meshed networks enhanced by DG systems suggested that the proposed algorithm could be extended for analyzing the impact of the DG system, which contains uncertainties of its inputs, locations, and capacities, none of which is known in the planning stage of a power system, on an urban distribution network. Thus, in the next chapter, this study will analyze the impact of DG systems, particularly PV systems, stochastically dispersed on an urban distribution network using a stochastic simulation algorithm combined with the proposed three-phase power-flow algorithm.

CHAPTER 3

STOCHASTIC METHODS FOR THE ANALYSIS OF STOCHASTICALLY DISTRIBUTED RENEWABLE GENERATION ON URBAN DISTRIBUTION NETWORKS

3.1 Overview

The objective of this study is to propose tools and algorithms useful for designing, analyzing, and operating urban distribution networks enhanced by stochastic renewable DG (distributed generation) systems, particularly PV (photovoltaic) systems, and to address some of the issues in the analysis of their impact on such networks. Nowadays, small-scale and decentralized DG systems, capacities of which vary in the range of several kW to hundreds of MW, have been dispersed into urban distribution networks. Because of the distributional characteristics of DG systems throughout such a network, the conventional algorithm for power-flow analysis, including Newton-Raphson and fast decoupled power-flow algorithms, is not capable of determining their impact on the urban distribution network, including their optimal position and capacity, without a stochastic process simulation such as a Monte Carlo method. Therefore, this study develops a stochastic algorithm combined with the fine-tuned three-phase power-flow algorithm developed in the previous chapter. In addition, since the stochastic methods rely on repeated random sampling, they cause a serious computational burden on rare events. Thus, to reduce the number of the computational burden, this study accelerates this combined algorithm with methods of variance reduction, including importance sampling, and the sampling of representative clusters and extreme points.

3.2 Introduction

Algorithms for analyzing the effect of the DG system can be classified as both non-stochastic (which typically uses the deterministic method) and stochastic methods [21, 26-33]. However, these both non-stochastic and stochastic studies did not examine the effect of the DG system from the standpoint of long-term, typically annual, operation. In addition, these studies did not examine the inherent high-dimensional uncertainty of the input, the location, and the capacity of the DG system, not known in the planning stage of the power system. The high-dimensionality of uncertainty requires a very large number of simulations, possible only with a fast-performing optimized algorithm. For this purpose, this study develops a stochastic simulation algorithm combined with the power-flow algorithm (developed in the previous chapter) and accelerated by not only importance sampling but also the sampling of representative clusters and extreme points. This study also uses the IEEE 123-bus test feeder as the urban distribution network and load profiles for residential customers, obtained from an actual utility in kW in hourly intervals in 2007. In addition, it assumes that residential PV systems as an example of a DG system are installed across the Atlanta area, an urban distribution area. Thus, it uses an energy mix of the state of Georgia. Lastly, it performs annual stochastic simulations in hourly intervals, quantifies the effects of the method of variance reduction, including importance sampling, and analyzes the impact of stochastically dispersed residential PV systems on the urban distribution network from the perspective of energy, particularly regarding peak power, electricity generation costs, and emissions.

3.3 Problem Statement

To analyze the effects of a DG system, particularly the PV system, on urban distribution networks, this study proposes a stochastic simulation algorithm that models the following uncertainties:

(1) *Location*. Residential small-capacity PV systems can be dispersed anywhere across

the distribution network.

(2) *Generation*. Since the generation of the PV system depends on a probabilistic quantity, its generation is not known in the planning stage.

(3) *Capacity and field orientation*. The capacity and the field orientation of individual PV systems may differ.

To model inherent uncertainties of the location, the capacity, and the field orientation of the PV system, the following two scenarios are examined:

(1) *The scenario of a single PV system*. This study selects twenty uniformly scattered buses on which a single PV system with a capacity scaled from ten to forty percent of total peak demand is installed across the distribution network, depicted in Figure 19. Then, the study repeats twenty annual stochastic simulations while the capacity of the PV system is fixed to ten percent of total peak demand. In each simulation, the study treats a single PV system as a negative load and then calculates the hourly power flow of the urban distribution network with residential load profile data (obtained from an actual utility in kW in hourly intervals in 2007). After the selection of the best performing bus from the twenty uniformly scattered buses, six of the annual stochastic simulations are repeated while the capacity of the PV system on the best performing bus increases from fifteen to forty percent of peak demand in five percent intervals.

(2) *The scenario of stochastically dispersed residential PV systems with various capacities*. This study determines the annual effect of not only savings in energy and emissions but also changes in generation costs resulting from residential PV systems stochastically dispersed throughout the urban distribution network that produce a capacity of ten percent of total peak demand. For this purpose, this study models the uncertainties of the location, the capacity, and the field orientation of stochastically dispersed residential PV systems.

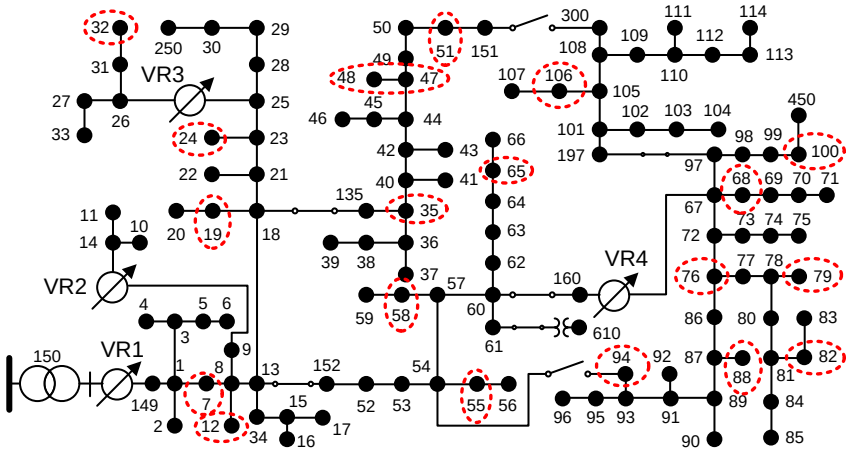

Figure 19. Twenty buses on which a single PV system is installed across the IEEE 123-bus test feeder.

3.4 Uncertainty Design for the Stochastic Simulation

3.4.1 Objective Function

In the scenario of dispersed residential PV systems, to determine the annual effect of the energy savings, the emissions savings, and the generation cost changes of residential PV systems with a capacity of ten percent of total peak demand dispersed throughout the urban distribution network, this study proposes the following objective function:

$$\theta = E[P, E, M, \text{and } C], \tag{25}$$

$$\text{Minimize } Var[\theta], \tag{26}$$

where P = the annual power generation of dispersed residential PV systems in kWh/year/household; and E, M, and C = the annual energy savings in kWh/year/household, emissions savings in kg/year/household or gallons/year/household, and the generation cost changes in $/year/household of PV systems with a capacity of ten percent of peak demand stochastically dispersed throughout the urban distribution network, respectively.

3.4.2 Uncertainty in PV Systems

To find the expectation value of the annual energy production of residential PV systems and their energy savings in urban distribution networks, this study defines

uncertainty in their input and output such as the capacity, the azimuth angle, the tilt angle, and the module material of the PV system. First, the capacity of the PV system for residential customers is affected by incentives, rebates, government subsidies, rooftop sizes, and daily, monthly, or annual load consumption patterns. As a result of these various factors, PV system capacity is not unique for individual residential customers. Therefore, this study surveyed the actual distribution of the capacity of residential PV systems, that is, the distribution of PV system capacities collected from 114,066 residential customers in California in 2014 [40] (because of unavailable data for Georgia), illustrated in Figure 20.

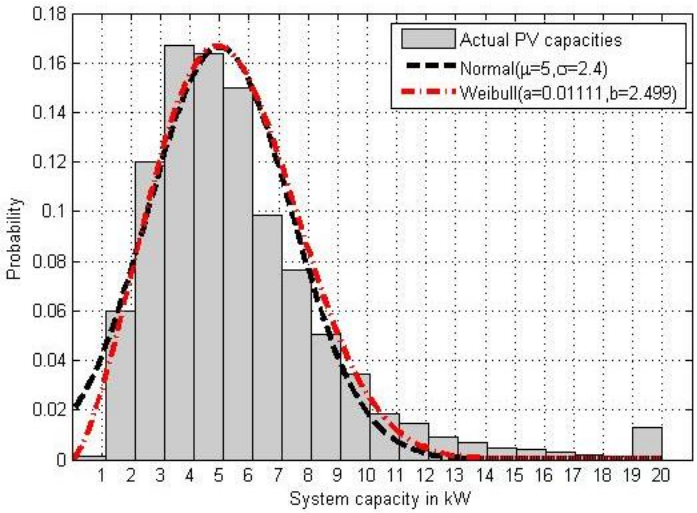

Figure 20. The distribution of residential PV system capacities in California.

Although the distribution of PV capacities illustrated in Figure 20 does not perfectly fit a truncated standard normal distribution (the root-mean-square deviation of which is 0.01341) or a Weibull distribution (the root-mean-square deviation of which is 0.01101), it reveals some characteristics of a normal distribution (such as more samples around a mean, a wide dispersion of probabilities, and increasing and decreasing patterns of probabilities along the system capacity in kW). Since the optimal distribution of importance sampling for a normal distribution can be found more easily than that for a Weibull distribution (which will be discussed in Sections 3.5.1 and 3.5.2), this study assumes that the PV system capacity follows a truncated normal distribution. In addition,

since the distribution of the azimuth angle of individual residential roofs in the urban distribution network is unknown, this study proposes uniformly distributed azimuth angles. However, since a south-facing PV system, which indicates an azimuth angle of 180°, is generally recommended for maximum energy production, this study uses a truncated normal distribution with a mean of 180° and a standard deviation determined by the range rule. Third, tilt angles of individual residential roofs can be either uniformly distributed or defined as typical pitch angles for residential roofs, which will be presented in Section 3.5.4. Lastly, PV module shipments for the residential sector in Georgia in 2010 are a 99.15% crystalline silicon (c-Si) type and a 0.85 % thin film type such as cadmium telluride (CdTe), amorphous silicon (a-Si), and copper indium gallium selenide (CIS) [37]. To sum up, to model the inherent uncertainties of the capacity and the field orientation of stochastically dispersed residential PV systems, this study proposes the following uncertainties:

Table 6. The uncertainty of stochastically dispersed residential PV systems

Random Variable	Value	Sample Size	Distribution
System capacity (inverter) in kW [40]	1 kW~20 kW in 1 kW intervals	20	1. Truncated Normal = $N(\mu$=5kW, approximate $\sigma)$ 2. Uniform = U(1kW, 20kW)
Azimuth angle in ° [38]	135°~ 225° in 0.1° intervals	901	1. Truncated Normal = $N(\mu$=180°, σ=range/4) 2. Uniform = U(135°,225°)
Tilt angle in ° [38, 39]	Typical roof pitch angles	10	1. Typical roof pitch angles with equal probabilities
PV module material [37]	99.15% c-Si type and 0.85% thin-film type (CdTe, a-Si, and CIS)	4	1. 99.15% c-Si type and 0.85% thin-film type

3.4.3 Stochastic Monte Carlo Simulation

In the scenario of stochastically dispersed residential PV systems, to remove their uncertainties and to determine their annual energy savings, this study performs a (naive) stochastic Monte Carlo simulation in the following steps:

Step 1. *Initialization*. It calculates the total number of households of the test feeder in Figure 19, selects representative commercial PV modules made of c-Si, CdTe, a-Si, and CIS (presented in Appendix E), and selects representative commercial

inverters with a capacity of 1 kW to 20 kW (also presented in Appendix E).

Step 2. *Random number generation for each random variable*. It generates uniformly and normally distributed random numbers for random variables such as the system capacity, the azimuth angle, the tilt angle, and the PV module. Each generated random number corresponds to a value of a random variable provided in Table 6.

Step 3. *Selection of households*. It assumes that PV systems with randomly generated modules and inverters are installed on the roof of individual houses throughout the urban distribution network. Then it randomly selects *N* households with their own PV systems that produce a capacity of ten percent of total peak demand and estimates the annual generation of the PV systems installed in the Atlanta area in hourly intervals during one year.

Step 4. *Calculation of annual power flow*. It calculates the annual power flow of the test feeder enhanced by *N* stochastically dispersed residential PV systems in hourly intervals, using the power-flow algorithm developed in Chapter 2.

Step 5. *Termination and normalization*. It repeats steps 3 and 4 for to complete the simulation period (which will be determined in the next section) and determines the annual effects of both reductions in energy consumption and emissions and changes in the costs of electricity generation of *N* residential PV systems stochastically dispersed throughout the urban distribution network.

3.4.4 Stochastic Simulation Period

If *N* stochastically dispersed residential PV systems selected in steps 3 and 4 in the previous section operate during one year, the enumeration of possible combinations for the selection of *N* PV systems with the uncertainties presented in Table 6 requires 20×901×10×4 years = 720,800 years. By the central limit theorem, which states that the sum of a sufficiently large number of independent and identical random variables can be approximated by a normal distribution, this study assumes that annual PV output in

kWh/year/household complies with the normal or Gaussian distribution defined in (27) as the total simulation period increases. After a preliminary simulation of 1,000 years, this study plotted the distribution of annual PV output, shown in Figure 21, with a mean of 589.92 kWh/year/household and a variance of 78.12 kWh/year/household, which complies with the following Gaussian distribution:

$$f_{Gaussian}(x) = a\mathrm{e}^{-(x-b)^2/c^2}, \qquad (27)$$

where a = 0.1313, b = 588.6, and c = 12.22.

This study also examined sample means and variances of annual PV output in kWh/year/household while increasing the sample size in year, depicted in Table 7. Since the sample variances of annual PV output in kWh/year/household converge as the sample size increases, this study performs a stochastic simulation of 1,000 years in hourly intervals in the scenario of N residential PV systems stochastically dispersed on an urban distribution network. The determination of a necessary simulation period of years to meet sufficient accuracy in a mean of annual PV output (which is calculated by averaging the power output of residential PV systems stochastically installed on N households that produce a capacity of ten percent of total peak demand in hourly intervals annually) is outside the scope of this study.

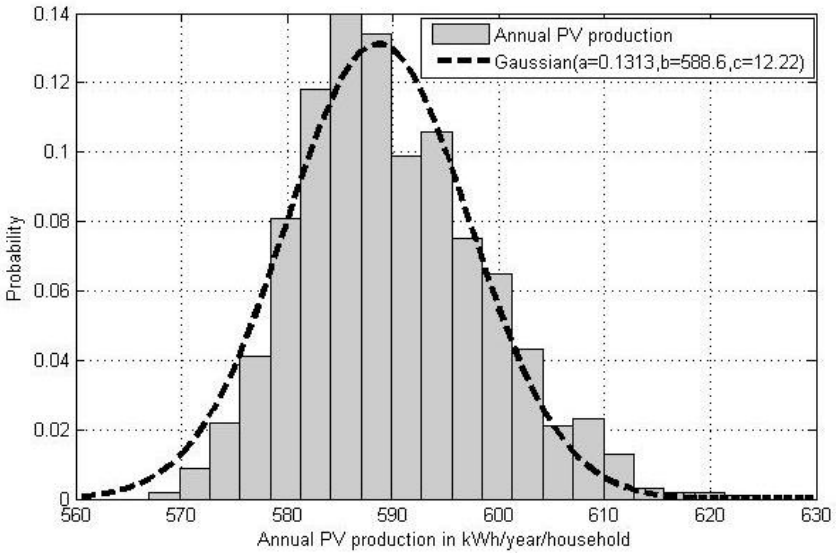

Figure 21. The distribution of annual PV output in kWh/year/household during 1,000 year.

Table 7. The sample variance of annual PV output in kWh/year/household

Sample Size	Sample Mean	Sample Variance
Year	kWh/year/household	kWh/year/household
10	592.25	139.34
20	591.21	102.94
50	590.56	97.01
100	590.19	86.44
200	589.73	77.42
500	589.77	77.46
1,000	589.92	78.12

3.5 Stochastic Methods for the Analysis of the Impact of DG

A naive Monte Carlo simulation, a stochastic simulation method of accounting for uncertainty, estimates the expected value of a random variable such as (1) annual reductions in energy consumption and emissions and (2) changes in the cost of electricity generation resulting from PV systems stochastically dispersed on an urban distribution network. To reduce variance in the expected value, in other words, to obtain the more accurate expected value, this study accelerates the stochastic simulation with the methods of variance reduction, including importance sampling for the system capacity and azimuth angle random variables and stratification sampling for the tilt angle random variable, both of which are typically the most effective. Figure 22 compares these two methods with other variance reduction methods.

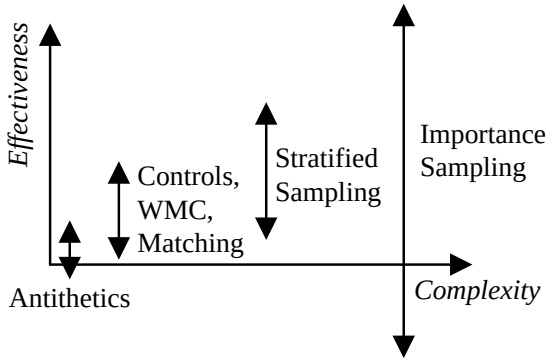

Figure 22. Comparison of the methods of variance reduction [35].

3.5.1 Importance Sampling

A stochastic simulation such as the naive Monte Carlo simulation is typically based on repeated random sampling, which creates a serious computation burden on rare

events that can be reduced by the method of importance sampling, which conducts random sampling more extensively close to a more important event. This study applies importance sampling to random sampling for the system capacity and azimuth angle random variables defined in Section 3.4.2. In other words, it reduces variance by sampling more extensively near the important area (which is defined by importance sampling) when finding an expectation value of annual PV power production defined in Equation (25), which is a function of the capacities, the azimuth and tilt angles, and the modules of PV systems. To describe how importance sampling can find more accurately the expectation value, this study assumes that annual PV power production depends on only their capacities that follow a normal distribution. Then, this study examines the expected value of random variable *x* by

$$\theta = E[x] = \int_{-\infty}^{\infty} x f_X(x) dx , \qquad (28)$$

where x = the random variable that contains samples of the system capacity and

$f_X(x)$ = the original probability density function of *x*.

This study introduces the new probability density function, *g(x)*, of importance sampling by

$$\theta = E[x] = \int_{-\infty}^{\infty} \frac{x f_X(x)}{g(x)} g(x) dx = E[\frac{x f_X(x)}{g(x)}] . \qquad (29)$$

If a shape that is similar but not equal to that of the original distribution, or $f_X(x)$, is selected for importance sampling, then $xf_X(x)/g(x)$ can be a constant and its variance zero [36]. The optimal distribution of the importance sampling is

$$g_{optimal}(x) = \frac{x f_X(x)}{constant} = \frac{x f_X(x)}{\theta} = \frac{x f_X(x)}{\int_{u \in support(xf)} u f_X(u) du} . \qquad (30)$$

The efficiency of importance sampling depends on the appropriate choice of *g(x)*. However, the constant in equation (30) cannot be calculated in practice because of the huge number of possible combinations or unknown original distributions. However, equation (30) suggests that the appropriate choice of *g(x)* with a shape that is similar but

not equal to that of $f_X(x)$ can reduce variance by sampling extensively near the area of large $f_X(x)$, which indicates an important event, and by sampling infrequently near the area of small $f_X(x)$, which indicates a non-important event.

The distribution of the system capacity of residential PV systems (as shown in Figure 20 presented in Section 3.4.2) can be approximated by the following truncated normal distribution with mean μ and standard deviation σ:

$$f_x(x) = \frac{1}{\sqrt{2\pi}\sigma} e^{-(x-\mu)^2/2\sigma^2}. \quad (31)$$

To apply importance sampling to random variable x of the system capacity, this study proposes a new distribution of importance sampling by the following near-normal distribution parameterized on λ:

$$g(x,\lambda) = \lambda e^{-\lambda(x-\mu)^2/2\sigma^2}. \quad (32)$$

To determine optimal λ^*, [36] proposed an upper bound on the variance, as follows:

$$\begin{aligned} Var(\theta) &= Var\left(\frac{xf_x(x)}{g(x,\lambda)}\right) = E\left[\left(\frac{xf_x(x)}{g(x,\lambda)}\right)^2\right] - E\left[\left(\frac{xf_x(x)}{g(x,\lambda)}\right)\right]^2 \\ &= \int_{-\infty}^{-\infty} \frac{x^2 f_x^{\,2}(x)}{g^2(x,\lambda)} g(x,\lambda)dx - \theta^2 \\ &\le M(x,\lambda)\int_{-\infty}^{\infty} xf_x(x)dx - \theta^2 \end{aligned} \quad ,(33)$$

where

$$M(x,\lambda) = \max_{x\in support(g)} \frac{xf_x(x)}{g(x,\lambda)}. \quad (34)$$

Optimal λ^* is 2/3 that satisfies the conditions of the following equation:

$$\frac{\partial M(x,\lambda)}{\partial x} = \frac{\partial M(x,\lambda)}{\partial \lambda} = 0. \quad (35)$$

Figure 23 compares optimal $g(x)$ to $f_X(x)$. Similarly, this study applies importance sampling to the azimuth angle random variable.

3.5.2 Example of Importance Sampling

To illustrate the effect of importance sampling on the stochastic simulation from

the point of view of reducing variance (which indicates that the estimated expectation value more closely approaches a true expectation value), this study proposes an example of identifying the expectation value of the sum of two normally distributed random variables, $X_1=N(0,1)$ and $X_2=N(0,0.5)$, in Figure 24.

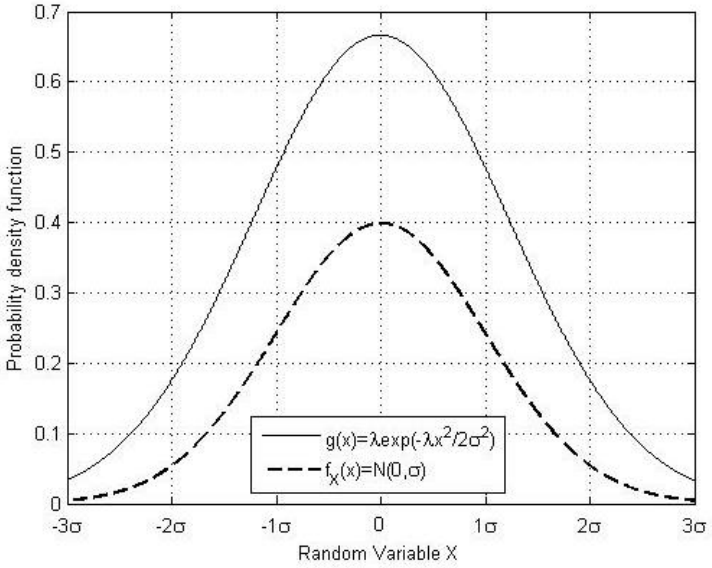

Figure 23. Optimal distribution of importance sampling.

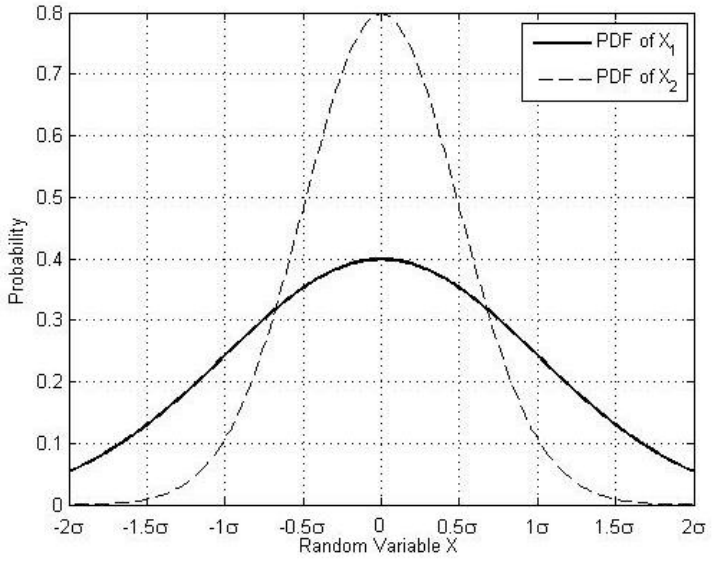

Figure 24. Probability density functions of $X_1=N(0,1)$ and $X_2=N(0,0.5)$.

The study defines a new random variable, $Y=X_1+X_2$, and estimates the expectation value and the variance of Y using both stochastic simulation and importance sampling. Stochastic simulation finds the expectation value in the following steps:

(1) It generates random samples for two normally distributed random variables, X_1' and X_2', in sample sizes of 100, 1,000, 10,000, 100,000, and 1,000,000, shown in Figure 25.

(2) It estimates the expectation value and the variance of $Y_{Stochastic} = X_1' + X_2'$.

By the definition of importance sampling presented in Section 3.5.1, $M\left(x,\lambda^*\right)$, for the normal distribution with a mean of 0 and a standard deviation of σ, can be calculated by

$$M\left(x,\lambda^*\right) = xf(x)/g(x) = \frac{xe^{(\frac{\lambda^*}{2\sigma^2}-\frac{1}{2\sigma^2})x^2}}{\sqrt{2\pi}\lambda^*\sigma}, \qquad (36)$$

where optimal λ^* is 2/3.

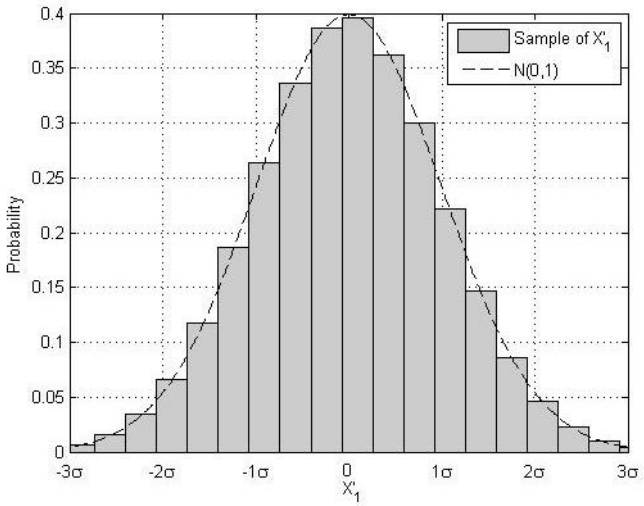

Figure 25. The probability density function of samples of X_1' with a sample size of 1,000,000.

This study then examines the expectation value and the variance of Y_{IS} using $M\left(x,\lambda^*\right)$ of importance sampling in the following steps:

(1) It generates random samples for two normally distributed random variables, X_1'' and X_2'', in sample sizes of 100, 1,000, 10,000, 100,000, and 1,000,000.

(2) It applies $M\left(x,\lambda^*\right)$ for the samples of X_1'' (presented in Figure 26) and X_2'' and calculates the expectation value and the variance of $Y_{IS} = X_1'' + X_2''$.

Figure 26 indicates that importance sampling conducts random sampling more extensively near a more important area ranging from -0.60σ to -0.60σ for a normal distribution with a standard deviation of σ. Table 8 presents a comparison of the stochastic simulation to importance sampling. Importance sampling with λ^*=2/3 reduces more variance than stochastic simulation as a sample size increases. For example, the variance (0.3328) of the stochastic simulation accelerated by importance sampling is less than that (1.2499) of stochastic simulation in the case of a sample size of 1,000,000. That is, the expectation value (-0.00006) estimated by importance sampling more closely approaches the true expectation value of *Y*, or zero, in this example.

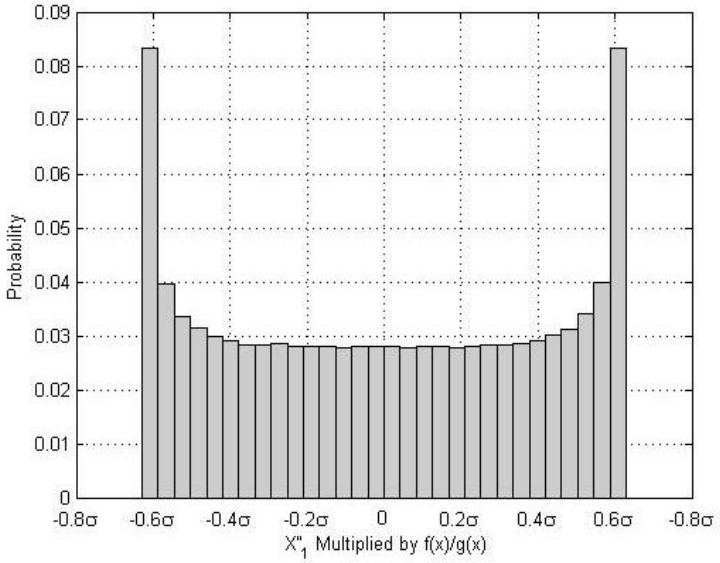

Figure 26. The probability density function of samples of X_1'' changed by importance sampling.

Table 8. Comparison of stochastic simulation to importance sampling

Sample Size	True Value	Stochastic Monte Carlo Simulation		Importance Sampling	
	$E[Y]$	$E[Y_{Stochastic}]$	$Var[Y_{Stochastic}]$	$E[Y_{IS}]$	$Var[Y_{IS}]$
100	0	0.02205	1.2436	0.01516	0.3349
1,000		0.00514	1.2506	0.00207	0.3337
10,000		0.00099	1.2508	0.00023	0.3332
100,000		-0.00039	1.2502	-0.00015	0.3329
1,000,000		-0.00016	1.2499	-0.00006	0.3328

3.5.3 System Capacity and Azimuth Angle Random Sampling Accelerated by Importance Sampling

This study introduces the new near-normal probability density function, *g(x)*, of importance sampling with optimal $\lambda^* = 2/3$ for the system capacity and azimuth angle random variables. To generate random numbers for the PV system capacity random variable in the stochastic simulation presented in Section 3.4.3, this study uses a truncated normal distribution with a mean of 5 kW and a standard deviation of 2.4 kW, both of which are determined by the non-linear least-squares method presented in Figure 20, and the probability density function of which is presented in Figure 27 (a). In addition, this study applies the near-normal distribution of importance sampling for the system capacity random variable. Figure 26 in previous Section 3.5.2 indicates that importance sampling conducts random sampling more extensively near a more important area ranging from -0.60σ to -0.60σ for a normal distribution with a standard deviation of σ. Since this study approximates a standard deviation of 2.4 kW for the system capacity random variable, it selects more samples near 3 to 7 kW in the PV system capacity. The probability density function of the system capacity random variable applying for importance sampling is presented in Figure 27 (b). To compare the effect of importance sampling on variance reduction, this study also uses uniformly distributed system capacities, the probability density function of which is presented in Figure 27 (c).

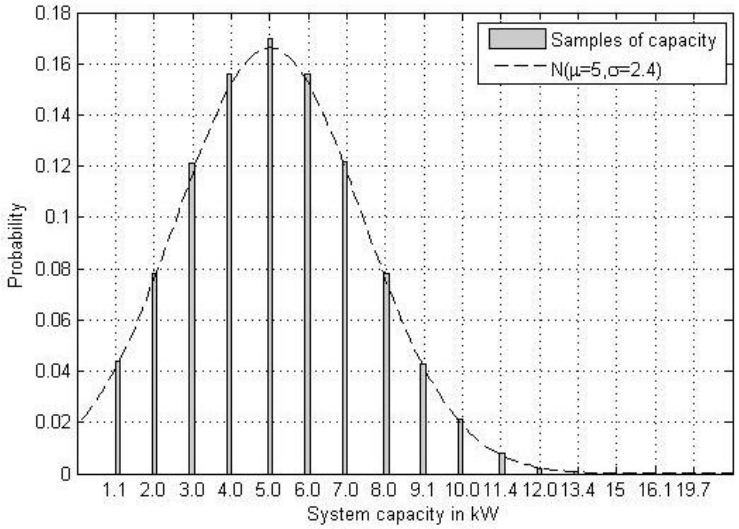

(a) Truncated normal distribution of system capacities

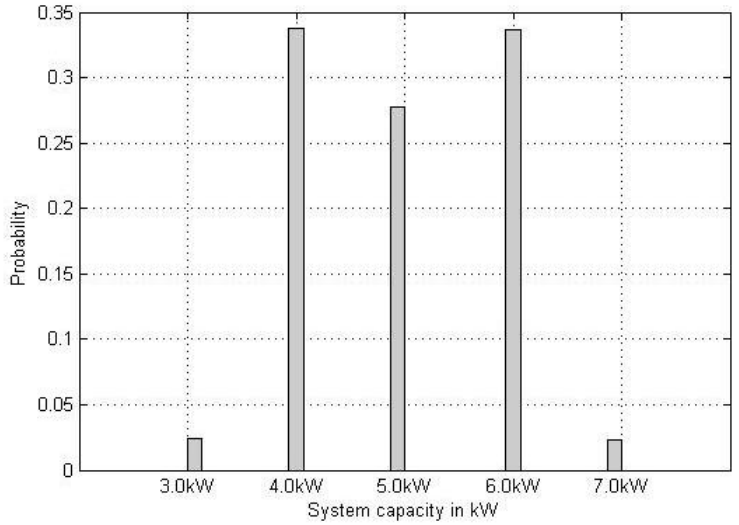

(b) Importance sampling of system capacities

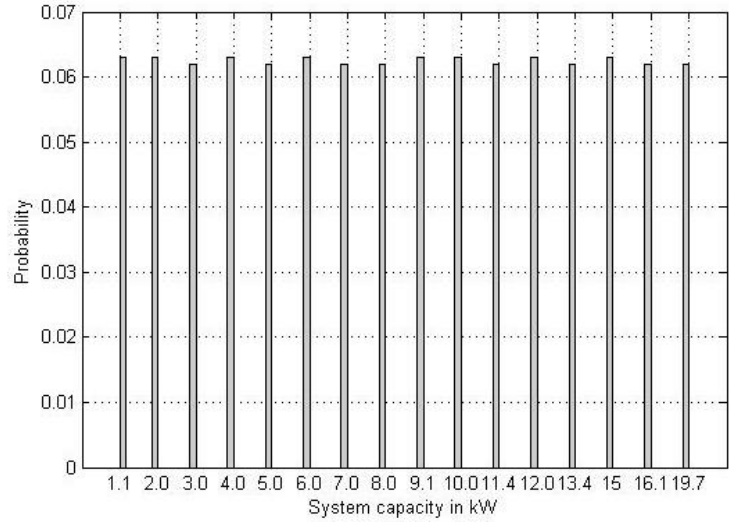

(c) Uniformly distributed system capacities

Figure 27. Importance sampling for the PV system capacity.

Since the distribution of the azimuth angle of individual residential roofs in the urban distribution network is unknown, this study initially conducts random sampling from uniformly distributed azimuth angles in the stochastic simulation presented in Section 3.4.3, the probability density function of which is presented in Figure 28 (a). However, a south-facing PV system, indicating one with an azimuth angle of 180°, is generally recommended [38]. In addition, we can either rotate a PV rack so that the PV module faces south [82] or install a south-facing panel in a yard, referred to as a "ground-mounted" solar array [83]. Thus, this study performs a second stochastic simulation that conducts random sampling from normally distributed azimuth angles with a mean of 180° and a standard deviation of 22.5°, or σ=90°/4, determined by the range rule, the probability density function of which is presented in Figure 28 (b). Lastly, this study applies the near-normal distribution of importance sampling for random variable of the azimuth angle, the probability density function of which is presented in Figure 28 (c).

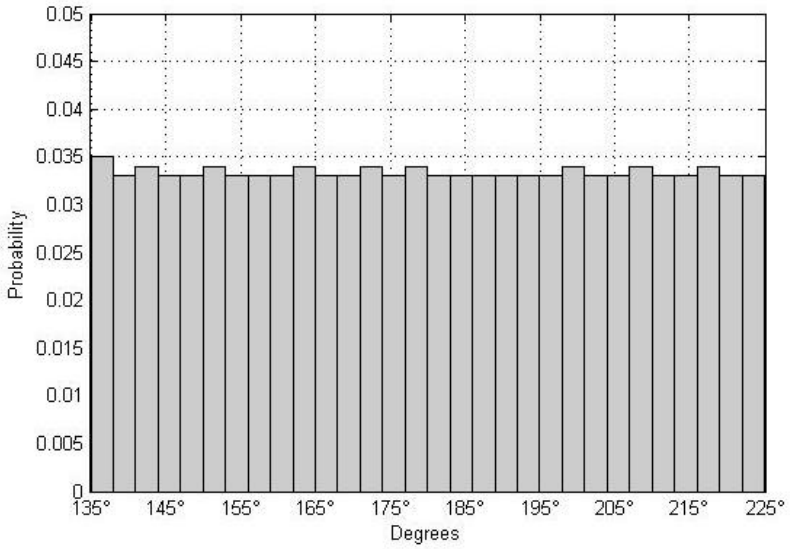

(a) Uniformly distributed azimuth angles

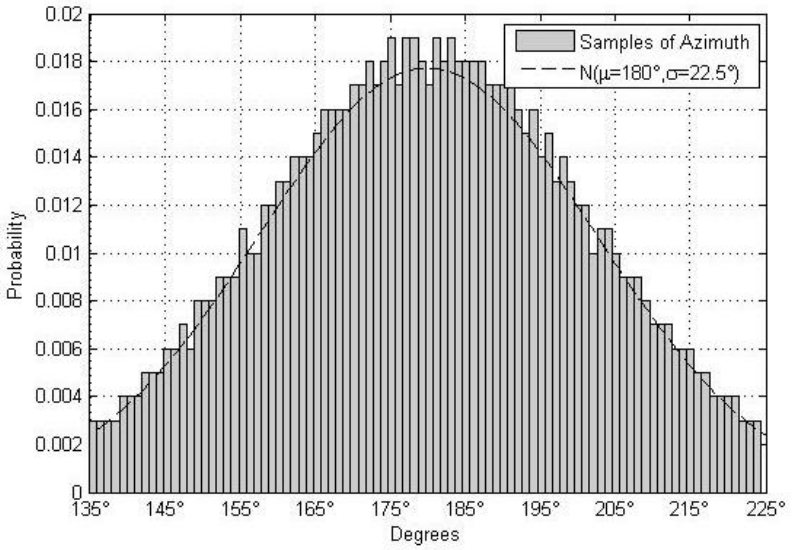

(b) Truncated normal distribution of azimuth angles

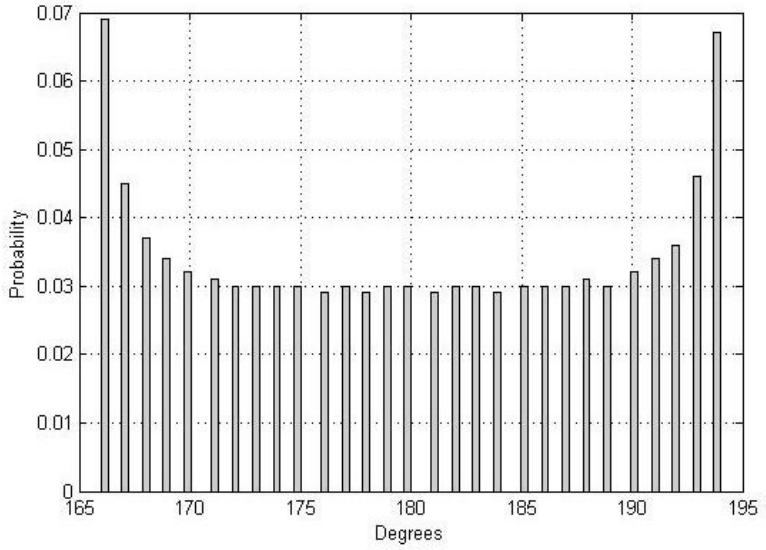

(c) Importance sampling

Figure 28. Importance sampling for the azimuth angle.

3.5.4 Stratification Sampling

In stratification sampling, random variable X can be split into mutually exclusive strata by $X \in \{S^{(i)}, i=1,2,..,m\}$ and then sampled from each stratum. This study defines the stratum of the tilt angle of the PV system as the typical pitch angle for residential roofs depicted in Table 9 and conducts random sampling from the strata of the tilt angle, as shown in Figure 29 (b).

Table 9. Typical pitch angles for residential roofs [39]

Pitch	Degree(°)	Pitch	Degree(°)	Pitch	Degree(°)	Pitch	Degree(°)
3/12	14.04	6/12	26.57	9/12	36.87	12/12	45.00
4/12	18.43	7/12	30.26	10/12	39.81	13/12	47.29
5/12	22.62	8/12	33.69	11/12	43.51	14/12	49.40

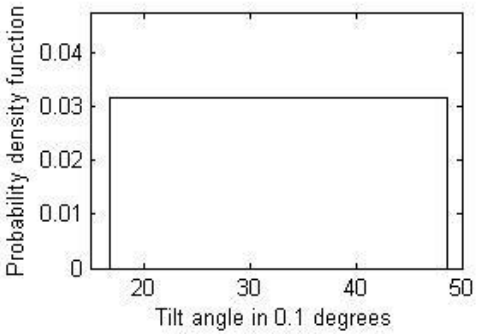

(a) Uniformly distributed tilt angles

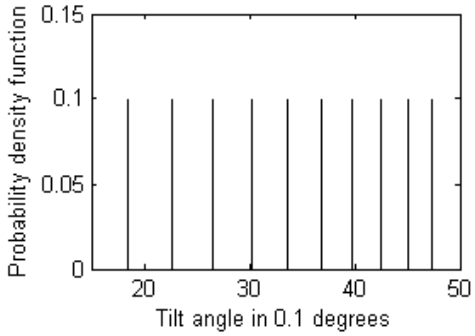

(b) Stratification sampling

Figure 29. Stratification sampling for the tilt angle.

3.5.5 Method of Sampling Representative Clusters and Extreme Points

Despite the acceleration of the stochastic method by importance sampling, repeated random sampling results in an extremely heavy computational burden. In fact, the number of possible combinations of uncertainties in Table 6 is 20× 901×10×4 years = 720,800 years = 6.31×10^9 power-flow calculations in hourly intervals, which consumes a prohibitive amount of computational time (e.g., 382.03 hours for a stochastic simulation of 1,000 years in hourly intervals presented in Table 16). Therefore, [32] proposed an additional method of sampling representative clusters and extreme points and this study applies the method to the proposed stochastic simulation algorithm. In fact, the power flow of the urban distribution network is calculated for only representative clusters and

extreme points that correspond to typical hours during which PV systems operate (i.e., hours derived from 8,760 hours of one year in hourly intervals). Figure 30 shows all of the data points of total active power scattered from the results of the power-flow calculation of the IEEE 123-bus test feeder with residential customers, superimposed with representative clusters and extreme points, for the generation of dispersed PV systems with a capacity of ten percent of total peak demand, or 3.55 MW. Figure 31 represents the duration curve of total active power approximated by 10, 50, and 100 representative clusters. Figure 31 reveals that the combination of representative clusters and extreme points does not destroy the intrinsic data structure, but it significantly reduces the number of power-flow calculations from 8,760 to 10, 50, and 100 in hourly intervals during the year. The duration curve approximated by only representative clusters of ten clusters shows a relatively good match. This study uses the Quickhull algorithm to detect extreme points of 10 to 20 and the K-means clustering algorithm to partition all the data points, or 8,760, into 100, in MATLAB.

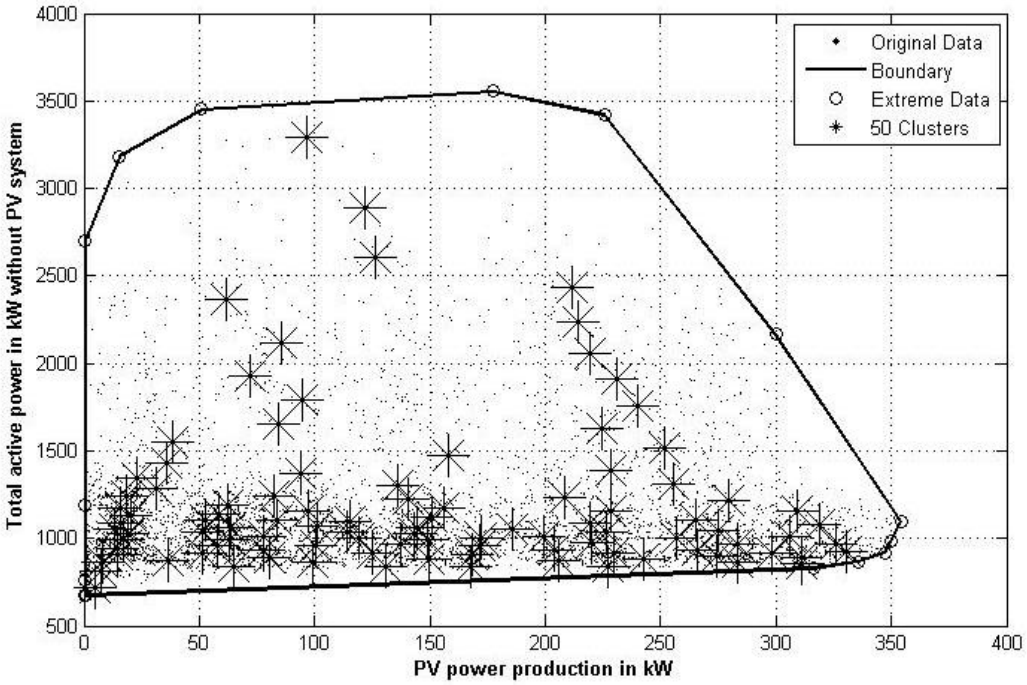

Figure 30. Original 8,760 boundary and cluster points of total active power scattered from the results of the power-flow calculation of the IEEE 123-bus test feeder with residential customers.

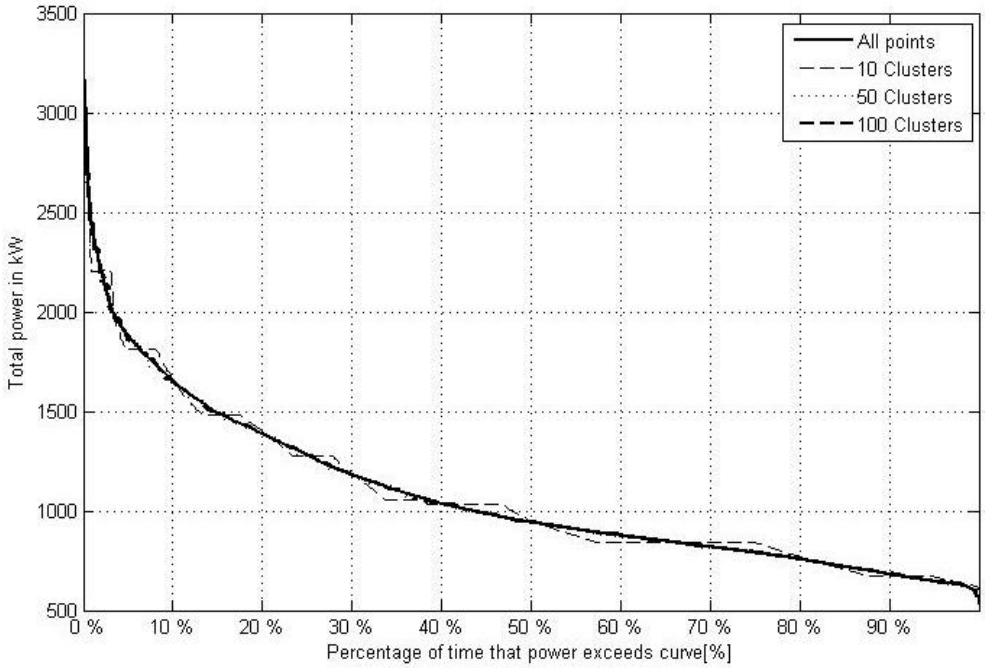

Figure 31. Duration curves of total active power approximated by representative clusters.

3.5.6 Variance Reduction Ratio

The variance reduction ratio (VRR) is the ratio of the variance of the stochastic simulation (without accelerated by the method of variance reduction) to that of the stochastic simulation accelerated by the method of variance reduction as follows:

$$VRR = \sigma^2_{Stochastic} / \sigma^2_{Variance-reduced\ Stochastic}. \qquad (37)$$

The VRR estimates the effect of importance sampling on variance reduction. Efficiency is defined as

$$Efficiency = VRR \times t_{Stochastic} / t_{Variance\text{-}reduced\ Stochastic}, \qquad (38)$$

where

$t_{Stochastic}$ = the elapsed time of the stochastic simulation without variance reduction,

$t_{Variance\text{-}reduced\ Stochastic}$ = the elapsed time of the stochastic simulation accelerated by the method of variance reduction.

Efficiency estimates the effect of the methods of variance reduction and the sampling of representative clusters and extreme points on the improvement of performance such as a stochastic simulation time in hours.

3.6 Implementation of the Stochastic Simulation Algorithm

This study implements the methods of variance reduction and the sampling of representative clusters and extreme points, both of which reduce the computational burden caused by the application of the stochastic method. Figure 32 shows the procedure of the developed algorithm.

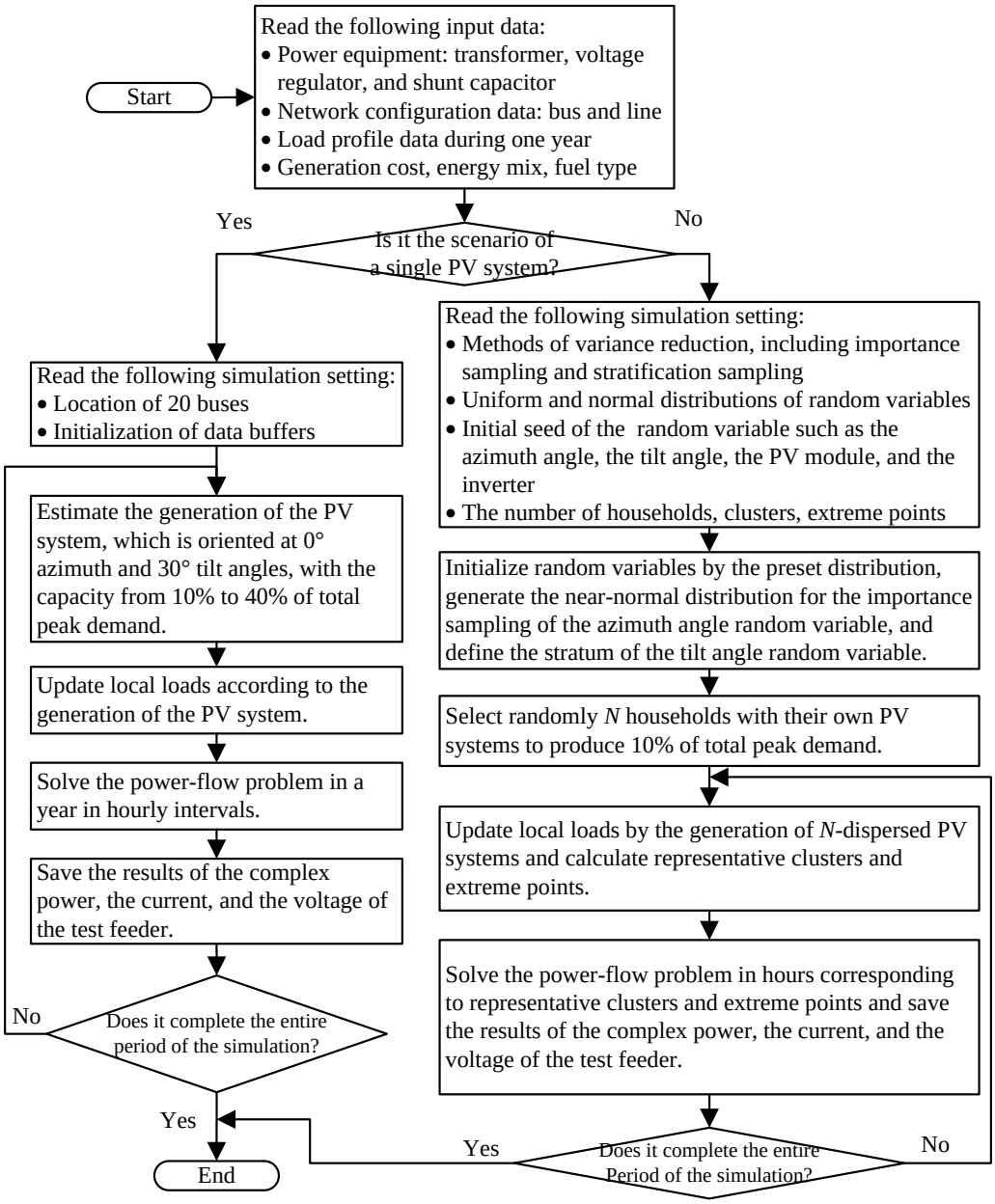

Figure 32. Flowchart of the developed stochastic simulation algorithm.

To perform the stochastic simulation of the scenarios of a single PV system and N

stochastically dispersed PV systems, the algorithm generates the uniform and truncated normal distributions of random variables such as the system capacity, the azimuth angle, and the tilt angle, produces the near-normal distribution of importance sampling with optimal λ^* for the system capacity and azimuth angle random variables, and defines the stratum of the tilt angle random variable of the PV system. To implement the stochastic algorithm, this study uses MATLAB, and to estimate the power output of *N* stochastically dispersed residential PV systems [72], it uses PV_LIB, which is based on TMY (typical meteorological year) version 3 weather data (1991 to 2005).

3.7 Case Study

3.7.1 Urban Distribution Network

This study uses the IEEE 123-bus test feeder as the urban distribution network in Figure 19 [23, 41]. The total capacity of the local loads of the test feeder, which is originally supplied by a three-phase transformer of 5 MVA, is 3,490 kW and 1,920 kVar. If a household has a maximum capacity of 4 kW but consumes an average of forty percent (which is a typical load factor in developed nations) of that amount, the test feeder can supply from 873 to 2,182 households with electricity. Therefore, in the scenario of a single PV system, this study assumes that the test feeder supplies 1,000 households with electricity. In the scenario of stochastically dispersed PV systems, this study selects *N* households that produce a capacity of ten percent of the total peak demand, which is used for the normalization of the simulation results.

3.7.2 Load Profile

The load profile is a graph of the total generation of electricity that varies continuously according to customer demand, which can be classified into residential, commercial, industrial, agricultural, and pumping demand, and large industrial customer demand. This study obtained load profile data from an actual utility in kW in hourly

intervals in 2007, which span one year [42]. Let the load profile data be a discrete function

$$P_{C,I} = \left\{ p_{c,i} \mid p_{c,i} \text{ is active power in kW}, i = 1,...,8760 \right\}, \quad (39)$$

$$Q_{C,I} = \left\{ q_{c,i} \mid q_{c,i} \text{ is reactive power in kVar}, i = 1,...,8760 \right\}, \quad (40)$$

where $C \in \{ c \mid c =$ residential, commercial, industrial, agricultural and pumping, and large industrial customers $\}$.

Because of the lack of available reactive power data, this study randomly generates reactive power consumption maintaining a power factor over 0.85. Total $P_{c,i}$ and $Q_{c,i}$ of individual loads at time i are scaled by the nominal peak active and reactive demand of the test feeder. To account statistically for a variety of types of loads, all the individual loads of each customer type in the distribution network follow an identical pattern. As a result of the preliminary power-flow analysis of each customer type in 2007, the duration curves of the total active power of each customer type, shown in Figure 33, indicates that the active power of a number of large industrial customers distributes close to the peak throughout the year and then descends in the following order: agricultural and pumping, industrial, commercial, and residential customers. Because of the losses of the distribution line and the transformer, the maximum total active and reactive power of the feeder throughout the year is 3,554.61 kW and 387.33 kVar.

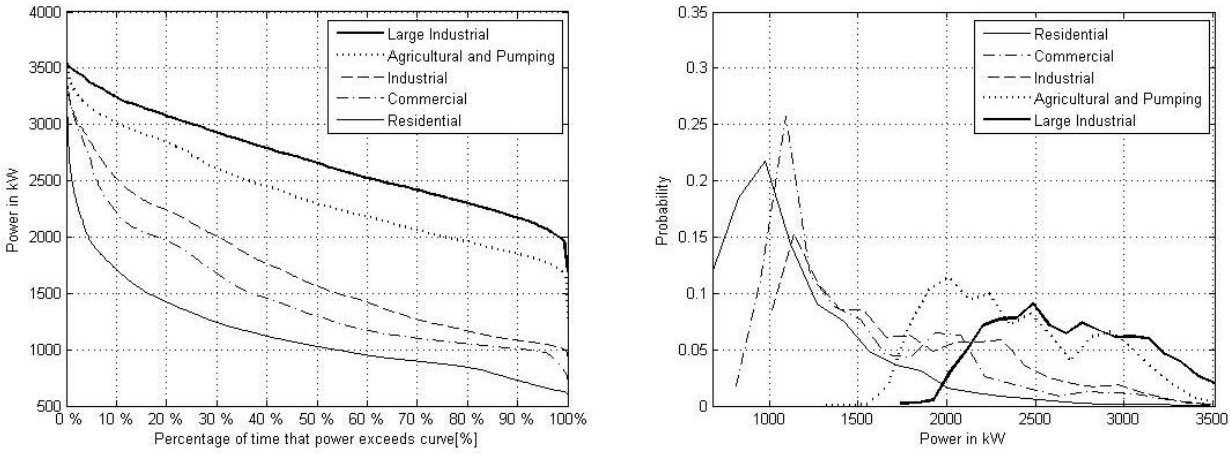

(a) Duration curve **(b) Probability curve**

Figure 33. Total active power of the IEEE 123-bus test feeder with each customer type in 2007.

3.7.3 Energy Mix

The interaction between DG utilization (particularly the PV system in this study) and the continuously varying demand of customers will affect the total costs of energy production. For a utility, the benefits of using DG are less demand for energy production during peak levels and a reduction in transmission and distribution losses. To analyze the impact of the DG system on the total costs of energy production, this study assumes that PV systems are installed across the Atlanta area, an urban distribution area. Thus, this study uses the energy mix of the state of Georgia as the input data of the case study. Table 10 presents the detailed data of the energy mix of the state from December 2010 [43, 84]. The data, supplied by the Georgia Power Company, pertain to the fuel type, the energy mix, and the electricity costs. Since the LCOE (levelized cost of electricity) of PV is continuously decreasing, as shown in Figure 4, this study uses the average levelized cost of electricity of PV entering new service in the United States in 2019 [85].

Table 10. Energy mix of the state of Georgia [84, 85]

Type	Capacity in kW	Fuel	Energy Mix	Cost in $/MWh
Base	0~746.468	Nuclear	21%	6.6
Intermediate	746.468~3128.057	Coal	67%	45.3
Peak	3128.057~3554.61	Gas and Hydro	Gas (10%) and Hydro (2%)	57.5
	10% of peak	PV	10%	118.60

3.8 Results of the Case Study

3.8.1 Scenario of a Single PV System

(1) Energy Savings of a PV System

This study assumes that a single PV system is installed in an urban distribution area, across the Atlanta metropolitan area. The main objective of the PV system is to reduce the consumption of electricity generated by non-solar plants. From the perspective of daily operations, Figure 34 presents the impact of the PV system on energy savings on the 244th day, which indicates that the PV system effectively reduces peak demand. Figure 35 presents a comparison of monthly total demand to the monthly generation of the PV system with a forty percent capacity of peak demand on the urban distribution

network, oriented at an azimuth angle of 180° (facing south) and a tilt angle of 30°. The PV system reduces total demand by the amount of monthly generation of the PV system.

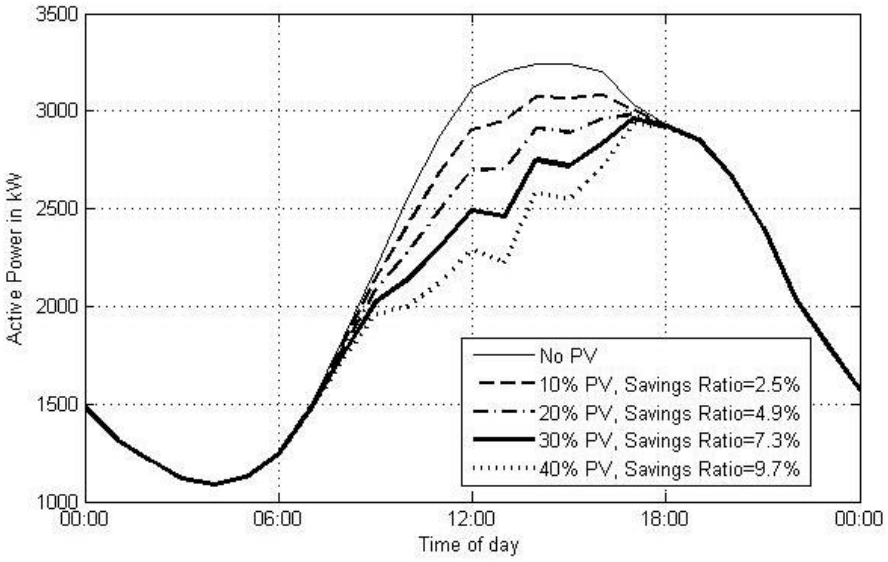

Figure 34. The effect of the PV system on residential customers on the 244th day in 2007.

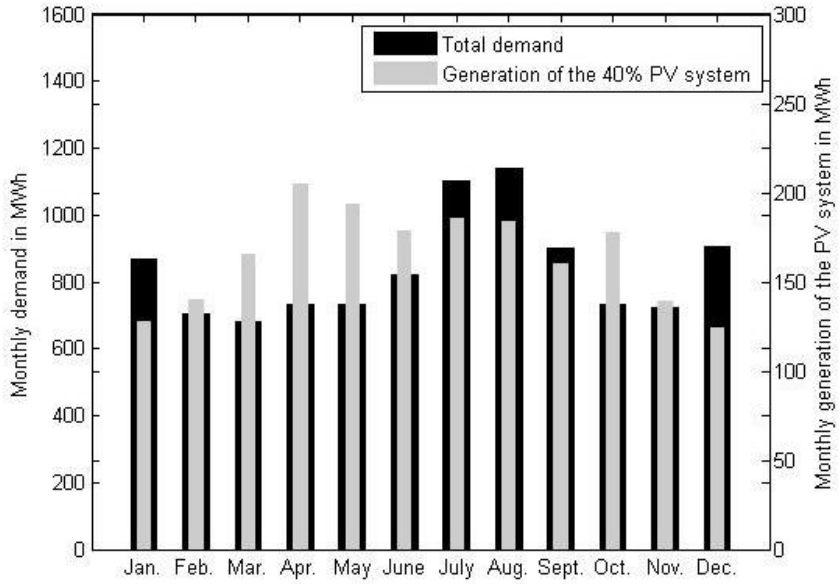

Figure 35. Monthly total demand and the monthly generation of the PV system for residential customers.

(2) Generation Cost Changes

The PV system, which reduces the amount of energy generated by non-solar plants from the perspective of daily and monthly operations, can also affect the costs of generating electricity. Table 11 shows savings in energy and changes in generation costs

of twenty buses on which a single PV system is installed for residential customers in hourly intervals in 2007. The cost of generating electricity of the PV system with a capacity of ten percent of total peak demand is 118.6 $/MWh, the predicted LCOE (levelized cost of electricity) of the United States for PV entering new service in 2019, which is still higher than the costs of the other generation types. Therefore, the PV system with a capacity of ten percent of total peak demand increases unit generation costs from 22.205 $/MWh to 25.680 $/MWh (the change rate of about +15.65 percent). Since the PV system operating on bus 79 saves the most energy, for simplicity, the results of other buses are omitted.

Table 11. Total energy, energy savings, and generation cost changes

Capacity of PV	PV Bus	Energy from Non-solar Plants	Energy Savings	Generation Costs	Cost Change	Unit Generation Costs
% of Peak		MWh/year/ household	kWh/year/ household	$/year/ household	$/year/ household	$/MWh
0%	-	10.0434	0	223.02	0	22.205
10%	79	9.4295	613.85	254.86	+31.84	25.680
15%	79	9.1725	870.87	275.12	+52.10	27.748
20%	79	8.9151	1128.32	297.05	+74.03	29.989
25%	79	8.6572	1386.17	319.98	+96.96	32.339
30%	79	8.3990	1644.38	343.55	+120.54	34.759
35%	79	8.1405	1902.88	367.73	+144.71	37.246
40%	79	7.8818	2161.61	392.41	+169.40	39.791

(3) Ecological Impact of the PV System

The PV system, while saving energy, also reduces the release of pollutants and greenhouse gases into the atmosphere by using less fuel from fossil-fuel plants. To analyze the ecological impact of the PV system, this study calculates the emission coefficients of each fuel type by averaging the amount of emissions emitted by each fuel type consumed for generating electricity divided by the amount of electricity generated from each fuel type in the United States from 1989 to 2008 [86]. Table 12 shows that while nuclear generation does not emit greenhouse gases and toxic pollutants, mining uranium, the enrichment process, and transportation of the fuel emit carbon dioxide [87]. The coefficients of water consumption by each fuel type are determined by the amount of

water required for cooling, which only accounts for the amount of evaporation [88, 89].

Table 12. Emission coefficients of various fuel types

Fuel	Emissions			Water
	CO_2 in kg/kWh	SO_2 in kg/kWh	NO_X in kg/kWh	Gallons/kWh
Coal	0.98053	0.0060729	0.00275	0.670
Gas	0.52532	0.0000029	0.00078	0.275
Nuclear	0.066	0	0	0.620
Hydroelectricity	0	0	0	18.000

Table 13 shows the ecological impact of the PV system. The PV system with a ten percent capacity of peak demand reduces CO_2 from 3.927 to 3.369 tons/year/household, SO_2 from 21.667 to 18.241 kg/year/household, NO_X from 9.802 to 8.250 kg/year/household, and water consumption from 6.414 to 5.998 kgal/year/household.

Table 13. Annual savings in emissions and water consumption of the PV system

Capacity of PV	PV Bus	Energy from Non-solar Plants	Emissions			Water
		MWh/year/ household	CO_2	SO_2	NO_X	kgal/ year/household
% of Peak			tons/year/household	kg/year/household	kg/year/household	
-	-	10.0434	3.927	21.667	9.802	6.414
10%	79	9.4295	3.369	18.241	8.250	5.998
15%	79	9.1725	3.199	17.224	7.790	5.830
20%	79	8.9151	3.062	16.426	7.429	5.663
25%	79	8.6572	2.946	15.771	7.133	5.498
30%	79	8.3990	2.844	15.207	6.878	5.333
35%	79	8.1405	2.753	14.717	6.656	5.169
40%	79	7.8818	2.673	14.294	6.465	5.005

3.8.2 Scenario of *N* Stochastically Dispersed PV Systems

(1) Energy Savings and Generation Cost Changes of N Stochastically Dispersed PV Systems

To analyze energy savings and changes in generation costs of stochastically dispersed PV systems, this study performs three stochastic simulations of 1,000 years. The unknown random variables are the system capacity, the azimuth angle, the tilt angle, and the module material of the PV system. Table 14 shows an annual statistical summary

of energy savings and generation cost changes, which indicates that PV systems with a ten percent capacity of total peak demand dispersed throughout the Atlanta area reduce the consumption of energy from 10.043 MWh/year/household to 9.367-9.658 MWh/year/household annually (change rates are from -3.8% to -6.7%). Since the costs of generating electricity of the PV system, 118.6 $/MWh, are still higher than those of the other generation types, the PV system increases the costs of generating electricity from 22.205 $/MWh to 27.808-28.467 $/MWh. In the first stochastic simulation, all random variables such as the system capacity, the azimuth angle, the tilt angle, and the module material of the PV system are uniformly distributed. In the second stochastic simulation, the system capacity and azimuth angle random variables are normally distributed, and in the third, this study applies importance sampling to the system capacity and azimuth angle random variables.

Table 14. Annual statistical summary of the energy savings and the generation cost changes of dispersed PV systems

Variance Reduction Method		Energy from Non-solar Plants	Energy Savings	Generation Cost	Unit Generation Cost
		MWh/year/household	kWh/year/household	$/year/household	$/MWh
Reference (No PV)		10.043	0	223.016	22.205
Naive (Uniform)	Min	9.367	436.020	263.842	28.166
	Avg	9.472	569.300	267.871	28.279
	Max	9.607	675.890	273.488	28.467
Naive (Truncated Normal)	Min	9.475	385.550	265.158	27.984
	Avg	9.552	490.720	269.137	28.175
	Max	9.658	568.160	272.844	28.251
Importance, stratification sampling	Min	9.504	410.340	264.297	27.808
	Avg	9.568	475.810	268.447	28.057
	Max	9.633	538.960	271.128	28.146

(2) Ecological Impact of N Stochastically Dispersed PV Systems

Table 15 presents an annual statistical summary of the ecological impact of *N* dispersed PV systems that decrease CO_2 from 3.927 to 3.328-3.555 tons/year/household (the change rates of which are from -9.5% to -15.3%), SO_2 from 21.667 to 17.996-19.373 kg/year/household (the change rates of which are -10.6% to -16.9%), NO_X from 9.802 to

8.139-8.763 kg/year/household (the change rates are from -10.6% to -17.0%), and water consumption from 6.414 to 5.957-6.150 kgal/year/household (the change rates are from -4.1% to -7.1%).

Table 15. Ecological impact of stochastically dispersed PV systems for the residential customer type

Variance Reduction Method		Energy from Non-solar Plants	Emissions			Water
		MWh/year/ household	CO_2 tons/year /household	SO_2 kg/year /household	NO_X kg/year /household	kgal/year/ household
Reference (No PV)		10.043	3.927	21.667	9.802	6.414
Naive (Uniform)	Min	9.367	3.328	17.996	8.139	5.957
	Avg	9.472	3.404	18.450	8.345	6.026
	Max	9.607	3.511	19.100	8.639	6.116
Naive (Truncated Normal)	Min	9.475	3.410	18.490	8.363	6.028
	Avg	9.552	3.469	18.844	8.523	6.080
	Max	9.658	3.555	19.373	8.763	6.150
Importance, stratification sampling	Min	9.504	3.433	18.628	8.426	6.048
	Avg	9.568	3.481	18.918	8.557	6.090
	Max	9.633	3.533	19.235	8.700	6.133

(3) Reduction of Variance and Stochastic Simulation Time

In the scenario of N residential PV systems stochastically dispersed throughout the urban distribution network, this study examines the expectation value of the annual output of PV systems, defined in equation (25), calculated by averaging the power output of residential PV systems stochastically installed on N households that produce a capacity of ten percent of total peak demand in hourly intervals annually.

To provide broader bounds for the metrics, this study applies, as a reference scenario, the interval arithmetic method, which often expresses the extent of uncertainty, to the proposed stochastic simulations. Typically, a south-facing PV system tilted at the latitude of the location on which it is installed receives maximum insolation [38, 82]. Therefore, an interval of the tilt angle random variable presented in Table 6 is [18.63°, 33.63°] or [33.63°, 48.63°] (in which the latitude of the Atlanta Hartsfield International Airport is 33.63°). An interval for the azimuth angle random variable is [135°, 180°] or [180°, 225°] (in which 180° indicates an azimuth angle facing south for maximum power production). An interval of the system capacity is [1kW, 20kW], which represents min

and max PV system capacities.

Table 16 shows that the expectation value and the variance of the annual power output of *N* dispersed PV systems in the reference scenario are 610.07 kWh/year/household and 151.14 kWh/year/household, respectively. In the second stochastic simulation, "Naive (Truncated Normal)" in Table 16, with the normally distributed system capacity and azimuth angle random variables, the expectation value and the variance of the annual power output of *N* dispersed PV systems are 569.39 kWh/year/household and 24.27 kWh/year/household, respectively. To reduce the variance of the annual power output of these PV systems, this study applies importance sampling to the random sampling of the system capacity and azimuth angle random variables and stratification sampling to the random sampling of the tilt angle random variable. As a result, the combination of both importance and stratification sampling reduces the variance of the power output of *N* dispersed residential PV systems from 151.14 kWh/year/household to 8.54 kWh/year/household with a variance reduction ratio of 17.69, calculated by equation (37). The reduced variance indicates that the expectation value more closely approaches the true value.

Table 16. Expectation value and variance of the annual output and the annual energy savings of *N* stochastically dispersed residential PV systems

Scenario	Period	Annual PV Production			Annual PV Energy Savings			Cluster	Time	Efficiency
		Expectation Value	Variance	VRR	Expectation Value	Variance	VRR			
	Year	kWh/year /household	kWh/year /household	-	kWh/year /household	kWh/year /household	-	-	Hour	-
Reference (Interval Arithmetic)	1,000	610.07	151.14	1.00	599.07	2573.50	1.00	No	382.03	1.00
Naive (Uniform)	1,000	589.92	78.12	1.93	569.30	1519.30	1.69	Yes	4.77	154.95
Naive (Truncated Normal)	1,000	569.39	24.27	6.23	490.72	671.56	3.83	Yes	5.72	415.92
Importance and Stratification Sampling	1,000	558.23	8.54	17.69	475.81	471.25	5.46	Yes	5.81	1163.11

This study determines the annual savings of the energy of PV systems

(determined by calculating the annual power flow of the test feeder enhanced by *N* stochastically dispersed residential PV systems in hourly intervals). The annual energy savings of the PV systems are less than the annual PV output because of the distribution loss of the test feeder in Table 16. Figure 36 shows variations among the annual energy savings of *N* stochastically dispersed residential PV systems in all scenarios, which indicates that the combination of importance sampling and stratification sampling reduces variance in the expectation value of the annual energy savings of PV systems, in other words, the expectation value approaches more closely to a true value.

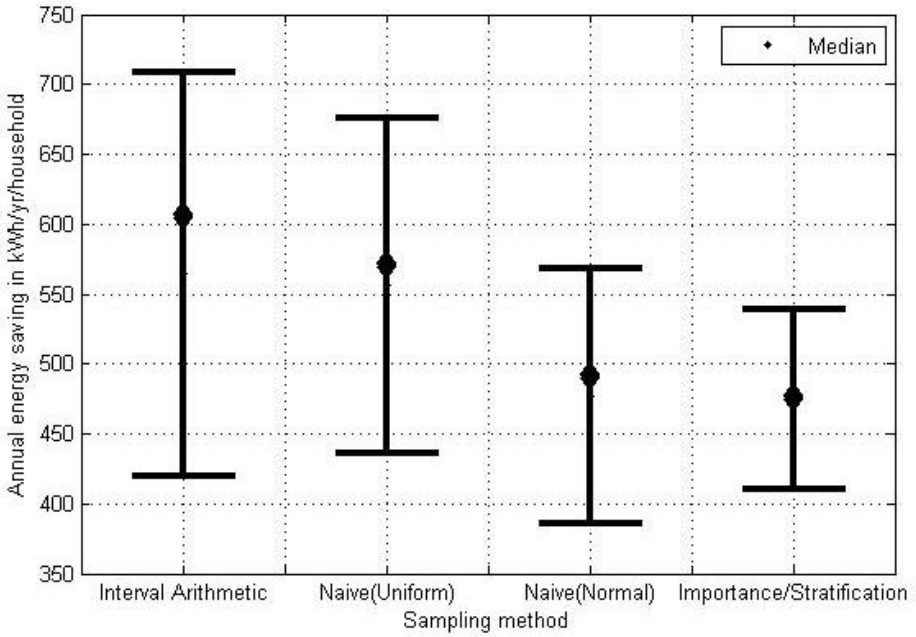

Figure 36. Annual energy savings of *N* dispersed PV systems with a capacity of ten percent of total peak demand during 1,000 years.

The power-flow calculation of the test feeder shows a tendency to increase variances in the energy savings of PV systems in kWh/year/household in Table 16. For example, in the scenario accelerated by importance and stratification sampling, the variance (471.25 kWh/year/household) in the energy savings of PV systems increases from that (8.54 kWh/year/household) of annual PV output. Figure 37 compares the histograms of the annual PV production to the annual energy savings of *N* dispersed PV systems in the scenario accelerated by importance and stratification sampling.

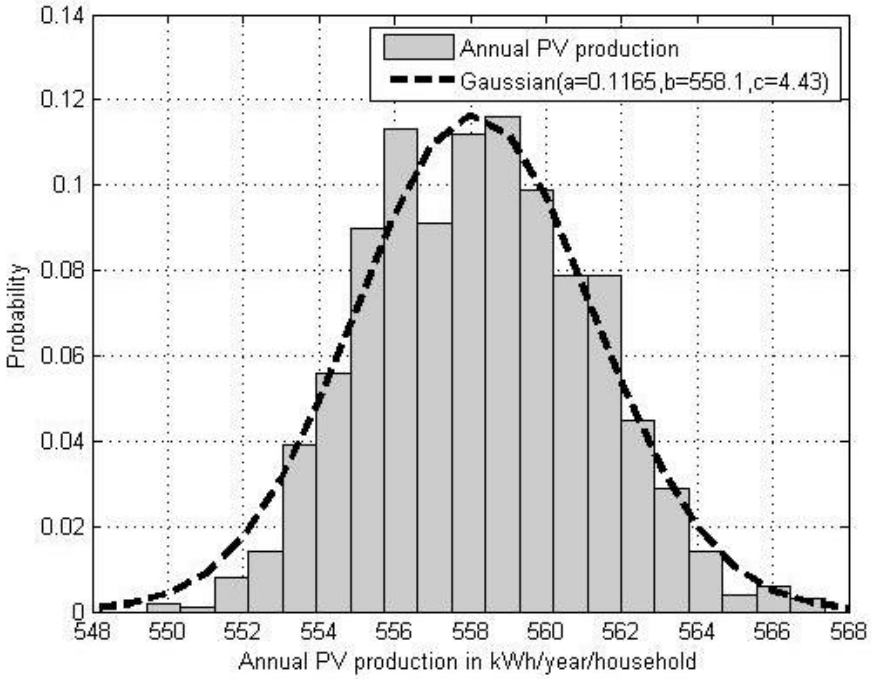

(a) Annual PV production

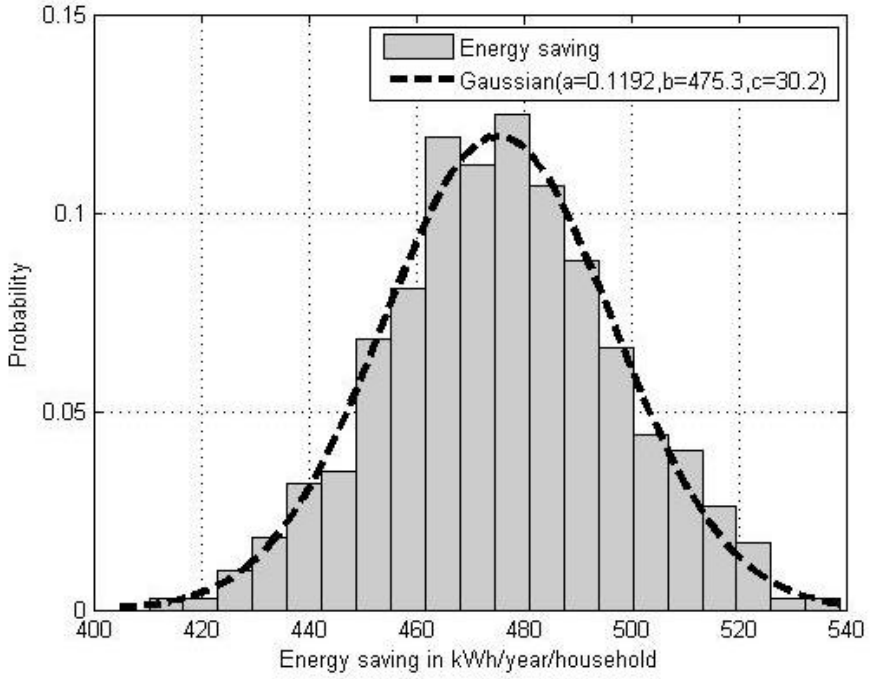

(b) Annual energy savings of PV systems

Figure 37. Histograms of the annual PV production and the annual energy savings of *N* dispersed PV systems in a scenario accelerated by importance and stratification sampling.

The annul PV outputs in Figure 37 (a) show a minimum of 548 kWh/year/household and a maximum of 568 kWh/year/household and the energy savings of PV systems in Figure 37 (b) indicate a minimum of 400 kWh/year/household and a

maximum of 540 kWh/year/household. The combination of importance and stratification sampling reduces variance in both the annual output and the energy savings of stochastically dispersed PV systems more than it does in other scenarios. In fact, in the case of the annual power output of PV systems, the combination of importance and stratification sampling decreases the variance of the annual power output of PV systems from 151.14 kWh/year/household to 8.54 kWh/year/household and the variance of energy savings from 2573.50 kWh/year/household to 471.25 kWh/year/household, which means these expectation values approach more closely to a true value.

To calculate power flow for 1,000 years in hourly intervals, the proposed algorithm takes an average of 0.157 seconds per power-flow calculation on a Dell OptiPlex 9020 desktop computer consisting of an Intel Core i7-4770 CPU with 32 GB of memory, a professional edition of Windows 7, and MATLAB 2014a. Therefore, without the acceleration by the sampling of representative clusters and extreme points, the stochastic simulations require $8{,}760 \times 1{,}000 \times 0.157$ sec ≈ 382.03 hours. To reduce the extremely heavy computational burden, a stochastic simulation time of 382.03 hours, this study applies the method of the sampling of representative clusters and extreme points to the proposed stochastic algorithm. As a result, the sampling of representative clusters and extreme points reduces the stochastic simulation time of 382.03 hours to 4.77-5.81 hours at an efficiency of 154.95-1163.11, calculated by equation (38).

3.9 Conclusion

The objective of this study has been (1) to propose tools and algorithms useful for designing, analyzing, and operating urban distribution networks enhanced by renewable DG (distributed generation) systems, particularly PV (photovoltaic) systems, (2) to address some of the issues in the analysis of their impact on such networks, and (3) to design a framework for streamlining the future development and the smooth integration of stochastic renewable DG systems into urban distribution networks. One difficulty in analyzing the impact of the DG system is the inherent uncertainties of its inputs, locations, and capacities, not known in the planning stage of the power system. Thus, to reduce the uncertainty of the DG system, this study has implemented a stochastic simulation algorithm combined with the algorithm for three-phase power-flow analysis based on the backward and forward sweep method developed in Chapter 2. Then, to reduce the number of computational steps, this study has accelerated this combined algorithm with the method of variance reduction, including the optimal near-normal distribution of importance sampling, and the sampling of representative clusters and extreme points. This study has proposed the IEEE 123-bus test feeder as a case study that incorporates load profiles obtained from an actual utility in kW in hourly intervals in 2007 and PV (photovoltaic) systems installed across the Atlanta area as the urban distribution area. Finally, this study has performed annual stochastic simulations in which a single PV system with a capacity scaled from ten to forty percent of total peak demand was installed across the distribution network. This study has also conducted three stochastic simulations of 1,000 years with unknown random variables: the azimuth angle, the title angle, the module, and the capacity of the residential PV system.

The results of the simulation of the case studies have shown that an urban distribution network enhanced by stochastically distributed PV systems can cope with peaks, save energy produced from non-solar plants, and reduce the release of pollutants

and greenhouse gases into the atmosphere by using less fuel from coal- and gas-fired plants. In fact, if (1) the power output of PV systems is estimated by solar radiation and meteorological data of the Atlanta area in TMY (typical meteorological year) data sets in hourly intervals and (2) the PV systems are stochastically dispersed throughout the IEEE 123-bus test feeder as an example of the urban distribution network with a capacity equal to ten percent of total peak demand, they can reduce the amount of energy produced from non-solar plants, particularly by about 3.8-6.7% in the case study (at the expense of higher costs of generating electricity resulting from high PV system costs). In the case study, they can also reduce about 9.5-15.3% of CO_2, 10.6-16.9% of SO_2, 10.6-17.0% of NO_X, and 4.1-7.1% of water consumption released by non-solar generating plants.

This study has presented a useful method for analyzing the impact of renewable DG systems, particularly PV systems, on urban distribution networks and produced useful results. For instance, this study has found that if unknown random variables in their input and output can be approximated by a (truncated) normal distribution, the optimal near-normal distribution of importance sampling can be extended so that it reduces variance in unknown random variables in the analysis of the effect of various DG systems (including PV systems, wind farms, and microturbines). In addition, this study has shown that the method of sampling representative clusters and extreme points effectively reduces a stochastic simulation time. However, these results did not apply to the rapidly decreasing price of commercial- and utility-scale PV systems, but they can be extended to such a case by modeling distribution networks enhanced by commercial- and utility-scale PV systems and determining their impact on such networks. In addition, this study did not apply to PV tracking systems, which produce much more energy than fixed PV systems. If this study conducts such an analysis, it can analyze the strong effect of PV systems on energy savings and changes in the generation costs.

CHAPTER 4

RELIABILITY ENHANCEMENT THROUGH A RECONFIGURATION OF URBAN DISTRIBUTION NETWORKS ENHANCED BY DISTRIBUTED GENERATION

4.1 Overview

One of the main concerns of utilities is to improve reliability or to minimize the frequency and the duration of failure of their distribution networks. A commonly used method of improving reliability is to optimally place protection devices such as breakers, switches, fuses, and reclosers within the distribution network. Nowadays, since small-scale, local, and decentralized DG (distributed generation) systems, particularly the PV (photovoltaic) system in this study, have been incorporated into power systems, the optimization problem for the strategic placement of protection devices has to be solved for urban distribution networks enhanced by DG systems. Thus, this study proposes a genetic algorithm that determines the optimal allocation of protection devices (i.e., the recloser, the fuse, and the switch) on urban distribution networks enhanced by the DG system and analyzes the impact of both the DG system and the protection device on the reliability of the urban distribution network.

4.2 Introduction

The method of evaluating the reliability of a distribution network can be classified into three methods: (1) the analytical method that provided a mathematical model of the reliability configuration and the mean value of the reliability index [44-46], (2) the stochastic method (or the Monte Carlo method) that evaluated the variability of the reliability index [47, 48], and (3) many heuristic search algorithms that proposed near-optimal solutions that maximize the reliability of conventional feeders protected by

reclosers and switches [51, 52, 57]. These analytical, stochastic methods, and evolutionary algorithms, however, are not capable of analyzing the urban distribution network housing a combination of fuses, switches, reclosers, and high-capacity DG systems. Therefore, the objective of this study is to propose tools and algorithms useful for planning, designing, and operating such a network from the standpoint of reliability and to address some of the issues in the analysis of the impact of DG systems and protection devices on the reliability of such a network. To determine the reliability index of a more practical distribution network housing a combination of fuses, switches, and reclosers, this study proposes an analytical method of implementing the backward and forward sweep method by KCL (Kirchhoff's current law) and KVL (Kirchhoff's voltage law) and presents a two-stage optimization method that improves the reliability of the urban distribution network enhanced by DG systems, particularly those with renewable PV systems and protection devices. In addition, the study verifies the proposed optimization algorithm using the IEEE 34-bus test feeder without the DG system and the IEEE 123-bus test feeder enhanced by twenty DG systems. Finally, it analyzes the impact of both the DG system, including the effect of the islanded operation of the DG system, and the protection device on the reliability of the urban distribution network.

4.3 Reliability Theory

4.3.1 Reliability Index

The objective of the reliability index is to quantify the reliability of the power system by calculating the average duration and the frequency of interruption. The standard reliability index that utilities have used for many years is formulated in [44]. Seven representative reliability indices are defined as follows:

$$System\ average\ interruption\ frequency\ index\ (SAIFI) = \frac{\sum \lambda_i N_i}{\sum N_i} in\ \ freq / customer / year\ , \qquad (41)$$

$$System\ average\ interruption\ duration\ index\ (SAIDI) = \frac{\sum \lambda_i r_i N_i}{\sum N_i}\ in\ hour / customer / year\ , \quad (42)$$

$$Customer\ average\ interruption\ duration\ index = \frac{\sum \lambda_i r_i N_i}{\sum \lambda_i N_i} = \frac{SAIDI}{SAIFI}\ in\ hour /\ freq\ , \quad (43)$$

$$Average\ service\ availability\ index\ (ASAI) = \left(8760 - SAIDI\right)/8760\ , \quad (44)$$

$$Average\ service\ unavailability\ index\ = 1 - ASAI\ , \quad (45)$$

$$Energy\ not\ supplied\ (ENS)\ index = \sum \lambda_i r_i L_i\ in\ kWh / year\ , \quad (46)$$

$$Average\ energy\ not\ supplied\ index = \frac{\sum \lambda_i r_i L_i}{\sum N_i}\ in\ kWh / customer / year\ , \quad (47)$$

where

λ_i = the failure rate in *freq/year* or *freq/year/km*,

N_i = the number of customers,

r_i = the repair time in *hours*,

L_i = demand in *kW*.

4.3.2 Reliability Evaluation by the Analytical Method

Methods for the evaluation of reliability can be classified into the analytical method [44, 45] and the time-sequential stochastic simulation method [47, 48]. The former represents the mathematical model of the network and calculates the mean values of the frequency and the duration of the system interruption of each load point (or bus) affected by faults on all main and lateral feeders. The latter method is to perform a time-sequential stochastic simulation that provides the variability of the reliability index.

In order to illustrate the analytical method, this study presents a simple radial distribution network in Figure 38, load points *A*, *B*, and *C*, which are protected by fuses on each first lateral feeder and connected to a main feeder. The basic parameters for the evaluation of the reliability of such a network are the average failure rate, λ, and the average outage duration, *r*. Individual failure data are as follows:

(1) *The main feeder*. The failure rate, λ_m, in *freq/year/km*, the average repair time, r_m, in *hours*, and the manually switching time of the disconnection switch, r_s, in *hours*.

(2) *The lateral feeder*. The failure rate, λ_l, in *freq/year/km* and the average repair time, r_l, in *hours*.

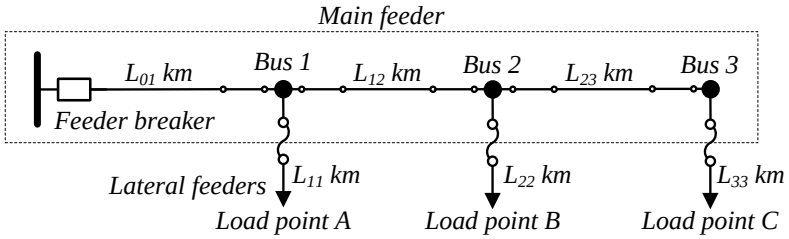

Figure 38. A distribution network with three buses.

The analytical method examines the failure effect on the main, lateral feeders, and the load points, shown in Table 17. This study assumes that the feeder breaker, the bus, and the substation transformer are completely reliable. The reliability indices of the simple radial distribution network can be calculated as follows:

$$SAIFI = \sum_{i=A}^{C} \lambda_i N_i \,/\, \sum_{i=A}^{C} N_i \,, \tag{48}$$

$$SAIDI = \sum_{i=A}^{C} \lambda_i r_i N_i \,/\, \sum_{i=A}^{C} N_i \,, \tag{49}$$

Other reliability indices can be calculated by (43)-(47).

Table 17. An example of evaluating reliability using the analytical method

Section		Load point *A*			Load point *B*			Load point *C*		
		λ	r	$\lambda \cdot r$	λ	r	$\lambda \cdot r$	λ	r	$\lambda \cdot r$
		freq/year	*hour/freq*	*hour/year*	*freq/year*	*hour/freq*	*hour/year*	*freq/year*	*hour/freq*	*hour/year*
Main	L_{01}	$\lambda_m \cdot L_{01}$	r_m	$\lambda_m \cdot L_{01} \cdot r_m$	$\lambda_m \cdot L_{01}$	r_m	$\lambda_m \cdot L_{01} \cdot r_m$	$\lambda_m \cdot L_{01}$	r_m	$\lambda_m \cdot L_{01} \cdot r_m$
	L_{12}	$\lambda_m \cdot L_{12}$	r_s	$\lambda_m \cdot L_{12} \cdot r_s$	$\lambda_m \cdot L_{12}$	r_m	$\lambda_m \cdot L_{12} \cdot r_m$	$\lambda_m \cdot L_{12}$	r_m	$\lambda_m \cdot L_{12} \cdot r_m$
	L_{23}	$\lambda_m \cdot L_{23}$	r_s	$\lambda_m \cdot L_{23} \cdot r_s$	$\lambda_m \cdot L_{23}$	r_s	$\lambda_m \cdot L_{23} \cdot r_s$	$\lambda_m \cdot L_{23}$	r_m	$\lambda_m \cdot L_{23} \cdot r_m$
Lateral	L_{11}	$\lambda_l \cdot L_{11}$	r_l	$\lambda_l \cdot L_{11} \cdot r_l$	-	-	-	-	-	-
	L_{22}	-	-	-	$\lambda_l \cdot L_{22}$	r_l	$\lambda_l \cdot L_{22} \cdot r_l$	-	-	-
	L_{33}	-	-	-	-	-	-	$\lambda_l \cdot L_{33}$	r_l	$\lambda_l \cdot L_{33} \cdot r_l$
Customers		N_A			N_B			N_C		
Σ	-	λ_A	r_A	$\lambda_A \cdot r_A$	λ_B	r_B	$\lambda_B \cdot r_B$	λ_C	r_C	$\lambda_C \cdot r_C$

4.3.3 Analytical Method for Modern Urban Distribution Networks

The analytical method for evaluating reliability is useful for planning, designing, and operating distribution networks because it can calculate the expected value of the reliability index. However, both the analytical and stochastic methods do not evaluate the reliability of the urban distribution network housing a combination of switches, fuses, reclosers, and the DG system. Thus, the mathematical representation of the reliability of the distribution network using the analytical method presented from [44] is extremely intricate.

As mentioned before, this study proposes an analytical method for the urban distribution network housing a combination of fuses and reclosers that implements the backward and forward sweep method, based on KCL (Kirchhoff's current law) and KVL (Kirchhoff's voltage law). The method, which analyzes the effect of the fuse, the switch, and the recloser on reliability, generates all possible permanent and transient faults on the main and lateral feeders in the following processes. First, the backward sweep sums up the fault current flowing at each bus. Since this method does not require the exact magnitude of the short-circuit current, the fault current is nonzero or zero. Then the second backward sweep searches all buses from the fault bus to the root bus. In the case of a transient fault, if a recloser detects the fault current, it will successfully reclose so that it can prevent downstream fuses from burning. In the case of a permanent fault, the upstream recloser disconnects more customers because it eventually opens, referred to as the "recloser lock-out state." If the recloser is not on the feeder, only the nearest upstream fuse will blow. If several reclosers are on the feeder, the method examines the priority of reclosers. Then the backward and forward sweeps calculate drops in the voltage, the on-off states of the line, and the frequency and the duration of the failure. Figure 39 shows the procedure of the analytical method for the urban distribution network. The optimal priority setting of reclosers is outside the scope of this study. The validation of this method is presented in Section 4.7.1.

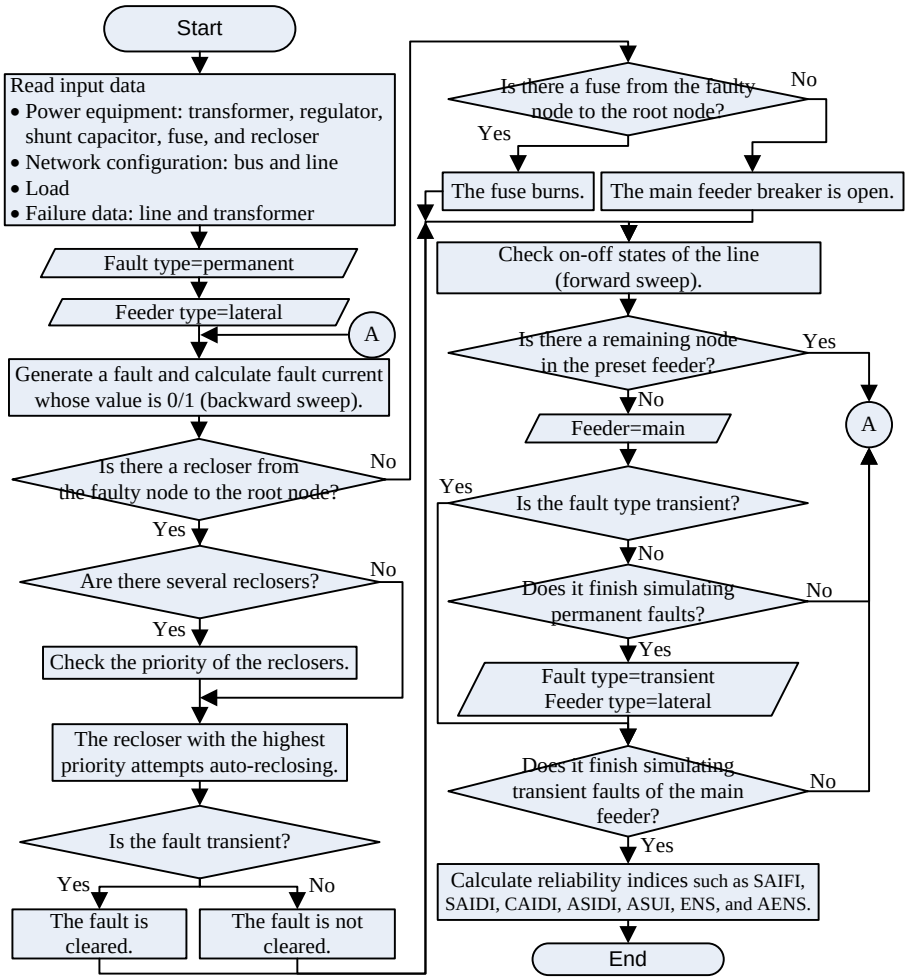

Figure 39. Flowchart of the analytical method for the urban distribution network.

4.4 Enhancement of Reliability

4.4.1 Effect of the Protection Device on Reliability

To enhance the reliability of distribution networks, many studies have investigated the effects of protection devices, particularly the recloser. One study suggested that a recloser placed in the middle of a distribution line might improve feeder-wide reliability by about 25 percent [51]. Another study showed that the three reclosing operations of the recloser could prevent nearly 93 percent of faults [58]. In addition, a recent study showed that downstream transient faults prevented by the recloser could improve the SAIDI, but not the SAIFI [59]. To determine the effect of protection devices on the reliability of the distribution network, [46] proposed various protection schemes,

or protection schemes 1-6, presented in Table 18.

Table 18. The protection schemes for the improvement of reliability

Protection Scheme Number	Fuse	Disconnect Switch	Alternative Supply	Transformer	Recloser on Main Branch	Recloser on Each Lateral
1 [45]	No	No	No	Repair	Not Applicable	Not Applicable
2 [45]	No	Yes	No	Repair	Not Applicable	Not Applicable
3 [45]	No	Yes	Yes	Repair	Not Applicable	Not Applicable
4 [45]	Yes	No	No	Repair	Not Applicable	Not Applicable
5 [45]	Yes	Yes	Yes	Repair	Not Applicable	Not Applicable
6 [45]	Yes	Yes	Yes	Replacement	Not Applicable	Not Applicable
7	Yes	Yes	No	Repair	No	No
8	Yes	Yes	No	Repair	Yes	No
9	Yes	Yes	No	Repair	Yes	Yes

To determine the effect of protection devices, particularly the recloser, on the reliability of the urban distribution network, this study adds protection schemes 7-9, presented in Table 18, and examines only the fuse-saving strategy typically used in urban distribution networks. Faults in the distribution network can be classified into both permanent (sustained) and transient (momentary) faults. In the case of the transient fault, the recloser initially operates before burning a fuse, so the recloser can prevent a downstream fuse from burning. That is, if a recloser detects the fault current, it opens at a pre-set time and then recloses, repeating auto-reclosing multiple times. This study assumes that the recloser prevents downstream transient faults at a success rate of 100 percent. In the case of a permanent fault, the recloser will eventually open because it still detects the fault current, referred to as the "recloser-lockout" state.

4.4.2 Islanded Operation of DG

In case of an outage, DG may be able to provide a distribution network with some power, especially when equipped with storage, so the network supplied by the DG, referred to as the "DG-enhanced distribution network," will not experience an outage. In fact, the distribution network becomes an "island" on which DG can continue providing power. A DG-enhanced distribution network requires the following conditions before, during, and after an islanded operation [14]:

(1) Before an islanded operation, DG should be able to supply the island with

sufficient power to maintain the voltage and the frequency within an acceptable range, typically within 0.95 to 1.05 PU of the rated (or nominal) voltage level and within the limits of 59.7 and 60.3 Hz of the frequency in the case of DG units with an aggregate rating of less than or equal 500 kVA. Protection devices within the island should be capable of communicating with protection devices outside of the island, detecting the islanded operation, and immediately disconnecting DG.

(2) If the power of DG and load matches within an acceptable range, the protection devices on the island can separate it from the nearby distribution system within two seconds and begin an islanded operation.

(3) After the islanded operation, if the fault is cleared, DG should be able to stop producing power, and protection devices should immediately be able to disconnect DG, referred to as an "anti-islanding operation."

The islanded operation of DG systems can reduce the outage time of customers and the strategic placement of protection devices (i.e., the recloser, the fuse, and the switch) and DG systems, particularly the PV systems in this study, can maximize reliability. To examine the effect of DG systems that enable an islanded operation from the perspective of long-term, typically annual operation, this study assumes that the DG-enhanced distribution network can begin an islanded operation if the following three conditions are satisfied:

(1) The total generation of DG systems within a particular zone, which indicates a possible "island" preset with the coordinating rule of protection in the planning stage of the power system, should exceed the total load of a zone. Figure 40 illustrates an islanded operation on a particular summer day for residential customers. The total generation of a zone with DG systems with a capacity of ten, twenty, and thirty percent of total demand does not exceed the total load of the zone, which suggests that the zone cannot become an island. However, the total generation of the zone with DG systems with a capacity of forty and eighty

percent of total demand exceeds the total load of the zone approximately three to eight hours a day, which corresponds to hours below zero in the y-axis in Figure 40 and indicates that the zone can become an island at that time.

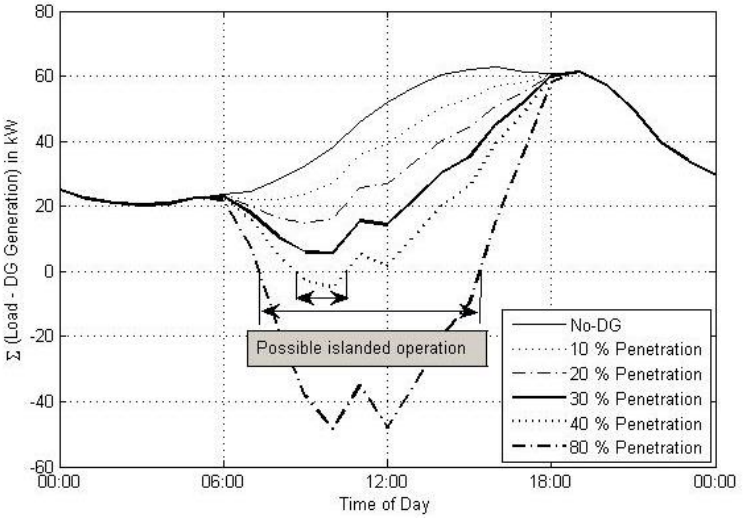

Figure 40. Reduction in the total load of the zone caused from DG systems with various capacities on a summer day.

(2) Protection devices that can communicate with protection devices outside of the zone should be installed at the connection point of the zone.

(3) This study assumes that protection devices such fuses and reclosers are fully reliable and voltage regulators located on urban distribution networks maintain voltages within a range of ± 5% of the rated voltage level (0.95 PU to 1.05 PU).

4.4.3 Determination of the Effect of Islanded Operation

An islanded operation of a DG-enhanced distribution network that satisfies the three conditions of sufficient generation, available protection devices, and fully reliable voltage regulators can improve reliability. In other words, an island operation reduces the duration of the fault by the time percentage of the total generation of DG systems within the zone that exceeds the total load of the zone. To determine the effect of an islanded operation from a long-term perspective, this study compares the total generation of DG systems within the zone to the total load within the zone during one year. Let the total load and the total generation of DG systems within the zone be discrete-time functions,

P_{LOAD} and P_{DG}, respectively. The time percentage of zone k that exceeds the total load of the zone is then calculated as follows [52]:

$$p_k = length\left(\sum_{i \in I} P_{i,LOAD} \le \sum_{i \in I} P_{i,DG}\right) / N \,, \qquad (50)$$

where

$I \in \{i | i$ = buses within the zone$\}$,

P_{LOAD} = the total load of the zone in kW in hourly intervals during one year,

P_{DG} = the total generation of DG systems of the zone in kW in hourly intervals during one year, and

N = the length of the entire time.

4.5 Genetic Algorithm

One of the most common methods of improving the reliability of the urban distribution network is to optimally place protection devices such as breakers, switches, fuses, and reclosers within such a network. The strategic placement of protection devices and DG systems can be formulated as an optimization problem. Because of the large size of the search space of the optimization problem and the inherent complexity of the power system, to solve the problem for the strategic placement of protection devices, this study proposes using a genetic algorithm. Mimicking the natural process of evolutionary reproduction toward better offspring, this algorithm approaches a globally optimal solution through the iterative selection of the "fittest" offspring, the reproduction of new offspring, the interchange of good genetic material by "crossover," and the exploration of new offspring by "mutation." The selection process evaluates the fitness of each population and selects better populations for reproduction. The algorithm implements the "survival of the fittest"; that is, the fittest offspring is likely to survive to the next generation. Many studies have presented selection models such as the fitness-based roulette model, the scaled roulette model, the tournament model, and the elitist model

[53-55]. The superiority of the genetic algorithm arises from its crossover and mutation operation. The crossover operation generates a better solution by exchanging genetic information. Crossover occurs with crossover probability (P_c) in the range of 0.5-1.0 [53, 56]. Better populations experiencing changes approach the best population in the mutation operation while avoiding convergence to the local minimum. Mutation occurs with mutation probability (P_m) in the range of 0.005-0.1 [53, 56].

4.5.1 Objective Function

The objective function of the proposed genetic algorithm minimizes (a) the SAIFI and the SAIDI of the urban distribution network without DG and (b) the SAIFI, the SAIDI, ENS, and loss of the DG-enhanced distribution network. Since protection scheme 2 in Table 18 has the same condition as protection schemes 7-9, excluding the condition of the fuse and the recloser, this study uses protection scheme 2 as the reference protection scheme, in which fuses, reclosers, and an alternative supply are not available, faulty transformers are repaired, and disconnect switches are available. Hence, the protection scheme 2 is the worst case. Then, this study normalizes the objective function by the reference reliability index (the index of the worst case).

(1) Urban Distribution Network Without DG

$$Minimize\, C_i\left(SAIFI_i, SAIDI_i\right) = W_{SAIFI}\frac{SAIFI_i}{SAIFI_{REF}} + W_{SAIDI}\frac{SAIDI_i}{SAIDI_{REF}}, \qquad (51)$$

$$\sum_{I\in\{SAIFI,SAIDI\}} W_I = 1, \qquad (52)$$

where $\{SAIFI, SAIDI\}_{REF}$ = the reliability indices of protection scheme 2 in Table 18.

(2) DG-Enhanced Urban Distribution Network

$$Minimize\, C_i(SAIFI_i, SAIDI_i, ENS_i, Loss_i) = W_{SAIFI}\frac{SAIFI_i}{SAIFI_{REF}} + W_{SAIDI}\frac{SAIDI_i}{SAIDI_{REF}} + W_{ENS}\frac{ENS_i}{ENS_{REF}} + W_{Loss}\frac{Loss_i}{Loss_{REF}}, \qquad (53)$$

$$\sum_{I \in \{SAIFI, SAIDI, ENS, Loss\}} W_I = 1, \tag{54}$$

where $\{SAIFI, SAIDI, ENS, Loss\}_{REF}$ = the reliability indices of protection scheme 2 in Table 18.

4.5.2 Implementation of the Genetic Algorithm

To solve the problem for the strategic placement of protection devices, this study implements the genetic algorithm in the following steps:

Step 1. Initialization. The genetic algorithm reads as input data power equipment, the network configuration, and reliability parameters of the urban distribution network and initializes a first-generation population with uniformly distributed random numbers. The population, referred to as "the solution," is a set of the positions of the protection devices.

Step 2. Calculation of fitness. The algorithm evaluates the fitness of the population. The objective function determines fitness using the analytical method presented in Section 4.3.3.

Step 3. Selection and reproduction. The algorithm calculates the probability of a scaled roulette, counts random picks on the roulette, and reproduces the population that continues to the next generation as a result of the number of counted picks.

Step 4. Crossover. The algorithm exchanges genetic information between two populations to create better populations by implementing arithmetic crossover operations with probabilities of 0.5, 0.8, or 1.0 [24, 53, 56].

Step 5. Mutation. The better populations experience mutation operations to avoid convergence to a local minimum. The algorithm implements uniform mutation operations with a probability of 0.018 per population [24, 53, 56].

Step 6. Convergence. If the algorithm determines a single best population (referred to as a "solution"), then it terminates. Otherwise, it repeats steps 2 through 5.

The parameters of crossover, mutation, a population size, and the number of

generations should typically be fine-tuned by pre-experimental assumptions. For example, a higher crossover probability (P_c) generates new solutions that disrupt fitness. However, lower P_c may not yield sufficient changes, so the genetic algorithm approaches a local minimum. A higher mutation probability (P_m) transforms the genetic algorithm into a random search algorithm, so it fails to converge while lower P_m can cause a premature problem. To solve the problem of the strategic placement of protection devices, a scaled roulette, an arithmetic crossover, a uniform mutation, and the parameters of the genetic algorithm are implemented by trial and error optimization. Table 19 shows the parameters of a genetic algorithm that solves the optimal allocation of protection devices.

Table 19. Parameters of the genetic algorithm

Operation	Method	Parameter
Selection	Scaled Roulette [24]	q=0.08
Crossover	Arithmetic Crossover [24, 53, 56]	P_c=1.0
Mutation	Uniform Mutation [24, 53, 56]	P_m=0.018
Weights	Feeder without DG	W_{SAIFI}=50%, W_{SAIDI}=50%
	DG-Enhanced Feeder	W_{SAIFI}=25%, W_{SAIDI}=25%, W_{ENS}=25%, W_{LOSS}=25%
Experiment Data	Population Size	50
	The Number of Generations	50
	The Number of Experiments	100

4.5.3 Two-Stage Optimization of the Genetic Algorithm

The main strength of the proposed genetic algorithm is to investigate the reliability of the urban distribution network housing a combination of fuses, switches, and reclosers. For this purpose, this study proposes two-stage optimization that addresses the following features of the modern distribution network:

(1) *The various operating characteristics of protection devices*. The fuse, typically located on incoming lateral feeders, interrupts the fault current by burning out. The recloser is a circuit breaker that can automatically reclose multiple times if it opens because of a transient fault.

(2) *The number of each protection device installed*. We commonly use the least costly protection device, a fuse. Because of its high cost, a recloser may not be installed on the distribution network. Thus, the number of fuses typically exceeds that of reclosers.

(3) *The problem of the size of the search space*. Simultaneously solving a problem pertaining to the optimal allocation of fuses and reclosers requires an enormous search space, so such an approach may not be possible.

Because of these characteristics, the proposed genetic algorithm initially finds the optimal positions of fuses on urban distribution networks. Then, it determines the optimal positions of reclosers, typically from one to three or one to five reclosers, on urban distribution networks optimized with fuses.

4.6 Case Study

4.6.1 Urban Distribution Networks

The IEEE PES Distribution System Analysis Subcommittee proposed 4-, 13-, 34-, 37-, 123-, and 8,500-bus feeders for research study purposes [23, 41]. These feeders, characterized by extremely complex configurations, several switches for alternative paths, voltage regulators, and shunt capacitor banks have the characteristics of urban distribution networks. Thus, this study uses the IEEE 34-bus test feeder as an urban distribution network without DG and the 123-bus test feeder as a DG-enhanced feeder. Table 20 shows the IEEE 123-bus test feeder enhanced by arbitrarily selected twenty DG systems, particularly the PV system in this study. This study selects, as the main feeder, buses from 800 to 840 of the IEEE 34-bus feeder and buses from 150 to 300 of the 123-bus test feeder and uses reliability parameters such as the typical failure rates and durations presented in [45] and in Appendix F. This study also assumes that the permanent and transient fault rates are 0.2 and 0.8, respectively [90].

Table 20. The IEEE 123-bus test feeder enhanced by twenty DG systems

DG	DG Position (20)	6,11,24,32,35,46,50,55,58,65,68, 75,79,82,88,95,100,104,106,114
	DG Type	PV oriented at the 180° azimuth (facing south) and 30° title angles
	Location (Weather Data)	Atlanta (TMY2)
	Total Capacity (% of Peak)	0%, 10%, 50%, 100%
Load	Feeder Type	IEEE 123-bus test feeder
	Peak Load	3,554.61 kW
	Load Profile (Customer Type) [42]	Residential load profile in hourly intervals in 2007
	Customers	1,000

Energy not supplied (ENS), which shows the effect of DG on reliability, is the expected value of energy not supplied as a result of a power outage. In fact, the more power DG injects into the distribution network, the less ENS the distribution network experiences because of the reduction in demand. To examine ENS from the standpoint of long-term operation when twenty DG systems are available, this study calculates the power flow of the IEEE 123-bus test feeder in hourly intervals of residential customers in 2007 (using the power-flow algorithm developed in Chapter 2) [91, 92].

4.6.2 Test Feeders Coordinated by a Simple Protection Strategy

Most optimization problems require an extremely large search space. For example, the total number of possible combinations of fuses in the IEEE 34-bus test feeder with 55 possible locations is $2^{55} \approx 3.603 \times 10^{16}$, the enumeration of which is computationally impossible. Thus, to reduce the number of possible locations, this study proposes the following two protection strategies [93]:

(1) A protection device that isolates the permanent faults of the local load, the transformer, and the voltage regulator is installed on the main feeder.

(2) In the IEEE 34-bus test feeder, the protection device that isolates the permanent faults of the lateral feeder is installed. To determine the effect of the islanded operation, this study divides the IEEE 123-bus test feeder into nineteen zones and installs the protection devices to isolate permanent faults in the zones in Figure 41. (The optimal partitioning of zones is outside the scope of this study.)

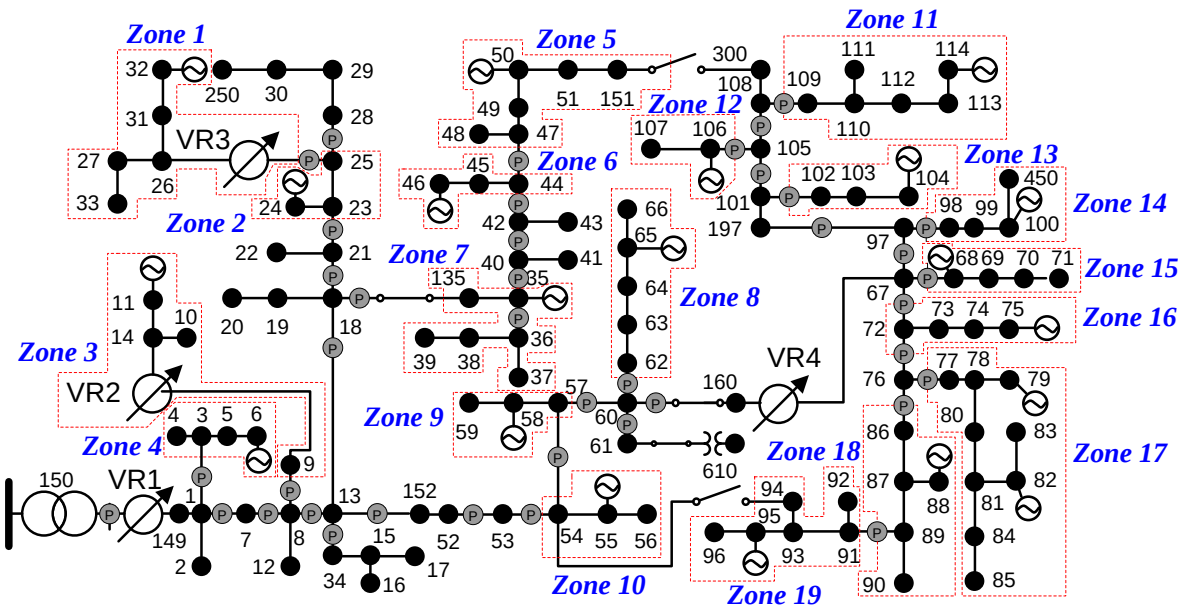

Figure 41. Zones of the IEEE 123-bus test feeder (19 zones and 40 possible locations of the protection device).

As a result of the two protection strategies, the number of possible locations of the protection device in the IEEE 34-bus test feeders decreases from 55 to 23 and in the IEEE 123-bus feeders from 131 to 40, shown in Table 21. A detailed illustration of the positions of the protection devices is presented in Appendix F. If the reduction in the number of protection devices significantly impacts the objective function, the solution that proposes a reduced number of protection devices cannot enhance reliability. Figure 42 shows the trend of the objective function for the number of fuses installed on the IEEE 123-bus test feeder; that is, the objective function decreases as more fuses are installed. However, the objective function is saturated when the number of fuses reaches approximately thirteen. In fact, thirteen or more fuses do not significantly decrease the objective function. In other words, it is neither practical nor economical for a fuse to be installed on every line segment. Therefore, this study selects a maximum number of protection devices, referred to as the "knee-point" number, of around 85 or more percentage reduction point of the objective function in Table 21. Similarly, since it may be wasteful for greater than five reclosers to be installed, this study finds the optimal positions of from either one to three or one to five reclosers.

Table 21. The number of possible protection devices

Test Feeder Name	DG	The Number of Possible Positions	The Reduced Number of Possible Positions	The Maximum Number of Positions of Protection Devices		The Maximum Number of Reclosers
				Knee-Point	Reduction Rate of the Objective Function	
IEEE 34-Bus	No	55	23	8	86.19 %	1~3
IEEE 123-Bus	Yes	131	40	13	87.59 %	1~5

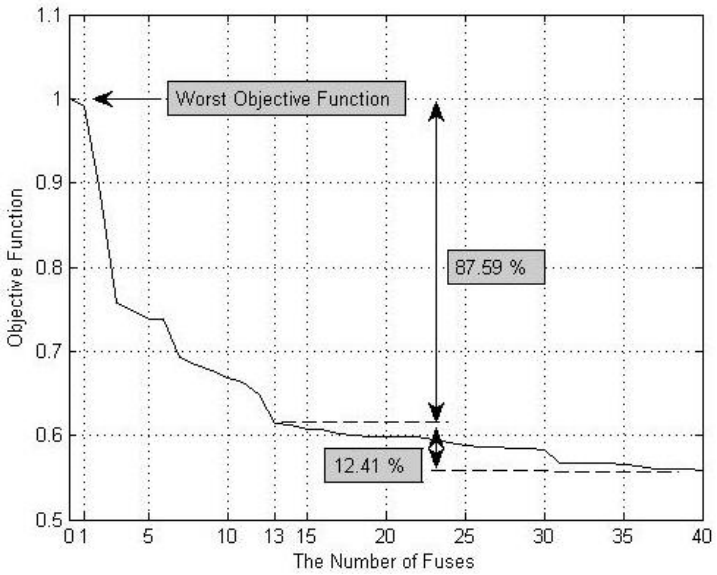

Figure 42. Objective function for the number of fuses in the IEEE 123-bus test feeder.

4.7 Results of the Case Study

4.7.1 Evaluation of Reliability

The Power System Research Group at the University of Saskatchewan developed an educational test system, the Roy Billinton Test System (RBTS), which consists of five load busbars from buses 2 to 6 and practical elements such as transformers, switches, busbars, lines, and cables [45]. This study evaluates the reliability of bus 4 of the RBTS in Table 22, in which the proposed algorithm shows the same results as those in [45]. In Table 22, this study also evaluates the reliability of the IEEE 34-bus test feeder with protection schemes 1 to 9, presented in Table 18. In Table 22 and Table 23, since protection schemes 4 to 7 contain fuses, they reduce the SAIFI considerably. Because protection schemes 5 and 6 provide the alterative supply, they significantly reduce the SAIDI. In protection schemes 7 and 8 in Table 23, downstream transient faults prevented

by the recloser and permanent faults causing the recloser-lockout state increase the SAIFI. However, in protection schemes 7 to 9, the reclosers installed on every lateral branch decrease the SAIDI.

Table 22. Reliability index of bus 4 of RBTS

Protection Scheme	Solution	SAIFI	SAIDI	ASAI	ENS	AENS
		freq/year /customer	hours/year /customer	-	kWh/year	kWh/year /customer
1	RBTS solution [45]	0.682	24.64	0.997187	374085	78.28
	Solution from proposed analytical method	0.682	24.64	0.997187	374075	78.28
2	RBTS solution [45]	0.682	12.45	0.998579	225985	47.29
	Solution from proposed analytical method	0.682	12.45	0.998579	225978	47.29
3	RBTS solution [45]	0.682	5.44	0.999379	88403	18.50
	Solution from proposed analytical method	0.682	5.44	0.999379	88400	18.50
4	RBTS solution [45]	0.300	4.42	0.999496	74013	15.49
	Solution from proposed analytical method	0.300	4.42	0.999496	74007	15.49
5	RBTS solution [45]	0.300	3.47	0.999604	54293	11.36
	Solution from proposed analytical method	0.300	3.47	0.999604	54291	11.36
6	RBTS solution [45]	0.300	0.62	0.999929	12740	2.67
	Solution from proposed analytical method	0.300	0.62	0.999929	12738	2.67

Table 23. Reliability index of the IEEE 34-bus test feeder

Protection Scheme	SAIFI	SAIDI	ASAI	ENS	AENS
	freq/year/customer	hour/year/customer	-	kWh/year	kWh/year/customer
1	5.644	39.922	0.995443	82372	82.372
2	5.644	35.821	0.995911	74165	74.165
3	5.644	7.274	0.999170	14915	14.915
4	3.963	29.331	0.996652	60412	60.412
5	3.963	5.382	0.999386	10999	10.999
6	3.963	4.658	0.999468	9565	9.565
7	3.963	26.722	0.996950	55190	55.190
8	5.644	9.769	0.998885	20207	20.207
9	3.995	7.981	0.999089	16481	16.481

4.7.2 Urban Distribution Network without DG

This study optimally allocated eight fuses and three reclosers on the IEEE 34-bus test feeder in Figure 43. Table 24 shows that they decrease the objective function and the SAIDI. As a result of the optimal allocation of fuses and reclosers, the SAIFI and the SAIDI at protection scheme 7 in Table 23 decrease to those without reclosers in Table 24.

In the case of a single recloser of the test feeder, it recloses three or four times if a permanent fault occurs, or it triggers a recloser-lockout state, thereby increasing the SAIFI by 53.92 percent. However, in the case of a transient fault, the recloser prevents downstream fuses from burning and decreases the SAIDI by as much as 63.41 percent.

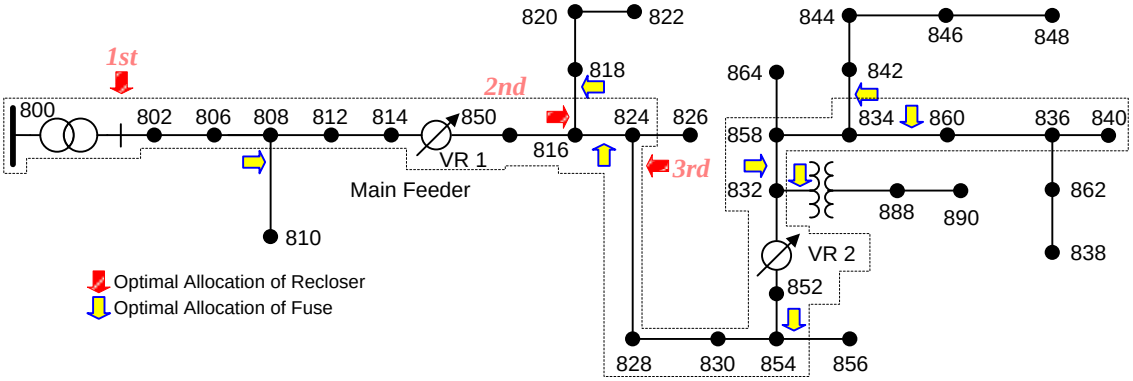

Figure 43. Optimal position of the fuse and the recloser of the IEEE 34-bus test feeder.

Table 24. Optimal allocation of the fuse and the recloser of the IEEE 34-bus test feeder

The Number of Reclosers	SAIFI		SAIDI		Objective Function	
	freq/year /customer	Change from Non-recloser case in %	hour/year /customer	Change from Non-recloser case in %	-	Change from Non-recloser case in %
0	3.66702	-	26.69395	-	0.69744	-
1	5.64440	+53.92%	9.76853	-63.41%	0.63635	-8.76%
2	4.62743	+26.19%	8.78752	-67.08%	0.53257	-23.64%
3	4.28303	+16.80%	8.74656	-67.23%	0.50149	-28.10%

4.7.3 Urban Distribution Network Enhanced by DG

To analyze the impact of protection devices and DG systems on the reliability of an urban distribution network enhanced by the DG system, this study optimally allocated thirteen fuses and five reclosers on the IEEE 123-bus test feeder enhanced by twenty DG systems with a total capacity of 0, 10, 50, and 100 percent of total peak demand. Figure 44 shows the thirteen fuses and five reclosers optimally allocated on the IEEE 123-bus test feeder enhanced by twenty DG systems.

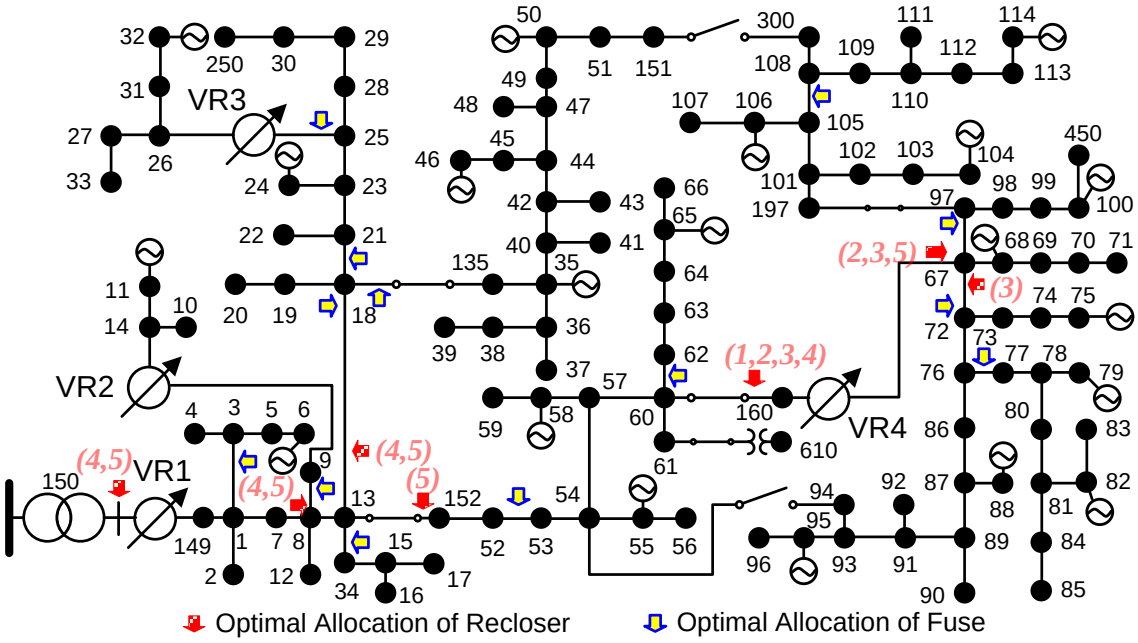

Figure 44. Thirteen fuses and five reclosers optimally allocated on the IEEE 123-bus test feeder.

This study minimizes the objective function consisting of the SAIFI, the SAIDI, ENS, and loss, illustrated in Figure 45. As either the capacity of the DG system or the number of reclosers increases, the objective function decreases. The more power DG injects into the distribution network, the more loss the distribution network experiences because of reverse power flow. Thus, the objective function of DG systems with a capacity of 100 percent of total peak demand increases slightly from that of DG systems with a capacity of 50 percent of total peak demand (which can be identified in Table 25). In general, as a result of their islanded operation, DG systems can reduce the SAIDI. As either the capacity of the DG system or the number of reclosers increases, the SAIDI decreases. However, since the total generation of the zone with DG systems with a total capacity of ten percent of total peak demand does not exceed the total load of the zone, the DG system does not reduce SAIDI, as shown in Figure 46 and Table 25. Since the DG system, particularly the PV system, produces power only during the daytime, the PV system slightly reduces the annual failure duration in hours/year/customer, even with a 100 percent capacity of total peak demand. In fact, if the assumed average time that the total generation of the zone exceeds the total load of the islanded zone is 4.5 hours/day,

the PV system can decrease by as much as 18.75 (=4.5/24) percent of the annual failure duration. The maximum limits of reliability improved by DG systems will be discussed in the next section. Figure 47 depicts the recloser locking out permanent faults, which increases the SAIFI. If an outage occurs, DG systems initiate the islanded operation, so they do not affect the SAIFI. In the case of the IEEE 123-bus test feeder with a single recloser without a DG system, the number of downstream transient faults prevented by the recloser and permanent faults causing the recloser-lockout state increase by as much as 40.01 percent of the SAIFI but decrease by 13.99 percent of the SAIDI (see Table 25). The test feeder enhanced by DG systems with a total capacity of 10, 50, and 100 percent of total peak demand shows a pattern increasing the SAIFI and decreasing the SAIDI.

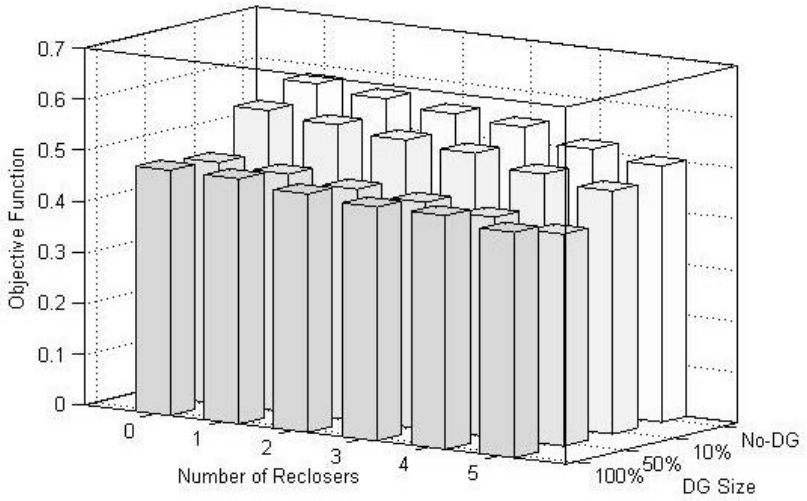

Figure 45. Objective function for the number of reclosers and the DG capacity.

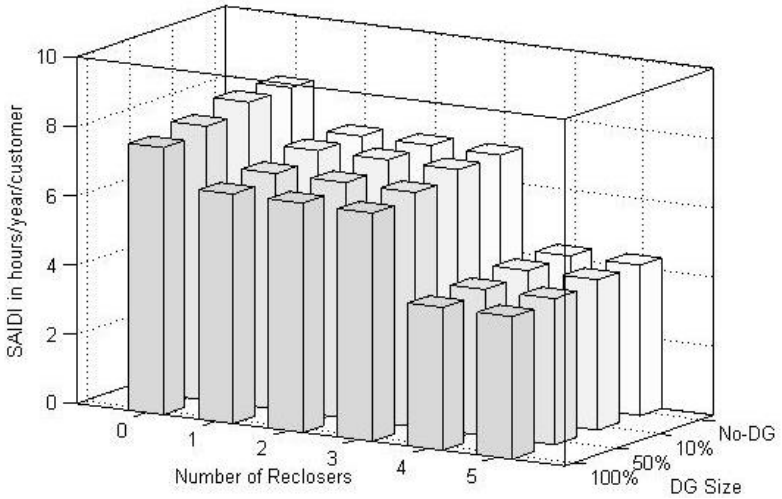

Figure 46. SAIDIs for the number of reclosers and the DG capacity.

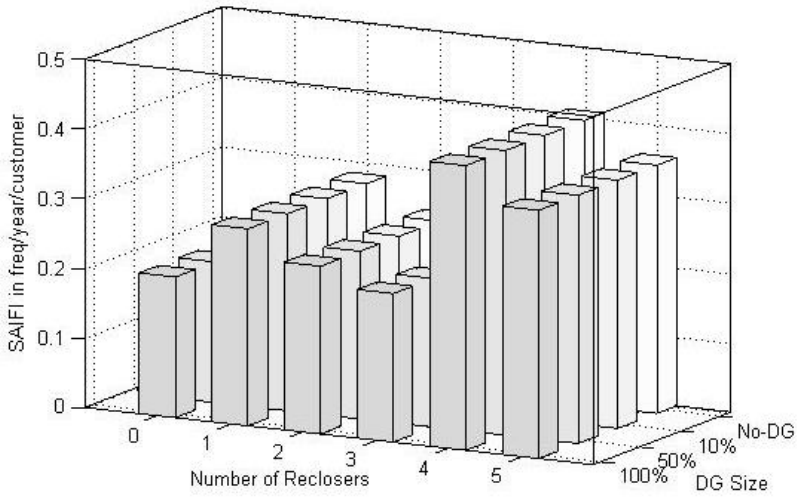

Figure 47. SAIFIs for the number of reclosers and the DG capacity.

Table 25. Optimal allocation of the fuse and the recloser of the IEEE 123-bus test feeder

DG Capacity in %	The # of Reclosers	SAIFI		SAIDI		ENS	Loss	Objective Function	
		freq/year /customer	Change from Non-recloser case in %	hour/year /customer	Change from Non-recloser case in %	MWh/year/ customer	kWh/year /customer	-	Change from Non-recloser case in %
No-DG	0	0.2021	-	8.17464	-	81.4832	89.9319	0.58085	-
	1	0.2829	+40.01%	7.03140	-13.99%	70.0006	89.9319	0.56804	-2.21%
	2	0.2409	+19.23%	7.02558	-14.06%	69.9403	89.9319	0.55491	-4.47%
	3	0.2134	+5.60%	6.99805	-14.39%	69.6794	89.9319	0.54555	-6.08%
	4	0.4090	+102.38%	4.34585	-46.84%	43.3714	89.9319	0.51883	-10.68%
	5	0.3565	+76.40%	4.33792	-46.93%	43.2999	89.9319	0.50241	-13.50%
10 %	0	0.2021	-	8.17464	-	77.2209	81.9311	0.55161	-
	1	0.2829	+40.01%	7.03140	-13.99%	66.4269	81.9311	0.53993	-2.12%
	2	0.2409	+19.23%	7.02558	-14.06%	66.3691	81.9311	0.52680	-4.50%
	3	0.2134	+5.60%	6.99805	-14.39%	66.1283	81.9311	0.51748	-6.19%
	4	0.4090	+102.38%	4.34585	-46.84%	41.2003	81.9311	0.49302	-10.62%
	5	0.3565	+76.40%	4.33792	-46.93%	41.1313	81.9311	0.47661	-13.60%
50 %	0	0.2021	-	7.90212	-	58.6170	66.1740	0.47276	-
	1	0.2829	+40.01%	6.79367	-14.03%	50.8256	66.1740	0.46658	-1.31%
	2	0.2409	+19.23%	6.78818	-14.10%	50.7800	66.1740	0.45348	-4.08%
	3	0.2134	+5.60%	6.76065	-14.45%	50.6206	66.1740	0.44429	-6.02%
	4	0.4090	+102.38%	4.21771	-46.63%	31.7877	66.1740	0.43165	-8.70%
	5	0.3565	+76.40%	4.21044	-46.72%	31.7323	66.1740	0.41526	-12.16%
100 %	0	0.2021	-	7.69959	-	37.6197	82.6304	0.48067	-
	1	0.2829	+40.01%	6.61818	-14.05%	33.2462	82.6304	0.48056	-0.02%
	2	0.2409	+19.23%	6.61294	-14.11%	33.2126	82.6304	0.46748	-2.74%
	3	0.2134	+5.60%	6.58541	-14.47%	33.1546	82.6304	0.45845	-4.62%
	4	0.4090	+102.38%	4.11994	-46.49%	21.0539	82.6304	0.45815	-4.69%
	5	0.3565	+76.40%	4.11289	-46.58%	21.0069	82.6304	0.44179	-8.09%

4.8 Maximum Reliability Improvement of PV Systems

This study examines the maximum limits of the reliability of the IEEE 123-bus test feeder as an example of urban distribution networks that can be improved by DG systems, particularly PV systems. It assumes that the test feeder is enhanced by twenty DG systems with their total capacity of 100 percent of total peak demand and divided by nineteen zones presented in Section 4.6.2. It also assumes the following conditions:

(1) *Constant power output of DG systems*. Twenty DG systems on the test feeder constantly operate at their full capacity during one year. However, twenty load buses (or points) of the test feeder are outside of the nineteen zones.

(2) *All the load buses perfectly coordinated by ideal islanded zones*. The total generation of DG systems in an islanded zone exceeds the total load of the zone throughout the year and all the load buses on main and lateral feeders of the IEEE 123-bus test feeder are perfectly coordinated by ideal islanded zones more than nineteen. In other words, all the load buses of the test feeder can begin an islanded operation if an outage occurs (while satisfying three conditions for the islanded operation presented in Section 4.4.2).

Table 26 shows the duration of failure (or the SAIDI) reduced by PV systems that satisfy the two assumptions. (Whenever only an outage occurs, DG systems initiate the islanded operation, so they do not affect the frequency of failure [the SAIFI]). Since 20 from 85 load buses of the test feeder are outside of the nineteen zones presented in Figure 41, PV systems that meet only condition (1) can reduce the duration of failure by as much as 31.38 percent to 55.49 percent. However, if PV systems satisfy both the conditions (1) and (2), which can be a projection of what might become a viable planning option for local and decentralized microgrids in the near future, can reduce the duration of failure to zero. However, this study assumes that protection devices such fuses and reclosers are fully reliable, their protection coordination with PV systems is ideal, and PV systems,

which consist of PV modules, inverters, electrical components, and mounting systems located on urban distribution networks, are also fully reliable.

Table 26. Maximum reduction of the duration of failure (SAIDI) of DG systems

Assumptions	Reference (No-DG)	Assumption (1)		Assumptions (1) and (2)	
The # of Reclosers	hour/year /customer	hour/year /customer	Change from Reference in %	hour/year /customer	Change from Reference in %
0	8.17464	3.63865	-55.49%	0	-100%
1	7.03140	3.44839	-50.96%	0	-100%
2	7.02558	3.43939	-51.04%	0	-100%
3	6.99805	3.43939	-50.85%	0	-100%
4	4.34585	2.99358	-31.12%	0	-100%
5	4.33792	2.97679	-31.38%	0	-100%

4.9 Conclusion

The main objective of this study has been (1) to propose tools and algorithms useful for planning, designing, and operating urban distribution networks enhanced by DG (distributed generation) systems, particularly the PV (photovoltaic) system analyzed in this study, from the standpoint of the reliability of such a network, (2) to address some of the issues in the analysis of the impact of DG systems and protection devices on the reliability of such a network, and (3) to suggest a framework for streamlining the smooth integration of DG systems into the urban distribution network. For this purpose, this study has implemented a genetic algorithm that determines the optimal allocation of protection devices, including fuses and reclosers, in two stages and improves the reliability of the urban distribution network enhanced by protection devices and DG systems. Using the backward and forward sweep method implemented by KCL (Kirchhoff's current law) and KVL (Kirchhoff's voltage law), this study has also presented an analytical method for an urban distribution network housing a combination of fuses, switches, reclosers, and high-capacity DG systems that generate all possible permanent and transient faults on the main and lateral feeders, sums up the fault current flowing at each bus, searches all buses from the fault bus to the root bus, and calculates voltage drops, the on-off states of the line, and the frequency and the duration of a failure.

Finally, this study has verified the proposed algorithm using IEEE 34- and 123-bus test feeders for distribution enhanced by protection devices and DG systems and analyzed the impact of both the DG system, including the effect of its islanded operation, and protection devices on the reliability of the urban distribution network.

The study discussed the process of detecting a fault current in a distribution network in which the recloser opens at a pre-set time and then recloses, repeating auto-reclosing multiple times, typically three or four times. In the case of a transient fault, the recloser can prevent a downstream fuse from burning, so fewer customers will experience outages. However, because of its reclosing capability and lockout state, it can increase the frequency of failure (the SAIFI). Since a single recloser installed on IEEE 34- and 123-bus test feeders without DG systems reclosed multiple times to prevent downstream transient faults and it was locked out by permanent faults, it increased the SAIFIs of the test feeders by 53.92 and 40.01 percent. The 123-bus test feeder enhanced by DG systems with a total capacity of 10, 50, and 100 percent of total peak demand exhibited a pattern of increasing the SAIFI. Second, the recloser reduced the failure duration, or the SAIDI. If three or five reclosers were installed on IEEE 34- and 123-bus test feeders without DG systems, they decreased the SAIDIs of the test feeders by 67.23 and 46.93 percent. The 123-bus test feeder enhanced by DG systems with a total capacity of 10, 50, and 100 percent of total peak demand exhibited a pattern of decreasing the SAIDI. Lastly, DG systems reduced the objective function and the annual failure duration. However, the PV system produces power only during the daytime, so it only slightly reduces the objective function and the annual failure duration. PV systems with an assumed average of 4.5 hours/day, during which the total generation of the zone exceeds the total load of the islanded zone, can reduce the annual failure duration by as much as 18.75 (=4.5/24) percent. However, if PV systems constantly operate at their full capacity during one year and all the load points of the 123-bus test feeder are perfectly coordinated by islanded zones, they can significantly reduce the annual failure duration, even up to zero at the

ideal conditions of fully reliable PV systems, fuses, reclosers, and their perfect protection coordination.

This study has proposed a useful method for analyzing the impact of renewable DG systems, particularly PV systems, and protection devices on the reliability of urban distribution networks and presented useful results. For example, it has found that because of the generation characteristics of the PV system (which produces power during daytime and peak power at around noon on a sunny day), even operating at 100 percent capacity of total peak demand, it only slightly reduces the annual failure duration of such a network. Thus, to maximize the enhancement of reliability, various DG types (including PV systems, wind farms, and microturbines), DG systems enhanced by a storage system, and methods of optimizing the location, the capacity, and the zone of the DG system must be further investigated. In addition, this study has presented a genetic algorithm that optimally allocates the fuse and the recloser in two stages within the urban distribution network enhanced by DG systems and an analytical method that evaluates the reliability of the urban distribution network housing a combination of fuses, switches, reclosers, and high-capacity DG systems. Both the genetic algorithm and the analytical method can be extended for analyses of the effects of various DG systems, including PV systems, wind farms, and microturbines, on the reliability of urban distribution networks.

CHAPTER 5

IMPACT OF GEOGRAPHICALLY DISTRIBUTED RENEWABLE GENERATION ON ENVIRONMENTALLY CONSTRAINED GENERATION RESOURCE ALLOCATION

5.1 Introduction

In 2010, the use of PV, which accounted for 0.28 percent of the renewable generation mix in the United States, has recently been growing at an annual rate of 222.44 percent in PV module shipments [94]. The increased number of PV systems offers not only opportunities such as a reduction in peak load and loss but also potential for use in Volt/VAr management and control. However, it also creates a need for additional spinning reserve that covers uncertainty involved in their output. In fact, the deployment of PV systems may increase the consumption of fossil fuels because of their intermittency, or sudden energy shortages or overages. In addition, viewed in hourly resolution (averaged every hour), the PV system seems to have a more stable output than usual. Rapid variations in short-term PV generation, typically in minute-averaging resolution, result from transient cloudiness in the atmosphere. Therefore, this study models the short-term intermittency of transient cloudiness, estimates the generation of PV systems geographically dispersed throughout a test bed, and analyzes the impact of their intermittency on energy, especially for peak power and spinning reserve, electricity generation costs, and emissions.

Fuel costs and emissions in resource allocation problems have been deemed constraints in many techniques [60, 61]. Many studies also introduced evolutionary algorithms that solved the problem of the non-commensurable objective function that minimizes emissions and the costs of generating electricity [62-66]. However, these studies do not address the ecological impact of water. Energy and water infrastructures

are closely or directly linked to production and consumption. With increasing awareness of the sustainability of energy and water infrastructures, this link may require the addition of the water consumption constraints to the objective function. Therefore, this study presents an algorithm for generating resource allocation with a scalar objective function that merges fuel costs and emissions with a water consumption constraint.

The objective of this study is (1) to present tools and algorithms useful for analyzing the impact of geographically dispersed DG systems, particularly PV systems in this study, on local, statewide, or nationwide generation resource allocation in hourly and minute intervals, (2) to address some of the issues in the analysis of the impact of DG systems on such resource allocation, and (3) to design a framework for streamlining the smooth integration of the DG system into such local, statewide, or nationwide grids. For this purpose, this study first develops an algorithm for generation resource allocation that minimizes ecological impact, including water consumption, and fuel costs, and synthesizes cubic-order output functions for costs, emissions, and water consumption from heat rate data, collected from a utility. Second, it proposes, as a test bed, the power system model of the state of Georgia in 2010, approximates the load consumption and the water inflow of the test bed, and estimates the power output of geographically dispersed PV systems in hourly and minute-by-minute resolutions and the hydroelectric resources of the test bed. Next, the study performs simulations for generation resource allocation in hourly and minute-by-minute resolutions. Finally, it analyzes the impact of geographically dispersed PV systems from a long-term, typically annual, perspective of energy, specifically for peak power and spinning reserve, electricity generation costs, and emissions.

5.2 Generation Resource Allocation

5.2.1 Emissions Modeling

An input-output model of generating unit *i*, which burns fossil fuel, can be

formulated as a function of its power output. The function is approximated by the following cubic-order equation [60]:

$$F_i\left(P_{Gi}\right) = a_i + b_i P_{Gi} + d_i P_{Gi}^{\,3}, \tag{55}$$

$$C_i\left(P_{Gi}\right) = fp_i F_i = a_i' + b_i' P_{Gi} + d_i' P_{Gi}^{\,3}. \tag{56}$$

The output of emissions such as SO_2, NO_X, and CO_2 and water from the generation unit is estimated by the following cubic-order equation of the power output [75].

$$EO_{SO_2,i}\left(P_{Gi}\right) = ef_{SO_2,i} F_i = \alpha'_{SO_2,i} + \beta'_{SO_2,i} P_{Gi} + \gamma'_{SO_2,i} P_{Gi}^{\,3}, \tag{57}$$

$$EO_{NO_X,i}\left(P_{Gi}\right) = ef_{NO_X,i} F_i = \alpha'_{NO_X,i} + \beta'_{NO_X,i} P_{Gi} + \gamma'_{NO_X,i} P_{Gi}^{\,3}, \tag{58}$$

$$EO_{CO_2,i}\left(P_{Gi}\right) = ef_{CO_2,i} F_i = \alpha'_{CO_2,i} + \beta'_{CO_2,i} P_{Gi} + \gamma'_{CO_2,i} P_{Gi}^{\,3}, \tag{59}$$

$$WO_{Water,i}\left(P_{Gi}\right) = ef_{Water,i} F_i = \alpha'_{Water,i} + \beta'_{Water,i} P_{Gi} + \gamma'_{Water,i} P_{Gi}^{\,3}. \tag{60}$$

5.2.2 Modeling of the Hydroelectric Unit

An input-output model of hydroelectric unit *i* with a constant head in Figure 48 can be approximated by first- and second-order equations [95].

$$q_i = q_i\left(P_{Hi}\right) = \begin{cases} a_{Hi} + b_{Hi} P_{Hi} & for\ 0 \le P_{Hi} \le P_{Hi,saddle} \\ c_{Hi} + d_{Hi} P_{Hi} + e_{Hi} P_{Hi}^2 & for\ P_{Hi,saddle} < P_{Hi} \le P_{Hi,max} \end{cases}. \tag{61}$$

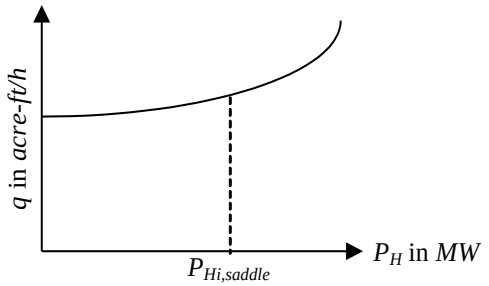

Figure 48. Hydroelectric unit input-output characteristics with a constant head.

5.2.3 Allocation Strategy

(1) Steam Turbine Generation

For *N* generating units, *m* buses, and *n* loads, the objective function can be formulated as follows:

$$Minimize \sum_{i=1}^{N} \left[C_i \left(P_{Gi} \right) + EO_i \left(P_{Gi} \right) \right], \tag{62}$$

subject to

$$\sum_{i=1}^{N} P_{Gi} = \sum_{i=1}^{n} P_{Load,i} + P_{Loss}(P_{G2}, P_{G3}, ..., P_{Gm}) = P_{Load} + P_{Loss}, \tag{63}$$

$$P_{Gi,Min} \le P_{Gi} \le P_{Gi,Max}, \tag{64}$$

$$r_{i,Min} \le \left| P_{Gi}(t) - P_{Gi}(t-1) \right| \le r_{i,Max}. \tag{65}$$

P_{Load} represents the total system load and P_{Loss} the total transmission or distribution losses expressed by the loss coefficient matrix [96]. Loss is calculated by solving the power-flow equations of real and reactive power constraints. However, since this study does not model transmission or distribution networks, it ignores such loss.

A Lagrangian function of the constrained problem can be represented by

$$\mathcal{L} = \sum_{i=1}^{N} (C_i \left(P_{Gi} \right) + EO_i (P_{Gi})) + \lambda (P_{Load} - \sum_{i=1}^{N} P_{Gi}). \tag{66}$$

An optimal solution to the constrained problem can be found from Kuhn-Tucker conditions. The optimal Lagrangian multiplier, λ, is found by the iterative bisection or secant search.

(2) Hydrothermal Coordination

The optimal coordination of hydroelectric generation units is more complex than that of thermal units since hydrothermal coordination requires both hydraulic and thermal unit constraints. For N_S steam turbines, N_H hydroelectric units, m buses, and n loads during i_{max} intervals, the coordination problem can then be formulated as follows:

$$Minimize \sum_{i=1}^{i_{\max}} \sum_{j=1}^{N_S} n_i F(P_{S_{j,i}}), \tag{67}$$

subject to

$$F\left(P_{S_{j,i}} \right) = a_{S_{j,i}} + b_{S_{j,i}} P_{S_{j,i}} + d_{S_{j,i}} {P_{S_{j,i}}}^3, \tag{68}$$

$$\sum_{i=1}^{i_{max}} n_i q_i = q_{Tot}\,, \tag{69}$$

$$\sum_{i=1}^{i_{max}} n_i = T\,. \tag{70}$$

The constraint for load balancing for $i \in \{1,...,i_{max}\}$ is as follows:

$$\sum_{j=1}^{N_S} P_{S_{j,i}} + \sum_{k=1}^{N_H} P_{H_{k,i}} = \sum_{j=1}^{n} P_{Load,j,i} + P_{Loss,i}(P_{G2}, P_{G3},..., P_{Gm}) = P_{Load} + P_{Loss}\,. \tag{71}$$

A Lagrangian function of the constrained problem can be represented by

$$\mathcal{L} = \sum_{i=1}^{i_{max}}[\sum_{j=1}^{N_S} n_i F\left(P_{S_{j,i}}\right) + \lambda_i (P_{Load} + P_{Loss} - \sum_{j=1}^{N_S} P_{S_{j,i}} - \sum_{k=1}^{N_H} P_{H_{k,i}})] + \gamma\left[\sum_{i=1}^{i_{max}}\sum_{k=1}^{N_H} n_i q_i\left(P_{H_{k,i}}\right) - q_{Tot}\right]. \tag{72}$$

An optimal solution to the constrained problem should satisfy the conditions of the following:

$$\frac{\partial \mathcal{L}}{\partial P_{S_{j,i}}} = \frac{\partial \mathcal{L}}{\partial P_{H_{k,i}}} = 0\,, \tag{73}$$

for $j = \{1,...,N_S\}$ and $k = \{1,...,N_H\}$.

Final coordination equations in interval i are formulated by [95]

$$n_i \frac{dF(P_{S_{j,i}})}{dP_{S_{j,i}}} + \lambda_i \frac{\partial P_{Loss}}{\partial P_{S_{j,i}}} = \lambda_i\,, \tag{74}$$

$$\gamma n_i \frac{dq_i(P_{H_{k,i}})}{dP_{H_{k,i}}} + \lambda_i \frac{\partial P_{Loss}}{\partial P_{H_{k,i}}} = \lambda_i\,. \tag{75}$$

5.3 Implementation of the Generation Resource Allocation Algorithm

5.3.1 Objective Function

To minimize costs, emissions, and water consumption with each weight, this study defines the objective function of the algorithm for generation resource allocation. The linear combination of the outputs of costs, emissions, and water consumption is formulated as follows:

$$Minimize[W_{Cost} C(P_G) + \sum_{i\in\{SO_2, NO_X, CO_2, Water\}} W_i EO_i(P_G)], \tag{76}$$

where

$$\sum_{i\in\{Cost,SO_2,NO_X,CO_2,Water\}} W_i = 1 . \qquad (77)$$

5.3.2 Procedures of the Algorithm for Generation Resource Allocation

This study uses MATLAB to implement the algorithm for generation resource allocation that minimizes costs, emissions, and water consumption in Figure 49 and Figure 50.

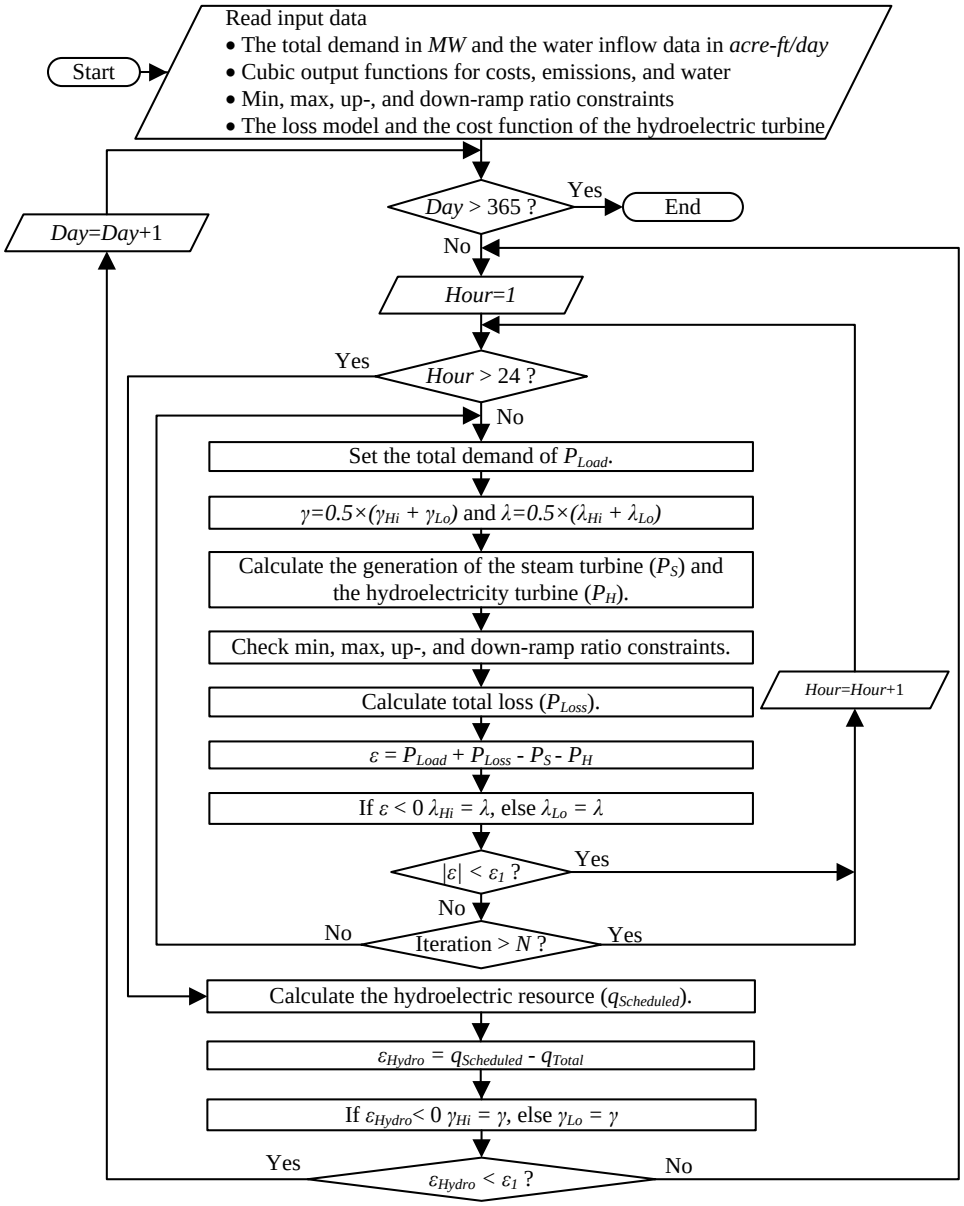

Figure 49. Flowchart of hydrothermal coordination.

Figure 49 shows the procedure of the proposed algorithm for hydrothermal coordination, which implements the method of the lambda-gamma iteration that schedules hydroelectric resources using Lagrangian optimization for load and water balancing. Then, the proposed algorithm schedules steam turbines and implements an iterative method that solves the constrained optimization problem using Lagrangian optimization in Figure 50.

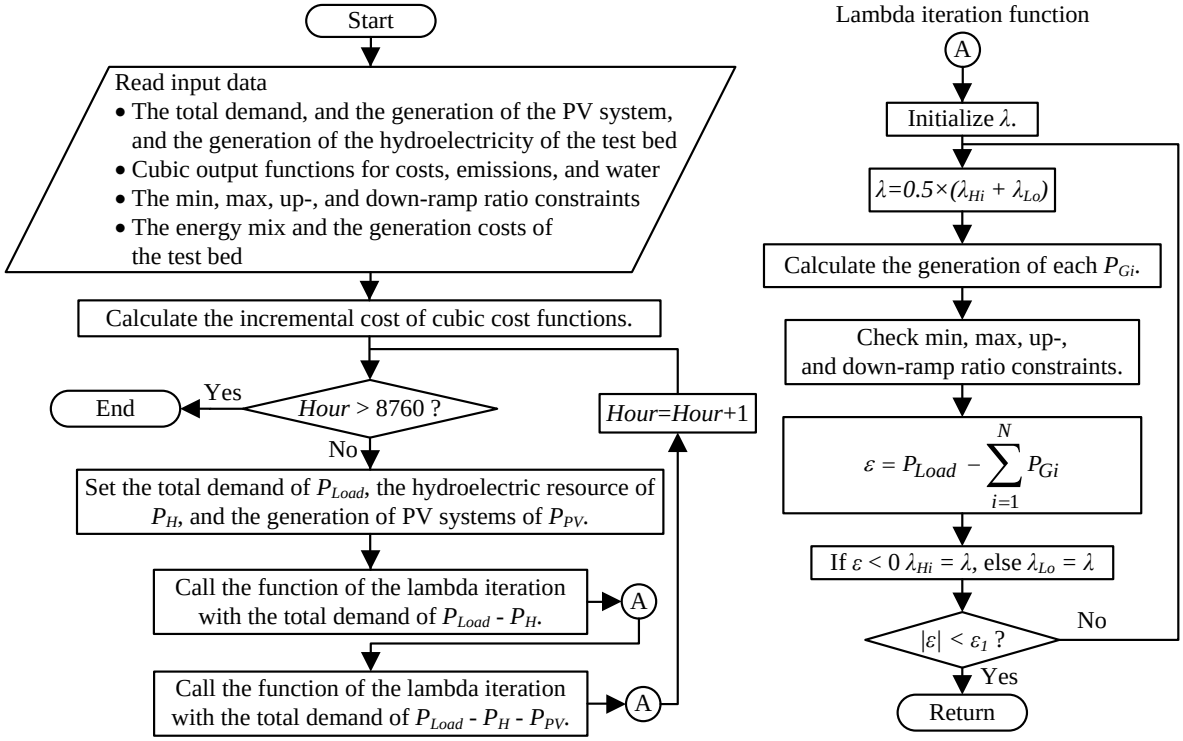

Figure 50. Flowchart of the proposed algorithm for the allocation of steam turbines.

5.4 Case Study

5.4.1 Modeling of Load Consumption

To evaluate the proposed algorithm, this study proposes, as a test bed, the power system model of the state of Georgia in 2010. Thus, this study obtained the load profile data for residential, commercial, and industrial customers from the actual utility in kW in hourly intervals in 2010 [79]. Let the composite load profile data be a discrete function, the linear combination of which is

$$\tilde{P}_{TB} = \sum_{c \in C} W_c P_c \,. \tag{78}$$

The unknown load profile of the test bed can be approximated by a combination of the profile of the composite load, the total actual generation of the test bed, and the total generation of the composite load profile in the following:

$$\hat{P}_{TB} = \tilde{P}_{TB} \frac{E_{TB}}{\tilde{E}_{TB}} \,. \tag{79}$$

This study iterates equation (79) until the composite load profile meets the peak demand and the total generation of the test bed. Figure 51 shows the duration curve of the approximate load consumption of the test bed satisfying a peak of 17.152 *GW* and total generation of 97,000 *GWh/year* in 2010 [43].

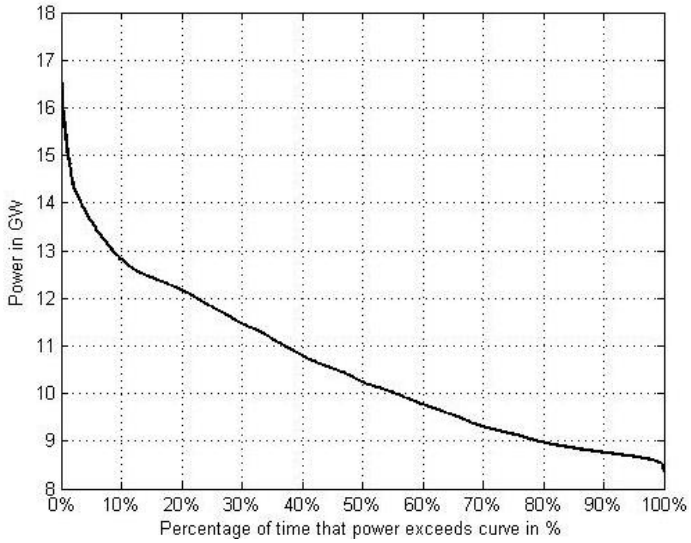

Figure 51. Load consumption of the test bed in hourly intervals in GW in 2010.

5.4.2 Water Inflow Modeling

Unfortunately, water inflow data for the test bed were not available. Thus, for hydrothermal coordination, this study obtained water inflow data from the Bartlett's Ferry Reservoir, a 5,850 acre reservoir on the Chattahoochee River that generated hydroelectric power to the western area of the test bed, in cubic feet per second during 1997 to 2009 [80], presented in Figure 52. Then, this study used the average water inflow data synthesized in hourly resolution as input data to six hydroelectric plants in the

western area of the test bed. As of December 31, 2010, since the capacity of the six plants has been 27.8 percent of that of all of the hydroelectric plants of the test bed [84], the total hydroelectric generation of the test bed is approximated by multiplying 3.597 (=1/0.278) to the hydroelectric generation of the six plants.

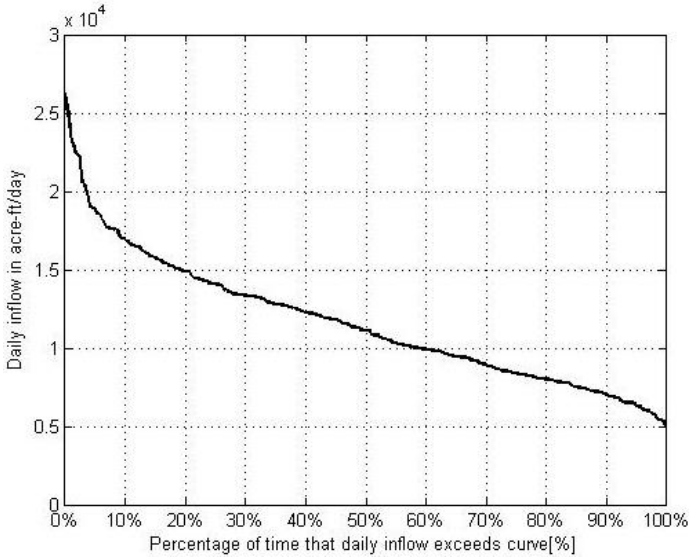

Figure 52. Daily water inflow of the Bartlett's Ferry Reservoir.

5.4.3 Unit Heat Rate Data

The heat rate of the modern thermal unit ranges from 8.6 to 10 *MBtu/MWh* [97] or from 9.8 to 11.4 *MBtu/MWh* [95] with overall efficiency between around 30 to 40 percent [95]. To model ten coal-fired, thirteen gas-fired, two nuclear plants of the test bed, this study synthesizes their heat-rate coefficients for costs, emissions, and water consumption from actual heat-rate data [76-78] presented in Appendices G and H.

5.4.4 Renewable Energy Generation

(1) Hydroelectric Generation

An input-output model of the hydroelectric unit with a constant head was presented in [95] and Appendix G. This study applies the model for hydrothermal coordination, which allocates hydroelectric resources. An electrical loss model of the hydroelectric unit and the load was proposed in [95], which is

$$P_{Loss} = c_{Loss} P_H^2 . \quad (80)$$

This study assumes that the hydroelectric unit is located at a short distance from steam turbine units, c_{Loss} = 0.00008 [95]. In hydrothermal coordination, this study employs the method of lambda-gamma iteration (presented in Figure 49) to search for Lagrangian multipliers for load and water balances.

(2) PV System Generation

This study analyzes the probable impact of the significant presence of renewable energy generation, particularly PV systems in this study, on the costs of operating the power systems of the test bed. To determine their impact, this study proposes two simulations for generation resource allocation in hourly and minute-by-minute resolutions. In hourly resolution, this study assumes that all PV systems oriented at an azimuth of 180° (facing south) and a tilt angle of 30° are geographically dispersed across the representative 19 locations of the test bed and generate ten percent of total peak demand, depicted in Figure 53.

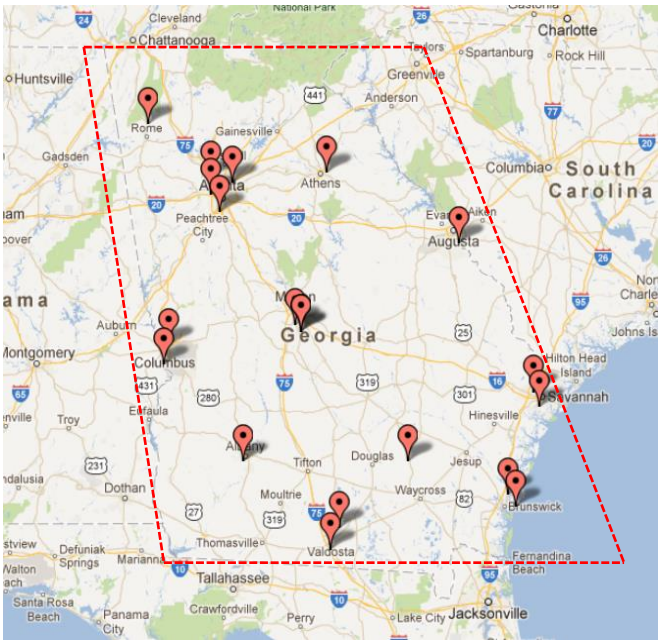

Figure 53. Hourly solar data obtained from 19 locations dispersed throughout the state of Georgia.

(3) Short-Term Intermittency of the PV System

Unfortunately, solar data in minute intervals for the test bed are not available from

the current national solar radiation database. Rapid variations in short-term, typically minute-averaging resolution, PV generation result from transient cloudiness and weather disturbances in the atmosphere. Since current PV generation affected by transient cloudiness depends only on previous generation, rapid variations in PV generation can be modeled by optimized Markov chain methods [69-71]. Thus, to model the short-term intermittency of the transient cloudiness of the test bed, this study uses a Markov chain Monte Carlo (MCMC) simulation. To calculate the transition probability matrix required as input data for a MCMC simulation, this study (1) obtained actual solar data in minute-by-minute resolution from nine test sites located in Colorado, Arizona, New Mexico, and Utah from 2008 to 2012 [74], (2) estimated their annual PV outputs using PV_LIB [72], and (3) selected the transition probability matrix calculated from the Milford area in Utah since it shows an annual output that most closely resembles that of the test bed. Then, as input data to the MCMC simulation, this study used hourly solar data obtained from the 19 locations of the test bed in the TMY3 format [73]. The results in Figure 54 show that the total generation of the PV systems geographically dispersed throughout the test bed that produce ten percent of peak demand in minute resolution exhibit rapid short-term intermittency.

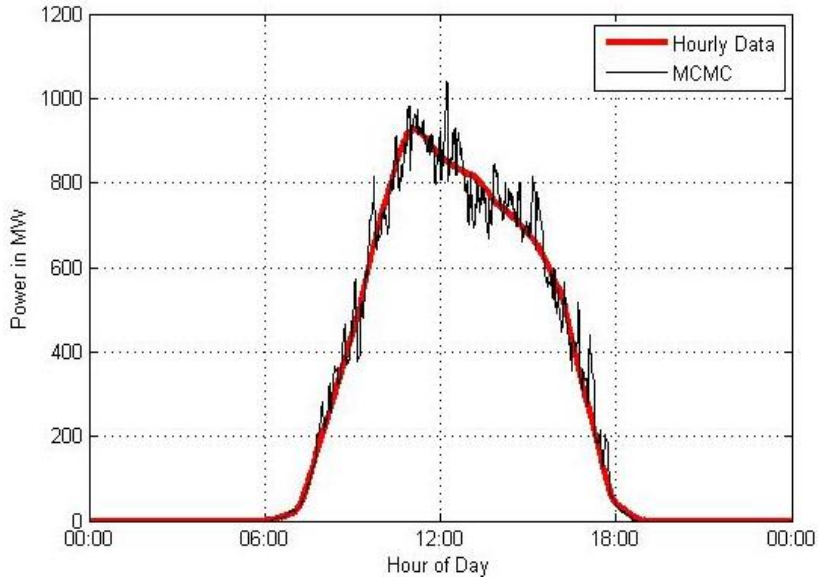

Figure 54. PV systems with rapid variations on a peak demand day, September 27, 2010.

A detailed simulation plan of generation resource allocation is presented in Table 27, which presents data from the Georgia Power Company that contain information about the fuel type, the energy mix, and electricity costs as of December 2010. Since the LCOE (levelized cost of electricity) of PV is continuously decreasing, as shown in Figure 4, this study uses the average levelized cost of PV entering new service in the United States for 2019 [85].

Table 27. Generation resource allocation of the test bed [43, 85, 98, 99]

Fuel Type	Total Generation	Source of Generation	Min Capacity	Max Capacity	Generation Cost	Ramp Rate (Up/Down)
	GWh/year	%	MW	MW	$/MWh	PU/min
PV	10% of Peak		0	1,715.20	118.60	-
Coal	97,000	67.0	4,913.45	9,485.43	45.30	0.01
Gas		10.0	0	5,979.61	57.50	0.10
Nuclear		21.0	1,959.85	1,959.85	6.60	0
Hydro		2.0	0	1,087.54	-	1.00
Spinning Reserve		-	1.10 GW of Hydro		-	-

5.5 Results of Simulations for Generation Resource Allocation

5.5.1 Simulation in Hourly Resolution

(1) Energy Savings of the PV System

PV systems can save energy, particularly during peak load, which typically burns the most expensive fuel. Energy savings are presented in Figure 55, which shows hourly unit allocation that minimizes the costs of generating electricity when the PV system is either available or not available on a peak demand day, September 27, 2010. Since the estimated maximum power output of the PV systems on the day presented in Figure 54 is about 1 GW, the PV systems save about 1 GW at around noon, shown in Figure 55 (b). Figure 56 displays weekly unit allocation from Friday to Thursday. Figure 55 and Figure 56 indicate that the PV system effectively reduces peak demand. In fact, the statewide power grid enhanced by geographically distributed PV systems with a capacity equal to ten percent of total peak demand is able to not only effectively cope with peak demand but also save energy generated from gas-fired plants. Table 28 depicts the normalized annual impact of the PV system on energy savings, especially for gas-fired generation. If

PV systems geographically dispersed throughout the test bed had a capacity equal to ten percent of total peak demand, they could decrease energy produced from non-solar plants, particularly by about 3.1 percent in the case study. The non-deployed spinning reserve without contingency is reserved.

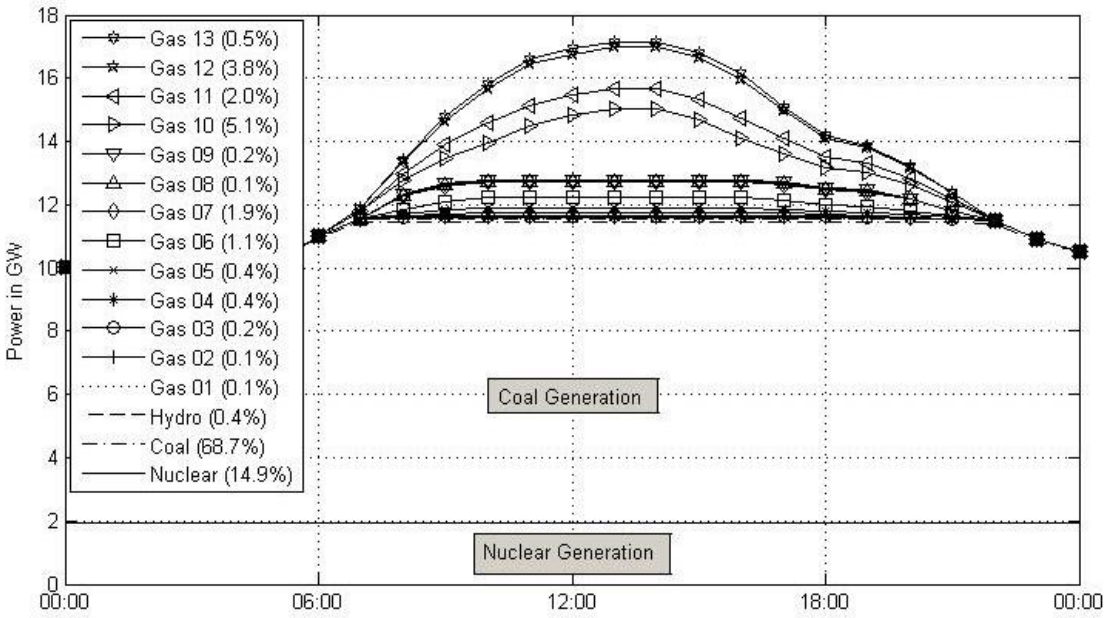

(a) Without the PV system

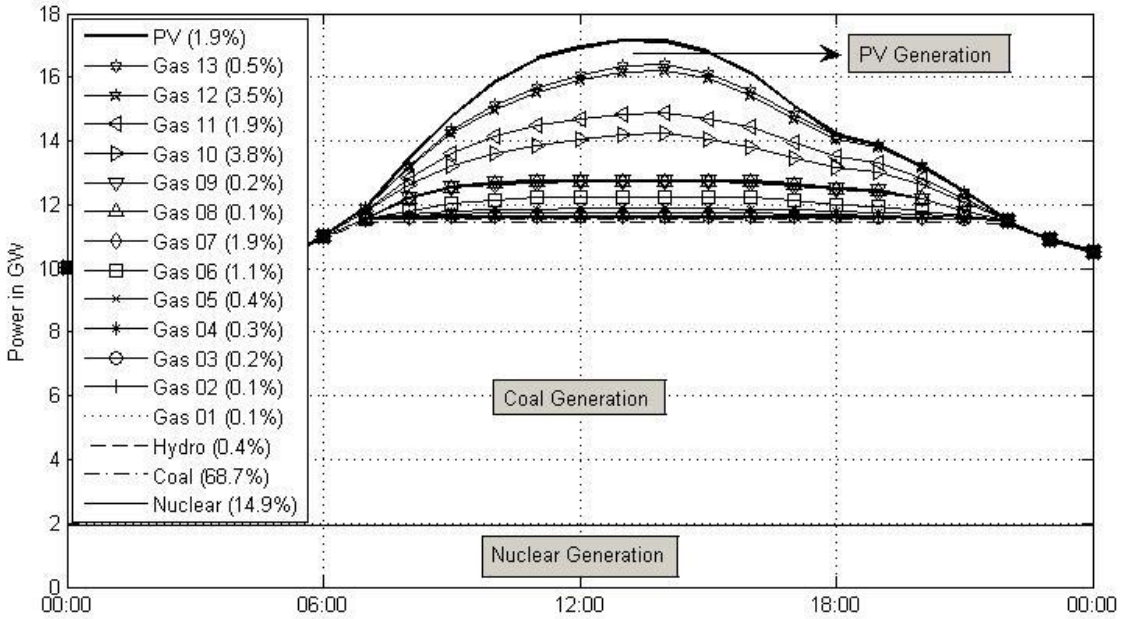

(b) With PV systems with a capacity of 10% of the total peak demand of the statewide power grid for Georgia

Figure 55. Daily generation profiles that minimize the costs of generating electricity on a peak demand day, September 27, 2010.

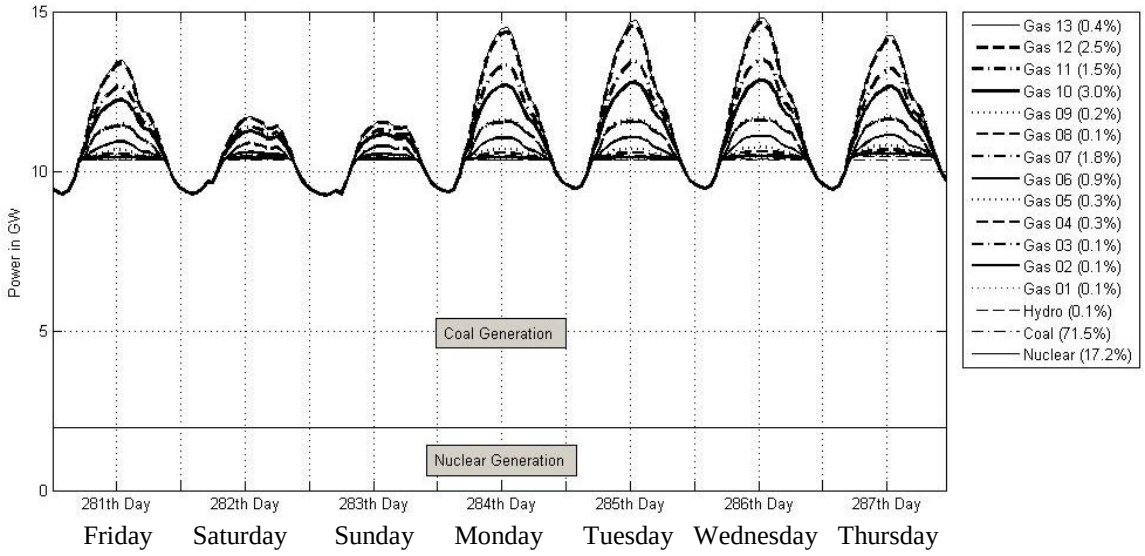

(a) Without the PV system from Friday to Thursday

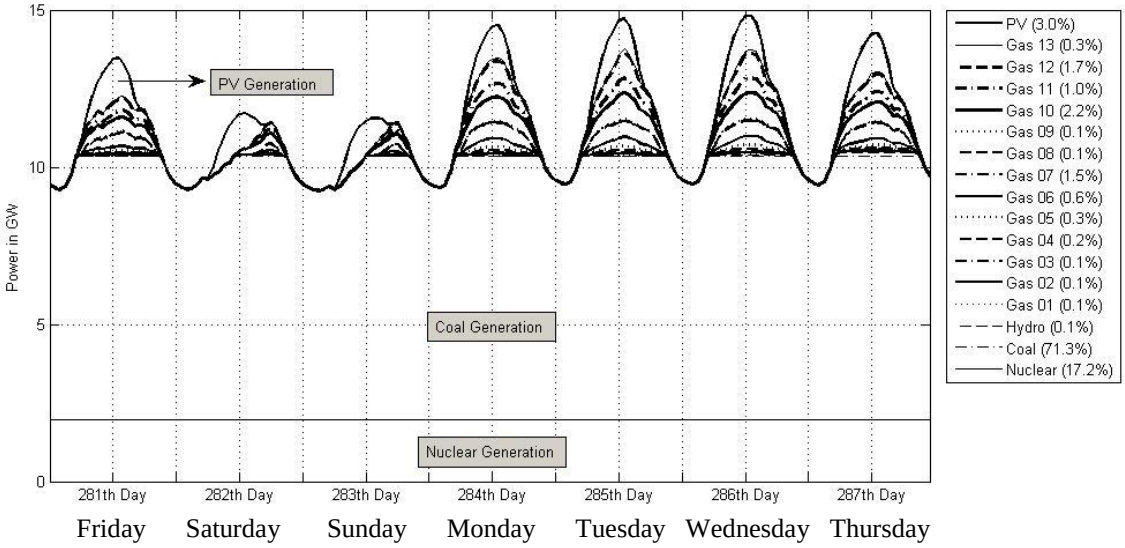

(b) With PV systems that can handle a capacity of 10% of peak demand from Friday to Thursday

Figure 56. Weekly generation profiles that minimize the costs of generating electricity.

Table 28. Annual energy savings of the PV system

Weight	Type	Non-solar Unit	Coal-Fired		Gas-Fired		Nuclear		Hydro		PV	
%	-	MWh/year/ household	MWh/year/ household	%	MWh/year/ household	%	MWh/year/ household	%	MWh/year/ household	%	MWh/year/ household	%
Cost= 100%	No-PV	15.01	10.63	70.8	1.56	10.4	2.66	17.7	0.16	1.1	0	0
	PV	14.55	10.56	70.4	1.17	7.8	2.66	17.7	0.16	1.1	0.46	3.1
	% Change from No-PV	-3.1%	-0.6%	-0.4	-25.1%	-2.6	0%	0	0%	0	-	+3.1

(2) Generation Costs and Emissions Savings of the PV System

PV systems, which save energy for gas-fired and peak generation, can also affect costs as a result of energy savings. Table 29 indicates the costs of generating electricity

when the PV systems are either available or not available. Such costs of the PV system indicate the amount required to produce ten percent of total peak demand. The costs of generating electricity of the PV system, 118.6 $/MWh (which is the LCOE [the levelized cost of electricity] of the United States for PV entering new service in 2019 and are still higher than the costs of the other systems), increase the total costs of all unit types from 45.53 to 64.87 $/MWh (the change rate of which is +42.5%). By contrast, since PV systems save energy for gas-fired and peak generation, they decrease the total costs of gas turbines from 104.33 to 78.14 $/year/household (the change rate of which is -25.1%), which typically burn expensive fuel. In this example, spinning reserve is not deployed, only reserved.

By using less fuel from gas- and coal-fired units, dispersed PV systems can also reduce the release of emissions. Table 30 shows the annual ecological impact of PV systems geographically dispersed on the test bed.

Table 29. Changes in the annual generation costs of the PV system

Weight	Type	All Unit Types	Gas-Fired Units	Unit Generation Costs
%	-	$/year/household	$/year/household	$/MWh
Cost= 100%	No-PV	683.21	104.33	45.53
	PV	973.38	78.14	64.87
	% Change from No-PV	+42.5%	-25.1%	+42.5%

Table 30. Annual results of emissions reductions

Weight	Type	Non-solar Unit	SO_2	NO_X	CO_2	Water
%		MWh/year/ household	kg/year/ household	Kg/year/ household	Ton/year/ household	kgallon /year/household
Cost= 100%	No-PV	15.01	64.5336	30.4094	11.3018	12.0826
	PV	14.55	64.1291	29.9196	11.0305	11.9301
	% Change from No-PV	-3.1%	-0.627%	-1.61%	-2.40%	-1.26%

5.5.2 Simulation in Minute-by-Minute Resolution

(1) Energy and Emissions Savings of the PV System

Viewed in hourly intervals, as shown in Figure 55, the PV system seems to have a more stable output than usual. Rapid variations in PV generation resulting from transient cloudiness and weather disturbances in the atmosphere create a need for additional spinning reserve that covers uncertainty involved in their output. In fact, they may increase fossil fuel consumption because of their intermittency, or sudden energy shortages or overages. Therefore, this study synthesized the short-term generation of PV systems in minute resolution geographically dispersed throughout the test bed, using the MCMC method. Figure 57 indicates minute-by-minute unit allocation that minimizes the costs of generating electricity on a peak demand day, September 27, 2010.

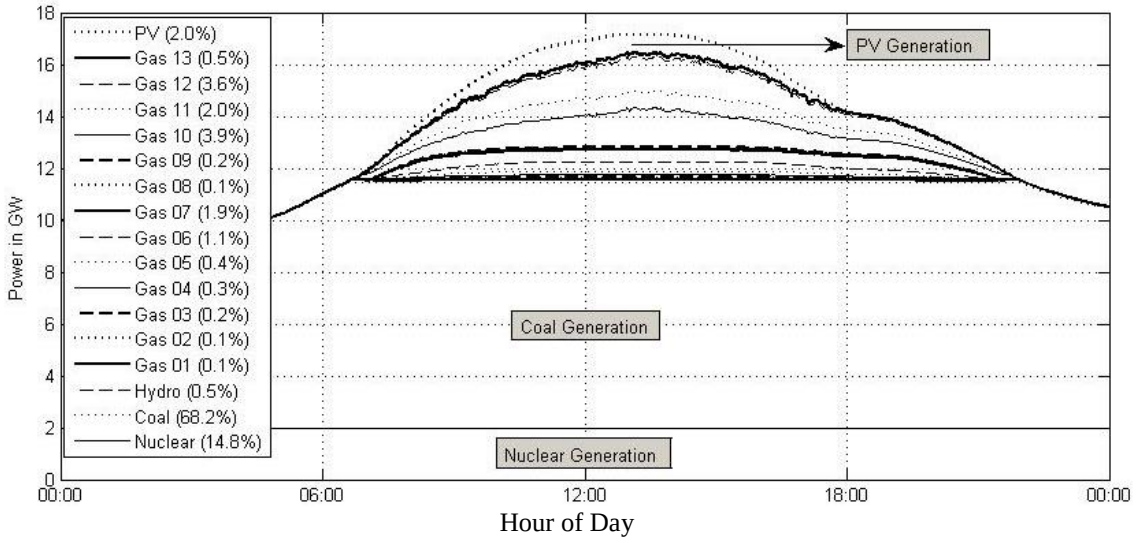

Figure 57. Generation profiles in minute resolution on a peak demand day, September 27, 2010.

Since the PV systems produce an amount of only ten percent of peak demand, rapid variations in their output presented in Figure 54 seem to be not significant in Figure 57. In Figure 57, when the PV output suddenly increases or decreases, faster dispatchable gas-fired units decrease or increase their output. In fact, the power system enhanced by geographically distributed PV systems is able to not only effectively cope with peak demand but also save energy generated from gas-fired plants. Table 31 depicts the impact

of PV systems on energy savings in minute resolution, especially for gas-fired generation. Lastly, Table 32 shows the ecological impact of the PV systems dispersed on the test bed.

Table 31. Daily energy savings of the PV systems in minute resolution on a peak demand day, September 27, 2010

Weight	Type	Energy from Non-solar	Coal-Fired		Gas-Fired		Nuclear		Hydro		PV	
%	-	MWh/day/ household	MWh/day/ household	%	MWh/day/ household	%	MWh/day/ household	%	MWh/day/ household	%	MWh/day/ household	%
Cost= 100%	No-PV	0.049	0.034	68.3	0.008	16.5	0.007	14.8	0.000	0.5	0.000	0
	10% PV	0.048	0.034	68.3	0.007	14.5	0.007	14.8	0.000	0.5	0.001	2.0
	% Change	-2.0%	0%	0	-12.3%	-2.0	0%	0	0%	0	-	+2.0

Table 32. Daily emissions savings in minute resolution on a peak demand day, September 27, 2010

Weight	Type	Energy from Non-solar	SO_2	NO_X	CO_2	Water
%		MWh/day/ household	kg/day/ household	kg/day/ household	ton/day/ household	kgallon/day/ household
Cost= 100%	No-PV	0.049	0.20412	0.0987	0.0374	0.0334
	10% PV	0.048	0.20411	0.0979	0.0369	0.0331
	% Change	-2.0%	-0.002%	-0.81%	-1.34%	-0.90%

(2) Short-Term Intermittency of PV Systems

When the PV output suddenly decreases, conventional units should increase their power output. On the other hand, when it suddenly increases, conventional units should decrease their power output to fully use the PV energy. In fact, because of its intermittency, or sudden energy shortages or overages, intermittent PV system output may increase the need for spinning reserve. To determine the impact of geographically dispersed PV systems on conventional units and spinning reserve in minute resolution, this study examines the time that the difference in total generation from one interval to another exceeds the limits of 17.152, 85.760, and 171.520 MW/min, which correspond to 0.001, 0.005, and 0.01 PU of peak/min, respectively. Table 33 shows that the PV systems increase short-term intermittency by 26.72 percent in the case study.

Table 33. Changes in total generation from one interval to another exceeding the limits on a peak demand day, September 27, 2010

Weight	Type	17.152 MW/min (=0.001 PU of peak/min)	85.760 MW/min (=0.005 PU of peak/min)	171.520 MW/min (=0.01 PU of peak/min)
%		hours/day		
Cost= 100%	No-PV	3.683	0	0
	10% PV	4.667	0.317	0.017
	% Change	+26.72%	-	-

5.6 Conclusion

The aim of this study has been (1) to propose tools and algorithms useful for analyzing the impact of geographically dispersed DG (distributed generation) systems on statewide and nationwide generation resource pools, (2) to address some of the issues in the analysis of the impact of DG systems on such resource pools, and (3) to design a framework for streamlining the smooth integration of the DG system into such resource pools. Therefore, this study has developed an algorithm for generating resource allocation that minimizes ecological impact, including water consumption, and fuel costs, using methods of Lagrangian optimization and hydrothermal coordination. This study has also proposed an example of a modified system in the state of Georgia with an added hypothetical PV (photovoltaic) system portfolio in the form of geographically dispersed systems with a capacity amounting to ten percent of the total peak load of the state. Finally, it has performed simulations for generation resource allocation in hourly and minute-by-minute resolutions and analyzed the impact of geographically dispersed PV systems from a long-term, typically annual, perspective of energy, particularly for peak power and spinning reserve, electricity generation costs, and emissions. Since the capacity of PV systems in this study is a peak of 1.7 GW while the added cumulative capacity of PV systems throughout the United States amounts to a peak of 2.6 GW in 2010 [37], the proposed scenario has been a projection of what might become a viable planning option for statewide or nationwide power grids in the near future.

The results of simulations for the generation resource allocation of the state in hourly resolution have shown that a statewide power grid for Georgia enhanced by PV systems geographically dispersed throughout the state can effectively cope with peaks and save energy generated from quickly dispatchable gas-fired plants, which typically burn expensive fuel at the expense of increased costs of generating electricity. If PV systems dispersed throughout the test bed had a capacity equal to ten percent of total peak

demand, they could decrease energy produced from non-solar plants, particularly by about 3.1 percent in the case study. They could also reduce the release of emissions such as SO_2, NO_X, and CO_2, and water consumption by 0.63, 1.61, 2.40, and 1.26 percent by using less fuel than coal- and gas-fired units.

Since the PV system appears to have a more stable output than expected, this study has modeled the short-term intermittency of transient cloudiness and weather disturbances in the atmosphere using the MCMC (Markov chain Monte Carlo) method and synthesized the generation of geographically dispersed PV systems in minute intervals. It has found that the statewide power grid enhanced by geographically distributed PV systems operating in one-minute intervals can still effectively cope with peaks. However, since PV systems operating in minute intervals increase short-term intermittency in the total generation of all generation units, including PV systems, they create an additional need for spinning reserve that copes with uncertainty involved in their output. In fact, because of their intermittency, PV systems can increase fossil fuel consumption of faster dispatchable spinning reserve, which typically burns the most expensive fuel.

This study has proposed a useful method for analyzing the impact of geographically dispersed DG systems, particularly PV systems in this study, on local, statewide, and nationwide generation resource pools and yielded useful results. For instance, this study has found that PV systems operating in hourly and minute intervals can produce benefits such as an effective reduction in peak load and loss. In addition, using the methods of Lagrangian optimization and hydrothermal coordination, this study has presented an algorithm for environmentally constrained generation resource allocation that minimizes both fuel costs and ecological impact, including water consumption, with each weight. The algorithm can be expanded for analyzing the effect of various DG systems, including PV systems, wind farms, and microturbines geographically dispersed on statewide and nationwide power grids. However, as more

renewables are deployed, the analysis of their impact becomes even more complicated because of intermittency in their output. In fact, renewables can increase the need for additional spinning reserve if they suddenly decrease their output. Therefore, for the smooth integration of renewables into statewide and nationwide power grids, the need for supplementary energy, especially for peak power and spinning reserve, and changes in electricity generation costs resulting from their intermittency must be further investigated.

CHAPTER 6

ACCOMPLISHMENTS, CONTRIBUTIONS, AND FUTURE WORK

6.1 Conclusion

The main objective of this study has been to analyze the impact of the DG (distributed generation) system in general and the PV (photovoltaic) system in particular on the urban distribution network. During the process of this analysis, the study has (1) developed tools, methods, and algorithms for both the analysis of the impact of the DG system and use in planning, designing, and operating such a network, (2) addressed some of the issues in the analysis of the impact of the DG system, and (3) established a framework for streamlining future designs and the smooth integration of the DG system into the urban distribution network.

In Chapter 2, using the backward and forward sweep method implemented in MATLAB, this study developed an algorithm for three-phase power flow that models power system components, including distribution systems, transformers, and PV systems, and calculates the three-phase power flow of the urban radial and meshed network enhanced by DG systems, particularly the PV system in this study. This study (1) implemented the backward and forward sweep method, a method of iterative compensation for the meshed network, and a method of representing the DG bus as a P-Q or P-V bus; (2) modeled common power system components such as the load, the transformer, the voltage regulator, and the shunt capacitor bank; and then (3) verified the algorithm using IEEE 4-, 13-, 34-, 37-, and 123-bus test feeders, which are well-defined and very complex distribution networks. The results of the power-flow analysis of the radial and meshed test feeders enhanced by the DG system have shown that the proposed algorithm is capable of solving power-flow problems accurately and analyzing the impact of the DG system, including the PV system, wind farms, and microturbines, which

contain uncertainties of its inputs, locations, and capacities, none of which are known in the planning stage of the power system, on urban distribution networks.

Chapter 3 of this study proposed a useful method for analyzing the impact of stochastic renewable DG systems, particularly PV systems in this study, that contain uncertainty in their input and output, on urban distribution networks. To model the influence of the inherent uncertainty of the input, the location, and the capacity of the PV system, this study implemented a stochastic simulation algorithm combined with the power-flow algorithm developed in Chapter 2. This study also accelerated the stochastic simulation algorithm using methods of variance reduction, including importance sampling with the optimal near-normal distribution, which reduced variance that occurred when finding the expectation value of the energy savings and emissions savings of N stochastically dispersed PV systems. It also reduced the extremely heavy computational burden caused from the stochastic simulation by the sampling of representative clusters and extreme points. Then, it presented, as the case study, the IEEE 123-bus test feeder, which incorporated residential load profiles obtained from the actual utility in kW in hourly intervals in 2007 and residential PV systems assumed to be installed across the Atlanta area as an urban distribution area. Finally, this study (1) performed stochastic simulations using the energy mix of the state of Georgia and residential PV systems that consisted of commercial PV modules and commercial inverters and that were stochastically dispersed throughout the urban distribution network, (2) quantified the effect of the methods of variance reduction, including importance sampling, and then (3) analyzed the impact of the PV systems from the perspective of energy, especially for peak power, the costs of generating electricity, and emissions.

The results of the simulation of the case studies indicated that PV systems could effectively save energy from the perspective of monthly and daily operations and reduce the release of pollutants and greenhouse gases into the atmosphere by using less fuel from coal- and gas-fired plants. In addition, it investigated methods of acceleration of the

stochastic simulation by the optimal near-normal distribution of importance sampling and defined the stratum of the tilt angle of the PV system as the typical pitch angle for residential roofs. In the proposed case study, the power output of PV systems is estimated by solar radiation and meteorological data of the Atlanta area in TMY (typical meteorological year) data sets in hourly intervals and they are dispersed stochastically throughout the IEEE 123-bus test feeder as an example of the urban distribution network with a capacity equal to ten percent of total peak demand. In the case study, as a result of the combination of both importance sampling and stratification sampling, this study was able to reduce the variance of the power output of N dispersed residential PV systems from 151.14 to 8.54 kWh/year/household with a variance reduction ratio of 17.69, which means the expectation value of annual PV output approaches more closely to a true value, in other words, the expectation value is more accurate. In addition, as a result of the sampling of representative clusters and extreme points, this study reduced a stochastic simulation time of 382.03 to 4.77-5.81 hours.

In Chapter 4, this study implemented algorithms and methods useful for planning, designing, and operating urban distribution networks enhanced by DG systems, particularly the PV system in this study, from the standpoint of the reliability of such networks. It presented a genetic algorithm that determines the optimal allocation of protection devices, including the fuse and the recloser, in two stages and improves the reliability of the urban distribution network enhanced by protection devices (such as fuses and reclosers) and the DG system. Using the backward and forward sweep method, it also proposed an analytical method of generating all possible permanent and transient faults on the main and lateral feeders for an urban distribution network housing a combination of fuses, switches, reclosers, and high-capacity DG systems; the method can also evaluate the failure frequency and duration of such urban distribution networks. Then it also analyzed the impact of both the DG system, including the effect of the islanded operation of the DG system, and protection devices on the reliability of the urban distribution

network.

The analysis of the reliability of IEEE 34- and 123-bus test feeders as case studies demonstrated that the recloser could reduce the duration of a system failure, or the SAIDI. However, the recloser installed on test feeders such as IEEE 34- and 123-bus test feeders exhibited a tendency to increase the frequency of failure, or the SAIFI, because of its multiple reclosing characteristics and lock-out state. In the case of a transient fault, the recloser prevents a downstream fuse from burning, so fewer customers experience outages. In addition, as a result of the islanded operation of the DG system, it has been able to reduce the objective function and the failure duration, or the SAIDI. However, the DG system, particularly the PV system in this study, produced power only during the daytime, so the PV system slightly reduced the annual failure duration. In fact, a PV system with an average of 4.5 hours/day (which is the assumed average time during which the total generation of a zone exceeds the total load of an islanded zone) can reduce the annual failure duration by as much as 18.75 (=4.5/24) percent. However, if PV systems constantly operate at their full capacity during one year and all the load points of the 123-bus test feeder are perfectly coordinated by islanded zones, they can significantly reduce the annual failure duration, even up to zero at the ideal conditions of fully reliable PV systems, fuses, reclosers, and their perfect protection coordination. Thus, to maximize improvement in the reliability of urban distribution networks, various DG types (including PV systems, wind farms, microturbines) enhanced by a storage system and methods of optimizing the location, the capacity, and the zone of the DG system would have to be further investigated.

In Chapter 5, to determine the impact of PV systems geographically dispersed throughout local, statewide, or nationwide grids on energy, especially for peak power and spinning reserve, the costs of generating electricity, and emissions, this study developed an algorithm for generation resource allocation that minimizes ecological impact and fuel costs, synthesized the short-term intermittency of transient cloudiness, and estimated the

generation of geographically dispersed PV systems. Then, it performed simulations for generation resource allocation in hourly and minute-by-minute resolutions. The results of the simulations for the generation resource allocation of a statewide power grid for Georgia in hourly and minute-by-minute resolutions showed that the statewide power grid enhanced by geographically dispersed PV systems could effectively cope with peaks and save energy generated from gas turbines, which typically burn expensive fuel, at the expense of increased costs of generating electricity. However, since PV systems operating in one-minute intervals increase short-term intermittency in the total generation of all generation units, including PV systems, they create an additional need for spinning reserve that copes with uncertainty involved in their output. In fact, because of their intermittency, or sudden energy shortages and overages, PV systems can increase fossil fuel consumption of faster dispatchable spinning reserve, which burns the most expensive fuel. Therefore, for the smooth integration of PV systems into the power grid, the need for supplementary energy, especially for peak power and spinning reserve, and changes in generation costs resulting from their intermittency must be further investigated.

6.2 Contributions

This study contributes to the body of knowledge in the analysis of impact of stochastic renewable distributed generation on urban distribution networks in the following ways:

Chapters 2 and 3: Impact of Stochastic Renewable Distributed Generation on Urban Distribution Networks and Stochastic Methods for the Analysis of Large Data Sets

- *The integration of a fine-tuned algorithm for three-phase power-flow analysis and the stochastic simulation algorithm*

  This study has developed an accurate and fast algorithm that (1) models power system components, including distribution systems, transformers, and the

DG system, particularly the PV system in this study, (2) calculates the three-phase power flow of urban radial and meshed networks enhanced by the DG system, and (3) represents a DG bus of high-penetration capacity as either a P-Q or P-V bus. The algorithm can be extended to the analysis of the impact of the DG system, including the PV system, wind farms, and microturbines. This study has also developed a stochastic simulation algorithm (in which the unknown random variables are the system capacity, the azimuth angle, the title angle, and the module of the residential PV system) and integrated the simulation program for the PV system into an algorithm for three-phase power-flow analysis.

- *The optimal distribution of importance sampling*

  This study has investigated the method of acceleration of the stochastic simulation by the optimal near-normal distribution of importance sampling and defined the stratum of the tilt angle of the PV system as the typical pitch angle for residential roofs. It has found that the optimal distribution of importance sampling can reduce the variance of unknown random variables approximated by a (truncated) normal distribution so that they approach the true expectation value more closely. Thus, the proposed optimal distribution of importance sampling can be used to reduce the variance of unknown random variables in studies of the effect of various DG systems (including PV systems, wind farms, and microturbines) if unknown random variables in their input and output can be approximated by a (truncated) normal distribution.

- *Reduction in the variance of large data sets and the simulation time in the analysis of renewable DG systems*

  In the proposed case study, combining both importance and stratification sampling can reduce the variance of the output of N stochastically dispersed residential PV systems from 151.14 kWh/year/household to 8.54 kWh/year/household with a variance reduction ratio of 17.69, which means the

expectation value of annual PV output approaches more closely to a true value, in other words, the expectation value is more accurate. The sampling of representative clusters and extreme points also has reduced the stochastic simulation time of 382.03 hours to 4.77-5.81 hours.

Chapter 4: Reliability Enhancement Through a Reconfiguration of Urban Distribution Networks Enhanced by DG

- *Analytical method for the evaluation of reliability*

  Using the backward and forward sweep method implemented by KCL (Kirchhoff's current law) and KVL (Kirchhoff's voltage law), this study has proposed an analytical method for the urban distribution network housing a combination of fuses, switches, reclosers, and high-capacity DG systems for evaluating the reliability of urban distribution networks. The proposed method generates all possible permanent and transient faults on the main and lateral feeders, sums the fault current flowing at each bus, searches all buses from the fault bus to the root bus, and calculates drops in voltage, the on-off states of the line, and the frequency and the duration of a failure.

- *Two-stage optimization of protection devices*

  Because of the various operational characteristics of the fuse and the recloser, this study has implemented a genetic algorithm that optimally allocates the fuse and the recloser in two stages within the urban distribution network enhanced by DG. It has optimally allocated both fuses on urban distribution networks and then reclosers, typically from one to three or one to five reclosers, on urban distribution networks optimized with fuses. Both the genetic algorithm and the analytical method can be extended to the analysis of the effect of DG systems, including PV systems, wind farms, and microturbines, on the reliability of the urban distribution network enhanced by DG.

- *Analysis of the impact of the DG system and protection devices*

  In general, because of its islanded operation, the DG system reduces the failure duration, or the SAIDI. However, this study has shown that since the DG system, particularly the PV system, in the proposed case study produces power only during the daytime, the PV system only slightly reduces the annual failure duration, even with a 100 percent capacity of total demand. However, if PV systems constantly operate at their full capacity during one year and all the load points of the 123-bus test feeder are perfectly coordinated by islanded zones, they can significantly reduce the annual failure duration, even up to zero at the ideal conditions of fully reliable PV systems, fuses, reclosers, and their perfect protection coordination. Thus, to maximize the enhancement of reliability, various DG types (including PV systems, wind farms, and microturbines) enhanced by a storage system and methods of optimizing the location, the capacity, and the zone of the DG system must be further investigated.

Chapter 5: Analysis of the Impact of Geographically Distributed Renewable DG Systems on Environmentally Constrained Generation Resource Allocation

- *Development of an algorithm for environmentally constrained generation resource allocation*

  This study has developed an algorithm for generation resource allocation that optimally allocates generation resources using the methods of Lagrangian optimization and hydrothermal coordination. It has implemented a scalar objective function that merges fuel costs and emissions with the water consumption constraint. That is, to minimize costs, emissions, and water consumption with each weight, it has defined the objective function of the algorithm for generation resource allocation. The proposed algorithm can be employed in analyzing the effect of DG systems, including geographically

dispersed PV systems, wind farms, and microturbines, on local, statewide or nationwide power grids.

- *Synthesizing of short-term intermittency in PV generation*

  Viewed in hourly intervals, the power output of geographically dispersed PV systems appears to be more stable than expected. Since current PV generation affected by transient cloudiness depends on only previous generation, this study has synthesized the short-term, typically minute-by-minute, intermittency of transient cloudiness using the MCMC (Markov chain Monte Carlo) method and estimated the generation of geographically dispersed PV systems in minute intervals. The proposed method can be useful for synthesizing short-term intermittency in the generation of weather-dependent renewables such as PV systems and wind farms installed on areas, minute-by-minute weather data of which are not available.

- *Analysis of the impact of geographically dispersed DG systems on generation resource allocation*

  This study has shown that a statewide power grid for Georgia enhanced by geographically dispersed DG systems, particularly the PV system, operating in hourly and minute intervals can effectively cope with peaks and save energy generated from gas turbines, which typically burn expensive fuel. However, since DG systems operating in one-minute intervals increase short-term intermittency in the total generation of all units, including DG systems, they can create an additional need for spinning reserve that copes with uncertainty involved in their output. Therefore, for their smooth integration into the power grid, the need for supplementary energy, particularly for peak power demand and spinning reserve, and changes in electricity generation costs resulting from their intermittency, or sudden energy shortages and overages, must be further investigated.

6.3 Recommendations for Future Work

Although this study has presented contributions to the body of knowledge in the analysis of the impact of stochastic renewable distributed generation on urban distribution networks, it recommends the following future research that can be built on the results presented in this study:

Chapters 2 and 3: Impact of Stochastic Renewable Distributed Generation on Urban Distribution Networks and Stochastic Methods for the Analysis of Large Data Sets

This study has developed an accurate and fast algorithm that models power system components, including distribution systems, transformers, and various DG systems, particularly the PV system in this study. The algorithm can be extended to the analysis of the impact of various other DG systems, including wind farms and microturbines, which are being installed on distribution networks. In addition, this study has analyzed the impact of the PV systems from the perspective of energy, especially for peak power, the costs of generating electricity, and emissions. However, the results do not apply to the rapidly decreasing price of commercial- and utility-scale PV systems, but it can be extended to such a case by modeling distribution networks enhanced by commercial- and utility-scale PV systems and determining their impact on such networks. It has also not applied to PV tracking systems, which produce much more energy than fixed PV systems. If future research conducts such an analysis, it can analyze the strong effect of PV systems on changes in the generation costs.

This study has conducted stochastic simulations of 1,000 years with unknown random variables: the azimuth angle, the title angle, the module, and the capacity of the residential PV system. If N stochastically dispersed residential PV systems operate during one year in hourly intervals, the enumeration of possible combinations for the selection of N PV systems with the uncertainties presented in Table 6 requires $20 \times 901 \times 10 \times 4$ years =

720,800 years. However, this study performed a stochastic simulation of only 1,000 years in hourly intervals because of a simulation time constraint of 8,760 × 1,000 × 0.157 sec ≈ 382.03 hours. (The proposed algorithm takes an average of 0.157 seconds per power-flow calculation on a Dell OptiPlex 9020 desktop computer consisting of an Intel Core i7-4770 CPU with 32 GB of memory, a professional edition of Windows 7, and MATLAB 2014a). Therefore, a necessary simulation period of years to meet sufficient accuracy in a mean of annual PV output (which is calculated by averaging the power output of residential PV systems stochastically installed on *N* households that produce a capacity of ten percent of total peak demand in hourly intervals annually) must be further investigated.

Chapter 4: Reliability Enhancement Through a Reconfiguration of Urban Distribution Networks Enhanced by DG

To maximize reliability, this study optimally has allocated fuses and reclosers on the test feeders (IEEE 34- and 123-bus test feeders) enhanced by DG systems, particularly the PV systems in this study. However, it has not examined costs of the protection device and the DG system, which may vary widely. Therefore, future research can investigate the improvement in reliability per dollar invested, referred to as economic sensitivity analysis. To determine the effect of the improvement in reliability per dollar invested in the protection device and the DG system, it can perform stochastic simulations such as a Monte Carlo simulation, in which the costs of the fuse, the recloser, the breaker, and the DG system are randomly generated within an acceptable range in the following steps:

(1) Investigation of actual costs for the protection device and the DG system

(2) Design and implementation of the stochastic simulation that investigates the improvement of reliability per dollar invested

(3) Economic sensitivity analysis of the protection device and the DG system

This study has presented a genetic algorithm that optimally allocates the fuse and the recloser in two stages within the urban distribution network enhanced by DG systems and an analytical method that evaluates the reliability of the urban distribution network housing a combination of fuses, switches, reclosers, and high-capacity DG systems. Both the genetic algorithm and the analytical method can be extended for analyses of the effects of various DG systems, including PV systems, wind farms, and microturbines, on the reliability of urban distribution networks. Therefore, as future work, to maximize improvement in the reliability, various DG types (including PV systems, wind farms, and microturbines), and DG systems enhanced by a storage system, and methods of optimizing the location, the capacity, and the zone of the DG system can be further investigated by the genetic algorithm and the analytical method developed in this study.

Chapter 5: Analysis of the Impact of Geographically Distributed Renewable DG Systems on Environmentally Constrained Generation Resource Allocation

This study has proposed a useful algorithm for analyzing the impact of geographically dispersed DG systems, particularly PV systems in this study, on local, statewide, and nationwide generation resource pools. The algorithm can be expanded for analyzing the effect of various DG systems, including geographically dispersed PV systems, wind farms, and microturbines, on local, statewide, or nationwide power grids, which are being enhanced by various DG systems. However, as more renewables are deployed, the analysis of their impact becomes even more complicated because of sudden shortages or overages of their output. In fact, renewables can increase the need for additional spinning reserve if they suddenly decrease their output. Therefore, for the smooth integration of renewables into statewide and nationwide power grids, the following future work must be further investigated:

(1) Modeling short-term intermittency in the generation of weather-dependent renewables such as PV systems and wind farms

(2) Parameterization of the distribution of the short-term intermittency of PV systems and wind farms

(3) Investigation of the need for supplementary energy, especially for peak power and spinning reserve, and changes in electricity generation costs resulting from the intermittency of PV systems and wind farms

(4) Simulation of various ramp ratios of coal- and gas-fired generation units

If PV systems suddenly decrease their output, although variability in their output decreases because of their geographical spread, they can increase a need for an additional spinning reserve thereby increasing generation costs, worsening the life of fast dispatchable generators for the spinning reserve (e.g., fast dispatchable gas turbines), and increasing maintenance cycles. Since the costs of faster dispatchable spinning reserves are more expensive than those of non-synchronized reserves, they can affect the costs of the spinning reserve. For example, the costs of generating electricity at peak time may be more expensive than those for base load at off-peak by more than twenty times. This study did not examine the realistic costs of different types of the spinning reserve controlled at peak and off-peak times in short-term resolution, typically from several seconds to hourly intervals. In addition, the study did not analyze the impact of operational uncertainty associated with weather-dependent renewables such as wind and centralized PV on the spinning reserve, all of which can be future work.

APPENDIX A

CONNECTION OF THE TRANSFORMER

Figure 58 shows the transformer connected by the delta-grounded wye, delta-delta, ungrounded wye-delta, and open grounded wye-open delta configuration.

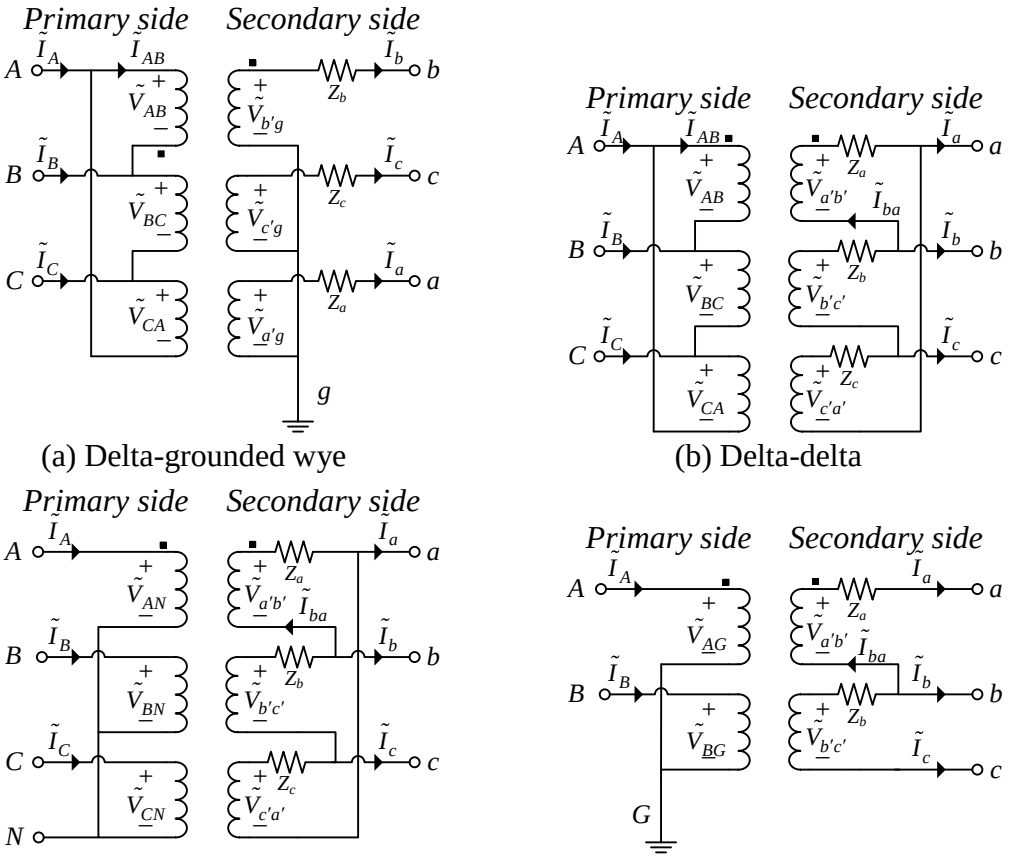

(a) Delta-grounded wye (b) Delta-delta

(c) Ungrounded wye-delta (d) Open wye-open delta

Figure 58. Connection of the transformer.

APPENDIX B

THREE-PHASE POWER-FLOW ALGORITHM USING THE BACKWARD AND FORWARD SWEEP METHOD

This study implemented the algorithm for solving three-phase power flow, which is based on the backward and forward sweep method in MATLAB and modeled common power system components such as various load types (i.e., constant power, constant current, and constant impedance loads), transformers, voltage regulators, and shunt capacitor banks, presented in Chapter 2. If you have any questions or comments regarding the following source codes and the modeling of other feeders, please send an email to kobekim@gmail.com to share the detailed codes or to discuss the modeling of other feeders using the codes.

(1) Main Design Function Codes

```
%%%%%%%%%%%%%%%%%%%%%%%%%%%%%%%%%%%%%%%%%%%%%%%%%%%%%%%%%%%%%%%%%%%%%%%%%%%%%%%%
%  Three-Phase Power-Flow Algorithm Using the Backward Forward Sweep Method
%                                                          kobekim@gmail.com
%                                                 Copyright 2014 by Insu Kim
%%%%%%%%%%%%%%%%%%%%%%%%%%%%%%%%%%%%%%%%%%%%%%%%%%%%%%%%%%%%%%%%%%%%%%%%%%%%%%%%

clear all;
close all;
clc

title_name='NAME:IEEE 123 NODE TEST FEEDER';

format long;

flag_v_pu=1;                    % 1-> PU 0->Actual Value
flag_i_pu=0;                    % 1-> PU 0->Actual Value
flag_disp_ieee=1;               % 0-> doesn't display the ieee result
flag_constant_power_display=0;  % 1-> disply 0->No display
flag_power_disply=0;
flg_i_display=0;
flag_v_display=0;
flag_v_line_display=0;
flag_breakpoint_diplay=1;
flag_breakpoint_locus_display=0;
flag_loss_display=0;
flag_vr_display=0;
flag_bus_seed=0;    % 1 -> predefined bus order while displaying.
flag_breakpoint_test=0; % Line impedance test, April, 4, 2014

mismatch_type=0;
mismatch_max_iteration=5;

BASE_KVA_3PH=60000;                             %[kVA]
BASE_J_PU=1;
SLACK_COEFFICIENT=1.00; % Voltage of Root Bus will be 1.05 pu
AD_COEFF=0.5;

FEET=0.3048/1609.3;                     % 1 Feet = 0.3048/1609.3 Mile
ACCURACY=0.1;
ACCURACY_MESHED=0.001;%0.1;0.001; % use 0.1(16 iterations) for the locus figure
MAX_ITERATION_LIMIT=120;

Ph=inline('mag*exp(j*ang/180*pi)','mag','ang');%argument: magnitude, degree
ALPHA=Ph(1,120);
```

```
%%%%%%%%%%%%%%%%%%%%%%%%%%%%%%%%%%%%%%%%%%%%%%%%%%%%%%%%%%%%%%%%%%%%%%%%%%%%%%%%
% IEEE Standard solution from http://ewh.ieee.org/soc/pes/dsacom/testfeeders/index.html
P_IEEE=[1463.861+582.101i 963.484+343.687i 1193.153+398.976i]*1000;
P_T_IEEE=(3620.498+1324.765i)*1000;
I_IEEE=[Ph(655.91,-21.69) Ph(425.91,-139.63) Ph(523.82,101.51)];
P_LOSS_IEEE=[50.540+102.653i 10.134+38.837i 34.937+52.237i];
%%%%%%%%%%%%%%%%%%%%%%%%%%%%%%%%%%%%%%%%%%%%%%%%%%%%%%%%%%%%%%%%%%%%%%%%%%%%%%%%

BUS_NUM=138;
ROOT_BUS_NO=117;

% First Column: 001:Sub Feeder 002:Main Feeder
% Second,Third,...: Node Number
% Warning: Last row should be the longest main feeder followed by the slack
SIMPLIFIED_BACK_LATERAL_DATA=[
001 002 001 000 000 000 000 000 000 000 000 000 000 000 000 000 000 000 000 000 000 000 000 000 000 000 000% # 01 Path
001 004 003 001 000 000 000 000 000 000 000 000 000 000 000 000 000 000 000 000 000 000 000 000 000 000 000% # 02 Path
001 006 005 003 001 000 000 000 000 000 000 000 000 000 000 000 000 000 000 000 000 000 000 000 000 000 000% # 03 Path
001 010 014 137 128 009 008 000 000 000 000 000 000 000 000 000 000 000 000 000 000 000 000 000 000 000 000% # 04 Path
001 011 014 137 128 009 008 000 000 000 000 000 000 000 000 000 000 000 000 000 000 000 000 000 000 000 000% # 05 Path
001 012 008 000 000 000 000 000 000 000 000 000 000 000 000 000 000 000 000 000 000 000 000 000 000 000 000% # 06 Path
001 016 015 034 013 000 000 000 000 000 000 000 000 000 000 000 000 000 000 000 000 000 000 000 000 000 000% # 07 Path
001 017 015 034 013 000 000 000 000 000 000 000 000 000 000 000 000 000 000 000 000 000 000 000 000 000 000% # 08 Path
001 020 019 018 000 000 000 000 000 000 000 000 000 000 000 000 000 000 000 000 000 000 000 000 000 000 000% # 09 Path
001 022 021 000 000 000 000 000 000 000 000 000 000 000 000 000 000 000 000 000 000 000 000 000 000 000 000% # 10 Path
001 024 023 000 000 000 000 000 000 000 000 000 000 000 000 000 000 000 000 000 000 000 000 000 000 000 000% # 11 Path
001 033 027 026 138 129 025 000 000 000 000 000 000 000 000 000 000 000 000 000 000 000 000 000 000 000 000% # 12 Path
001 032 031 026 138 129 025 000 000 000 000 000 000 000 000 000 000 000 000 000 000 000 000 000 000 000 000% # 13 Path
001 123 030 029 028 025 000 000 000 000 000 000 000 000 000 000 000 000 000 000 000 000 000 000 000 000 000% # 14 Path
001 037 036 035 000 000 000 000 000 000 000 000 000 000 000 000 000 000 000 000 000 000 000 000 000 000 000% # 15 Path
001 039 038 036 035 000 000 000 000 000 000 000 000 000 000 000 000 000 000 000 000 000 000 000 000 000 000% # 16 Path
001 041 040 000 000 000 000 000 000 000 000 000 000 000 000 000 000 000 000 000 000 000 000 000 000 000 000% # 17 Path
001 043 042 000 000 000 000 000 000 000 000 000 000 000 000 000 000 000 000 000 000 000 000 000 000 000 000% # 18 Path
001 046 045 044 000 000 000 000 000 000 000 000 000 000 000 000 000 000 000 000 000 000 000 000 000 000 000% # 19 Path
001 118 051 050 049 047 000 000 000 000 000 000 000 000 000 000 000 000 000 000 000 000 000 000 000 000 000% # 20 Path
001 048 047 000 000 000 000 000 000 000 000 000 000 000 000 000 000 000 000 000 000 000 000 000 000 000 000% # 21 Path
001 056 055 054 000 000 000 000 000 000 000 000 000 000 000 000 000 000 000 000 000 000 000 000 000 000 000% # 22 Path
001 059 058 057 000 000 000 000 000 000 000 000 000 000 000 000 000 000 000 000 000 000 000 000 000 000 000% # 23 Path
001 066 065 064 063 062 060 000 000 000 000 000 000 000 000 000 000 000 000 000 000 000 000 000 000 000 000% # 24 Path
001 126 131 061 060 000 000 000 000 000 000 000 000 000 000 000 000 000 000 000 000 000 000 000 000 000 000% # 25 Path
001 096 095 093 000 000 000 000 000 000 000 000 000 000 000 000 000 000 000 000 000 000 000 000 000 000 000% # 26 Path
001 094 093 000 000 000 000 000 000 000 000 000 000 000 000 000 000 000 000 000 000 000 000 000 000 000 000% # 27 Path
001 133 092 091 000 000 000 000 000 000 000 000 000 000 000 000 000 000 000 000 000 000 000 000 000 000 000% # 28 Path
001 134 090 089 000 000 000 000 000 000 000 000 000 000 000 000 000 000 000 000 000 000 000 000 000 000 000% # 29 Path
001 135 088 087 000 000 000 000 000 000 000 000 000 000 000 000 000 000 000 000 000 000 000 000 000 000 000% # 30 Path
001 132 083 082 081 080 078 077 076 000 000 000 000 000 000 000 000 000 000 000 000 000 000 000 000 000 000% # 31 Path
001 085 084 081 080 078 077 076 000 000 000 000 000 000 000 000 000 000 000 000 000 000 000 000 000 000 000% # 32 Path
001 079 078 077 076 000 000 000 000 000 000 000 000 000 000 000 000 000 000 000 000 000 000 000 000 000 000% # 33 Path
001 075 074 073 072 000 000 000 000 000 000 000 000 000 000 000 000 000 000 000 000 000 000 000 000 000 000% # 34 Path
001 071 070 069 068 067 000 000 000 000 000 000 000 000 000 000 000 000 000 000 000 000 000 000 000 000 000% # 35 Path
001 125 100 099 098 097 000 000 000 000 000 000 000 000 000 000 000 000 000 000 000 000 000 000 000 000 000% # 36 Path
001 104 103 102 101 000 000 000 000 000 000 000 000 000 000 000 000 000 000 000 000 000 000 000 000 000 000% # 37 Path
001 107 106 105 000 000 000 000 000 000 000 000 000 000 000 000 000 000 000 000 000 000 000 000 000 000 000% # 38 Path
001 114 113 112 110 109 108 000 000 000 000 000 000 000 000 000 000 000 000 000 000 000 000 000 000 000 000% # 39 Path
001 111 110 109 108 000 000 000 000 000 000 000 000 000 000 000 000 000 000 000 000 000 000 000 000 000 000% # 40 Path
001 124 108 000 000 000 000 000 000 000 000 000 000 000 000 000 000 000 000 000 000 000 000 000 000 000 000% # 41 Path
002 108 105 101 122 097 067 000 000 000 000 000 000 000 000 000 000 000 000 000 000 000 000 000 000 000 000% #1 Main Feeder
002 047 044 042 040 035 115 018 000 000 000 000 000 000 000 000 000 000 000 000 000 000 000 000 000 000 000% #2 Main Feeder
002 025 023 021 018 013 000 000 000 000 000 000 000 000 000 000 000 000 000 000 000 000 000 000 000 000 000% #3 Main Feeder
002 093 091 089 087 086 076 072 067 136 130 120 060 057 054 053 052 119 013 008 007 001 116 127 117% #4 Main Feeder
];


% From Bus | To Bus | Root Bus | Path 1 | Path 2 |
% Phase Info(0:3 Phs, 1:A, 2:B, 3:C, 4:AB, 5:BC, 6:CA)

MESHED_DATA=[
% 118 124 ROOT_BUS_NO 20 41 0 % loop #1
% 054 094 ROOT_BUS_NO 22 27 1 % loop #5
% 114 071 ROOT_BUS_NO 39 35 1 % loop #4
% 020 011 ROOT_BUS_NO 09 05 1 % loop #3
% 075 085 ROOT_BUS_NO 34 32 3 % loop #2
];

MESHED_BACK_LATERAL_DATA=[
002 001 116 127 117 000 000 000 000 000 000 000 000 000 000 000 000 000 000 000 000 000 000 000 000 000 000 % 01
004 003 001 116 127 117 000 000 000 000 000 000 000 000 000 000 000 000 000 000 000 000 000 000 000 000 000 % 02
006 005 003 001 116 127 117 000 000 000 000 000 000 000 000 000 000 000 000 000 000 000 000 000 000 000 000 % 03
010 014 137 128 009 008 007 001 116 127 117 000 000 000 000 000 000 000 000 000 000 000 000 000 000 000 000 % 04
011 014 137 128 009 008 007 001 116 127 117 000 000 000 000 000 000 000 000 000 000 000 000 000 000 000 000 % 05
012 008 007 001 116 127 117 000 000 000 000 000 000 000 000 000 000 000 000 000 000 000 000 000 000 000 000 % 06
016 015 034 013 008 007 001 116 127 117 000 000 000 000 000 000 000 000 000 000 000 000 000 000 000 000 000 % 07
017 015 034 013 008 007 001 116 127 117 000 000 000 000 000 000 000 000 000 000 000 000 000 000 000 000 000 % 08
020 019 018 013 008 007 001 116 127 117 000 000 000 000 000 000 000 000 000 000 000 000 000 000 000 000 000 % 09
022 021 018 013 008 007 001 116 127 117 000 000 000 000 000 000 000 000 000 000 000 000 000 000 000 000 000 % 10
024 023 021 018 013 008 007 001 116 127 117 000 000 000 000 000 000 000 000 000 000 000 000 000 000 000 000 % 11
033 027 026 138 129 025 023 021 018 013 008 007 001 116 127 117 000 000 000 000 000 000 000 000 000 000 000 % 12
032 031 026 138 129 025 023 021 018 013 008 007 001 116 127 117 000 000 000 000 000 000 000 000 000 000 000 % 13
123 030 029 028 025 023 021 018 013 008 007 001 116 127 117 000 000 000 000 000 000 000 000 000 000 000 000 % 14
037 036 035 115 018 013 008 007 001 116 127 117 000 000 000 000 000 000 000 000 000 000 000 000 000 000 000 % 15
039 038 036 035 115 018 013 008 007 001 116 127 117 000 000 000 000 000 000 000 000 000 000 000 000 000 000 % 16
```

```
041 040 035 115 018 013 008 007 001 116 127 117 000 000 000 000 000 000 000 000 000 000 000 000 000 000 000 % 17
043 042 040 035 115 018 013 008 007 001 116 127 117 000 000 000 000 000 000 000 000 000 000 000 000 000 000 % 18
046 045 044 042 040 035 115 018 013 008 007 001 116 127 117 000 000 000 000 000 000 000 000 000 000 000 000 % 19
118 051 050 049 047 044 042 040 035 115 018 013 008 007 001 116 127 117 000 000 000 000 000 000 000 000 000 % 20
048 047 044 042 040 035 115 018 013 008 007 001 116 127 117 000 000 000 000 000 000 000 000 000 000 000 000 % 21
056 055 054 053 052 119 013 008 007 001 116 127 117 000 000 000 000 000 000 000 000 000 000 000 000 000 000 % 22
059 058 057 054 053 052 119 013 008 007 001 116 127 117 000 000 000 000 000 000 000 000 000 000 000 000 000 % 23
066 065 064 063 062 060 057 054 053 052 119 013 008 007 001 116 127 117 000 000 000 000 000 000 000 000 000 % 24
126 131 061 060 057 054 053 052 119 013 008 007 001 116 127 117 000 000 000 000 000 000 000 000 000 000 000 % 25
096 095 093 091 089 087 086 076 072 067 136 130 120 060 057 054 053 052 119 013 008 007 001 116 127 117 000 % 26
094 093 091 089 087 086 076 072 067 136 130 120 060 057 054 053 052 119 013 008 007 001 116 127 117 000 000 % 27
133 092 091 089 087 086 076 072 067 136 130 120 060 057 054 053 052 119 013 008 007 001 116 127 117 000 000 % 28
134 090 089 087 086 076 072 067 136 130 120 060 057 054 053 052 119 013 008 007 001 116 127 117 000 000 000 % 29
135 088 087 086 076 072 067 136 130 120 060 057 054 053 052 119 013 008 007 001 116 127 117 000 000 000 000 % 30
132 083 082 081 080 078 077 076 072 067 136 130 120 060 057 054 053 052 119 013 008 007 001 116 127 117 000 % 31
085 084 081 080 078 077 076 072 067 136 130 120 060 057 054 053 052 119 013 008 007 001 116 127 117 000 000 % 32
079 078 077 076 072 067 136 130 120 060 057 054 053 052 119 013 008 007 001 116 127 117 000 000 000 000 000 % 33
075 074 073 072 067 136 130 120 060 057 054 053 052 119 013 008 007 001 116 127 117 000 000 000 000 000 000 % 34
071 070 069 068 067 136 130 120 060 057 054 053 052 119 013 008 007 001 116 127 117 000 000 000 000 000 000 % 35
125 100 099 098 097 067 136 130 120 060 057 054 053 052 119 013 008 007 001 116 127 117 000 000 000 000 000 % 36
104 103 102 101 122 097 067 136 130 120 060 057 054 053 052 119 013 008 007 001 116 127 117 000 000 000 000 % 37
107 106 105 101 122 097 067 136 130 120 060 057 054 053 052 119 013 008 007 001 116 127 117 000 000 000 000 % 38
114 113 112 110 109 108 105 101 122 097 067 136 130 120 060 057 054 053 052 119 013 008 007 001 116 127 117 000 % 39
111 110 109 108 105 101 122 097 067 136 130 120 060 057 054 053 052 119 013 008 007 001 116 127 117 000 000 % 40
124 108 105 101 122 097 067 136 130 120 060 057 054 053 052 119 013 008 007 001 116 127 117 000 000 000 000 % 41
];

%%%%%%%%%%%%%%%%%%%%%%%%%%%%%%%%%%%%%%%%%%%%%%%%%%%%%%%%%%%%%%%%%%%%%%%%%%%%%%%
%   Bus Data
%%%%%%%%%%%%%%%%%%%%%%%%%%%%%%%%%%%%%%%%%%%%%%%%%%%%%%%%%%%%%%%%%%%%%%%%%%%%%%%
% 1. Bus Number
% 2. Load Type(0: constant power 1: constant current 2: constnat impedance)
%    (0,1,2<--Wye connected, a-g, b-g, c-g
%    (3<--Reserved
%    (4, Delta connected(ab, bc, ca) Constant Power
%        Nominal Volt(kV)->Input a-g voltage
%    (5, Delta connected Constant Current Load)
%    (6, Delta connected Constant Impedance Load)
% 3. Real Power(KW) -> if 4000 kW, Input 4000*KVA
% 4. Reactive Power(KVAR)
% 5. Power Factor
% 6. Voltage Regulator( Bet 1 and 2 ->  Input VR ID at Bus 2)
% 7. Shunt Capacitor of the Bus(KVA)
% 8. Nominal Voltage(If 4.16 kV, Input Nominal Volt: (4.16/sqrt(3))/BASE_KV)
KVA=1000;

bus_data=[
% Bus No LoadType   kW          kVar            PF     VR ID Sh.Cap[kVA]    Nominal Volt(LL Volt)
1           0       40*KVA      20*KVA            0       0       0*KVA     4160
1           0        0*KVA       0*KVA            0       0       0*KVA     4160
1           0        0*KVA       0*KVA            0       0       0*KVA     4160
2           0        0*KVA       0*KVA            0       0       0*KVA     4160
2           0       20*KVA      10*KVA            0       0       0*KVA     4160
2           0        0*KVA       0*KVA            0       0       0*KVA     4160
3           0        0*KVA       0*KVA            0       0       0*KVA     4160
3           0        0*KVA       0*KVA            0       0       0*KVA     4160
3           0        0*KVA       0*KVA            0       0       0*KVA     4160
4           0        0*KVA       0*KVA            0       0       0*KVA     4160
4           0        0*KVA       0*KVA            0       0       0*KVA     4160
4           0       40*KVA      20*KVA            0       0       0*KVA     4160
5           0        0*KVA       0*KVA            0       0       0*KVA     4160
5           0        0*KVA       0*KVA            0       0       0*KVA     4160
5           1       20*KVA      10*KVA            0       0       0*KVA     4160
6           0        0*KVA       0*KVA            0       0       0*KVA     4160
6           0        0*KVA       0*KVA            0       0       0*KVA     4160
6           2       40*KVA      20*KVA            0       0       0*KVA     4160
7           0       20*KVA      10*KVA            0       0       0*KVA     4160
7           0        0*KVA       0*KVA            0       0       0*KVA     4160
7           0        0*KVA       0*KVA            0       0       0*KVA     4160
8           0        0*KVA       0*KVA            0       0       0*KVA     4160
8           0        0*KVA       0*KVA            0       0       0*KVA     4160
8           0        0*KVA       0*KVA            0       0       0*KVA     4160
9           0       40*KVA      20*KVA            0       0       0*KVA     4160
9           0        0*KVA       0*KVA            0       0       0*KVA     4160
9           0        0*KVA       0*KVA            0       0       0*KVA     4160
10          1       20*KVA      10*KVA            0       0       0*KVA     4160
10          0        0*KVA       0*KVA            0       0       0*KVA     4160
10          0        0*KVA       0*KVA            0       0       0*KVA     4160
11          2       40*KVA      20*KVA            0       0       0*KVA     4160
11          0        0*KVA       0*KVA            0       0       0*KVA     4160
11          0        0*KVA       0*KVA            0       0       0*KVA     4160
12          0        0*KVA       0*KVA            0       0       0*KVA     4160
12          0       20*KVA      10*KVA            0       0       0*KVA     4160
12          0        0*KVA       0*KVA            0       0       0*KVA     4160
13          0        0*KVA       0*KVA            0       0       0*KVA     4160
13          0        0*KVA       0*KVA            0       0       0*KVA     4160
13          0        0*KVA       0*KVA            0       0       0*KVA     4160
14          0        0*KVA       0*KVA            0       0       0*KVA     4160
14          0        0*KVA       0*KVA            0       0       0*KVA     4160
14          0        0*KVA       0*KVA            0       0       0*KVA     4160
15          0        0*KVA       0*KVA            0       0       0*KVA     4160
15          0        0*KVA       0*KVA            0       0       0*KVA     4160
15          0        0*KVA       0*KVA            0       0       0*KVA     4160
16          0        0*KVA       0*KVA            0       0       0*KVA     4160
```

16	0	0*KVA	0*KVA	0	0	0*KVA	4160
16	0	40*KVA	20*KVA	0	0	0*KVA	4160
17	0	0*KVA	0*KVA	0	0	0*KVA	4160
17	0	0*KVA	0*KVA	0	0	0*KVA	4160
17	0	20*KVA	10*KVA	0	0	0*KVA	4160
18	0	0*KVA	0*KVA	0	0	0*KVA	4160
18	0	0*KVA	0*KVA	0	0	0*KVA	4160
18	0	0*KVA	0*KVA	0	0	0*KVA	4160
19	0	40*KVA	20*KVA	0	0	0*KVA	4160
19	0	0*KVA	0*KVA	0	0	0*KVA	4160
19	0	0*KVA	0*KVA	0	0	0*KVA	4160
20	1	40*KVA	20*KVA	0	0	0*KVA	4160
20	0	0*KVA	0*KVA	0	0	0*KVA	4160
20	0	0*KVA	0*KVA	0	0	0*KVA	4160
21	0	0*KVA	0*KVA	0	0	0*KVA	4160
21	0	0*KVA	0*KVA	0	0	0*KVA	4160
21	0	0*KVA	0*KVA	0	0	0*KVA	4160
22	0	0*KVA	0*KVA	0	0	0*KVA	4160
22	2	40*KVA	20*KVA	0	0	0*KVA	4160
22	0	0*KVA	0*KVA	0	0	0*KVA	4160
23	0	0*KVA	0*KVA	0	0	0*KVA	4160
23	0	0*KVA	0*KVA	0	0	0*KVA	4160
23	0	0*KVA	0*KVA	0	0	0*KVA	4160
24	0	0*KVA	0*KVA	0	0	0*KVA	4160
24	0	0*KVA	0*KVA	0	0	0*KVA	4160
24	0	40*KVA	20*KVA	0	0	0*KVA	4160
25	0	0*KVA	0*KVA	0	0	0*KVA	4160
25	0	0*KVA	0*KVA	0	0	0*KVA	4160
25	0	0*KVA	0*KVA	0	0	0*KVA	4160
26	0	0*KVA	0*KVA	0	0	0*KVA	4160
26	0	0*KVA	0*KVA	0	0	0*KVA	4160
26	0	0*KVA	0*KVA	0	0	0*KVA	4160
27	0	0*KVA	0*KVA	0	0	0*KVA	4160
27	0	0*KVA	0*KVA	0	0	0*KVA	4160
27	0	0*KVA	0*KVA	0	0	0*KVA	4160
28	1	40*KVA	20*KVA	0	0	0*KVA	4160
28	0	0*KVA	0*KVA	0	0	0*KVA	4160
28	0	0*KVA	0*KVA	0	0	0*KVA	4160
29	2	40*KVA	20*KVA	0	0	0*KVA	4160
29	0	0*KVA	0*KVA	0	0	0*KVA	4160
29	0	0*KVA	0*KVA	0	0	0*KVA	4160
30	0	0*KVA	0*KVA	0	0	0*KVA	4160
30	0	0*KVA	0*KVA	0	0	0*KVA	4160
30	0	40*KVA	20*KVA	0	0	0*KVA	4160
31	0	0*KVA	0*KVA	0	0	0*KVA	4160
31	0	0*KVA	0*KVA	0	0	0*KVA	4160
31	0	20*KVA	10*KVA	0	0	0*KVA	4160
32	0	0*KVA	0*KVA	0	0	0*KVA	4160
32	0	0*KVA	0*KVA	0	0	0*KVA	4160
32	0	20*KVA	10*KVA	0	0	0*KVA	4160
33	1	40*KVA	20*KVA	0	0	0*KVA	4160
33	0	0*KVA	0*KVA	0	0	0*KVA	4160
33	0	0*KVA	0*KVA	0	0	0*KVA	4160
34	0	0*KVA	0*KVA	0	0	0*KVA	4160
34	0	0*KVA	0*KVA	0	0	0*KVA	4160
34	2	40*KVA	20*KVA	0	0	0*KVA	4160
35	4	40*KVA	20*KVA	0	0	0*KVA	4160
35	0	0*KVA	0*KVA	0	0	0*KVA	4160
35	0	0*KVA	0*KVA	0	0	0*KVA	4160
36	0	0*KVA	0*KVA	0	0	0*KVA	4160
36	0	0*KVA	0*KVA	0	0	0*KVA	4160
36	0	0*KVA	0*KVA	0	0	0*KVA	4160
37	2	40*KVA	20*KVA	0	0	0*KVA	4160
37	0	0*KVA	0*KVA	0	0	0*KVA	4160
37	0	0*KVA	0*KVA	0	0	0*KVA	4160
38	0	0*KVA	0*KVA	0	0	0*KVA	4160
38	1	20*KVA	10*KVA	0	0	0*KVA	4160
38	0	0*KVA	0*KVA	0	0	0*KVA	4160
39	0	0*KVA	0*KVA	0	0	0*KVA	4160
39	0	20*KVA	10*KVA	0	0	0*KVA	4160
39	0	0*KVA	0*KVA	0	0	0*KVA	4160
40	0	0*KVA	0*KVA	0	0	0*KVA	4160
40	0	0*KVA	0*KVA	0	0	0*KVA	4160
40	0	0*KVA	0*KVA	0	0	0*KVA	4160
41	0	0*KVA	0*KVA	0	0	0*KVA	4160
41	0	0*KVA	0*KVA	0	0	0*KVA	4160
41	0	20*KVA	10*KVA	0	0	0*KVA	4160
42	0	20*KVA	10*KVA	0	0	0*KVA	4160
42	0	0*KVA	0*KVA	0	0	0*KVA	4160
42	0	0*KVA	0*KVA	0	0	0*KVA	4160
43	0	0*KVA	0*KVA	0	0	0*KVA	4160
43	2	40*KVA	20*KVA	0	0	0*KVA	4160
43	0	0*KVA	0*KVA	0	0	0*KVA	4160
44	0	0*KVA	0*KVA	0	0	0*KVA	4160
44	0	0*KVA	0*KVA	0	0	0*KVA	4160
44	0	0*KVA	0*KVA	0	0	0*KVA	4160
45	1	20*KVA	10*KVA	0	0	0*KVA	4160
45	0	0*KVA	0*KVA	0	0	0*KVA	4160
45	0	0*KVA	0*KVA	0	0	0*KVA	4160
46	0	20*KVA	10*KVA	0	0	0*KVA	4160
46	0	0*KVA	0*KVA	0	0	0*KVA	4160
46	0	0*KVA	0*KVA	0	0	0*KVA	4160
47	1	35*KVA	25*KVA	0	0	0*KVA	4160
47	1	35*KVA	25*KVA	0	0	0*KVA	4160
47	1	35*KVA	25*KVA	0	0	0*KVA	4160

48	2	70*KVA	50*KVA	0	0	0*KVA	4160
48	2	70*KVA	50*KVA	0	0	0*KVA	4160
48	2	70*KVA	50*KVA	0	0	0*KVA	4160
49	0	35*KVA	25*KVA	0	0	0*KVA	4160
49	0	70*KVA	50*KVA	0	0	0*KVA	4160
49	0	35*KVA	20*KVA	0	0	0*KVA	4160
50	0	0*KVA	0*KVA	0	0	0*KVA	4160
50	0	0*KVA	0*KVA	0	0	0*KVA	4160
50	0	40*KVA	20*KVA	0	0	0*KVA	4160
51	0	20*KVA	10*KVA	0	0	0*KVA	4160
51	0	0*KVA	0*KVA	0	0	0*KVA	4160
51	0	0*KVA	0*KVA	0	0	0*KVA	4160
52	0	40*KVA	20*KVA	0	0	0*KVA	4160
52	0	0*KVA	0*KVA	0	0	0*KVA	4160
52	0	0*KVA	0*KVA	0	0	0*KVA	4160
53	0	40*KVA	20*KVA	0	0	0*KVA	4160
53	0	0*KVA	0*KVA	0	0	0*KVA	4160
53	0	0*KVA	0*KVA	0	0	0*KVA	4160
54	0	0*KVA	0*KVA	0	0	0*KVA	4160
54	0	0*KVA	0*KVA	0	0	0*KVA	4160
54	0	0*KVA	0*KVA	0	0	0*KVA	4160
55	2	20*KVA	10*KVA	0	0	0*KVA	4160
55	0	0*KVA	0*KVA	0	0	0*KVA	4160
55	0	0*KVA	0*KVA	0	0	0*KVA	4160
56	0	0*KVA	0*KVA	0	0	0*KVA	4160
56	0	20*KVA	10*KVA	0	0	0*KVA	4160
56	0	0*KVA	0*KVA	0	0	0*KVA	4160
57	0	0*KVA	0*KVA	0	0	0*KVA	4160
57	0	0*KVA	0*KVA	0	0	0*KVA	4160
57	0	0*KVA	0*KVA	0	0	0*KVA	4160
58	0	0*KVA	0*KVA	0	0	0*KVA	4160
58	1	20*KVA	10*KVA	0	0	0*KVA	4160
58	0	0*KVA	0*KVA	0	0	0*KVA	4160
59	0	0*KVA	0*KVA	0	0	0*KVA	4160
59	0	20*KVA	10*KVA	0	0	0*KVA	4160
59	0	0*KVA	0*KVA	0	0	0*KVA	4160
60	0	20*KVA	10*KVA	0	0	0*KVA	4160
60	0	0*KVA	0*KVA	0	0	0*KVA	4160
60	0	0*KVA	0*KVA	0	0	0*KVA	4160
61	0	0*KVA	0*KVA	0	0	0*KVA	4160
61	0	0*KVA	0*KVA	0	0	0*KVA	4160
61	0	0*KVA	0*KVA	0	0	0*KVA	4160
62	0	0*KVA	0*KVA	0	0	0*KVA	4160
62	0	0*KVA	0*KVA	0	0	0*KVA	4160
62	2	40*KVA	20*KVA	0	0	0*KVA	4160
63	0	40*KVA	20*KVA	0	0	0*KVA	4160
63	0	0*KVA	0*KVA	0	0	0*KVA	4160
63	0	0*KVA	0*KVA	0	0	0*KVA	4160
64	0	0*KVA	0*KVA	0	0	0*KVA	4160
64	1	75*KVA	35*KVA	0	0	0*KVA	4160
64	0	0*KVA	0*KVA	0	0	0*KVA	4160
65	6	35*KVA	25*KVA	0	0	0*KVA	4160
65	6	35*KVA	25*KVA	0	0	0*KVA	4160
65	6	70*KVA	50*KVA	0	0	0*KVA	4160
66	0	0*KVA	0*KVA	0	0	0*KVA	4160
66	0	0*KVA	0*KVA	0	0	0*KVA	4160
66	0	75*KVA	35*KVA	0	0	0*KVA	4160
67	0	0*KVA	0*KVA	0	0	0*KVA	4160
67	0	0*KVA	0*KVA	0	0	0*KVA	4160
67	0	0*KVA	0*KVA	0	0	0*KVA	4160
68	0	20*KVA	10*KVA	0	0	0*KVA	4160
68	0	0*KVA	0*KVA	0	0	0*KVA	4160
68	0	0*KVA	0*KVA	0	0	0*KVA	4160
69	0	40*KVA	20*KVA	0	0	0*KVA	4160
69	0	0*KVA	0*KVA	0	0	0*KVA	4160
69	0	0*KVA	0*KVA	0	0	0*KVA	4160
70	0	20*KVA	10*KVA	0	0	0*KVA	4160
70	0	0*KVA	0*KVA	0	0	0*KVA	4160
70	0	0*KVA	0*KVA	0	0	0*KVA	4160
71	0	40*KVA	20*KVA	0	0	0*KVA	4160
71	0	0*KVA	0*KVA	0	0	0*KVA	4160
71	0	0*KVA	0*KVA	0	0	0*KVA	4160
72	0	0*KVA	0*KVA	0	0	0*KVA	4160
72	0	0*KVA	0*KVA	0	0	0*KVA	4160
72	0	0*KVA	0*KVA	0	0	0*KVA	4160
73	0	0*KVA	0*KVA	0	0	0*KVA	4160
73	0	0*KVA	0*KVA	0	0	0*KVA	4160
73	0	40*KVA	20*KVA	0	0	0*KVA	4160
74	0	0*KVA	0*KVA	0	0	0*KVA	4160
74	0	0*KVA	0*KVA	0	0	0*KVA	4160
74	2	40*KVA	20*KVA	0	0	0*KVA	4160
75	0	0*KVA	0*KVA	0	0	0*KVA	4160
75	0	0*KVA	0*KVA	0	0	0*KVA	4160
75	0	40*KVA	20*KVA	0	0	0*KVA	4160
76	5	105*KVA	80*KVA	0	0	0*KVA	4160
76	5	70*KVA	50*KVA	0	0	0*KVA	4160
76	5	70*KVA	50*KVA	0	0	0*KVA	4160
77	0	0*KVA	0*KVA	0	0	0*KVA	4160
77	0	40*KVA	20*KVA	0	0	0*KVA	4160
77	0	0*KVA	0*KVA	0	0	0*KVA	4160
78	0	0*KVA	0*KVA	0	0	0*KVA	4160
78	0	0*KVA	0*KVA	0	0	0*KVA	4160
78	0	0*KVA	0*KVA	0	0	0*KVA	4160
79	2	40*KVA	20*KVA	0	0	0*KVA	4160
79	0	0*KVA	0*KVA	0	0	0*KVA	4160

79	0	0*KVA	0*KVA	0	0	0*KVA	4160
80	0	0*KVA	0*KVA	0	0	0*KVA	4160
80	0	40*KVA	20*KVA	0	0	0*KVA	4160
80	0	0*KVA	0*KVA	0	0	0*KVA	4160
81	0	0*KVA	0*KVA	0	0	0*KVA	4160
81	0	0*KVA	0*KVA	0	0	0*KVA	4160
81	0	0*KVA	0*KVA	0	0	0*KVA	4160
82	0	40*KVA	20*KVA	0	0	0*KVA	4160
82	0	0*KVA	0*KVA	0	0	0*KVA	4160
82	0	0*KVA	0*KVA	0	0	0*KVA	4160
83	0	0*KVA	0*KVA	0	0	200*KVA	4160
83	0	0*KVA	0*KVA	0	0	200*KVA	4160
83	0	20*KVA	10*KVA	0	0	200*KVA	4160
84	0	0*KVA	0*KVA	0	0	0*KVA	4160
84	0	0*KVA	0*KVA	0	0	0*KVA	4160
84	0	20*KVA	10*KVA	0	0	0*KVA	4160
85	0	0*KVA	0*KVA	0	0	0*KVA	4160
85	0	0*KVA	0*KVA	0	0	0*KVA	4160
85	0	40*KVA	20*KVA	0	0	0*KVA	4160
86	0	0*KVA	0*KVA	0	0	0*KVA	4160
86	0	20*KVA	10*KVA	0	0	0*KVA	4160
86	0	0*KVA	0*KVA	0	0	0*KVA	4160
87	0	0*KVA	0*KVA	0	0	0*KVA	4160
87	0	40*KVA	20*KVA	0	0	0*KVA	4160
87	0	0*KVA	0*KVA	0	0	0*KVA	4160
88	0	40*KVA	20*KVA	0	0	50*KVA	4160
88	0	0*KVA	0*KVA	0	0	0*KVA	4160
88	0	0*KVA	0*KVA	0	0	0*KVA	4160
89	0	0*KVA	0*KVA	0	0	0*KVA	4160
89	0	0*KVA	0*KVA	0	0	0*KVA	4160
89	0	0*KVA	0*KVA	0	0	0*KVA	4160
90	0	0*KVA	0*KVA	0	0	0*KVA	4160
90	1	40*KVA	20*KVA	0	0	50*KVA	4160
90	0	0*KVA	0*KVA	0	0	0*KVA	4160
91	0	0*KVA	0*KVA	0	0	0*KVA	4160
91	0	0*KVA	0*KVA	0	0	0*KVA	4160
91	0	0*KVA	0*KVA	0	0	0*KVA	4160
92	0	0*KVA	0*KVA	0	0	0*KVA	4160
92	0	0*KVA	0*KVA	0	0	0*KVA	4160
92	0	40*KVA	20*KVA	0	0	50*KVA	4160
93	0	0*KVA	0*KVA	0	0	0*KVA	4160
93	0	0*KVA	0*KVA	0	0	0*KVA	4160
93	0	0*KVA	0*KVA	0	0	0*KVA	4160
94	0	40*KVA	20*KVA	0	0	0*KVA	4160
94	0	0*KVA	0*KVA	0	0	0*KVA	4160
94	0	0*KVA	0*KVA	0	0	0*KVA	4160
95	0	0*KVA	0*KVA	0	0	0*KVA	4160
95	0	20*KVA	10*KVA	0	0	0*KVA	4160
95	0	0*KVA	0*KVA	0	0	0*KVA	4160
96	0	0*KVA	0*KVA	0	0	0*KVA	4160
96	0	20*KVA	10*KVA	0	0	0*KVA	4160
96	0	0*KVA	0*KVA	0	0	0*KVA	4160
97	0	0*KVA	0*KVA	0	0	0*KVA	4160
97	0	0*KVA	0*KVA	0	0	0*KVA	4160
97	0	0*KVA	0*KVA	0	0	0*KVA	4160
98	0	40*KVA	20*KVA	0	0	0*KVA	4160
98	0	0*KVA	0*KVA	0	0	0*KVA	4160
98	0	0*KVA	0*KVA	0	0	0*KVA	4160
99	0	0*KVA	0*KVA	0	0	0*KVA	4160
99	0	40*KVA	20*KVA	0	0	0*KVA	4160
99	0	0*KVA	0*KVA	0	0	0*KVA	4160
100	0	0*KVA	0*KVA	0	0	0*KVA	4160
100	0	0*KVA	0*KVA	0	0	0*KVA	4160
100	2	40*KVA	20*KVA	0	0	0*KVA	4160
101	0	0*KVA	0*KVA	0	0	0*KVA	4160
101	0	0*KVA	0*KVA	0	0	0*KVA	4160
101	0	0*KVA	0*KVA	0	0	0*KVA	4160
102	0	0*KVA	0*KVA	0	0	0*KVA	4160
102	0	0*KVA	0*KVA	0	0	0*KVA	4160
102	0	20*KVA	10*KVA	0	0	0*KVA	4160
103	0	0*KVA	0*KVA	0	0	0*KVA	4160
103	0	0*KVA	0*KVA	0	0	0*KVA	4160
103	0	40*KVA	20*KVA	0	0	0*KVA	4160
104	0	0*KVA	0*KVA	0	0	0*KVA	4160
104	0	0*KVA	0*KVA	0	0	0*KVA	4160
104	0	40*KVA	20*KVA	0	0	0*KVA	4160
105	0	0*KVA	0*KVA	0	0	0*KVA	4160
105	0	0*KVA	0*KVA	0	0	0*KVA	4160
105	0	0*KVA	0*KVA	0	0	0*KVA	4160
106	0	0*KVA	0*KVA	0	0	0*KVA	4160
106	0	40*KVA	20*KVA	0	0	0*KVA	4160
106	0	0*KVA	0*KVA	0	0	0*KVA	4160
107	0	0*KVA	0*KVA	0	0	0*KVA	4160
107	0	40*KVA	20*KVA	0	0	0*KVA	4160
107	0	0*KVA	0*KVA	0	0	0*KVA	4160
108	0	0*KVA	0*KVA	0	0	0*KVA	4160
108	0	0*KVA	0*KVA	0	0	0*KVA	4160
108	0	0*KVA	0*KVA	0	0	0*KVA	4160
109	0	40*KVA	20*KVA	0	0	0*KVA	4160
109	0	0*KVA	0*KVA	0	0	0*KVA	4160
109	0	0*KVA	0*KVA	0	0	0*KVA	4160
110	0	0*KVA	0*KVA	0	0	0*KVA	4160
110	0	0*KVA	0*KVA	0	0	0*KVA	4160
110	0	0*KVA	0*KVA	0	0	0*KVA	4160
111	0	20*KVA	10*KVA	0	0	0*KVA	4160

```
111         0        0*KVA      0*KVA            0       0       0*KVA     4160
111         0        0*KVA      0*KVA            0       0       0*KVA     4160
112         1       20*KVA     10*KVA            0       0       0*KVA     4160
112         0        0*KVA      0*KVA            0       0       0*KVA     4160
112         0        0*KVA      0*KVA            0       0       0*KVA     4160
113         2       40*KVA     20*KVA            0       0       0*KVA     4160
113         0        0*KVA      0*KVA            0       0       0*KVA     4160
113         0        0*KVA      0*KVA            0       0       0*KVA     4160
114         0       20*KVA     10*KVA            0       0       0*KVA     4160
114         0        0*KVA      0*KVA            0       0       0*KVA     4160
114         0        0*KVA      0*KVA            0       0       0*KVA     4160
115         0        0*KVA      0*KVA            0       0       0*KVA     4160
115         0        0*KVA      0*KVA            0       0       0*KVA     4160
115         0        0*KVA      0*KVA            0       0       0*KVA     4160
116         0        0*KVA      0*KVA            0       0       0*KVA     4160
116         0        0*KVA      0*KVA            0       0       0*KVA     4160
116         0        0*KVA      0*KVA            0       0       0*KVA     4160
117         0        0*KVA      0*KVA            0       0       0*KVA     4160
117         0        0*KVA      0*KVA            0       0       0*KVA     4160
117         0        0*KVA      0*KVA            0       0       0*KVA     4160
118         0        0*KVA      0*KVA            0       0       0*KVA     4160
118         0        0*KVA      0*KVA            0       0       0*KVA     4160
118         0        0*KVA      0*KVA            0       0       0*KVA     4160
119         0        0*KVA      0*KVA            0       0       0*KVA     4160
119         0        0*KVA      0*KVA            0       0       0*KVA     4160
119         0        0*KVA      0*KVA            0       0       0*KVA     4160
120         0        0*KVA      0*KVA            0       0       0*KVA     4160
120         0        0*KVA      0*KVA            0       0       0*KVA     4160
120         0        0*KVA      0*KVA            0       0       0*KVA     4160
121         0        0*KVA      0*KVA            0       0       0*KVA     4160
121         0        0*KVA      0*KVA            0       0       0*KVA     4160
121         0        0*KVA      0*KVA            0       0       0*KVA     4160
122         0        0*KVA      0*KVA            0       0       0*KVA     4160
122         0        0*KVA      0*KVA            0       0       0*KVA     4160
122         0        0*KVA      0*KVA            0       0       0*KVA     4160
123         0        0*KVA      0*KVA            0       0       0*KVA     4160
123         0        0*KVA      0*KVA            0       0       0*KVA     4160
123         0        0*KVA      0*KVA            0       0       0*KVA     4160
124         0        0*KVA      0*KVA            0       0       0*KVA     4160
124         0        0*KVA      0*KVA            0       0       0*KVA     4160
124         0        0*KVA      0*KVA            0       0       0*KVA     4160
125         0        0*KVA      0*KVA            0       0       0*KVA     4160
125         0        0*KVA      0*KVA            0       0       0*KVA     4160
125         0        0*KVA      0*KVA            0       0       0*KVA     4160
126         0        0*KVA      0*KVA            0       0       0*KVA     480
126         0        0*KVA      0*KVA            0       0       0*KVA     480
126         0        0*KVA      0*KVA            0       0       0*KVA     480
127         0        0*KVA      0*KVA            0       1       0*KVA     4160
127         0        0*KVA      0*KVA            0       1       0*KVA     4160
127         0        0*KVA      0*KVA            0       1       0*KVA     4160
128         0        0*KVA      0*KVA            0       2       0*KVA     4160
128         0        0*KVA      0*KVA            0       2       0*KVA     4160
128         0        0*KVA      0*KVA            0       2       0*KVA     4160
129         0        0*KVA      0*KVA            0       3       0*KVA     4160
129         0        0*KVA      0*KVA            0       3       0*KVA     4160
129         0        0*KVA      0*KVA            0       3       0*KVA     4160
130         0        0*KVA      0*KVA            0       4       0*KVA     4160
130         0        0*KVA      0*KVA            0       4       0*KVA     4160
130         0        0*KVA      0*KVA            0       4       0*KVA     4160
131         0        0*KVA      0*KVA            0       5       0*KVA     480
131         0        0*KVA      0*KVA            0       5       0*KVA     480
131         0        0*KVA      0*KVA            0       5       0*KVA     480
132         0        0*KVA      0*KVA            0       0       0*KVA     4160
132         0        0*KVA      0*KVA            0       0       0*KVA     4160
132         0        0*KVA      0*KVA            0       0       0*KVA     4160
133         0        0*KVA      0*KVA            0       0       0*KVA     4160
133         0        0*KVA      0*KVA            0       0       0*KVA     4160
133         0        0*KVA      0*KVA            0       0       0*KVA     4160
134         0        0*KVA      0*KVA            0       0       0*KVA     4160
134         0        0*KVA      0*KVA            0       0       0*KVA     4160
134         0        0*KVA      0*KVA            0       0       0*KVA     4160
135         0        0*KVA      0*KVA            0       0       0*KVA     4160
135         0        0*KVA      0*KVA            0       0       0*KVA     4160
135         0        0*KVA      0*KVA            0       0       0*KVA     4160
136         0        0*KVA      0*KVA            0       0       0*KVA     4160
136         0        0*KVA      0*KVA            0       0       0*KVA     4160
136         0        0*KVA      0*KVA            0       0       0*KVA     4160
137         0        0*KVA      0*KVA            0       0       0*KVA     4160
137         0        0*KVA      0*KVA            0       0       0*KVA     4160
137         0        0*KVA      0*KVA            0       0       0*KVA     4160
138         0        0*KVA      0*KVA            0       0       0*KVA     4160
138         0        0*KVA      0*KVA            0       0       0*KVA     4160
138         0        0*KVA      0*KVA            0       0       0*KVA     4160
];

BASE_V_LNS=bus_data(:,8)/sqrt(3);                 %[V]
BASE_V_LL=BASE_V_LNS((ROOT_BUS_NO-1)*3+1)*sqrt(3);%[V]
BASE_V_LN=BASE_V_LNS((ROOT_BUS_NO-1)*3+1);        %[V]
BASE_I=BASE_KVA_3PH*1000/(sqrt(3)*BASE_V_LL);     %[A]
BASE_OHM=BASE_V_LN/BASE_I;                        %[Ohm]

BUS_SEED=[01,14,02,03,04,05,06,07,08,09,10,11,12, 13];
bus_name=[
'001';'002';'003';'004';'005';'006';'007';'008';'009';'010';'011';'012';'013';'014';'015';
```

```
'016';'017';'018';'019';'020';'021';'022';'023';'024';'025';'026';'027';'028';'029';'030';
'031';'032';'033';'034';'035';'036';'037';'038';'039';'040';'041';'042';'043';'044';'045';
'046';'047';'048';'049';'050';'051';'052';'053';'054';'055';'056';'057';'058';'059';'060';
'061';'062';'063';'064';'065';'066';'067';'068';'069';'070';'071';'072';'073';'074';'075';
'076';'077';'078';'079';'080';'081';'082';'083';'084';'085';'086';'087';'088';'089';'090';
'091';'092';'093';'094';'095';'096';'097';'098';'099';'100';'101';'102';'103';'104';'105';
'106';'107';'108';'109';'110';'111';'112';'113';'114';'135';'149';'150';'151';'152';'160';
'195';'197';'250';'300';'450';'610';'VR1';'VR2';'VR3';'VR4';'TR1';'132';'133';'134';'135';
'136';'137';'138'
];

%%%%%%%%%%%%%%%%%%%%%%%%%%%%%%%%%%%%%%%%%%%%%%%%%%%%%%%%%%%%%%%%%%%%%%%%%%%%%%%
%   Line Data
%%%%%%%%%%%%%%%%%%%%%%%%%%%%%%%%%%%%%%%%%%%%%%%%%%%%%%%%%%%%%%%%%%%%%%%%%%%%%%%
% 1. Starting Node
% 2. End Node
% 3. Impedance Matrix Numer(1, 2, 3, ...)
% 4. Length(Mile), 2500*FEET -> 2500*0.3048/1609.3 Mile, 1 -> 1 Mile
% 5. Equivalent Shunt Capacitor(ID)
line_data=[
1     2  10     175*FEET    10
1     3  11     250*FEET    11
1     7   1     300*FEET    1
3     4  11     200*FEET    11
3     5  11     325*FEET    11
5     6  11     250*FEET    11
7     8   1     200*FEET    1
8    12  10     225*FEET    10
8     9   9     225*FEET    9
8    13   1     300*FEET    1
9   128   9       0*FEET    9
13   34  11     150*FEET    11
13   18   2     825*FEET    2
14   11   9     250*FEET    9
14   10   9     250*FEET    9
15   16  11     375*FEET    11
15   17  11     350*FEET    11
18   19   9     250*FEET    9
18   21   2     300*FEET    2
19   20   9     325*FEET    9
21   22  10     525*FEET    10
21   23   2     250*FEET    2
23   24  11     550*FEET    11
23   25   2     275*FEET    2
25  129   9       0*FEET    9
25   28   2     200*FEET    2
26   27   7     275*FEET    7
26   31  11     225*FEET    11
27   33   9     500*FEET    9
28   29   2     300*FEET    2
29   30   2     350*FEET    2
30  123   2     200*FEET    2
31   32  11     300*FEET    11
34   15  11     100*FEET    11
35   36   8     650*FEET    8
35   40   1     250*FEET    1
36   37   9     300*FEET    9
36   38  10     250*FEET    10
38   39  10     325*FEET    10
40   41  11     325*FEET    11
40   42   1     250*FEET    1
42   43  10     500*FEET    10
42   44   1     200*FEET    1
44   45   9     200*FEET    9
44   47   1     250*FEET    1
45   46   9     300*FEET    9
47   48   4     150*FEET    4
47   49   4     250*FEET    4
49   50   4     250*FEET    4
50   51   4     250*FEET    4
52   53   1     200*FEET    1
53   54   1     125*FEET    1
54   55   1     275*FEET    1
54   57   3     350*FEET    3
55   56   1     275*FEET    1
57   58  10     250*FEET    10
57   60   3     750*FEET    3
58   59  10     250*FEET    10
60   61   5     550*FEET    5
60   62  12     250*FEET    12
62   63  12     175*FEET    12
63   64  12     350*FEET    12
64   65  12     425*FEET    12
65   66  12     325*FEET    12
67   68   9     200*FEET    9
67   72   3     275*FEET    3
67   97   3     250*FEET    3
68   69   9     275*FEET    9
69   70   9     325*FEET    9
70   71   9     275*FEET    9
72   73  11     275*FEET    11
72   76   3     200*FEET    3
73   74  11     350*FEET    11
74   75  11     400*FEET    11
```

```
 76   77   6     400*FEET    6
 76   86   3     700*FEET    3
 77   78   6     100*FEET    6
 78   79   6     225*FEET    6
 78   80   6     475*FEET    6
 80   81   6     475*FEET    6
 81   82   6     250*FEET    6
 81   84  11     675*FEET    11
 82   83   6     250*FEET    6
 84   85  11     475*FEET    11
 86   87   6     450*FEET    6
 87   88   9     175*FEET    9
 87   89   6     275*FEET    6
 89   90  10     225*FEET    10
 89   91   6     225*FEET    6
 91   92  11     300*FEET    11
 91   93   6     225*FEET    6
 93   94   9     275*FEET    9
 93   95   6     300*FEET    6
 95   96  10     200*FEET    10
 97   98   3     275*FEET    3
 98   99   3     550*FEET    3
 99  100   3     300*FEET    3
100 125   3     800*FEET    3
101 102  11     225*FEET    11
101 105   3     275*FEET    3
102 103  11     325*FEET    11
103 104  11     700*FEET    11
105 106  10     225*FEET    10
105 108   3     325*FEET    3
106 107  10     575*FEET    10
108 109   9     450*FEET    9
108 124   3    1000*FEET    3
109 110   9     300*FEET    9
110 111   9     575*FEET    9
110 112   9     125*FEET    9
112 113   9     525*FEET    9
113 114   9     325*FEET    9
115  35   4     375*FEET    4
116   1   1     400*FEET    1
119  52   1     400*FEET    1
120 130   6       0*FEET    6
130 136   6       0*FEET    6
136  67   6     350*FEET    6
122 101   3     250*FEET    3
127 116   1       0*FEET    1
117 127   1       0*FEET    1
128 137   1       0*FEET    1 %vr02
137  14   9     425*FEET    9
129 138   7       0*FEET    7
138  26   7     350*FEET    7 %vr03
129  25   1       0*FEET    1
130 120   1       0*FEET    1
115  18   1       0*FEET    1
118  51   1      10*FEET    1
13  119   1       0*FEET    1
131 126   1       0*FEET    1
61  131   1       0*FEET    1
120 130   1       0*FEET    1
60  120   1       0*FEET    1
97  122   1       0*FEET    1
83  132   1       0*FEET    1
92  133   1       0*FEET    1
90  134   1       0*FEET    1
88  135   1       0*FEET    1
54   94   1       0*FEET    1
121 95    1       0*FEET    1
];

%%%%%%%%%%%%%%%%%%%%%%%%%%%%%%%%%%%%%%%%%%%%%%%%%%%%%%%%%%%%%%%%%%%%%%%%%%%%
%   Voltage Regulator & Xfmrs
%%%%%%%%%%%%%%%%%%%%%%%%%%%%%%%%%%%%%%%%%%%%%%%%%%%%%%%%%%%%%%%%%%%%%%%%%%%%
% 1. Voltage Regulator or Xfmr
%    Type A VR --> 1: PH A   2:PH B   3:PH C
%    Type B VR --> 4: PH A   5:PH B   6:PH C
%    Type A Open AB & CB --> 7: Open Delta AB  8: Open Delta:CB 9: Reserved
%    Type B OPen AB & CB --> 10: Open Delta AB  11: Open Delta:CB 12: Reserved
%
% 1. XFMR
% 1.1  Gr Wye-Gr Wye              101: PH A 102:PH B 103:PH C
% 1.2  Delta-Delta                104: PH A 105:PH B 106:PH C
% 1.3  Delta-Gr Wye(Gr Wye-Delta) 107: PH A 108:PH B 109:PH C
% 1.4  Wye-Delta                  110: PH A 108:PH B 109:PH C
% 1.5  Open Wye-Open Delta        113: PH A 108:PH B 109:PH C
% 2. VR: VOLT HOLD         XFMR: None
% 3. VR: R-VOLT            XFMR: R % -> 1% pu-->0.01 pu
% 4. VR: X-VOLT            XFMR: X %
% 5. VR: PT RATIO          XFMR: None
% 6. VR: CT RATE           XFMR: None
% 7. VR: TAP               XFMR: Turns Ratio
% 8. VR: MAGNITDE PER TAP  XFMR: 1-Phase [VA]
% 9. VR: TARGET LEVEL      XFMR: Primary Line to Line Voltage
%10. VR: BASE VOLT         XFMR: Seconday Line to Line Voltage
% 3 rows -> VR ID: 1
```

```
% Next 3 rows -> VR ID: 2
% 125.232(120V Base) is used to boost voltage to 1.0436 PU that IEEE specifies
voltage_reg=[
%1  2 3 4  5   6    7          8        9      10
1 122 3 9 20 700    0       0.75      125.232 120% VR 01
2 122 3 9 20 700    0       0.75      125.244 120
3 122 3 9 20 700    0       0.75      125.232 120
1 122 3 9 20 700    0       0.75      120.958 120% VR 02
2 122 3 9 20 700    0       0.75      120       120
3 122 3 9 20 700    0       0.75      120       120
1 122 3 9 20 700    0       0.75      119.671 120% VR 03
2 122 3 9 20 700    0       0.75      120     120
3 122 3 9 20 700    0       0.75      120.335 120
1 122 3 9 20 700    0       0.75      124.487 120% VR 04
2 122 3 9 20 700    0       0.75      123.843 120
3 122 3 9 20 700    0       0.75      124.398 120
% 3 single phase xfmrs(s_base=1500[kVA]/3)
104 0 1.27  2.72 1 1 4160/480 150000/3 4160 480 % XFMR 1
105 0 1.27  2.72 1 1 4160/480 150000/3 4160 480
106 0 1.27  2.72 1 1 4160/480 150000/3 4160 480
];

%%%%%%%%%%%%%%%%%%%%%%%%%%%%%%%%%%%%%%%%%%%%%%%%%%%%%%%%%%%%%%%%%%%%%%%%%%%%
%   Impedance Data
%%%%%%%%%%%%%%%%%%%%%%%%%%%%%%%%%%%%%%%%%%%%%%%%%%%%%%%%%%%%%%%%%%%%%%%%%%%%
% [Ohm/mile]
% 3X3 -> ID: 1 -> impedance_data(1:3,:)
% Next 3X3 -> ID: 2 -> impedance_data(4:6,:)
impedance_data=[
0.4576+1.0780i   0.1560+0.5017i   0.1535+0.3849i    % ID 1
0.1560+0.5017i   0.4666+1.0482i   0.1580+0.4236i
0.1535+0.3849i   0.1580+0.4236i   0.4615+1.0651i

0.4666+1.0482i   0.1580+0.4236i   0.1560+0.5017i    % ID 2
0.1580+0.4236i   0.4615+1.0651i   0.1535+0.3849i
0.1560+0.5017i   0.1535+0.3849i   0.4576+1.0780i

0.4615+1.0651i   0.1535+0.3849i   0.1580+0.4236i    % ID 3
0.1535+0.3849i   0.4576+1.0780i   0.1560+0.5017i
0.1580+0.4236i   0.1560+0.5017i   0.4666+1.0482i

0.4615+1.0651i   0.1580+0.4236i   0.1535+0.3849i    % ID 4
0.1580+0.4236i   0.4666+1.0482i   0.1560+0.5017i
0.1535+0.3849i   0.1560+0.5017i   0.4576+1.0780i

0.4666+1.0482i   0.1560+0.5017i   0.1580+0.4236i   % ID 5
0.1560+0.5017i   0.4576+1.0780i   0.1535+0.3849i
0.1580+0.4236i   0.1535+0.3849i   0.4615+1.0651i

0.4576+1.0780i   0.1535+0.3849i   0.1560+0.5017i    % ID 6
0.1535+0.3849i   0.4615+1.0651i   0.1580+0.4236i
0.1560+0.5017i   0.1580+0.4236i   0.4666+1.0482i

0.4576+1.0780i   0.0000+0.0000i   0.1535+0.3849i    % ID 7
0.0000+0.0000i   0.0000+0.0000i   0.0000+0.0000i
0.1535+0.3849i   0.0000+0.0000i   0.4615+1.0651i

0.4576+1.0780i   0.1535+0.3849i   0.0000+0.0000i    % ID 8
0.1535+0.3849i   0.4615+1.0651i   0.0000+0.0000i
0.0000+0.0000i   0.0000+0.0000i   0.0000+0.0000i

1.3292+1.3475i   0.0000+0.0000i   0.0000+0.0000i    % ID 9
0.0000+0.0000i   0.0000+0.0000i   0.0000+0.0000i
0.0000+0.0000i   0.0000+0.0000i   0.0000+0.0000i

0.0000+0.0000i   0.0000+0.0000i   0.0000+0.0000i    % ID 10
0.0000+0.0000i   1.3292+1.3475i   0.0000+0.0000i
0.0000+0.0000i   0.0000+0.0000i   0.0000+0.0000i

0.0000+0.0000i   0.0000+0.0000i   0.0000+0.0000i    % ID 11
0.0000+0.0000i   0.0000+0.0000i   0.0000+0.0000i
0.0000+0.0000i   0.0000+0.0000i   1.3292+1.3475i

1.5209+0.7521i   0.5198+0.2775i   0.4924+0.2157i    % ID 12
0.5198+0.2775i   1.5329+0.7162i   0.5198+0.2775i
0.4924+0.2157i   0.5198+0.2775i   1.5209+0.7521i

];

%impedance_data=impedance_data/BASE_OHM;

%%%%%%%%%%%%%%%%%%%%%%%%%%%%%%%%%%%%%%%%%%%%%%%%%%%%%%%%%%%%%%%%%%%%%%%%%%%%
%   Admittance Data
%%%%%%%%%%%%%%%%%%%%%%%%%%%%%%%%%%%%%%%%%%%%%%%%%%%%%%%%%%%%%%%%%%%%%%%%%%%%
% [micro Siemens per mile]=[10^-6 Siemens per mile]
% 3X3 -> ID: 1 -> admittance_data(1:3,:)
% Next 3X3 -> ID: 2 -> admittance_data(4:6,:)

admittance_data=[
```

```
5.6765   -1.8319   -0.6982  % ID 1
-1.8319   5.9809   -1.1645
-0.6982  -1.1645    5.3971

5.9809   -1.1645   -1.8319  % ID 2
-1.1645   5.3971   -0.6982
-1.8319  -0.6982   5.6765

5.3971   -0.6982   -1.1645  % ID 3
-0.6982   5.6765   -1.8319
-1.1645   -1.8319   5.9809

5.3971   -1.1645   -0.6982  % ID 4
-1.1645   5.9809   -1.8319
-0.6982  -1.8319    5.6765

5.9809   -1.8319   -1.1645  % ID 5
-1.8319   5.6765   -0.6982
-1.1645  -0.6982    5.3971

5.6765   -0.6982   -1.8319  % ID 6
-0.6982   5.3971   -1.1645
-1.8319  -1.1645    5.9809

5.1154    0.0000   -1.0549  % ID 7
     0    0.0000    0.0000
-1.0549   0         5.1704

5.1154   -1.0549    0.0000  % ID 8
0         5.1704    0.0000
0         0         0.0000

4.5193    0.0000    0.0000  % ID 9
0         0.0000    0.0000
0         0         0.0000

0.0000    0.0000    0.0000  % ID 10
0         4.5193    0.0000
0         0         0.0000

0.0000    0.0000    0.0000  % ID 11
0         0.0000    0.0000
0         0         4.5193

67.2242   0.0000    0.0000  % ID 12
0         67.2242   0.0000
0         0        67.2242

]*10^-6*1i;



%%%%%%%%%%%%%%%%%%%%%%%%%%%%%%%%%%%%%%%%%%%%%%%%%%%%%%%%%%%%%%%%%%%%%%%%%%%%%%%
%   FAST Backward Forward Sweep Method
%%%%%%%%%%%%%%%%%%%%%%%%%%%%%%%%%%%%%%%%%%%%%%%%%%%%%%%%%%%%%%%%%%%%%%%%%%%%%%%
% System State Vector
% Difference between pfmc123 and pf123
% Initial Guesses
v_bus=BASE_V_LNS.*ones(BUS_NUM*3,1);
v_bus(2:3:BUS_NUM*3)=v_bus(2:3:BUS_NUM*3)*ALPHA^2;
v_bus(3:3:BUS_NUM*3)=v_bus(3:3:BUS_NUM*3)*ALPHA;

v_slack=ones(3,1)*BASE_V_LN*SLACK_COEFFICIENT;
v_slack(2)=v_slack(2)*ALPHA^2;
v_slack(3)=v_slack(3)*ALPHA;

i_bus=zeros(BUS_NUM*3, 1);
s_bus=zeros(BUS_NUM*3, 1);
s_loss_bus=zeros(BUS_NUM*3, 1);
p_loss_bus=zeros(BUS_NUM*3, 1);

[reg_r,~]=size(voltage_reg);
m_factors=ones(reg_r,1);
vr_bus=zeros(reg_r, 8);

% timer
t_b_sw=zeros(120,1);
t_f_sw=zeros(120,1);
t_p_sw=zeros(120,1);
s_dev=zeros(3*MAX_ITERATION_LIMIT,1);

iter_cnt=1;
flag=1;

% timer
t_start=tic;
```

```
while(flag)
    % timer
    t_timer=tic;

    i_bus=bsw(v_bus, bus_data, line_data, admittance_data, voltage_reg, ...
        m_factors, SIMPLIFIED_BACK_LATERAL_DATA, MESHED_DATA, [], BUS_NUM, ...
        AD_COEFF, 0, 0, 0);

    % timer
    t_b_sw(iter_cnt)=toc(t_timer);
    t_timer=tic;

    [v_bus, m_factors, vr_bus]=fsw3(0,i_bus, v_slack, bus_data, line_data, ...
        impedance_data, voltage_reg, m_factors, vr_bus, ...
        SIMPLIFIED_BACK_LATERAL_DATA, BUS_NUM, ROOT_BUS_NO, ...
        BASE_V_LNS, v_bus);

    % timer
    t_f_sw(iter_cnt)=toc(t_timer);
    t_timer=tic;

    [s_bus, s_loss_bus, flag, s_total_loss]=psw(s_bus, v_bus, ...
        i_bus, bus_data, line_data, admittance_data, voltage_reg, ...
        SIMPLIFIED_BACK_LATERAL_DATA, BUS_NUM, AD_COEFF, ...
        mismatch_type, mismatch_max_iteration, iter_cnt, ACCURACY);

    if(flag==0)
        % to return outputs at the end of the simulation
        p_loss_bus=s_loss_bus;% Total loss(kW)
    end

    % timer
    t_p_sw(iter_cnt)=toc(t_timer);

    iter_cnt=iter_cnt+1;

    if(iter_cnt==MAX_ITERATION_LIMIT)
        disp('WARNING: Sorry, We failed to converge in BFSW');
        break;
    end
end



% timer
t_timer=tic;



%%%%%%%%%%%%%%%%%%%%%%%%%%%%%%%%%%%%%%%%%%%%%%%%%%%%%%%%%%%%%%%%%%%%%%%%%%%%%%%
%   Backward Forward Sweep Method for MESHED Networks
%%%%%%%%%%%%%%%%%%%%%%%%%%%%%%%%%%%%%%%%%%%%%%%%%%%%%%%%%%%%%%%%%%%%%%%%%%%%%%%

% Step 1. Breakpoint Impedance Matrix Z
[mesh_row,~]=size(MESHED_DATA);
if(mesh_row>0)
    bp_imp=br_point2(impedance_data, line_data, MESHED_DATA, MESHED_BACK_LATERAL_DATA, ...
        BASE_J_PU, ROOT_BUS_NO, BUS_NUM, mesh_row,...
        bus_data, voltage_reg, m_factors, vr_bus,...
        SIMPLIFIED_BACK_LATERAL_DATA, BASE_V_LNS);

    % Line impedance test, April, 4, 2014
    %bp_imp=bp_imp*1e7;%1e3=1000;
end

% Step #2. Iterative Compensation Process
J=zeros(3*mesh_row,1);
prev_J=J;
buf_bp_i=zeros(1, MAX_ITERATION_LIMIT+1);
buf_bp_v=zeros(1, MAX_ITERATION_LIMIT);

flag=1;
iter_cnt_mesh=1;
while(flag && mesh_row>0)
    i_bus=bsw(v_bus, bus_data, line_data, admittance_data, voltage_reg, ...
        m_factors, SIMPLIFIED_BACK_LATERAL_DATA, MESHED_DATA, [], BUS_NUM, ...
        AD_COEFF, J, 1, 0);

    [v_bus, m_factors, vr_bus]=fsw3(0, i_bus, v_slack, bus_data, line_data, ...
        impedance_data, voltage_reg, m_factors, vr_bus, ...
        SIMPLIFIED_BACK_LATERAL_DATA, BUS_NUM, ROOT_BUS_NO, ...
        BASE_V_LNS, v_bus);

    [v_1, i_1, J, prev_J, flag]=psw_meshed(v_bus, prev_J, MESHED_DATA, bp_imp, mesh_row,...
        ACCURACY_MESHED);

    buf_bp_i(iter_cnt_mesh+1)=i_1;
    buf_bp_v(iter_cnt_mesh)=v_1;

    if(flag==0)
```

```
        % flag==0 means convergence is met, we will exit the bfsw routine
        [s_bus, s_loss_bus, flag, s_total_loss]=psw(s_bus, v_bus, i_bus, bus_data, line_data, ...
            admittance_data, voltage_reg, ...
            SIMPLIFIED_BACK_LATERAL_DATA, BUS_NUM, AD_COEFF, ...
            3, mismatch_max_iteration, iter_cnt, ACCURACY);

        % to return outputs at the end of the simulation
        p_loss_bus=s_loss_bus;% Total loss(kW)
    end

    iter_cnt_mesh=iter_cnt_mesh+1;

    if(iter_cnt_mesh==MAX_ITERATION_LIMIT)
        disp('WARNING: Sorry, We failed to converge in MESHED BFSW');
        break;
    end
end


% timer
t_loop=toc(t_timer);
t_total=toc(t_start);

% Displays elpased times
disp('=======================END=====================================================');
t_elapsed_total=toc(t_start);

fprintf('Total Simulation Time= %.2f [sec]\n',t_total);
fprintf('1. Backward Sweep= %.2f [sec]\n',sum(t_b_sw));
fprintf('2. Forward Sweep= %.2f [sec]\n',sum(t_f_sw));
fprintf('3. Mismatch & Loss Sweep= %.2f [sec]\n',sum(t_p_sw));
fprintf('4. Loop Sweep= %.2f [sec]\n',t_loop);
```

(2) Backward Sweep Codes

```
function i_bus=bsw(v_bus, bus_data, line_data, ...
    admittance_data, voltage_reg, m_factors, ...
    SIMPLIFIED_BACK_LATERAL_DATA, MESHED_DATA, DG_DATA, BUS_NUM, ...
    AD_COEFF, J, flag_meshed, i_qs)

%%%%%%%%%%%%%%%%%%%%%%%%%%%%%%%%%%%%%%%%%%%%%%%%%%%%%%%%%%%%%%%%%%%%%%%%%%%%%%%
%       FAST Backward Sweep(Sub Feeder->Main->Longest Main Feeder Scanning)
%                                                   Copyright 2014 by Insu Kim
%%%%%%%%%%%%%%%%%%%%%%%%%%%%%%%%%%%%%%%%%%%%%%%%%%%%%%%%%%%%%%%%%%%%%%%%%%%%%%%
%flag_meshed=1, it has to analyze the meshed network
%            2, it is used to analyze pv no mismatch

Ph=inline('mag*exp(j*ang/180*pi)','mag','ang');%argument: magnitude, degree
ALPHA=Ph(1,120);
D_V=[1 -1 0;0 1 -1;-1 0 1];

i_bus=zeros(BUS_NUM*3, 1);
i_ad_status=zeros(BUS_NUM, 1);      % for shunt admittance of the d. lines
i_bus_status=zeros(BUS_NUM*3, 1);   % for scheduled power

if(flag_meshed==1)
    % This is for meshed network analysis
    bp_from_status=zeros(BUS_NUM,1);
    bp_to_status=zeros(BUS_NUM,1);
end

pvnode_from_status=zeros(BUS_NUM,1);

[row, col]=size(SIMPLIFIED_BACK_LATERAL_DATA);

for n=1:row
    % Temperary buffer for currents of one radial path.
    i_bus_buf=zeros(BUS_NUM*3, 1);
    prev_bus_no=0;

    for mm=2:col
        feeder_id=SIMPLIFIED_BACK_LATERAL_DATA(n,1);
        bus_no=SIMPLIFIED_BACK_LATERAL_DATA(n,mm);

        if(bus_no>0)
            for m=1:3
                load_type=bus_data((bus_no-1)*3+m, 2);
                vr_id=bus_data((bus_no-1)*3+m, 6);
                v_nom=bus_data((bus_no-1)*3+m, 8)/sqrt(3);%LL->LN
                % Difference between bsw and bsw_mc
                s_known=bus_data((bus_no-1)*3+m, 3)+bus_data((bus_no-1)*3+m,4)*1i;
                v_a=v_bus((bus_no-1)*3+m);

                J_tmp=0;

                if(vr_id==0)
                    if(feeder_id==2)
                        % Main Feeder
                        J_tmp=i_bus((bus_no-1)*3+m);
                        i_bus((bus_no-1)*3+m)=0;
                        % After zero setting, and in the end of the one path scanning rout it will
                        % be updated again.
                    end

                    if(mm>2)% It means the middle layer
                        J_tmp=J_tmp+i_bus_buf((prev_bus_no-1)*3+m);
                    end

                    if(i_bus_status((bus_no-1)*3+m)==0)
                        if((load_type==0 || load_type==10))
                            % Constant Power Load
```

```
                        i_tmp=conj(s_known/v_a);
                    elseif(load_type==1 || load_type==11)
                        % Constant Current Load
                        if(m==2)
                            v_nom=v_nom*ALPHA^2;
                        elseif(m==3)
                            v_nom=v_nom*ALPHA;
                        end
                        i_tmp_mag=abs(conj(s_known/v_nom));
                        i_tmp_ang=(angle(v_a)-angle(s_known))*180/pi;

                        i_tmp=Ph(i_tmp_mag, i_tmp_ang);
                    elseif(load_type==2 || load_type==12)
                        % Constant Impedance Load
                        constant_z=abs(v_nom)^2/conj(s_known);
                        i_tmp=v_bus((bus_no-1)*3+m)/constant_z;
                    elseif(load_type==3)
                        % Reserved
                    elseif(load_type==4 || load_type==14)
                        % Delta Connected Constant Power Load
                        v_abc=v_bus((bus_no-1)*3+1:bus_no*3);
                        v_line=D_V*v_abc;

                        i_ab=conj(s_known/v_line(m));
                    elseif(load_type==5 || load_type==15)
                        % Delta Connected Constant Current Load
                        v_abc=v_bus((bus_no-1)*3+1:bus_no*3);
                        if(m==2)
                            v_nom=v_nom*ALPHA^2;
                        elseif(m==3)
                            v_nom=v_nom*ALPHA;
                        end
                        v_nom=v_nom*sqrt(3)*Ph(1, 30);
                        v_line=D_V*v_abc;
                        i_line=conj(s_known/v_nom);
                        i_ab_abs=abs(i_line);
                        i_ab_ang=(angle(v_line(m))-angle(s_known))*180/pi;

                        i_ab=Ph(i_ab_abs, i_ab_ang);
                    elseif(load_type==6 || load_type==16)
                        % Delta Connected Constant Impedance Load
                        v_abc=v_bus((bus_no-1)*3+1:bus_no*3);
                        z=abs(v_nom*sqrt(3))^2/conj(s_known);
                        v_line_abc=D_V*v_abc;
                        i_delta=v_line_abc/z;

                        i_ab=i_delta(m);
                    end

                    % Jan/23/2014
                    if isnan(i_tmp)
                        i_tmp=0;
                    end

                    % Delta connected Loads
                    if(load_type==4 || load_type==5 || load_type==6 || load_type==14 || load_type==15 || load_type==16)
                        i_bus_buf((bus_no-1)*3+m)=i_bus_buf((bus_no-1)*3+m)+i_ab;
                        if(m==1)% a-b connection
                            i_bus_buf((bus_no-1)*3+m+1)=i_bus_buf((bus_no-1)*3+m+1)-i_ab;
                        elseif(m==2)% b-c connection
                            i_bus_buf((bus_no-1)*3+m+1)=i_bus_buf((bus_no-1)*3+m+1)-i_ab;
                        else% c-a connection
                            i_bus_buf((bus_no-1)*3+m-2)=i_bus_buf((bus_no-1)*3+m-2)-i_ab;
                        end
                    else % Wye connected Loads
                        i_bus_buf((bus_no-1)*3+m)=i_bus_buf((bus_no-1)*3+m)+i_tmp;
                    end

                    % Difference between bsw and bsw_mc
                    % Shunt elements of the bus, capacitor bank
                    s_c=-1i*bus_data((bus_no-1)*3+m, 7);
                    if(s_c~=0)
                        % Consider it as CONSTANT IMPEDANCE LOAD
                        constant_z=abs(v_nom)^2/conj(s_c);
                        i_sc=v_bus((bus_no-1)*3+m)/constant_z;
                        i_bus_buf((bus_no-1)*3+m)=i_bus_buf((bus_no-1)*3+m)+i_sc;
                    end

                    i_bus_status((bus_no-1)*3+m)=1;
                end

                i_bus_buf((bus_no-1)*3+m)=i_bus_buf((bus_no-1)*3+m)+J_tmp;
            else
                ph_type=voltage_reg((vr_id-1)*3+m,1);
                i_pri=xfmr_conn(0, i_bus_buf, m_factors, ...
                    prev_bus_no, vr_id, voltage_reg, m, ph_type);
                i_bus_buf((bus_no-1)*3+1:bus_no*3)=i_bus_buf((bus_no-1)*3+1:bus_no*3)+i_pri;
            end
        end

        % To avoid calculatig twice or more.
        if(prev_bus_no>0 && i_ad_status(prev_bus_no)==0)
            [yy_id, yy_len]=find_admittance(bus_no, prev_bus_no, line_data);
            if(yy_id==0)
                yy=zeros(3,3);
            else
                yy=AD_COEFF*admittance_data((yy_id-1)*3+1:yy_id*3,:);
            end

            yy=yy*yy_len;

            i_shunt_line=yy*v_bus((bus_no-1)*3+1:bus_no*3);
            i_bus_buf((bus_no-1)*3+1:bus_no*3)=i_bus_buf((bus_no-1)*3+1:bus_no*3)+i_shunt_line;

            i_ad_status(prev_bus_no)=1;
        end

        % Updating Breakpoint Current
        if(flag_meshed==1)
            [rr,~]=size(MESHED_DATA);
            for iter=1:rr
                bus_no_from=MESHED_DATA(iter,1);
                bus_no_to=MESHED_DATA(iter,2);
```

```
                    if(bus_no==bus_no_from && bp_from_status(bus_no)==0)
                        i_bus_buf((bus_no-1)*3+1:bus_no*3)=i_bus_buf((bus_no-1)*3+1:bus_no*3)-J((iter-1)*3+1:iter*3);
                        bp_from_status(bus_no)=1;
                        break;
                    elseif(bus_no==bus_no_to && bp_to_status(bus_no)==0)
                        i_bus_buf((bus_no-1)*3+1:bus_no*3)=i_bus_buf((bus_no-1)*3+1:bus_no*3)+J((iter-1)*3+1:iter*3);
                        bp_to_status(bus_no)=1;
                        break;
                    end
                end
            end

            % Injects the reactive power injection and calculating the Q
            if(flag_meshed==2)
                idx=find(DG_DATA(:,1)==1);
                [r,~]=size(idx);
                for k=1:r
                    dg_bus=DG_DATA(idx(k), 2);
                    if(dg_bus==bus_no && pvnode_from_status(dg_bus)==0)
                        i_bus_buf((dg_bus-1)*3+1:dg_bus*3)=...
                            i_bus_buf((dg_bus-1)*3+1:dg_bus*3)+i_qs(:,k);
                        pvnode_from_status(dg_bus)=1;
                    end
                end
            end

        else
            break;%Move the next line
        end
        prev_bus_no=bus_no;
    end

    %%%%%%%%%%%%%%%%%%%%%%%%%%%%%%%%%%%%%%%%
    i_bus=i_bus+i_bus_buf;
end


end
```

(3) Forward Sweep Codes

```
function [v_bus, m_factors,  vr_bus]=fsw3(flag_vr, i_bus, v_slack, bus_data, line_data, ...
        impedance_data, voltage_reg, m_factors, vr_bus, ...
        SIMPLIFIED_BACK_LATERAL_DATA, BUS_NUM, ROOT_BUS_NO, ...
        BASE_V_LNS, v_bus)

%%%%%%%%%%%%%%%%%%%%%%%%%%%%%%%%%%%%%%%%%%%%%%%%%%%%%%%%%%%%%%%%%%%%%%%%%%%%%%%
% Forward Sweep(Copyright 2014 by Insu Kim)
%%%%%%%%%%%%%%%%%%%%%%%%%%%%%%%%%%%%%%%%%%%%%%%%%%%%%%%%%%%%%%%%%%%%%%%%%%%%%%%

% flag_vr=1->it is used only for calculating the break point impedances

% Ph=inline('mag*exp(j*ang/180*pi)','mag','ang');%argument: magnitude, degree
% ALPHA=Ph(1,120);
D_V=[1 -1 0;0 1 -1;-1 0 1];
D_I=[1 0 -1; -1 1 0; 0 -1 1];
A_T=1/3*[2 -1 -1;-1 2 -1;-1 -1 2];
B_T=1/3*[1 0 0;0 1 0;-1 -1 0];
%B_T=1/3*[1 0 0;0 1 0;0 0 1];
% Since Ia+Ib+Ic=0, B_T in line 17 and 18 are the same!
B_T2=1/3*[2 0 -1;-1 0 -1;-1 0 2];
A_I=[1 0 0;-1 1 0;0 -1 0];
A_T2=1/3*[2 1 0;0 2 1;1 0 2];
A_T3=1/3*[2 1 0;-1 1 0;-1 -2 0];

% v_bus=BASE_V_LNS.*ones(BUS_NUM*3,1);
% v_bus(2:3:BUS_NUM*3)=v_bus(2:3:BUS_NUM*3)*ALPHA^2;
% v_bus(3:3:BUS_NUM*3)=v_bus(3:3:BUS_NUM*3)*ALPHA;

bus_rd_status=zeros(BUS_NUM*3, 1);% To avoid calculating two or more
[row,col]=size(SIMPLIFIED_BACK_LATERAL_DATA);
% Why reverse order?
% Warning: Last row should be the longest main feeder followed by the slack
for mm=row:-1:1
    prev_bus_no=0;
    for nn=col:-1:2
        bus_no=SIMPLIFIED_BACK_LATERAL_DATA(mm, nn);
        if(bus_no>0)
           % Root layer or SLACK
            if(bus_no==ROOT_BUS_NO)
                if(bus_rd_status((bus_no-1)*3+1)==0)
                    v_bus((bus_no-1)*3+1:bus_no*3)=v_slack;
                    bus_rd_status((bus_no-1)*3+1:bus_no*3)=1;
                end
            elseif(prev_bus_no>0)
                i_tmp=zeros(3,1);
                [zz_id, zz_len]=find_impedance(bus_no, prev_bus_no, line_data);

                for m=1:3%m->phase number->1(a ph), 2(b ph), 3(c ph)
                    if(bus_rd_status((bus_no-1)*3+m)==0)
                        % Checking of the voltage regulator
                        vr_id=bus_data((bus_no-1)*3+m, 6);

                        if(vr_id==0) % No VR
                            i_tmp(m)=i_bus((bus_no-1)*3+m);

                            if(m==3) % Matrix(3X1) calulation for 3 phase voltage drop...
                                zz=impedance_data((zz_id-1)*3+1:zz_id*3,:);
                                zz=zz*zz_len;
                                v_drop=zz*i_tmp;

                                v_bus((bus_no-1)*3+1:bus_no*3)=...
                                    v_bus((prev_bus_no-1)*3+1:prev_bus_no*3)-v_drop;
                            end
                        else
                            ph=voltage_reg((vr_id-1)*3+m,1);
                            if(ph>=1 && ph<=3)
                                % Type A, Voltage regulator
                                %r_c=voltage_reg((vr_id-1)*3+m,3);
                                %x_c=voltage_reg((vr_id-1)*3+m,4);
```

```
                %pt_ratio=voltage_reg((vr_id-1)*3+m,5);
                %ct_pri_rating=voltage_reg((vr_id-1)*3+m,6);
                %tap=voltage_reg((vr_id-1)*3+m,7);
                one_tap_size=voltage_reg((vr_id-1)*3+m,8);
                target_level=voltage_reg((vr_id-1)*3+m,9);
                v_base=voltage_reg((vr_id-1)*3+m,10);

                v_l=v_bus((prev_bus_no-1)*3+m)/BASE_V_LNS((prev_bus_no-1)*3+m);
                v_l_base=abs(v_l)*v_base;

                tap_size=((target_level-v_l_base)/one_tap_size);
                %tap_size=round((target_level-v_l_base)/one_tap_size);
                v_2_base=v_l_base+tap_size*one_tap_size;
                multiply_factor=v_l_base/v_2_base;

                if(flag_vr==1)%for only breakpoint impedances
                    multiply_factor=m_factors((vr_id-1)*3+m);
                end

                v_bus((bus_no-1)*3+m)=v_bus((prev_bus_no-1)*3+m)/multiply_factor;
            elseif(ph>=4 && ph<=6)
                % Type B, Voltage regulator
                % Loads the voltage regulator specification
                r_c=voltage_reg((vr_id-1)*3+m,3);
                x_c=voltage_reg((vr_id-1)*3+m,4);
                pt_ratio=voltage_reg((vr_id-1)*3+m,5);
                ct_pri_rating=voltage_reg((vr_id-1)*3+m,6);
                tap=voltage_reg((vr_id-1)*3+m,7);
                one_tap_size=voltage_reg((vr_id-1)*3+m,8);
                target_level=voltage_reg((vr_id-1)*3+m,9);
                v_base=voltage_reg((vr_id-1)*3+m,10);

                % Calculates the compensator impedance
                z_tmp=(r_c+x_c*1i);
                z_c=z_tmp*ct_pri_rating/pt_ratio;
                z_c_ohm=z_c/5;

                i_line=i_bus((prev_bus_no-1)*3+m);
                i_relay=i_line/(ct_pri_rating/5);
                v_drop=z_c_ohm*i_relay;

                v_l=v_bus((prev_bus_no-1)*3+m)/BASE_V_LNS((prev_bus_no-1)*3+m);
                v_l_base=v_l*v_base;

                % There should be voltage drop through the compensation circuit
                v_R=v_l_base-v_drop;

                if(flag_vr==0)
                    if(tap==0)
                        tap_size=round((target_level-1-abs(v_R))/0.75);
                        multiply_factor=(1-0.00625*tap_size);

                        % Boosts the volage of regulator terminal
                        i_L=i_bus((bus_no-1)*3+m);
                        v_bus((bus_no-1)*3+m)=v_bus((prev_bus_no-1)*3+m)/multiply_factor-z_tmp*i_L;

                        % Changing the tap after checking the target voltage
                        vr_flag=1;
                        while (vr_flag)
                            v_2_base=v_bus((bus_no-1)*3+m)*v_base/BASE_V_LNS((bus_no-1)*3+m);

                            if(abs(v_2_base) < target_level)
                                tap_size=tap_size+1;
                                multiply_factor=(1-0.00625*tap_size);

                                % Boosts the volage of regulator terminal
                                v_bus((bus_no-1)*3+m)=v_bus((prev_bus_no-1)*3+m)/multiply_factor-z_tmp*i_L;
                            else
                                vr_flag=0;
                            end
                        end
                    else
                        tap_size=(target_level-abs(v_l_base))/one_tap_size;
                        v_2_base=abs(v_l_base)+tap_size*one_tap_size;
                        multiply_factor=abs(v_l_base)/v_2_base;

                        v_bus((bus_no-1)*3+m)=v_bus((prev_bus_no-1)*3+m)/multiply_factor;
                    end
                elseif(flag_vr==1)%for only breakpoint impedances
                    multiply_factor=m_factors((vr_id-1)*3+m);
                    v_bus((bus_no-1)*3+m)=v_bus((prev_bus_no-1)*3+m)/multiply_factor;
                end
            elseif(ph==7)
                % Type A Open Delta AB & CB
                % It takes 3 phases at a time, it is related to ph=4,5,6
                tap=voltage_reg((vr_id-1)*3+1,7);
                target_level=voltage_reg((vr_id-1)*3+1,9);
                v_base=voltage_reg((vr_id-1)*3+1,10);

                if(tap==0)
                    a_rab=v_base/target_level;
                    %tap=(target_level-v_base)/one_tap_size;
                else
                    a_rab=1-0.00625*tap;
                end

                tap=voltage_reg((vr_id-1)*3+2,7);
                %one_tap_size=voltage_reg((vr_id-1)*3+2,8);
                target_level=voltage_reg((vr_id-1)*3+2,9);
                v_base=voltage_reg((vr_id-1)*3+2,10);

                if(tap==0)
                    a_rcb=v_base/target_level;
                    %tap=(target_level-v_base)/one_tap_size;
                else
                    a_rcb=1-0.00625*tap;
                end

                v_ab=v_bus((prev_bus_no-1)*3+1)-v_bus((prev_bus_no-1)*3+2);
                v_bc=v_bus((prev_bus_no-1)*3+2)-v_bus((prev_bus_no-1)*3+3);
                v_ca=v_bus((prev_bus_no-1)*3+1)-v_bus((prev_bus_no-1)*3+1);
                v_tmp=[v_ab;v_bc;v_ca];

                % See Distribution System and Modeling Analysis(pp.185)
```

```
            A_LL=[1/a_rab 0 0;0 1/a_rcb 0;-1/a_rab -1/a_rcb 0];
            if(flag_vr==0)
                v_bus((bus_no-1)*3+1:bus_no*3)=pinv(D_V)*A_LL*v_tmp;
            elseif(flag_vr==1)%for only breakpoint impedances
                multiply_factor=m_factors((vr_id-1)*3+m);
                v_bus((bus_no-1)*3+1:bus_no*3)=v_bus((prev_bus_no-1)*3+1:prev_bus_no*3)/multiply_factor;
            end

            % For output display
            tap_size=tap;
            multiply_factor=a_rcb;
        elseif(ph==10)
            % Type B Open Delta AB & CB

        elseif(ph==101)
            % Gr Wye-Gr Wye XFMR
            turnsratio=voltage_reg((vr_id-1)*3+1,7);
            v_base_line_sec=voltage_reg((vr_id-1)*3+1,10);
            z_eq=voltage_reg((vr_id-1)*3+1,3)/100+voltage_reg((vr_id-1)*3+1,4)/100*1i;
            s_base=voltage_reg((vr_id-1)*3+1,8);

            z_base=v_base_line_sec^2/s_base;
            z=z_eq*z_base;

            i_sec=i_bus((bus_no-1)*3+1:bus_no*3)*turnsratio;
            v_pri=v_bus((prev_bus_no-1)*3+1:prev_bus_no*3);
            v_sec=v_pri/turnsratio-z*i_sec;

            v_bus((bus_no-1)*3+1:bus_no*3)=v_sec;

            % For output display
            tap_size=0;
            multiply_factor=turnsratio;
        elseif(ph==104)
            % Delta-Delta XFMR
            turnsratio=voltage_reg((vr_id-1)*3+1,7);
            v_base_line_sec=voltage_reg((vr_id-1)*3+1,10);
            z_eq=voltage_reg((vr_id-1)*3+1,3)/100+voltage_reg((vr_id-1)*3+1,4)/100*1i;
            s_base=voltage_reg((vr_id-1)*3+1,8);

            z_base=v_base_line_sec^2/s_base;
            z=z_eq*z_base;

            i_sec=i_bus((bus_no-1)*3+1:bus_no*3)*turnsratio;
            v_pri=v_bus((prev_bus_no-1)*3+1:prev_bus_no*3);
            v_sec=A_T/turnsratio*v_pri-z*B_T*i_sec;

            v_bus((bus_no-1)*3+1:bus_no*3)=v_sec;

            % For output display
            tap_size=0;
            multiply_factor=turnsratio;
        elseif(ph==107)
            % Delta-Gr Wye(Grounded Wye Connected) XFMR
            turnsratio=voltage_reg((vr_id-1)*3+1,7)*sqrt(3);
            v_base_line_sec=voltage_reg((vr_id-1)*3+1,10);
            z_eq=voltage_reg((vr_id-1)*3+1,3)/100+voltage_reg((vr_id-1)*3+1,4)/100*1i;
            s_base=voltage_reg((vr_id-1)*3+1,8);

            z_base=v_base_line_sec^2/s_base;
            z=z_eq*z_base;

            %i_sec=pinv(D_V)*i_bus((bus_no-1)*3+1:bus_no*3)*turnsratio;
            i_sec=1/3*D_I*i_bus((bus_no-1)*3+1:bus_no*3)*turnsratio;
            v_pri=v_bus((prev_bus_no-1)*3+1:prev_bus_no*3);
            v_sec=D_I/turnsratio*v_pri-z*i_sec;

            v_bus((bus_no-1)*3+1:bus_no*3)=v_sec;

            % For output display
            tap_size=0;
            multiply_factor=turnsratio;
        elseif(ph==110)
            % Wye-Delta XFMR
            turnsratio=voltage_reg((vr_id-1)*3+1,7)/sqrt(3);
            v_base_line_sec=voltage_reg((vr_id-1)*3+1,10);
            z_eq=voltage_reg((vr_id-1)*3+1,3)/100+voltage_reg((vr_id-1)*3+1,4)/100*1i;
            s_base=voltage_reg((vr_id-1)*3+1,8);

            z_base=v_base_line_sec^2/s_base;
            z=z_eq*z_base;

            i_sec=D_I*i_bus((bus_no-1)*3+1:bus_no*3)*turnsratio;
            v_pri=v_bus((prev_bus_no-1)*3+1:prev_bus_no*3);
            v_sec=A_T2/turnsratio*v_pri-z*B_T*i_sec;

            v_bus((bus_no-1)*3+1:bus_no*3)=v_sec;

            % For output display
            tap_size=0;
            multiply_factor=turnsratio;
        elseif(ph==113)
            % Open Wye-Open Delta XFMR
            turnsratio=voltage_reg((vr_id-1)*3+1,7)/sqrt(3);
            v_base_line_sec=voltage_reg((vr_id-1)*3+1,10);
            z_eq=voltage_reg((vr_id-1)*3+1,3)/100+voltage_reg((vr_id-1)*3+1,4)/100*1i;
            s_base=voltage_reg((vr_id-1)*3+1,8);

            z_base=v_base_line_sec^2/s_base;
            z=z_eq*z_base;

            i_sec=A_I*i_bus((bus_no-1)*3+1:bus_no*3)*turnsratio;
            v_pri=v_bus((prev_bus_no-1)*3+1:prev_bus_no*3);
            v_sec=A_T3/turnsratio*v_pri-z*B_T2*i_sec;

            v_bus((bus_no-1)*3+1:bus_no*3)=v_sec;

            % For output display
            tap_size=0;
            multiply_factor=turnsratio;
        end

        % For output display
        vr_bus((vr_id-1)*3+m,1)=bus_no;
```

```
                            vr_bus((vr_id-1)*3+m,2)=voltage_reg((vr_id-1)*3+m,1);
                            vr_bus((vr_id-1)*3+m,3)=voltage_reg((vr_id-1)*3+m,2);
                            vr_bus((vr_id-1)*3+m,4)=voltage_reg((vr_id-1)*3+m,3);
                            vr_bus((vr_id-1)*3+m,5)=voltage_reg((vr_id-1)*3+m,4);
                            vr_bus((vr_id-1)*3+m,6)=voltage_reg((vr_id-1)*3+m,5);
                            vr_bus((vr_id-1)*3+m,7)=voltage_reg((vr_id-1)*3+m,6);
                            vr_bus((vr_id-1)*3+m,8)=tap_size;
                            if (ph>=4 && ph<=6)% Type B
                                vr_bus((vr_id-1)*3+m,9)=multiply_factor;
                            else% Type A
                                vr_bus((vr_id-1)*3+m,9)=1/multiply_factor;
                            end
                            m_factors((vr_id-1)*3+m)=multiply_factor;
                        end

                        bus_rd_status((bus_no-1)*3+m)=1;
                    end
                end
            end
            prev_bus_no=bus_no;
        end
    end
end


end
```

(4) Power Mismatch Codes

```
function [s_bus, s_loss_bus, flag, s_total_loss]=...
    psw(s_bus, v_bus, i_bus, bus_data, line_data, ...
    admittance_data, voltage_reg, ...
    SIMPLIFIED_BACK_LATERAL_DATA, BUS_NUM, AD_COEFF, ...
    mismatch_type, mismatch_max_iteration, iter_cnt, accuracy)

%%%%%%%%%%%%%%%%%%%%%%%%%%%%%%%%%%%%%%%%%%%%%%%%%%%%%%%%%%%%%%%%%%%%%%%%%%%%%%%
% Power Mismatch Equations(Copyright 2014 by Insu Kim)
%%%%%%%%%%%%%%%%%%%%%%%%%%%%%%%%%%%%%%%%%%%%%%%%%%%%%%%%%%%%%%%%%%%%%%%%%%%%%%%

s_loss_bus=zeros(BUS_NUM*3, 1);
flag=0;
loss_rd_status=zeros(BUS_NUM*3, 1);% To avoid calculating two or more
s_total_loss=zeros(3,1);

if(mismatch_type==0)
    % This is for test to know how the times needs to iterate by the
    % fixed iteration number.

    s_bus=v_bus.*conj(i_bus);

    [row,col]=size(SIMPLIFIED_BACK_LATERAL_DATA);
    for mm=1:row
        prev_bus_no=0;
        for nn=col:-1:2
            bus_no=SIMPLIFIED_BACK_LATERAL_DATA(mm, nn);
            if(bus_no>0)
                for m=1:3

                    % mismatch checking
                    % It doesn't need

                    % loss calculation
                    if(mismatch_max_iteration==iter_cnt && ...
                            prev_bus_no>0 && loss_rd_status((bus_no-1)*3+m)==0)

                        vr_id=bus_data((bus_no-1)*3+m, 6);

                        [yy_id, yy_len]=find_admittance(bus_no, prev_bus_no, line_data);
                        if(yy_id==0)
                            yy=zeros(3,3);
                        else
                            yy=AD_COEFF*admittance_data((yy_id-1)*3+1:yy_id*3,:);
                        end

                        yy=yy*yy_len;
                        i_sh=yy*v_bus((prev_bus_no-1)*3+1:prev_bus_no*3);

                        if(vr_id==0)
                            s_in=v_bus((prev_bus_no-1)*3+m)*conj(i_bus((bus_no-1)*3+m)+i_sh(m));
                            s_out=v_bus((bus_no-1)*3+m).*conj(i_bus((bus_no-1)*3+m));
                            loss=s_in-s_out;
                        else
                            ph_no=voltage_reg((vr_id-1)*3+m,1);
                            turnsratio=voltage_reg((vr_id-1)*3+2,7);

                            if(ph_no>100)
                                % Transformers-Consider Loss!!!
                                s_in=v_bus((prev_bus_no-1)*3+m)*conj(i_bus((bus_no-1)*3+m)+i_sh(m));
                                s_out=v_bus((bus_no-1)*3+m).*conj(i_bus((bus_no-1)*3+m)*turnsratio);
                                loss=s_in-s_out;
                            else
                                % Voltage regulators-No loss!!!
                                loss=0;
                            end
                        end

                        s_loss_bus((bus_no-1)*3+m)=loss/1000;
                        loss_rd_status((bus_no-1)*3+m)=1;
                    end
                end
                prev_bus_no=bus_no;
            end
        end
    end

    if(mismatch_max_iteration==iter_cnt)
        flag=0;%it means EXIT
    else
        flag=1;%it means reiterate
    end
```

```
elseif(mismatch_type==1)

    s_bus=v_bus.*conj(i_bus);

    [row,col]=size(SIMPLIFIED_BACK_LATERAL_DATA);
    for mm=1:row
        prev_bus_no=0;
        for nn=col:-1:2
            bus_no=SIMPLIFIED_BACK_LATERAL_DATA(mm, nn);
            if(bus_no>0)
                for m=1:3
                    load_type=bus_data((bus_no-1)*3+m, 2);
                    % Difference psw and psw_mc
                    s_scheduled=bus_data((bus_no-1)*3+m, 3)+bus_data((bus_no-1)*3+m, 4)*1i;

                    % mismatch checking
                    if(nn==2 && (load_type==0 || load_type==4))

                        if(s_scheduled>0)
                            s_now=s_bus((bus_no-1)*3+m);
                            del_P=abs(s_now-s_scheduled);
                            if(del_P>accuracy)
                                flag=1;
                            end
                        end
                    end

                    % loss calculation
                    if(prev_bus_no>0 && loss_rd_status((bus_no-1)*3+m)==0)

                        vr_id=bus_data((bus_no-1)*3+m, 6);

                        [yy_id, yy_len]=find_admittance(bus_no, prev_bus_no, line_data);
                        if(yy_id==0)
                            yy=zeros(3,3);
                        else
                            yy=AD_COEFF*admittance_data((yy_id-1)*3+1:yy_id*3,:);
                        end

                        yy=yy*yy_len;
                        i_sh=yy*v_bus((prev_bus_no-1)*3+1:prev_bus_no*3);

                        if(vr_id==0)
                            s_in=v_bus((prev_bus_no-1)*3+m)*conj(i_bus((bus_no-1)*3+m)+i_sh(m));
                            s_out=v_bus((bus_no-1)*3+m).*conj(i_bus((bus_no-1)*3+m));
                            loss=s_in-s_out;
                        else
                            ph_no=voltage_reg((vr_id-1)*3+m,1);
                            turnsratio=voltage_reg((vr_id-1)*3+2,7);

                            if(ph_no>100)
                                % Transformers-Consider Loss!!!
                                s_in=v_bus((prev_bus_no-1)*3+m)*conj(i_bus((bus_no-1)*3+m)+i_sh(m));
                                s_out=v_bus((bus_no-1)*3+m).*conj(i_bus((bus_no-1)*3+m)*turnsratio);
                                loss=s_in-s_out;
                            else
                                % Voltage regulators-No loss!!!
                                loss=0;
                            end
                        end

                        s_loss_bus((bus_no-1)*3+m)=loss/1000;
                        loss_rd_status((bus_no-1)*3+m)=1;
                    end
                end
                prev_bus_no=bus_no;
            end
        end
    end
elseif(mismatch_type==2)

    [row,col]=size(SIMPLIFIED_BACK_LATERAL_DATA);
    for mm=1:row
        prev_bus_no=0;
        for nn=col:-1:2
            bus_no=SIMPLIFIED_BACK_LATERAL_DATA(mm, nn);
            if(bus_no>0)
                for m=1:3
                    load_type=bus_data((bus_no-1)*3+m, 2);
                    % Difference psw and psw_mc
                    s_scheduled=bus_data((bus_no-1)*3+m, 3)+bus_data((bus_no-1)*3+m, 4)*1i;

                    % mismatch checking
                    if(load_type==0 || load_type==4)
                        if(s_scheduled>0)
                            s_now=v_bus((bus_no-1)*3+1:bus_no*3).*conj(i_bus((bus_no-1)*3+1:bus_no*3));
                            s_prev=s_bus((bus_no-1)*3+1:bus_no*3);
                            del_P=abs(s_now-s_prev);
                            if(del_P>accuracy)
                                flag=1;
                            end
                        end
                    end

                    % loss calculation
                    if(prev_bus_no>0 && loss_rd_status((bus_no-1)*3+m)==0)

                        vr_id=bus_data((bus_no-1)*3+m, 6);

                        [yy_id, yy_len]=find_admittance(bus_no, prev_bus_no, line_data);
                        if(yy_id==0)
                            yy=zeros(3,3);
                        else
                            yy=AD_COEFF*admittance_data((yy_id-1)*3+1:yy_id*3,:);
                        end

                        yy=yy*yy_len;
                        i_sh=yy*v_bus((prev_bus_no-1)*3+1:prev_bus_no*3);

                        if(vr_id==0)
                            s_in=v_bus((prev_bus_no-1)*3+m)*conj(i_bus((bus_no-1)*3+m)+i_sh(m));
                            s_out=v_bus((bus_no-1)*3+m).*conj(i_bus((bus_no-1)*3+m));
                            loss=s_in-s_out;
                        else
```

```
                            ph_no=voltage_reg((vr_id-1)*3+m,1);
                            turnsratio=voltage_reg((vr_id-1)*3+2,7);

                            if(ph_no>100)
                                % Transformers-Consider Loss!!!
                                s_in=v_bus((prev_bus_no-1)*3+m)*conj(i_bus((bus_no-1)*3+m)+i_sh(m));
                                s_out=v_bus((bus_no-1)*3+m).*conj(i_bus((bus_no-1)*3+m)*turnsratio);
                                loss=s_in-s_out;
                            else
                                % Voltage regulators-No loss!!!
                                loss=0;
                            end
                        end

                        s_loss_bus((bus_no-1)*3+m)=loss/1000;
                        loss_rd_status((bus_no-1)*3+m)=1;
                    end
                end
                prev_bus_no=bus_no;
            end
        end
    end

    s_bus=v_bus.*conj(i_bus);
elseif(mismatch_type==3)
    % This is just calculating the loss only
    s_bus=v_bus.*conj(i_bus);
    [row,col]=size(SIMPLIFIED_BACK_LATERAL_DATA);
    for mm=1:row
        prev_bus_no=0;
        for nn=col:-1:2
            bus_no=SIMPLIFIED_BACK_LATERAL_DATA(mm, nn);
            if(bus_no>0)
                for m=1:3
                    % loss calculation
                    if(prev_bus_no>0 && loss_rd_status((bus_no-1)*3+m)==0)

                        vr_id=bus_data((bus_no-1)*3+m, 6);

                        [yy_id, yy_len]=find_admittance(bus_no, prev_bus_no, line_data);
                        if(yy_id==0)
                            yy=zeros(3,3);
                        else
                            yy=AD_COEFF*admittance_data((yy_id-1)*3+1:yy_id*3,:);
                        end

                        yy=yy*yy_len;
                        i_sh=yy*v_bus((prev_bus_no-1)*3+1:prev_bus_no*3);

                        if(vr_id==0)
                            s_in=v_bus((prev_bus_no-1)*3+m)*conj(i_bus((bus_no-1)*3+m)+i_sh(m));
                            s_out=v_bus((bus_no-1)*3+m).*conj(i_bus((bus_no-1)*3+m));
                            loss=s_in-s_out;
                        else
                            ph_no=voltage_reg((vr_id-1)*3+m,1);
                            turnsratio=voltage_reg((vr_id-1)*3+2,7);

                            if(ph_no>100)
                                % Transformers-Consider Loss!!!
                                s_in=v_bus((prev_bus_no-1)*3+m)*conj(i_bus((bus_no-1)*3+m)+i_sh(m));
                                s_out=v_bus((bus_no-1)*3+m).*conj(i_bus((bus_no-1)*3+m)*turnsratio);
                                loss=s_in-s_out;
                            else
                                % Voltage regulators-No loss!!!
                                loss=0;
                            end
                        end

                        s_loss_bus((bus_no-1)*3+m)=loss/1000;
                        loss_rd_status((bus_no-1)*3+m)=1;
                    end
                end
                prev_bus_no=bus_no;
            end
        end
    end
end

if(flag==0)
    % flag==0 means convergence is met, we will exit the bfsw routine
    % to display output at the end of the simulation
    s_total_loss(1)=sum(s_loss_bus(1:3:BUS_NUM*3));% Total A Ph loss
    s_total_loss(2)=sum(s_loss_bus(2:3:BUS_NUM*3));% Total B Ph loss
    s_total_loss(3)=sum(s_loss_bus(3:3:BUS_NUM*3));% Total C Ph loss
end


end
```

APPENDIX C

IEEE TEST FEEDERS FOR DISTRIBUTION

The IEEE PES Distribution System Analysis Subcommittee developed test networks for a distribution system that consists of well-defined, extremely complex distribution networks such as 4-, 13-, 34-, 37-, 123-, and 8,500-bus test feeders [23]. This study verifies the proposed power-flow algorithm using IEEE 4-, 13-, 34-, 37-, and 123-bus test feeders, in Figure 59-Figure 63. Power equipment (e.g., transformers, voltage regulators, and shunt capacitor banks), the network configuration (e.g., the configuration of buses, overhead and underground lines, and cables), load data (e.g., local and distributed loads), and distribution line data (e.g., specification data, spacing models, and the impedance of conductors and cables) used in this study are from [23, 41].

(1) IEEE 4-Bus Test Feeder

This study verifies all of the connections of the three-phase transformer, presented Appendix A, using the IEEE 4-bus test feeder, depicted in Figure 59.

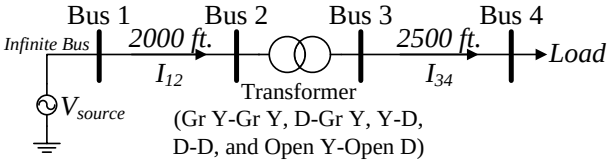

Figure 59. The IEEE 4-bus test feeder.

(2) IEEE 13-Bus Test Feeder

Shown in Figure 60, this feeder, which consists of the voltage regulator, two three-phase transformers with rating voltages of 115/4.16 kV and 4.16/0.48 kV, capacitor banks, and several types of loads, is appropriate for testing a power-flow algorithm for a small distribution feeder.

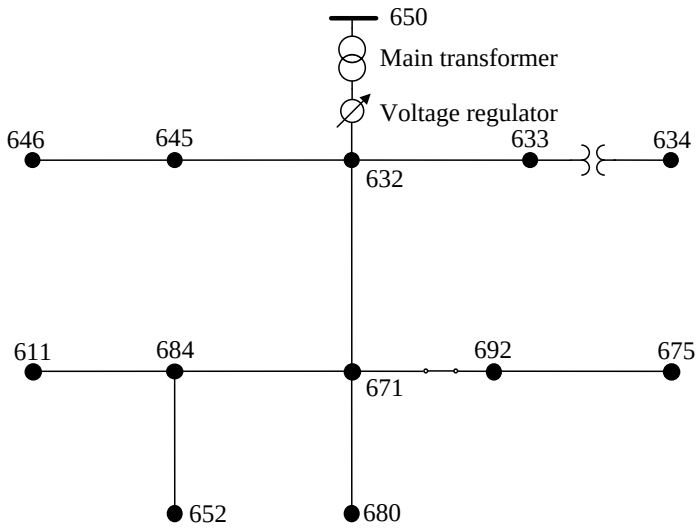

Figure 60. The IEEE 13-bus test feeder.

(3) IEEE 34-Bus Test Feeder

Illustrated in Figure 61, this feeder, characterized by very long but lightly loaded lines and distributed loads is the actual feeder in the state of Arizona, which operates at a 24.9 kV rating voltage.

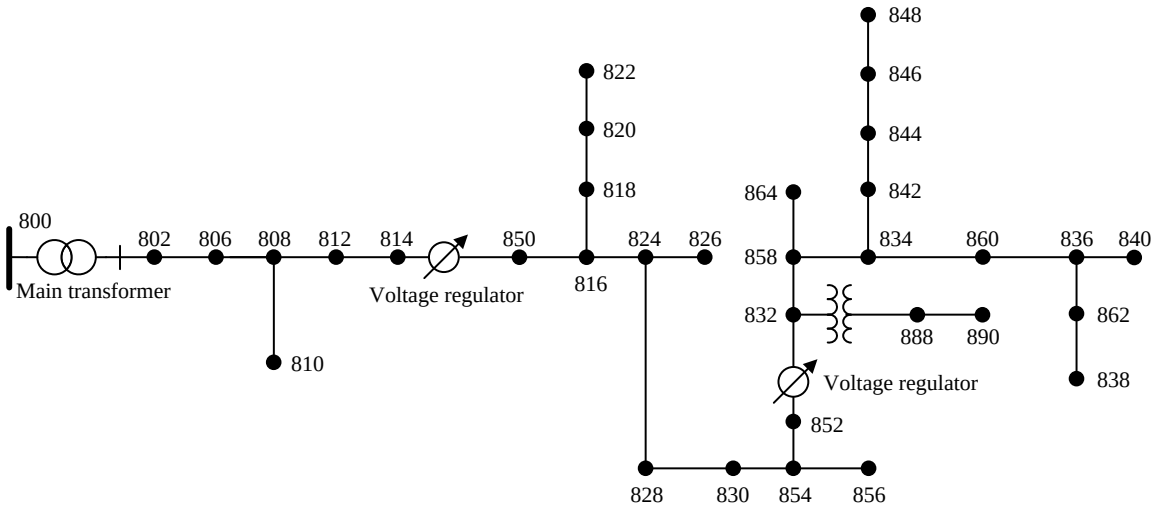

Figure 61. The IEEE 34-bus test feeder.

(4) IEEE 37-Bus Test Feeder

Shown in Figure 62, this feeder, all lines of which are underground cables and all the loads of which are highly unbalanced, is the actual feeder in the state of California, which operates at a nominal voltage of 4.8 kV.

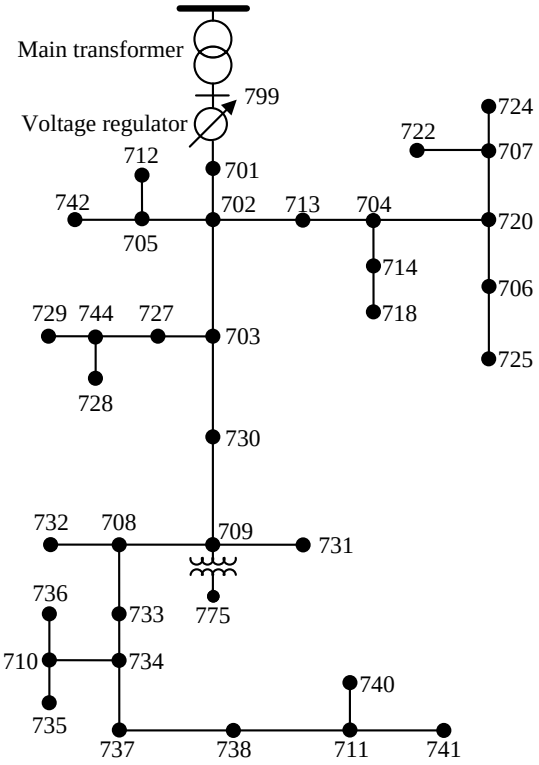

Figure 62. The IEEE 37-bus test feeder.

(5) IEEE 123-Bus Test Feeder

Illustrated in Figure 63, this feeder, which is characterized by an extremely complex configuration and several switches for the alternative path, is appropriate for testing the problem of the voltage drop through very long lines, voltage regulators, and shunt capacitor banks.

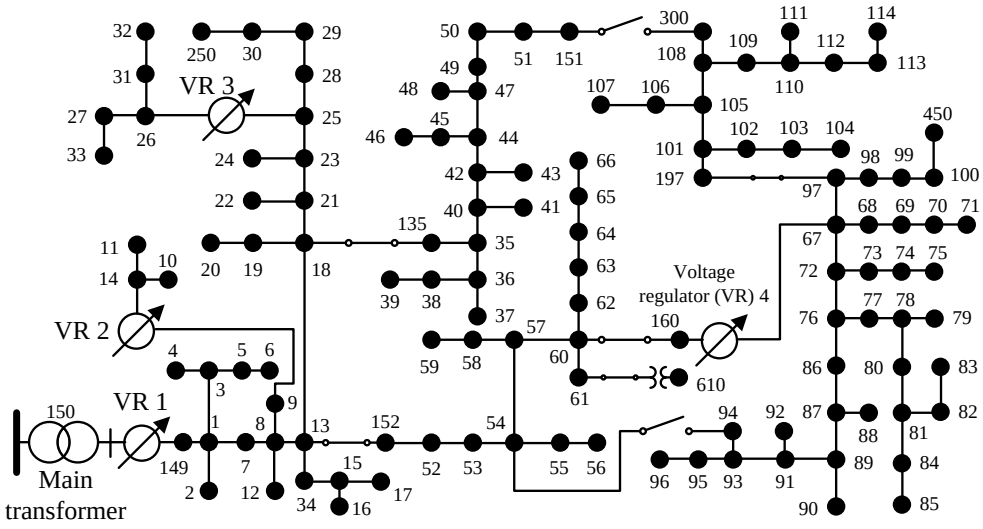

Figure 63. The IEEE 123-bus test feeder.

Table 34 shows the summary of main transformers, voltage regulators, capacitor banks, and load data of the test feeders.

Table 34. IEEE test feeders for the distributed system

Number of Buses	Capacity	Main Transformer (LL=Line-to-line)		Connection	Voltage Regulator	Capacitor Bank	Load(Lagging PF)			Distributed Load
	kVA	kV_{LL}	kV_{LL}				Phase *A*	Phase *B*	Phase *C*	
4	6,000	12.47	4.16	Gr Y-Gr Y, D-Gr Y,Y-D, D-D, Open Gr Y-Open D	-	-	1,800 kW (0.9)	1,800 kW (0.9)	1,800 kW (0.9)	-
	6,000	12.47	24.9				1,275 kW (0.85)	1,800 kW (0.9)	2,375 kW (0.95)	-
	2,000	12.47	4.16				1,200 kW (0.9)	1,200 kW (0.9)	1,200 kW (0.9)	-
	2,000	12.47	24.9				850 kW (0.85)	1,200 kW (0.9)	1,583 kW (0.95)	-

Number of Buses	Capacity in kVA	Main Transformer in kV_{LL}		Transformer in kV_{LL}	Voltage Regulator	Capacitor Bank (Total Capacity)	Local load						Distributed Load
							Y-PQ	Y-I	Y-Z	D-PQ	D-I	D-Z	
13	5,000	115	4.16	4.16/0.48	1	2	3	1	1	1	1	1	1
		D-Gr Y		Gr Y-Gr Y		700 kVar	8 loads, total 3,266 kW+1,986 kVar						200 kW +116 kVar
34	2,500	69	24.9	24.9/4.16	2	2	1	1	1	1	1	1	19
		D-Gr Y		Gr Y-Gr Y		750 kVar	6 loads, total 1,047 kW+677 kVar						722 kW +367 kVar
37	2,500	230	4.8	4.8/0.48	1	-	0	0	0	13	6	6	-
		D-D		D-D		-	25 loads, total 2,457 kW+1,201 kVar						-
123	5,000	115	4.16	4.16/0.48	4	4	56	12	14	1	1	1	-
		D-Gr Y		D-D		750 kVar	85 loads, total 3,490 kW+1,920 kVar						-

APPENDIX D

COMPARISON OF IEEE SOLUTIONS AND SOLUTIONS CALCULATED BY THE PROPOSED THREE-PHASE POWER-FLOW ALGORITHM

Table 35 and Table 39 show the detailed comparisons of voltage profiles presented from [41] and those from the proposed algorithm for IEEE 4-, 13-, 34-, 37-, and 123-bus test feeders. The solutions of the proposed power-flow algorithm are the same as those from [41]. The results of the IEEE 123-bus test feeder are omitted for brevity.

Table 35. A comparison of the voltage profiles of the IEEE 4-bus feeder with the step-down transformer in the case of balanced loading-1

Connection	Gr Y - Gr Y				Gr Y-D				Y-D			
	IEEE Solution		Solution from Proposed Algorithm		IEEE Solution		Solution from Proposed Algorithm		IEEE Solution		Solution from Proposed Algorithm	
	Magnitude	Angle(°)	Magnitude	Angle(°)	Magnitude	Angle(°)	Magnitude	Angle(°)	Magnitude	Angle(°)	Magnitude	Angle(°)
Bus 2												
Va	7107.0	-0.3	7106.5	-0.3	7113.0	-0.3	7111.6	-0.3	7112.0	0.0	7111.6	-0.3
Vb	7140.0	-120.3	7139.7	-120.3	7132.0	-120.3	7132.1	-120.4	7133.0	-120.4	7132.1	-120.4
Vc	7121.0	119.6	7120.7	119.6	7123.0	119.6	7123.1	119.6	7124.0	119.6	7123.1	119.6
Bus 3												
Va	2247.6	-3.7	2247.4	-3.7	3906.0	-3.5	3905.7	-3.5	3906.0	-3.4	3905.7	-3.5
Vb	2269.0	-123.5	2268.5	-123.5	3915.0	-123.6	3914.8	-123.6	3915.0	-123.6	3914.8	-123.6
Vc	2256.0	116.4	2255.8	116.4	3909.0	116.3	3909.3	116.3	3909.0	116.3	3909.3	116.3
Bus 4												
Va	1918.0	-9.1	1917.7	-9.1	3437.0	-7.8	3437.3	-7.8	3437.0	-7.8	3437.3	-7.8
Vb	2061.0	-128.3	2061.3	-128.3	3497.0	-129.3	3496.8	-129.3	3497.0	-129.3	3496.8	-129.3
Vc	1981.0	110.9	1980.7	110.9	3388.0	110.6	3388.4	110.6	3388.0	110.6	3388.4	110.6
Current between Buses 1 and 2												
Ia	347.9	-34.9	347.9	-34.9	334.8	-34.5	335.8	-34.7	335.8	-34.7	335.8	-34.7
Ib	323.7	-154.2	323.7	-154.2	335.4	-154.9	336.0	-154.6	335.9	-154.6	336.0	-154.6
Ic	336.8	85.0	336.9	85.0	337.4	85.4	335.9	85.3	335.9	85.3	335.9	85.3
Current between Buses 3 and 4												
Ia	1042.8	-34.9	1042.9	-34.9	1006.6	-64.7	1006.6	-64.7	1006.6	-64.7	1006.6	-64.7
Ib	970.2	-154.2	970.3	-154.2	1006.7	175.4	1006.7	175.4	1006.7	175.4	1006.7	175.4
Ic	1009.6	85.0	1009.7	85.0	1007.2	55.3	1007.2	55.3	1007.2	55.3	1007.2	55.3

Table 36. A comparison of the voltage profiles of the IEEE 4-bus feeder with the step-down transformer in the case of balanced loading-2

Connection	D-D				Open Gr Y-Open D			
	IEEE Solution		Proposed Algorithm		IEEE Solution		Proposed Algorithm	
	Magnitude	Angle(°)	Magnitude	Angle(°)	Magnitude	Angle(°)	Magnitude	Angle(°)
Bus 2								
Va	12339.0	29.7	12338.7	29.7	6984.0	0.4	6983.9	0.5
Vb	12349.0	-90.4	12348.6	-90.4	7167.0	-121.7	7166.5	-121.7
Vc	12321.0	149.6	12321.2	149.6	7293.0	120.5	7293.0	120.5
Bus 3								
Va	3911.0	26.5	3910.6	26.5	3701.0	-0.9	3701.2	-0.9
Vb	3914.0	-93.6	3914.3	-93.6	4076.0	-126.5	4075.7	-126.5
Vc	3905.0	146.4	3905.0	146.4	3572.0	110.9	3572.1	110.9
Bus 4								
Va	3442.0	22.3	3442.0	22.3	3384.0	-3.5	3384.1	-3.5
Vb	3497.0	-99.4	3496.8	-99.4	3804.9	-130.2	3804.9	-130.2
Vc	3384.0	140.7	3383.7	140.7	3246.0	106.5	3245.6	106.5
Current between Buses 1 and 2								
Ia	335.8	-34.7	335.8	-34.7	380.9	-65.2	381.0	-65.2
Ib	335.8	-154.6	335.8	-154.6	387.4	-125.2	387.5	-125.2
Ic	336.0	85.4	336.0	85.4	0.0	0.0	0.0	0.0
Current between Buses 3 and 4								
Ia	1006.7	-34.7	1006.7	-34.7	659.3	-65.2	659.3	-65.2
Ib	1006.7	-154.6	1006.7	-154.6	665.7	175.6	665.7	175.6
Ic	1007.2	85.4	1007.2	85.4	670.5	54.8	670.6	54.8

Table 37. A comparison of the line-to-neutral voltage profiles of the IEEE 13-bus test feeder

Bus	IEEE Line-to-Neutral Voltage Solution in PU						Line-to-Neutral Voltage from the Proposed Algorithm in PU					
	Phase *A*		Phase *B*		Phase *C*		Phase *A*		Phase *B*		Phase *C*	
	Magnitude	Angle (°)	Magnitude	Angle (°)	Magnitude	Angle (°)	Magnitude	Angle (°)	Magnitude	Angle (°)	Magnitude	Angle (°)
650	1.0000	0.00	1.0000	-120.00	1.0000	120.00	1.0000	0.00	1.0000	-120.00	1.0000	120.00
VRP	1.0625	0.00	1.0500	-120.00	1.0687	120.00	1.0625	0.00	1.0500	-120.00	1.0687	120.00
VRS	1.0625	0.00	1.0500	-120.00	1.0687	120.00	1.0625	0.00	1.0500	-120.00	1.0687	120.00
632	1.0210	-2.49	1.0420	-121.72	1.0174	117.83	1.0211	-2.49	1.0420	-121.72	1.0174	117.83
633	1.0180	-2.56	1.0401	-121.77	1.0148	117.82	1.0180	-2.55	1.0401	-121.77	1.0148	117.82
XFP	0.9941	-3.23	1.0218	-122.22	0.9960	117.35	0.9941	-3.23	1.0218	-122.22	0.9960	117.35
XFS	0.9941	-3.23	1.0218	-122.22	0.9960	117.35	0.9941	-3.23	1.0218	-122.22	0.9960	117.35
634	0.9940	-3.23	1.0218	-122.22	0.9960	117.34	0.9941	-3.23	1.0218	-122.22	0.9960	117.35
645			1.0329	-121.90	1.0155	117.86			1.0328	-121.90	1.0155	117.86
646			1.0311	-121.98	1.0134	117.90			1.0311	-121.98	1.0134	117.90
671	0.9900	-5.30	1.0529	-122.34	0.9778	116.02	0.9900	-5.29	1.0529	-122.34	0.9779	116.03
680	0.9900	-5.30	1.0529	-122.34	0.9778	116.02	0.9900	-5.29	1.0529	-122.34	0.9779	116.03
684	0.9881	-5.32			0.9758	115.92	0.9881	-5.32			0.9759	115.92
611					0.9738	115.78					0.9739	115.78
652	0.9825	-5.25					0.9825	-5.24				
692	0.9900	-5.31	1.0529	-122.34	0.9777	116.02	0.9900	-5.29	1.0529	-122.34	0.9779	116.03
675	0.9835	-5.56	1.0553	-122.52	0.9758	116.03	0.9835	-5.54	1.0553	-122.52	0.9760	116.04

Table 38. A comparison of the line-to-neutral voltage profiles of the IEEE 34-bus test feeder

Bus	IEEE Line-to-Neutral Voltage Solution in PU						Line-to-Neutral Voltage from the Proposed Algorithm in PU					
	Phase *A*		Phase *B*		Phase *C*		Phase *A*		Phase *B*		Phase *C*	
	Magnitude	Angle (°)	Magnitude	Angle (°)	Magnitude	Angle (°)	Magnitude	Angle (°)	Magnitude	Angle (°)	Magnitude	Angle (°)
800	1.0500	0.00	1.0500	-120.00	1.0500	120.00	1.0500	0.00	1.0500	-120.00	1.0500	120.00
802	1.0475	-0.05	1.0484	-120.07	1.0484	119.95	1.0475	-0.05	1.0484	-120.07	1.0484	119.95
806	1.0457	-0.08	1.0474	-120.11	1.0474	119.92	1.0457	-0.08	1.0474	-120.11	1.0474	119.91
808	1.0136	-0.75	1.0296	-120.95	1.0289	119.30	1.0136	-0.74	1.0295	-120.94	1.0287	119.31
810			1.0294	-120.95					1.0294	-120.95		
812	0.9763	-1.57	1.0100	-121.92	1.0069	118.59	0.9761	-1.56	1.0098	-121.90	1.0066	118.59
814	0.9467	-2.26	0.9945	-122.70	0.9893	118.01	0.9464	-2.25	0.9943	-122.68	0.9890	118.02
VR1	1.0177	-2.26	1.0255	-122.70	1.0203	118.01	1.0177	-2.25	1.0255	-122.68	1.0203	118.02
850	1.0176	-2.26	1.0255	-122.70	1.0203	118.01	1.0177	-2.25	1.0255	-122.68	1.0203	118.02
816	1.0172	-2.26	1.0253	-122.71	1.0200	118.01	1.0173	-2.25	1.0252	-122.69	1.0200	118.01
818	1.0163	-2.27					1.0164	-2.25				
820	0.9926	-2.32					0.9925	-2.30				
822	0.9895	-2.33					0.9894	-2.30				
824	1.0082	-2.37	1.0158	-122.94	1.0116	117.76	1.0082	-2.36	1.0158	-122.91	1.0116	117.76
826			1.0156	-122.94					1.0156	-122.91		
828	1.0074	-2.38	1.0151	-122.95	1.0109	117.75	1.0075	-2.37	1.0151	-122.93	1.0109	117.74
830	0.9894	-2.63	0.9982	-123.39	0.9938	117.25	0.9895	-2.63	0.9982	-123.36	0.9938	117.24
854	0.9890	-2.64	0.9978	-123.40	0.9934	117.24	0.9890	-2.64	0.9977	-123.38	0.9934	117.23
856			0.9977	-123.41					0.9976	-123.38		
852	0.9581	-3.11	0.9680	-124.18	0.9637	116.33	0.9580	-3.09	0.9679	-124.14	0.9636	116.34
VR2	1.0359	-3.11	1.0345	-124.18	1.0360	116.33	1.0359	-3.09	1.0345	-124.14	1.0360	116.34
832	1.0359	-3.11	1.0345	-124.18	1.0360	116.33	1.0359	-3.09	1.0345	-124.14	1.0360	116.34
TR3	0.9997	-4.63	0.9983	-125.73	1.0000	114.82	0.9995	-4.62	0.9983	-125.69	0.9999	114.81
888	0.9996	-4.64	0.9983	-125.73	1.0000	114.82	0.9995	-4.62	0.9983	-125.69	0.9999	114.81
890	0.9167	-5.19	0.9235	-126.78	0.9177	113.98	0.9166	-5.17	0.9235	-126.74	0.9176	113.98
858	1.0336	-3.17	1.0322	-124.28	1.0338	116.22	1.0336	-3.15	1.0321	-124.23	1.0338	116.23
864	1.0336	-3.17					1.0336	-3.15				
834	1.0309	-3.24	1.0295	-124.39	1.0313	116.09	1.0309	-3.22	1.0294	-124.34	1.0313	116.10
842	1.0309	-3.25	1.0294	-124.39	1.0313	116.09	1.0308	-3.23	1.0294	-124.35	1.0312	116.09
844	1.0307	-3.27	1.0291	-124.42	1.0311	116.06	1.0306	-3.25	1.0290	-124.37	1.0310	116.07
846	1.0309	-3.32	1.0291	-124.46	1.0313	116.01	1.0309	-3.30	1.0290	-124.42	1.0313	116.01
848	1.0310	-3.32	1.0291	-124.47	1.0314	116.00	1.0309	-3.30	1.0291	-124.43	1.0313	116.01
860	1.0305	-3.24	1.0291	-124.39	1.0310	116.09	1.0305	-3.22	1.0290	-124.34	1.0309	116.09
836	1.0303	-3.23	1.0287	-124.39	1.0308	116.09	1.0302	-3.21	1.0286	-124.35	1.0308	116.09
840	1.0303	-3.23	1.0287	-124.39	1.0308	116.09	1.0302	-3.21	1.0286	-124.35	1.0308	116.10
862	1.0303	-3.23	1.0287	-124.39	1.0308	116.09	1.0302	-3.21	1.0286	-124.35	1.0308	116.09
838			1.0285	-124.39					1.0285	-124.35		

Table 39. A comparison of the line-to-line voltage profiles of the IEEE 37-bus test feeder

Bus	IEEE Line-to-Line Voltage Solution in PU						Line-to-Line Voltage from the Proposed Algorithm in PU					
	Phases *A-B*		Phases *B-C*		Phases *C-A*		Phases *A-B*		Phases *B-C*		Phases *C-A*	
	Magnitude	Angle (°)	Magnitude	Angle (°)	Magnitude	Angle (°)	Magnitude	Angle (°)	Magnitude	Angle (°)	Magnitude	Angle (°)
799	1.0000	0.00	1.0000	-120.00	1.0000	120.00	1.00000	0.00	1.00000	-120.00	1.00000	120.00
VRP	1.0437	0.00	1.0250	-120.00	1.0345	120.00	1.04370	0.00	1.02500	-120.00	1.03448	120.90
701	1.0317	-0.08	1.0144	-120.39	1.0183	120.61	1.03167	-0.08	1.01444	-120.39	1.01832	120.61
702	1.0248	-0.14	1.0088	-120.58	1.0101	120.43	1.02473	-0.14	1.00885	-120.58	1.01005	120.42
705	1.0241	-0.13	1.0075	-120.59	1.0088	120.46	1.02409	-0.13	1.00752	-120.59	1.00878	120.45
712	1.0240	-0.11	1.0073	-120.61	1.0082	120.46	1.02396	-0.11	1.00734	-120.61	1.00816	120.46
742	1.0238	-0.15	1.0067	-120.59	1.0086	120.48	1.02375	-0.15	1.00669	-120.59	1.00859	120.48
713	1.0234	-0.15	1.0070	-120.6	1.0083	120.44	1.02337	-0.14	1.00698	-120.60	1.00826	120.44
704	1.0217	-0.17	1.0044	-120.61	1.0065	120.46	1.02163	-0.17	1.00443	-120.61	1.00644	120.46
714	1.0214	-0.17	1.0043	-120.6	1.0064	120.46	1.02137	-0.17	1.00434	-120.60	1.00635	120.45
718	1.0201	-0.16	1.0041	-120.57	1.0060	120.42	1.02003	-0.16	1.00411	-120.57	1.00594	120.42
720	1.0205	-0.21	1.0011	-120.66	1.0041	120.53	1.02041	-0.21	1.00111	-120.66	1.00403	120.52
707	1.0187	-0.3	0.9959	-120.62	1.0025	120.67	1.01862	-0.30	0.99593	-120.62	1.00248	120.67
722	1.0185	-0.3	0.9954	-120.62	1.0023	120.68	1.01844	-0.30	0.99540	-120.62	1.00230	120.68
724	1.0184	-0.32	0.9950	-120.61	1.0023	120.69	1.01830	-0.32	0.99498	-120.61	1.00230	120.69
706	1.0204	-0.22	1.0007	-120.66	1.0039	120.54	1.02031	-0.22	1.00068	-120.66	1.00390	120.53
725	1.0202	-0.23	1.0003	-120.65	1.0039	120.55	1.02019	-0.22	1.00033	-120.65	1.00384	120.54
703	1.0178	-0.17	1.0051	-120.7	1.0034	120.2	1.01778	-0.17	1.00505	-120.70	1.00340	120.19
727	1.0167	-0.16	1.0044	-120.69	1.0025	120.19	1.01666	-0.16	1.00442	-120.69	1.00243	120.19
744	1.0160	-0.16	1.0041	-120.68	1.0021	120.17	1.01596	-0.16	1.00405	-120.68	1.00203	120.17
729	1.0157	-0.15	1.0040	-120.67	1.0019	120.17	1.01560	-0.15	1.00399	-120.67	1.00192	120.16
728	1.0156	-0.15	1.0037	-120.68	1.0017	120.18	1.01557	-0.15	1.00368	-120.68	1.00164	120.18
730	1.0127	-0.12	1.0021	-120.73	0.9981	120.1	1.01269	-0.12	1.00215	-120.73	0.99812	120.10
709	1.0111	-0.11	1.0012	-120.73	0.9967	120.07	1.01108	-0.11	1.00123	-120.73	0.99666	120.07
731	1.0109	-0.13	1.0004	-120.74	0.9964	120.1	1.01088	-0.13	1.00038	-120.74	0.99639	120.09
708	1.0087	-0.08	1.0002	-120.73	0.9945	120.02	1.00863	-0.08	1.00023	-120.73	0.99447	120.01
732	1.0086	-0.07	1.0001	-120.74	0.9941	120.02	1.00854	-0.07	1.00011	-120.74	0.99405	120.02
733	1.0063	-0.05	0.9993	-120.73	0.9925	119.96	1.00624	-0.05	0.99928	-120.73	0.99252	119.96
734	1.0029	-0.01	0.9978	-120.74	0.9893	119.88	1.00286	-0.01	0.99780	-120.74	0.98928	119.88
736	1.0019	-0.02	0.9951	-120.75	0.9875	119.95	1.00182	-0.02	0.99515	-120.75	0.98746	119.95
710	1.0024	0.01	0.9968	-120.77	0.9878	119.91	1.00236	0.01	0.99675	-120.76	0.98778	119.91
735	1.0023	0.03	0.9966	-120.78	0.9873	119.91	1.00225	0.03	0.99660	-120.78	0.98725	119.91
737	0.9996	0.02	0.9969	-120.71	0.9872	119.79	0.99954	0.02	0.99685	-120.71	0.98718	119.79
738	0.9985	0.04	0.9965	-120.71	0.9861	119.76	0.99842	0.04	0.99647	-120.71	0.98608	119.76
711	0.9982	0.06	0.9963	-120.74	0.9852	119.76	0.99815	0.06	0.99629	-120.74	0.98517	119.75
740	0.9981	0.07	0.9961	-120.75	0.9847	119.76	0.99804	0.07	0.99614	-120.75	0.98464	119.76
741	0.9981	0.07	0.9962	-120.75	0.9849	119.76	0.99806	0.07	0.99623	-120.75	0.98487	119.75
XF7	1.0111	-0.11	1.0012	-120.73	0.9967	120.07	1.01108	-0.11	1.00123	-120.73	0.99666	120.07
775	1.0111	-0.11	1.0012	-120.73	0.9967	120.07	1.01108	-0.11	1.00123	-120.73	0.99666	120.07

APPENDIX E

PV MODULES AND INVERTERS OF STOCHASTICALLY DISPERSED PV SYSTEMS

Table 40 and Table 41 show PV modules and inverters used in the scenario of *N* stochastically dispersed PV systems.

Table 40. PV modules used in the scenario of *N* dispersed PV systems [72]

Model	Year	Material	Area	V_{oc}	I_{mp}	V_{mp}	P_{mp}
			m^2	V	A	V	W
Suniva Titan 240	2009	c-Si	1.643	37.5	7.93	30.78	244.1
First Solar FS-275	2007	CdTe	0.72	92	1.08	69.4	75.0
Uni-Solar PVL-124	2006	3-a-Si	1.973	42	4.1	30	123.0
Shell Solar ST36	2003	CIS	0.424	22.9	2.28	15.8	36.0

Table 41. Inverters used in the scenario of *N* dispersed PV systems [72]

Model	Year	Rating in kW	V_{ac}	V_{dc}	V_{dcmax}	I_{dcmax}
			V	V	V	A
GEPVe-1100-NA-120	2009	1.1 kW	120	182.39	-	-
Sunteams 2000	2011	2 kW	240	384.88	500	10
GS-3000	2011	3 kW	208	306.83	500	15
Beacon M4	2006	4 kW	120	54.50	110	100
Conext TX 5000 NA	2011	5 kW	240	300.36	600	22.5
IG Plus 6.0-1 uni(208)	2010	6 kW	208	364.25	600	28.1
SB7000US	2007	7 kW	208	310.02	-	-
SPR-8000m	2010	8 kW	277	345.50	600.00	30
SB9000TL-US	2010	9.1 kW	208	347.82	600.00	31
PVI-10.0-I-OUTD-x-US-208-y	2011	10 kW	208	320.73	520.00	24
SPR-11401f-3 Delta (208Vac)	2010	11.4 kW	208	364.64	600.00	53.3
SPR-12001f-3-277WYE	2010	12 kW	277	329.58	600.00	53.3
PVI 13 kW 480 V	2007	13.4 kW	480	269.74	-	-
Ingecon Sun 15U 208V	2010	15 kW	208	350.43	-	-
Refusol (16 kW)	2011	16.1 kW	480	720.18	500.00	33
Refusol (20 kW)	2011	19.7 kW	480	720.65	500.00	37.5

APPENDIX F

RELIABILITY PARAMETERS

Table 42 shows the failure data used in this study [45]. The failure rate of the line is higher than that of the cable, and the repair time of the line is longer than that of the cable. Figure 64 illustrates the trend in the objective function for the number of fuses installed on the IEEE 34-bus test feeder. Table 43 and Table 44 present possible locations of the protection device decreased as a result of two protection strategies presented in Section 4.6.2.

Table 42. Reliability parameters

Element	Failure rate	Repair time in hours	Replacement time in hours	Switching time in hour(s)
Line	0.065 freq/(year-km)	5	-	1
Cable	0.040 freq/(year-km)	30	-	3
Transformer in the line system	0.015 freq/(year)	200	10	1
Transformer in the cable system	0.015 freq/(year)	200	10	3

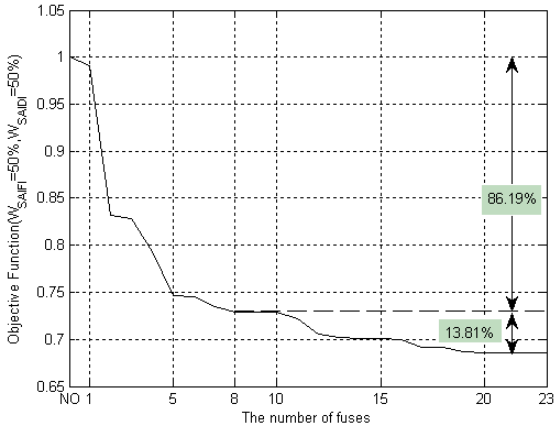

Figure 64. The objective function according to the number of fuses of the IEEE 34-bus test feeder.

Table 43. Possible positions of fuses and reclosers of the IEEE 34-bus test feeder

Device Type	Position	
	Main	Lateral
Fuse (23)	800-802, 802-806, 814-850, 816-824, 824-828, 830F[1]-830, 828-830F, 852-832, 832-858, 858-834, 834-860F, 860F-860, 860-836, 836-840F, 840F-840	808-810, 816-818, 824-826, 854-856, 832-888, 858-864, 834-842, 836-862
Recloser (23)	The same as fuse	The same as fuse

where [1]830F means a fictitious bus in front of bus 830.

Table 44. Possible positions of fuses and reclosers of the IEEE 123-bus test feeder

Device Type	Position	
	Main	Lateral
Fuse (40)	150-149,1-7,7-8,8-13,13-152, 52-53,53-54,54-57,57-60,60-160,67-97,97-197,101-105,105-108	1-3,8-9,13-18,13-34,18-135,18-21,21-23,25-26,25-28,35-36,35-40,40-42,42-44,44-47,60-61,60-62,67-68,67-72,72-76,76-77,76-86,89-91,97-98,101-102,105-106,108-109
Recloser (40)	The same as fuse	The same as fuse

APPENDIX G

HEAT-RATE DATA

Table 45. Heat-rate data of a nuclear plant [77]

Fuel	Rating	Unit output in Btu/kWh		
	MW	90%	80%	65%
Nuclear	1,000	9,847	9,914	10,133

Table 46. Heat-rate data of a coal-fired plant [76]

Fuel	Rating	Unit output in Btu/kWh		
	MW	90%	60%	40%
Coal	1,000	8,279	8,305	8,349

Table 47. Heat-rate data of gas-fired plants [78]

Fuel	Rating in MW	Unit output in Btu/kWh		
Gas	65	100%	66%	46%
		10,255	10,426	10,808
	110	100%	50%	25%
		10,773	11,028	12,092
	126	100%	56%	33%
		11,229	12,599	14,935
	150	100%	50%	25%
		9,768	10,107	11,219
	350	100%	51%	26%
		10,530	11,577	14,020
	560	100%	54%	32%
		10,065	10,320	10,770
	640	100%	50%	25%
		9,731	10,354	12,071
	960	100%	69%	38%
		9,509	9,691	10,479

Table 48. Coefficients of the input-output model of the hydroelectric unit [95]

Coefficient	a_{Hi}	b_{Hi}	c_{Hi}	d_{Hi}	e_{Hi}	$P_{Hi,saddle}$
Value	330	4.97	4330	-88	0.05	1,000MW

Table 49. The number of power system customers of the state of Georgia as of December 2010 [43]

Customer type	Population size	Percentage	Variable
Residential	2,049,770	86.80	W_R
Commercial	296,140	12.54	W_C
Industrial	8,136	0.34	W_I
Other	7,309	0.32	-

Table 50. Load profile data of each customer type in hourly intervals in kW [79]

Customer type	Year	Description	Raw measurement data in kW			Variable (hourly)
			Min	Mean	Max	
Residential	2010	Domestic single	0.39	0.71	2.11	P_R
Commercial		Small commercial	0.59	1.10	2.56	P_C
Industrial		Medium commercial/industrial	8.01	14.12	30.91	P_I

APPENDIX H

COST AND EMISSION OUTPUT FUNCTIONS

This study synthesizes cubic-order output functions for the costs and the emissions of steam-turbine generating units in *$/hour*, *kg/hour*, or *gallon/hour* using heat-rate data presented in Table 45-Table 47, the equivalent fuel prices of generating units (generation costs) in *$/MWh* presented in Table 27, and the emission factors in *kg/kWh* or *gallons/kWh* presented in Table 12.

Table 51. Coefficients of cubic-order cost functions in $/hour

Fuel Type	Index	$C_i(P_{Gi}) = fp_i F_i = a_i' + b_i' P_{Gi} + d_i' P_{Gi}^3$ in *$/hour*		
		a_i'	b'	d'
Coal	1~10	734.5277	108.9850	0.00000013975
Gas	11	757.3970	155.6331	0.00130883034
Gas	12	757.3970	155.6331	0.00130883034
Gas	13	757.3970	155.6331	0.00130883034
Gas	14	1059.5203	164.7993	0.00058785630
Gas	15	4050.9652	153.9108	0.00019951438
Gas	16	7828.3413	149.8850	0.00004242976
Gas	17	3446.6513	162.1236	0.00000425702
Gas	18	757.3970	155.6331	0.00130883034
Gas	19	757.3970	155.6331	0.00130883034
Gas	20	12122.1348	142.6421	0.00000539754
Gas	21	9621.8918	142.9032	0.00001476413
Gas	22	12122.1348	142.6421	0.00000539754
Gas	23	1483.8003	149.1440	0.00024765893
Nuclear	24~25	2327.4529	15.5382	0.00000113918

Table 52. Coefficients of cubic-order output functions for CO_2 in kg/hour

Fuel Type	Index	$EO_{CO_2,i}(P_{Gi}) = ef_{CO_2,i} F_i = \alpha'_{CO_2,i} + \beta'_{CO_2,i} P_{Gi} + \gamma'_{CO_2,i} P_{Gi}^3$ in *kg/hour*		
		$\alpha'_{CO_2,i}$	$\beta'_{CO_2,i}$	$\gamma'_{CO_2,i}$
Coal	1~10	15899.0394	2359.0079	0.00000302493
Gas	11	6919.5790	1421.8636	0.01195747399
Gas	12	6919.5790	1421.8636	0.01195747399
Gas	13	6919.5790	1421.8636	0.01195747399
Gas	14	9679.7776	1505.6063	0.00537065515
Gas	15	37009.6177	1406.1288	0.00182276338
Gas	16	71519.7265	1369.3497	0.00038763830
Gas	17	31488.6060	1481.1608	0.00003889213
Gas	18	6919.5790	1421.8636	0.01195747399
Gas	19	6919.5790	1421.8636	0.01195747399
Gas	20	110747.8240	1303.1782	0.00004931193
Gas	21	87905.6038	1305.5636	0.00013488506
Gas	22	110747.8240	1303.1782	0.00004931193
Gas	23	13555.9995	1362.5794	0.00226261199
Nuclear	24~25	23274.5288	155.3819	0.00001139175

Table 53. Coefficients of cubic-order output functions for SO_2 in kg/hour

Fuel Type	Index	$EO_{SO_2,i}(P_{Gi}) = ef_{SO_2,i}F_i = \alpha'_{SO_2,i} + \beta'_{SO_2,i}P_{Gi} + \gamma'_{SO_2,i}P_{Gi}^3$ in *kg/hour*		
		$\alpha'_{SO_2,i}$	$\beta'_{SO_2,i}$	$\gamma'_{SO_2,i}$
Coal	1~10	98.4705	14.6105	0.00000001874
Gas	11	0.0382	0.0078	0.00000006601
Gas	12	0.0382	0.0078	0.00000006601
Gas	13	0.0382	0.0078	0.00000006601
Gas	14	0.0534	0.0083	0.00000002965
Gas	15	0.2043	0.0078	0.00000001006
Gas	16	0.3948	0.0076	0.00000000214
Gas	17	0.1738	0.0082	0.00000000022
Gas	18	0.0382	0.0078	0.00000006601
Gas	19	0.0382	0.0078	0.00000006601
Gas	20	0.6114	0.0072	0.00000000027
Gas	21	0.4853	0.0072	0.00000000075
Gas	22	0.6114	0.0072	0.00000000027
Gas	23	0.0748	0.0075	0.00000001249
Nuclear	24~25	0.0000	0.0000	0.00000000000

Table 54. Coefficients of cubic-order output functions for NO_X in kg/hour

Fuel Type	Index	$EO_{NO_X,i}(P_{Gi}) = ef_{NO_X,i}F_i = \alpha'_{NO_X,i} + \beta'_{NO_X,i}P_{Gi} + \gamma'_{NO_X,i}P_{Gi}^3$ in *kg/hour*		
		$\alpha'_{NO_X,i}$	$\beta'_{NO_X,i}$	$\gamma'_{NO_X,i}$
Coal	1~10	44.5905	6.6161	0.00000000848
Gas	11	10.2743	2.1112	0.00001775457
Gas	12	10.2743	2.1112	0.00001775457
Gas	13	10.2743	2.1112	0.00001775457
Gas	14	14.3726	2.2355	0.00000797440
Gas	15	54.9522	2.0878	0.00000270646
Gas	16	106.1932	2.0332	0.00000057557
Gas	17	46.7546	2.1992	0.00000005775
Gas	18	10.2743	2.1112	0.00001775457
Gas	19	10.2743	2.1112	0.00001775457
Gas	20	164.4394	1.9350	0.00000007322
Gas	21	130.5231	1.9385	0.00000020028
Gas	22	164.4394	1.9350	0.00000007322
Gas	23	20.1281	2.0232	0.00000335955
Nuclear	24~25	0.0000	0.0000	0.00000000000

Table 55. Coefficients of cubic-order output functions for water consumption in gallon/hour

Fuel Type	Index	$WO_{Water,i}(P_{Gi}) = ef_{Water,i}F_i = \alpha'_{Water,i} + \beta'_{Water,i}P_{Gi} + \gamma'_{Water,i}P_{Gi}^3$ in g*allons/hour*		
		$\alpha'_{Water,i}$	$\beta'_{Water,i}$	$\gamma'_{Water,i}$
Coal	1~10	10863.8761	1611.9193	0.00000206700
Gas	11	3622.3335	744.3320	0.00625962300
Gas	12	3622.3335	744.3320	0.00625962300
Gas	13	3622.3335	744.3320	0.00625962300
Gas	14	5067.2711	788.1705	0.00281148700
Gas	15	19374.1812	736.0950	0.00095419900
Gas	16	37439.8934	716.8415	0.00020292500
Gas	17	16483.9843	775.3735	0.00002036000
Gas	18	3622.3335	744.3320	0.00625962300
Gas	19	3622.3335	744.3320	0.00625962300
Gas	20	57975.4275	682.2013	0.00002581400
Gas	21	46017.7436	683.4501	0.00007061100
Gas	22	57975.4275	682.2013	0.00002581400
Gas	23	7096.4362	713.2973	0.00118445600
Nuclear	24~25	218639.5126	1459.6481	0.00010701300

APPENDIX I

ADAPTATION OF COST FUNCTIONS

Methods for the calculation of total operating costs can be classified into the average cost method and the cost function method. The former presents the unit cost (i.e., the total costs divided by the amount of produced electricity in *$/MWh* or *¢/kWh* presented as $C_{i,average}(P_{Gi})$ in Figure 65). The latter method calculates total operating costs using the cubic-order cost function presented in (56) (i.e., $C_i(P_{Gi})$ in Figure 65). Because of the differences in operating costs estimated by both the methods in *$/h* in Figure 65, to adapt proposed cubic-order cost functions to the average cost function (i.e., the straight line, $C_{i,average}(P_{Gi})$, in Figure 65), this study applies an affine transformation, a linear transformation followed by a translation represented by

$$C_i'(P_{Gi}) = aC_i(P_{Gi}) + b \quad . \tag{81}$$

By translating the original cubic-order cost function into an origin and selecting one of the points on the average cost function between $P_{Gi,Min}$ and $P_{Gi,Max}$, this study determines unknowns, or *a* and *b* in (81). Since base-load generation units such as nuclear plants produce constant power, the discrepancy in total operating costs between the transformed cubic-order cost function and the average cost method should be zero.

To determine the effect of the proposed affine transformation on the estimates of total generation costs, this study examines the total operating costs of ten coal-fired, thirteen gas-fired, and two nuclear plants of the power system model of the state of Georgia in 2010 by

$$C = \sum_{i=1}^{8760}\sum_{j=1}^{N_{Nuclear}} C'_{Nuclear}(P_{Nuclear,i,j}) + \sum_{i=1}^{8760}\sum_{j=1}^{N_{Coal}} C'_{Coal}(P_{Coal,i,j}) + \sum_{i=1}^{8760}\sum_{j=1}^{N_{Gas}} C'_{Gas}(P_{Gas,i,j}) \quad . \tag{82}$$

Table 56 presents a comparison of total operating costs determined by not only an average of generation costs of the Georgia Power Company, listed in Table 27, but also

the proposed cubic-order cost functions modified by the affine transformation. Since nuclear generation produces base power, or nearly constant output, the discrepancy in operating costs determined by both the methods is zero. Since gas-firing generating units, however, have their various min and max generation capacities, even from zero to their full capacity, the discrepancy increases by about 5.42%. Since this study does not use heat-rate data collected from actual plants operating in Georgia, total operating costs estimated by both the methods show a discrepancy of 3.46%.

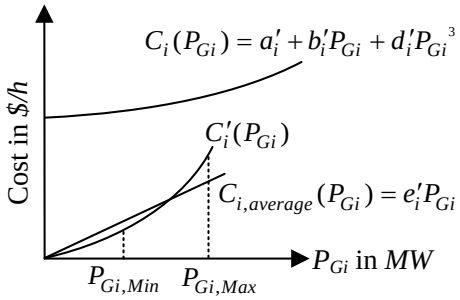

Figure 65. Adaptation of the cubic-order cost functions using an affine transformation.

Table 56. Comparison of total operating costs determined by averaging generation costs and the proposed cubic-order cost function

Fuel Type	Total Costs Determined by Average Generation Costs	Total Costs Determined by Cubic Cost Function	Discrepancy
	$/year	$/year	%
Coal	2.944E+09	3.040E+09	3.25%
Gas	5.578E+08	5.880E+08	5.42%
Nuclear	1.344E+08	1.344E+08	0.00%
Total	3.636E+09	3.762E+09	3.46%

REFERENCES

[1] A. R. Rohatgi, A. Ristow, A. Das, S. Ramanathan, "Road to Cost Effective Silicon PV," International Photovoltaic Science and Engineering Conference, 2009.

[2] T. Bradford, *Solar Revolution*, Cambridge, Massachusetts: MIT Press, 2006.

[3] A. Ristow, "Numerical modeling of uncertainty and variability in the technology, manufacturing, and economics of crystalline silicon photovoltaics," Ph.D. dissertation, Dept. Electrical Eng., Georgia Institute of Technology, 2008.

[4] International Energy Agency, *IEA energy statistics-electricity for United States*, Available: http://www.iea.org/statistics, 2007.

[5] International Energy Agency, *IEA energy statistics-electricity for world*, Available: http://www.iea.org/statistics, 2007.

[6] International Energy Agency, "World Energy Outlook 2011," Tech. Rep., 2011.

[7] International Energy Agency, "Technology Roadmap Solar Photovoltaic Energy," Tech. Rep., 2010.

[8] M. M. Begovic, Insu Kim, Damir Novosel, Julio Romero Aguero, Ajeet Rohatgi, "Integration of Photovoltaic Distributed Generation in the Power Distribution Grid," Hawaii International Conference System Science, 2012.

[9] National Renewable Energy Laboratory, "Best research photovoltaic cell efficiencies," US Department of Energy, Rev. 08-01-2014, 2014.

[10] A. Froitzheim, et al., "International Technology Roadmap for Photovoltaic Results 2012," International Technology Roadmap for Photovoltaic, Tech. Rep., 2013.

[11] Gaëtan Masson, Sinead Orlandi, Manoël Rekinger, "Global Market Outlook for Photovoltaics 2014-2018," European Photovoltaic Industry Association, Tech. Rep., 2014.

[12] C. Jorant, "The implications of Fukushima: The European perspective," Bulletin of the Atomic Scientists, vol. 67, pp. 14-17, 2011.

[13] Julio Romero Agüero, Steve J. Steffel, "Integration challenges of photovoltaic distributed generation on power distribution systems," IEEE Power and Energy Society General Meeting, 2011.

[14] *IEEE Application Guide for IEEE Std 1547(TM), IEEE Standard for Interconnecting Distributed Resources with Electric Power Systems*, IEEE Standard 1547-2008, 2009.

[15] M. M. Begovic and I. Kim, "Distributed renewable PV generation in urban distribution networks," Power Systems Conference and Exposition, 2011.

[16] M. H. Haque, "Efficient load flow method for distribution systems with radial or mesh configuration," *IEE Proceedings Generation, Transmission and Distribution*, pp. 33-38, 1996

[17] C. S. Cheng and D. Shirmohammadi, "A three-phase power flow method for real-time distribution system analysis," *IEEE Trans. Power Systems*, vol. 10, pp. 671-679, 1995.

[18] D. Shirmohammadi, H. W. Hong, A. Semlyen, and G. X. Luo, "A compensation-based power flow method for weakly meshed distribution and transmission networks," *IEEE Trans on Power Systems*, vol. 3, pp. 753-762, 1988.

[19] G. Gross and H. W. Hong, "A Two-Step Compensation Method for Solving Short Circuit Problems," *IEEE Trans. on Power Apparatus and Systems*, vol. 101, pp. 1322-1331, 1982.

[20] W. F. Tinney, "Compensation Methods for Network Solutions by Optimally Ordered Triangular Factorization," *IEEE Trans. on Power Apparatus and Systems*, vol. 91, pp. 123-127, 1972.

[21] S. Khushalani, J. M. Solanki, and N. N. Schulz, "Development of Three-Phase Unbalanced Power Flow Using PV and PQ Models for Distributed Generation and Study of the Impact of DG Models," *IEEE Trans. on Power Systems*, vol. 22, pp. 1019-1025, 2007.

[22] W. H. Kersting, *Distribution system modeling and analysis*, Boca Raton: CRC Press, pp. 199, 2002.

[23] W. H. Kersting, "Radial distribution test feeders," *IEEE Trans. on Power Systems*, vol. 6, pp. 975-985, 1991.

[24] A. Pregelj, "Impact of Distributed Generation on Power Network Operation," Ph.D. dissertation, Dept. Electrical Eng., Georgia Institute of Technology, 2003.

[25] *IEEE Standard Requirements, Terminology, and Test Code for Step-Voltage and Induction-Voltage Regulators*, ANSI/IEEE Standard C57.15-1986, 1988.

[26] D. S. Shugar, "Photovoltaics in the utility distribution system: The evaluation of system and distributed benefits," *Photovoltaic Specialists Conference*, 1990.

[27] T. Hoff and D. S. Shugar, "The value of grid-support photovoltaics in reducing distribution system losses," *IEEE Transactions on Energy Conversion*, vol. 10, pp. 569-576, 1995.
[28] N. Srisaen and A. Sangswang, "Effects of PV Grid-Connected System Location on a Distribution System," *IEEE Asia Pacific Conference on Circuits and Systems*, 2006.
[29] N. D. Hatziargyriou, T. S. Karakatsanis, and M. Papadopoulos, "Probabilistic load flow in distribution systems containing dispersed wind power generation," *IEEE Transactions on Power Systems*, vol. 8, pp. 159-165, 1993.
[30] P. Jorgensen, J. S. Christensen, and J. O. Tande, "Probabilistic load flow calculation using Monte Carlo techniques for distribution network with wind turbines," *International Conference On Harmonics and Quality of Power Proceedings*, 1998.
[31] M. Begovic, A. Pregelj, A. Rohatgi, D. Novosel, "Impact of renewable distributed generation on power systems," *Proceedings of the 34th Annual Hawaii International Conference on System Sciences*, 2001.
[32] A. Pregelj, M. Begovic, and A. Rohatgi, "Quantitative techniques for analysis of large data sets in renewable distributed generation," *IEEE Transactions on Power Systems*, vol. 19, pp. 1277-1285, 2004.
[33] S. Conti and S. Raiti, "Probabilistic load flow using Monte Carlo techniques for distribution networks with photovoltaic generators," *Solar Energy*, vol. 81, pp. 1473-1481, 2007.
[34] E. Rothfield, "Solar Photovoltaic Installation in California: Understanding the Likelihood of Adoption Given Incentives, Electricity Pricing and Consumer Characteristics," Thesis, Dept. Arts and Sciences, Duke University, 2010.
[35] P. Glasserman, *Monte Carlo methods in financial engineering*, New York: Springer, pp. 277, 2004.
[36] J. Dagpunar, *Simulation and Monte Carlo: with applications in finance and MCMC*, John Wiley, pp. 83, 2007.
[37] US Energy Information Administration, "Solar Photovoltaic Cell/Module Shipments Report 2010," Office of Energy Statistics, Washington, DC, Tech. Rep., 2012.
[38] W. Brooks and J. Dunlop, "Photovoltaic (PV) Installer Resource Guide," The North American Board of Certified Energy Practitioners (NABCEP), Tech. Rep., 2012.
[39] Atlantech, *Roof Pitch Diagram Chart*, Available from: http://www.atlantechsolar.com/roof_pitch_angle_diagram_chart.html.
[40] State of California, California Energy Commission and California Public Utilities Commission, California Solar Statistics, Available from: http://californiasolarstatistics.ca.gov/.
[41] Distribution Test Feeder Working Group, *Distribution Test Feeders*, Available from: http://ewh.ieee.org/soc/pes/dsacom/testfeeders/index.html.
[42] Southern California Edison, *2007 Static Load Profiles*, Available from: http://www.sce.com/AboutSCE/Regulatory/loadprofiles/2007loadprofiles.htm.
[43] Georgia Power Company, "2010 Annual Report," February 25, 2011.
[44] R. Billinton and R. N. Allan, *Reliability evaluation of power systems*, New York: Plenum Press, 1996.
[45] R. N. Allan, R. Billinton, I. Sjarief, L. Goel, and K. S. So, "A reliability test system for educational purposes-basic distribution system data and results," *IEEE Transactions on Power Systems*, vol. 6, pp. 813-820, 1991.
[46] R. Billinton, S. Kumar, N. Chowdhury, K. Chu, K. Debnath, L. Goel, E. Khan, P. Kos, G. Nourbakhsh, and J. Oteng-Adjei, "A Reliability Test System for Educational Purposes-Basic Data," *Power Engineering Review*, vol. 9, pp. 67-68, 1989.
[47] R. Billinton and W. Peng, "Teaching distribution system reliability evaluation using Monte Carlo simulation," *IEEE Transactions on Power Systems*, vol. 14, pp. 397-403, 1999.
[48] R. Billinton and S. Jonnavithula, "A test system for teaching overall power system reliability assessment," *IEEE Transactions on Power Systems*, vol. 11, pp. 1670-1676, 1996.
[49] B. In-Su and O. K. Jin, "Reliability Evaluation of Distributed Generation Based on Operation Mode," *IEEE Transactions on Power Systems*, vol. 22, pp. 785-790, 2007.
[50] D. Midence, S. Rivera, and A. Vargas, "Reliability assessment in power distribution networks by logical and matrix operations," *2008 IEEE/PES Transmission and Distribution Conference and Exposition*, 2008.

[51] D. H. Popovic, J. A. Greatbanks, M. Begovic, and A. Pregelj, "Placement of distributed generators and reclosers for distribution network security and reliability," *International Journal of Electrical Power & Energy Systems*, pp. 398–408, 2005.
[52] A. Pregelj, M. Begovic, and A. Rohatgi, "Recloser allocation for improved reliability of DG-enhanced distribution networks," *IEEE Transactions on Power Systems*, vol. 21, pp. 1442-1449, 2006.
[53] K. A. De Jong, "An analysis of the behavior of a class of genetic adaptive systems," Ph.D. dissertation, Dept. Computer and Communication Sciences, University of Michigan, Ann Arbor, 1975.
[54] C. R. Houck, J. A. Joines, and M. G. Kay "A genetic algorithm for function optimization: A MATLAB implementation," North Carolina State University, 1995.
[55] Z. Michalewicz, *Genetic algorithms + data structures = evolution programs*, New York: Springer-Verlag, 1996.
[56] D.E. Goldberg, *Genetic Algorithms in Search, Optimization, and Machine Learning*, Addison-Wesley, 1989.
[57] T. Jen-Hao and L. Yi-Hwa, "A novel ACS-based optimum switch relocation method," *IEEE Transactions on Power Systems*, vol. 18, pp. 113-120, 2003.
[58] B. Ravindranath and M. Chander, *Power System Protection and Switchgear*, New York: Wiley, pp. 180, 1977.
[59] S. Eckles, "Simple Strategies to Improve Power Reliability," *Electric Light & Power*, 2006.
[60] J. W. Lamont and E. V. Obessis, "Emission dispatch models and algorithms for the 1990s," *IEEE Transactions on Power Systems*, vol. 10, pp. 941-947, 1995.
[61] J. S. Dhillon, S. C. Parti, and D. P. Kothari, "Stochastic economic emission load dispatch," *Electric Power Systems Research*, vol. 26, pp. 186-197, 1993.
[62] G. B. Sheble and K. Brittig, "Refined genetic algorithm-economic dispatch example," *IEEE Transactions on Power Systems*, vol. 10, pp. 117-124, 1995.
[63] Y. H. Song, G. S. Wang, P. Y. Wang, and A. T. Johns, "Environmental/economic dispatch using fuzzy logic controlled genetic algorithms," *IEEE Proceedings Generation, Transmission and Distribution*, vol. 144, pp. 377-382, 1997.
[64] W. Kit Po and J. Yuryevich, "Evolutionary-programming-based algorithm for environmentally-constrained economic dispatch," *IEEE Transactions on Power Systems*, vol. 13, pp. 301-306, 1998.
[65] T. Thakur, K. Sem, S. Saini, S. Sharma, "A Particle Swarm Optimization Solution to NO_2 and SO_2 Emissions for Environmentally Constrained Economic Dispatch Problem," *Transmission & Distribution Conference and Exposition: Latin America*, 2006.
[66] W. J. Tang, Q. H. Wu, and J. R. Saunders, "Bacterial Foraging Algorithm For Dynamic Environments," *IEEE Congress on Evolutionary Computation*, 2006.
[67] A. Mills and R. Wiser, "Implications of Wide-Area Geographic Diversity for Short-Term Variability of Solar Power," Lawrence Berkeley National Laboratory, Tech. Rep., 2010
[68] A. D. Mills and R. H. Wiser, "Implications of geographic diversity for short-term variability and predictability of solar power," *Power and Energy Society General Meeting*, 2011.
[69] C. Mustacchi, V. Cena, and M. Rocchi, "Stochastic simulation of hourly global radiation sequences," *Solar Energy*, vol. 23, pp. 47-51, 1979.
[70] R. J. Aguiar, M. Collares-Pereira, and J.P. Conde, "Simple procedure for generating sequences of daily radiation values using a library of Markov transition matrices," *Solar Energy*, vol. 40, pp. 269-279, 1988.
[71] D.A. McCracken, "Synthetic High Resolution Solar Data," M.S. thesis, Dept. Mechanical Eng., University of Strathclyde, 2011.
[72] PVPMC, *PV_LIB Toolbox*, Available from: http://pvpmc.org/pv-lib/.
[73] NREL, *National Solar Radiation Data Base*, Available from: http://rredc.nrel.gov/solar/old_data/nsrdb/1991-2005/tmy3/.
[74] NREL, *Measurement and Instrumentation Data Center (MIDC)*, Available from: http://www.nrel.gov/midc/.
[75] E. V. M. Obessis and J. W. Lamont, "An Emissions-constrained Scheduling algorithm," *Proceedings of Joint International Power Conference*, Athens Power Tech, 1993.
[76] D. Hasler, "New Coal-Fired Power Plant Performance and Cost Estimates," Sargent & Lundy, Tech. Rep., Aug. 2009.

[77] A. Leyzerovich, *Wet-steam turbines for nuclear power plants*, Oklahoma: PennWell Corp, pp. 268, 2005.
[78] J. B. Klein, "The Use of Heat Rates in Production Cost Modeling and Market Modeling," California Energy Commission, 1998.
[79] Southern California Edison, *2010 Static Load Profiles*, Available from: http://www.sce.com/AboutSCE/Regulatory/loadprofiles/2010loadprofiles.htm.
[80] Georgia Power Company, "Project Operations and Drought Management Plan Study-Bartletts Ferry Hydroelectric Project," Tech. Rep., March 2011.
[81] NREL, *System Advisor Model*, Available from: https://sam.nrel.gov/.
[82] Z. Yewdall, "PV Orientation," *Home Power Magazine*, vol. 93, pp. 24-28, 2003.
[83] GetSolar.com, *How Solar Home Energy Works*, Available from: http://www.getsolar.com/residential_solar-home-energy-overview.php.
[84] Georgia Power, *Facts & Figures*, Available from: http://www.georgiapower.com/about/facts.asp.
[85] US Energy Information Administration, "Levelized Cost of New Generation Resources in the Annual Energy Outlook 2014," Office of Energy Statistics, Washington, DC, Tech. Rep., 2014.
[86] U.S. Energy Information Administration, "Annual Energy Review 2009," Tech. Rep., 2010.
[87] K. Sovacool, "Valuing the greenhouse gas emissions from nuclear power: A critical survey," Centre on Asia and Globalization, National University of Singapore, Tech. Rep., 2008.
[88] A. Leitner, "Fuel from the sky: Solar power's potential for western energy supply," NREL, Tech. Rep., 2002.
[89] P. Torcellini, N. Long, and R. Judkoff, "Consumptive Water Use for U.S. Power Production," NREL, Tech. Rep., 2003.
[90] B. M. Weedy, *Electric power systems*, New York: J. Wiley, pp. 26, 1972.
[91] I. Kim and M. Begovic, "Power-flow Algorithm for the Integration of Stochastic Renewable Distributed Photovoltaic Systems and Urban Distribution Networks (Unpublished)."
[92] I. Kim and M. Begovic, "Impact of Stochastically Distributed Renewable Generation on Urban Distribution Networks and Variance Reduction Using Optimal Importance Sampling for a Normal Distribution (Unpublished)."
[93] P. M. Anderson, *Power system protection*, New York: McGraw-Hill: IEEE Press, 1999.
[94] U.S. Energy Information Administration, "Annual Energy Review 2011," Office of Energy Statistics, Washington, DC. Tech. Rep., 2012.
[95] A. J. Wood and B. F. Wollenberg, *Power generation, operation, and control*, New York: J. Wiley & Sons, 1996.
[96] D. Hazarika and P. K. Bordoloi, "Modified loss coefficients in the determination of optimum generation scheduling," *IEEE Proceedings Generation, Transmission and Distribution*, vol. 138, pp. 166-172, 1991.
[97] A. R. Bergen and V. Vittal, *Power systems analysis*, NJ: Prentice Hall, 2000.
[98] A. Vuorinen, *Planning of Optimal Power Systems*, Ekoenergo Oy, 2008.
[99] Georgia Power Company, "Morgan Falls Hydro," Tech. Rep., 2007.

VITA

Insu Kim

Insu Kim (Korean [Hangul]: 김인수), who received his master's degree from Sungkyunkwan University in South Korea in 2002, worked five years in electrical systems engineering for Hyosung Corporation, where he developed software for various electric power systems. He is currently a graduate research assistant working on his doctoral degree in electrical and computer engineering at Georgia Tech, under the supervision of Dr. Miroslav Begovic and Dr. Ronald Harley. His major research interests have been (1) analyzing the impact of stochastic renewable distributed generation such as photovoltaic systems, wind farms, and microturbines on urban distribution networks, using the three-phase power-flow algorithm, the stochastic Monte Carlo simulation method, the environmentally-constrained generation resource allocation algorithm, and the genetic algorithm for the reliability optimization of such networks, and (2) researching the transient behavior of distribution networks when distributed generation systems are injecting active and reactive power. He published seven international conference papers, two book chapters, four Korean journal papers, twelve Korean conference papers, and a registered patent on his research area.